

**Development of analytical and remediation methods
for highly polycyclic aromatic hydrocarbon
contaminated soils**

Dissertation

zur Erlangung des akademischen Grades eines
Doktors der Naturwissenschaften

– Dr. rer. nat. –

vorgelegt von

Ruoji Luo

Aus Chongqing, China
geboren

Fakultät für Chemie
der
Universität Duisburg-Essen

2020

DuEPublico

Duisburg-Essen Publications online

UNIVERSITÄT
DUISBURG
ESSEN

Offen im Denken

ub | universitäts
bibliothek

Diese Dissertation wird via DuEPublico, dem Dokumenten- und Publikationsserver der Universität Duisburg-Essen, zur Verfügung gestellt und liegt auch als Print-Version vor.

DOI: 10.17185/duepublico/73506

URN: urn:nbn:de:hbz:465-20230704-104214-0

Alle Rechte vorbehalten.

Die vorliegende Arbeit wurde im Zeitraum von Oktober 2015 bis Mai 2019 im Arbeitskreis von Prof. Dr. Wolfgang Schrader am Max-Planck-Institut für Kohlenforschung im Mülheim an der Ruhr durchgeführt.

Tag der Disputation: 19.11.2020

Gutachter: Prof. Dr. Wolfgang Schrader

Prof. Dr. Torsten C. Schmidt

Vorsitzender: Prof. Dr. Alexander Probst

知人者智，自知者明。

胜人者有力，自胜者强。

知足者富。强行者有志。

不失其所者久。死而不亡者寿。

老子

Kurzfassung

Polyzyklische aromatische Kohlenwasserstoffe (PAK) sind als allgegenwärtige Kontaminanten in der Umwelt bekannt. In den letzten 40 Jahren werden die von PAK kontaminierten Böden aus Industrieanlagen gemäß einer Liste von 16 PAK der United States Environmental Protection Agency (EPA) überwacht. Im kontaminierten Boden können jedoch auch (alkylierte) PAK mit hochmolekularen Massen sowie polyzyklische aromatische Heterozyklen (PAXH, X = N, S, O) vorkommen. Daher müssen Fragen gestellt werden, wie die folgenden: „Wie komplex sind die von PAK kontaminierten Böden?“ oder „Wie verhalten sich andere Kontaminanten als die 16 EPA PAK mit verschiedenen Sanierungsmethoden?“ Um diese Fragen zu beantworten, muss eine neue analytische Strategie angewendet werden. Dies kann durch die Anwendung der modernsten analytischen Instrumente, z.B. Fourier-Transformations-Massenspektrometrie (FTMS), auf eine Non-Target Vorgehensweise, realisiert werden.

In einem ersten Schritt wurden die Extraktionseffizienz der Extraktionsmethoden, darunter die Soxhlet Extraktion mit verschiedenen Lösungsmitteln sowie die Extraktion mit überkritischen CO₂, mittels Non-Target Analyse von PAXH in einer Modellprobe (Sand mit Erdöl versetzt) verglichen. Dichlormethan erwies sich als das am besten geeignete Lösungsmittel bei Verwendung der Soxhlet Extraktion für die Non-Target Analyse von PAXH in kontaminierten Böden.

Anschließend wurde ein stark PAXH kontaminierter Boden (mit $64.500 \pm 9.500 \text{ mg kg}^{-1}$ lösungsmittlextrahierbaren organischen Stoffen (SEO)) mittels FTMS mit drei Ionisationsmethoden bei Atmosphärendruck (API) in beiden Polaritäten charakterisiert. Insgesamt konnten 21.958 verschiedene elementare Zusammensetzungen für diese einzelne Probe zugeordnet werden. Die Ergebnisse zeigten, dass sich hoch aromatische PAK mit Doppelbindungsäquivalent (DBE) über 70 sowie PAXH, insbesondere Azaarenes, im kontaminierten Boden zu finden waren. Der pyrogene Ursprung dieses kontaminierten Bodens konnte durch die charakteristischen DBE vs. Kohlenstoffzahlen Verteilungen von PAXH nachgewiesen werden.

Nach der Charakterisierung des kontaminierten Bodens wurde dieser den unterschiedlichen Sanierungstechniken unterzogen, darunter der physikalischen Sanierung mittels Dichtentrennung und Lösungsmittlextraktion sowie der thermischen Sanierung mittels Pyrolyse. Durch die Anwendung integrierter Sanierungstechniken wurde die SEO im

kontaminierten Boden auf $860 \pm 280 \text{ mg kg}^{-1}$ reduziert, was einer Sanierungseffizienz von 98,7% entspricht. Zusätzlich wurde mit Hilfe der API-FTMS und Gaschromatographie (GC)-FTMS eine detaillierte Analyse des kontaminierten Bodens vor und nach der Sanierung auf molekularer Ebene erzielt. Dies ermöglichte ein tieferes Verständnis ausgewählter Sanierungsprozesse und, was noch wichtiger ist, lieferte wertvolle Informationen darüber, wie sich unterschiedliche PAXH unter verschiedenen Sanierungstechniken verhalten.

Abstract

Polycyclic aromatic hydrocarbons (PAH) are known as omnipresent contaminants in the environment. Over the last 40 years, PAH contaminated soils from industrial sites are monitored according to a list of 16 United States Environmental Protection Agency (EPA) PAH. However, high molecular weight (alkylated) PAH along with polycyclic aromatic heterocycles (PAXH, X = N, S, O) can occur in the contaminated soil as well. Questions have been arisen, such as: “How complex are PAH contaminated soils?” or “How do contaminants other than 16 EPA PAH behave under different remediation conditions?” In order to answer these questions, a new analytical strategy has to be applied. This can be realized by applying the state-of-the-art analytical instrumentation, for instance Fourier transform mass spectrometry (FTMS), by a non-targeted approach.

As the first step, the extraction efficiency of different extraction methods, including Soxhlet extraction with various extraction solvents as well as supercritical fluid extraction (SFE) using CO₂, were compared for the non-targeted analysis of PAXH in a model sample (sand with crude oil spiked). Dichloromethane turned out to be the most suitable solvent when using Soxhlet extraction for the non-targeted analysis of PAXH in contaminated soils.

Subsequently, a highly PAXH contaminated soil (with $64,500 \pm 9,500 \text{ mg kg}^{-1}$ solvent extractable organics (SEO)) was characterized using FTMS with three atmospheric pressure ionization (API) methods in both polarities. In total, 21,958 distinct elemental compositions could be assigned for this single sample. Results revealed that highly aromatized PAH with double bond equivalent (DBE) over 70 and PAXH, especially azaarenes, co-occurred in the contaminated soil. The pyrogenic origin of this contaminated soil could be proven by the unique DBE vs. carbon count distributions of PAXH.

After the characterization of the contaminated soil, it was subjected to different remediation techniques, including physical remediation via density separation and solvent extraction as well as thermal remediation via pyrolysis. By applying integrated remediation techniques the SEO in the contaminate soil was reduced to $860 \pm 280 \text{ mg kg}^{-1}$, which represent a remediation efficiency of 98.7%. Additionally, with the help of API-FTMS and gas chromatography (GC)-FTMS a detailed analysis of contaminated soil before and after remediation on a molecular level was achieved. This enabled a deeper understanding of selected remediation processes and, more importantly, provided valuable information about the how different PAXH behave under different remediation techniques.

Content

Chapter 1. General Introduction.....	1
1.1. Analysis of PA(X)H	4
1.2. Remediation techniques for PA(X)H contaminated soils	9
1.3. Introduction to instrumentation	12
1.4. Scope of the study	18
1.5. References	20
Chapter 2. Development of a Non-Targeted Method to Study Petroleum Polyaromatic Hydrocarbons in Soil by Ultrahigh Resolution Mass Spectrometry Using Multiple Ionization Methods.....	29
2.1. Abstract.....	29
2.2. Introduction	30
2.3. Material and Methods.....	31
2.4. Results and Discussion	33
2.5. Conclusion.....	43
2.6. References	44
Appendix for Chapter 2.....	49
Chapter 3. Getting a Better Overview of a Highly PAH Contaminated Soil: a Non-Targeted Approach Assessing the Real Environmental Risk.....	57
3.1. Abstract.....	57
3.2. Introduction	58
3.3. Materials and Methods	59
3.4. Results and Discussion	60
3.5. Conclusion.....	70
3.6. References	70
Appendix for Chapter 3.....	75
Chapter 4. Physical Separation of Highly PAXH Contaminated Soil as Well as Analysis of Its Fractions and Corresponding Water Phase Using Fourier Transform Mass Spectrometry	83

4.1. Abstract.....	83
4.2. Introduction	84
4.3. Materials and Methods	85
4.4. Results and Discussion	87
4.5. Conclusion.....	96
4.6. References	96
Appendix for Chapter 4.....	100
Chapter 5. Investigation of Solvent Extraction for Highly PAH Contaminated Soil Using Used Cooking Oil Methyl Ester	107
5.1. Abstract.....	107
5.2. Introduction	108
5.3. Materials and Methods	109
5.4. Results and Discussion	111
5.5. Conclusion.....	119
5.6. References	119
Chapter 6. Pyrolytic Remediation of Highly PAH Contaminated Soil, Analyzed Using Ultrahigh Resolution Atmospheric Pressure Photon Ionization (APPI) Fourier Transform Mass Spectrometry and Gas Chromatography-APPI-Mass Spectrometry	123
6.1. Abstract.....	123
6.2. Introduction	124
6.3. Materials and Methods	125
6.4. Results and Discussion	127
6.4.3. Characterization of pyrolyzed oil	136
6.5. Conclusion.....	138
6.6. References	139
Appendix for Chapter 6.....	143
Chapter 7. Conclusion.....	147
Chapter 8. Appendix	151

8.1. List of abbreviations	151
8.2. List of schemes	154
8.3. List of figures	155
8.4. List of tables	163
8.5. List of publications	164
8.6. Curriculum Vitae	166
8.7. Erklärung	167
8.8. Acknowledgment.....	168

Chapter 1. General Introduction

Polycyclic aromatic compounds are a group of organic compounds, which are typically considered to consist of two or more fused aromatic five or six-membered rings in a two-dimensional arrangement. Several thousand individual compounds belong to this large family, which can be further divided into polycyclic aromatic hydrocarbons (PAH) and polycyclic aromatic heterocycles (PAXH, X = N, S or O).¹ Figure 1-1 shows some examples of such compounds. While PAH are omnipresent in the environment, their individual occurrence varies largely. High differences between individual compounds are also observed for their human or eco-toxicity as well as their physicochemical properties, which ultimately lead to different transformation processes in the environment.

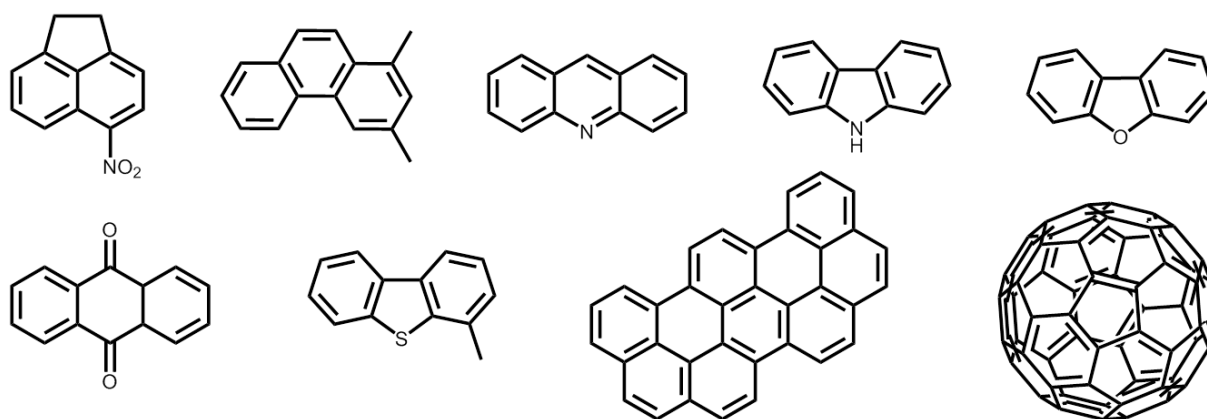


Figure 1-1. Examples of polycyclic aromatic compounds.

PAH can be brought into the environment through different processes, the most important of which are summarized in Figure 1-2. These can be categorized into biogenic, petrogenic or pyrogenic processes.² PAH of biogenic origin are formed from natural organic compounds through biological processes.³ Petrogenic PAH are generated under geologic temperature and pressure over a relatively long period (geological time scale), whereas pyrogenic PAH are naturally generated through volcanic eruptions and forest fires.⁴

Besides these natural processes, PAH can be anthropogenically generated or transferred into the environment. The major anthropogenic sources for petrogenic PAH in the environment are the crude oil related activities (e.g. its exploitation, transportation, storage, usage). These include, for example, oceanic or land-based oil spills, and pollution from petroleum refineries. Pyrogenic PAHs can be formed from industrial sites, for instance from manufactured gas or coking plants, or through the combustion of organic matters (fossil fuels) at relatively high temperature over a short time period.⁵ Other sources of anthropogenic PAH involve the incineration of wastes.

No matter the origin of PAH (biogenic, petrogenic or pyrogenic; natural or anthropogenic), once they are present in the environment, they undergo transfer processes between the atmosphere, lithosphere, hydrosphere and biosphere, and are subjected to chemical and biological transformations. The transfer and transformation processes of PAH in the environment is discussed in the following paragraphs.

As one of the primary emission sources for PAH into the atmosphere, burning of biofuel contributed more than half of the total emission. The other sources of PAH are wildfire, consumer products, traffic oil combustion and domestic coal combustion (Figure 1-2).⁶ Revolatilization of semi-volatile PAH from other compartments (vegetation, soils, and water surfaces), in which PAH have been accumulated historically, into the atmosphere is considered as secondary emission.⁷ Atmospheric PAH are present in the gas and particulate phase. Here, the gas-particle partitioning of individual PAH plays an essential role in determining in which phase they are predominantly present. Generally, smaller PAH with two to three rings tend to stay in the gas phase, while larger compounds are more likely found within atmospheric particles.⁸ Additionally, seasonal and geological variations in the ratio of PAH concentration in the gas and particulate phase can be observed, which are influenced through various parameters, such as land-sea circulation or monsoon activities.⁹

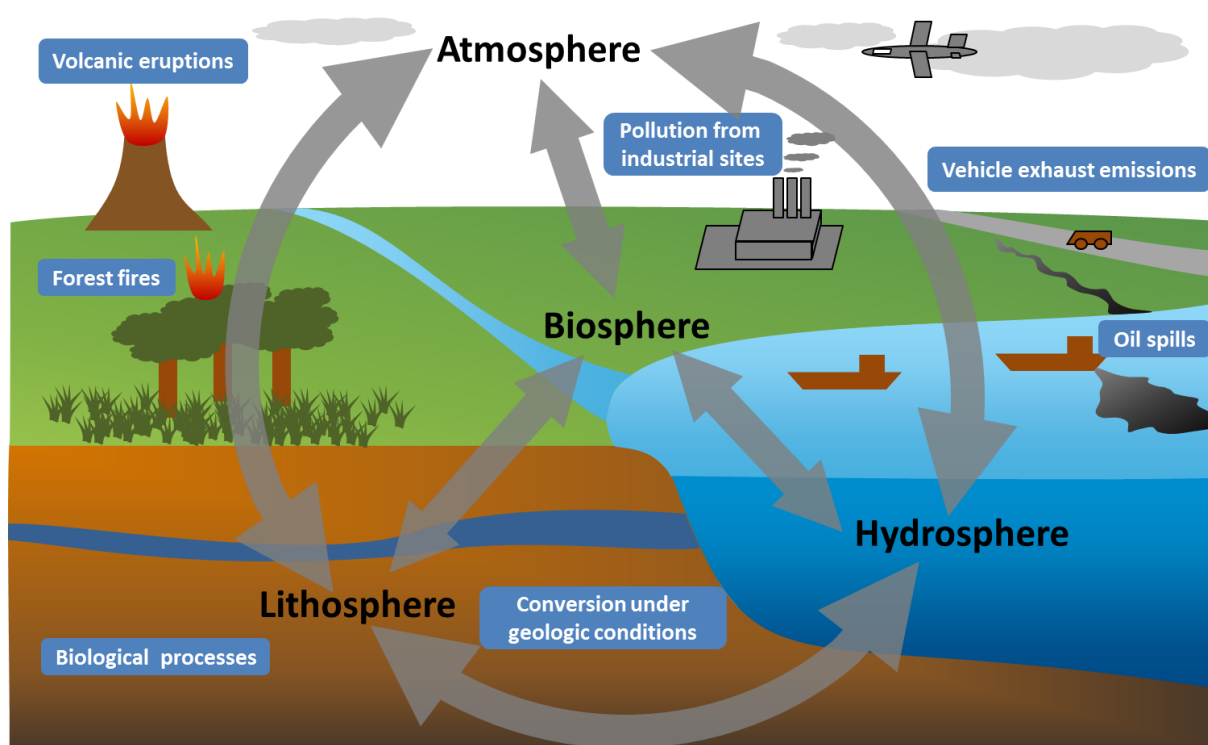


Figure 1-2. Occurrence and transfer of PAH in the environment.

Atmospheric PAH can be transferred to the lithosphere and hydrosphere through dry or wet deposition processes.¹⁰ Other inputs of PAH into the lithosphere and hydrosphere include natural or anthropogenic oil spills occurred on land or in the sea. PAH coming from these sources can be released into ground water, surface water or directly into the ocean. According to their octanol-water partitioning coefficients, PAH tend to accumulate in the sediment or soil rather than in the hydrosphere.¹¹ However, the hydrosphere endows PAH with more mobility, thus rendering them more accessible for micro- or macro-organisms.

While PAH are retaining in and/or transferring between different environments, they undergo a series of physical, biological and chemical processes, which include volatilization, leaching, adsorption to/desorption from soil particles, biodegradation, bioaccumulation, photooxidation and chemical oxidation.¹² In the atmosphere, the hydroxyl radical, which is predominantly generated by the photolysis of ozone in the presence of water vapor, plays a key role in the transformation of PAH. Also ozone itself can react with atmospheric PAH. A full understanding of the mechanisms of reactions involving PAH in the atmosphere is not achieved. Most of the reaction products still remain unidentified because of the analytical difficulties.⁷ The degree of difficulty increases, when the matrix is changing from air to water and soil, where other biological and chemical processes are increasingly involved.

The original or transformed PAH represent a threat to the living beings in the environment. They are carcinogenic, mutagenic and teratogenic for human, other mammals, invertebrates, and fish. Their uptake occurs via three main routes: ingestion, inhalation and dermal contact.¹³ While it is not entirely clear, which kind of short-term health effects PAH can induce in humans, they may cause diarrhea, eye irritation, nausea, vomiting, and confusion. A long-term exposure to PAHs can result in kidney, lung and liver damage, as well as abnormality in cataracts and skin inflammation.¹⁴ The transformation of PAH in the human body comprises mainly three pathways: the cytochrome P450 monooxygenase and epoxide hydrolase pathway, cytochrome P450 peroxidase pathway, and aldo-keto reductase pathway. During the metabolism PAH are firstly transformed into phenols, catechols, and quinones, which can then be further transformed into radical cations, diol-epoxides, or o-quinones. These reactive species may react with deoxyribonucleic acid (DNA) or proteins to produce DNA or protein adducts, and initiate carcinogenesis or mutagenesis.¹⁵

According PAH's (eco)toxicological effects, they are constantly the focus of researchers. A deeper understanding of the occurrence, transfer, and transformation of PAH will help researcher to develop appropriate remediation techniques, and accordingly reduce the amount

of PAH in the environment. This is supported by the establishment of reliable analytical methods.

1.1. Analysis of PA(X)H

The investigation on sources of PAHs in the environment started in the early to middle of 1970s.¹⁶ This was due to the growing interest and concern of their presence, which is driven by scientists with interdisciplinary knowledge in geochemistry, environmental chemistry, toxicology and analytical chemistry. After more than 40 years of research on this exciting topic, much has been achieved. However, the more investigations have been conducted, more questions are raised.

1.1.1. The 16 EPA PAH

The analysis of PAHs, their origin and fate in environmental samples is today almost entirely based on a list of 16 PAHs that are among others deemed priority pollutants by the United States Environmental Protection Agency (U.S. EPA)¹⁶ It was not until recently that scientists started to question why these particular PAHs were chosen as representatives for the whole group?¹⁷

The chosen PAH (which are shown together with their molecular mass and double bond equivalent (DBE) in Figure 1-3) were not necessarily included into the list according their relevance in terms of environmental issues. In fact, one needs to consider that during the 1970s, when the EPA list was put together, the analytical possibilities were somewhat limited, especially when it comes to the analysis of organic contaminants in the ppb range. At that time all steps of an analysis were typically performed manually, on an analog instrumentation and therefore very time consuming. As for analytical instrumentation gas-chromatographs

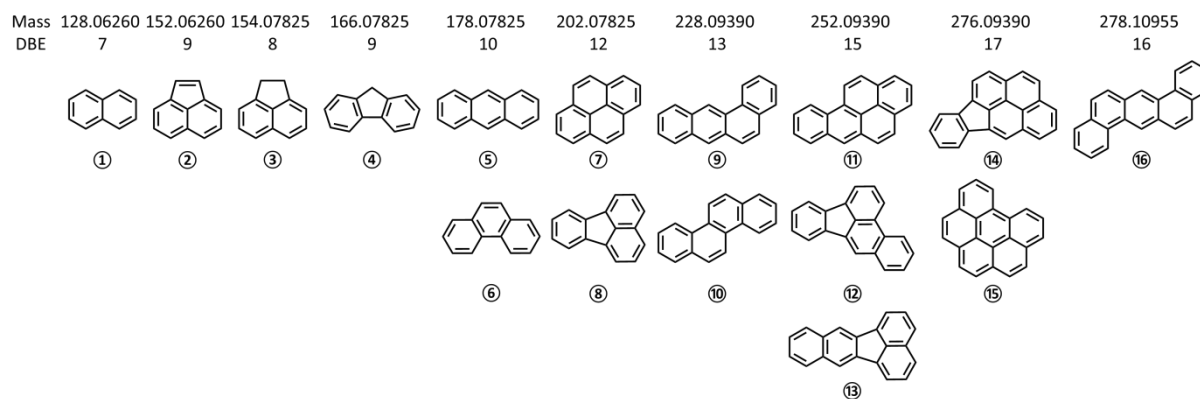


Figure 1-3. Masses, double bond equivalents (DBEs) and chemical structures for 16 EPA PAH. ①: Naphthalene, ②: Acenaphthene, ③: Acenaphthene, ④: Fluorene, ⑤: Anthracene, ⑥: Phenanthrene, ⑦: Pyrene, ⑧: Fluoranthene, ⑨: Benzo[*a*]anthracene, ⑩: Chrysene, ⑪: Benzo[*a*]pyrene, ⑫: Benzo[*b*]fluoranthene, ⑬: Benzo[*k*]fluoranthene, ⑭: Dibenzo[*a,h*]anthracene, ⑮: Benzo[*ghi*]perylene, ⑯: Indeno[*1,2,3-cd*]pyrene.

where often still operated using inefficient packed columns and the first commercial mass spectrometers had just become available.¹⁷

Still, when it was realized that a definitive list of compounds would be needed for the monitoring of this important group of compounds, 16 PAH were chosen based on different criteria. Among these were a known carcinogenicity (acenaphthylene, fluorene and phenanthrene), frequent appearance on coal related industrial sites (anthracene, pyrene and benzo[*ghi*]perylene) or simply the availability as a pure reference standard (benz[*a*]anthracene, chrysene, benzo[*a*]pyrene, benzo[*b*]fluoranthene, benzo[*k*]fluoranthene, dibenz[*a,h*]anthracene, and indeno[*1,2,3-cd*]pyrene). Such a limited definitive list has certain advantages:¹⁸

- limited analytical complexity and moderate analytical costs
- analytical standards are commercially available
- established for monitoring over the years
- good comparability worldwide

However, this list of 16 PAH also has its limitations, especially after 40 years of intensive research. One of the major drawbacks is that some commonly occurring PAH with higher toxicity are not listed and therefore completely neglected. For example, dibenz[*a,h*]pyrene, dibenz[*a,i*]pyrene and dibenz[*a,l*]pyrene have 10-fold and benzo[*c*]fluoranthene even 20 fold higher carcinogenic potential than benzo[*a*]pyrene.¹⁹ Another limitation is that alkylated PAH are not considered, although some of them have higher toxicity and their distribution in environmental samples may offer valuable information about their origin.²⁰ In addition to this, PAXH, which co-occur together with PAH in the environment, are not included, either.

During the years, numerous attempts have been made to analyze other (alkylated) PA(X)H in the environment. However, from the analytical point of view this is not an easy task. With increasing number of carbon atoms in side chains the number of isomers increases exponentially, while the concentration of the corresponding isomers decreases accordingly.¹⁸ When the standard gas chromatography-mass spectrometry (GC-MS) method for the quantitative analysis of the 16 EPA PAHs is applied for the analysis of substituted PAHs, false positive and negative assignments can occur.²¹ The situation will become even worse, if such analysis is applied for quantifying PAH in complex environmental samples, e.g. sediment or soil. To overcome this problem and to gain a more comprehensive view on PAH

related contaminants from industrial sites, where a high concentration as well as diversity of PA(X)H are suspected, modern analytical techniques are needed.

1.1.2. Sample preparation for PA(X)H analysis in soils

In the environmental analysis, sample preparation, especially extraction, is a crucial step.²² Any error introduced during this very first step, no matter how precise and accurate the analytical instrument is, the gained data will render doubtful. Various standard extraction methods for organic compounds from solid materials, such as soils, sludges, and wastes, have been published by the U.S. EPA. These include Soxhlet extraction,²³ supercritical fluid extraction (SFE),²⁴ ultrasonic extraction²⁵ and microwave-assisted extraction (MAE)²⁶ (see Figure 1-4). Shaking extraction and accelerated solvent extraction (ASE) are other extraction methods, which are suggested from the International Organization for Standardization (ISO).²⁷ These methods are validated for the extraction of the 16 EPA PAH. However, little is known about the extraction efficiency of other (alkylated) PA(X)H. Here, the advantages and disadvantages of the above mentioned extraction methods are firstly discussed, in order to select a suitable one for the extraction of PA(X)H from contaminated sites.

Soxhlet extraction is one of the most conventional methods, which is easy to operate and allows a high sample load. The major solvents or solvent mixtures used for the extraction are dichloromethane, toluene, *n*-heptane, ethyl acetate, acetone/*n*-hexane (1:1, *v/v*) or acetone/dichloromethane (1:1, *v/v*).²⁸⁻³¹ Major drawbacks of this method are that it is usually time consuming and requires a relatively large amount of organic solvent.³² However, this method can be automatized, which increases the sample throughput and reduces solvent use and costs.³³

In comparison to the Soxhlet extraction, SFE is considered much more environmentally friendly.³⁴ The solvent commonly used during the extraction is supercritical carbon dioxide (CO₂), which is chemically very inert, inexpensive, nontoxic, noncorrosive and nonflammable.

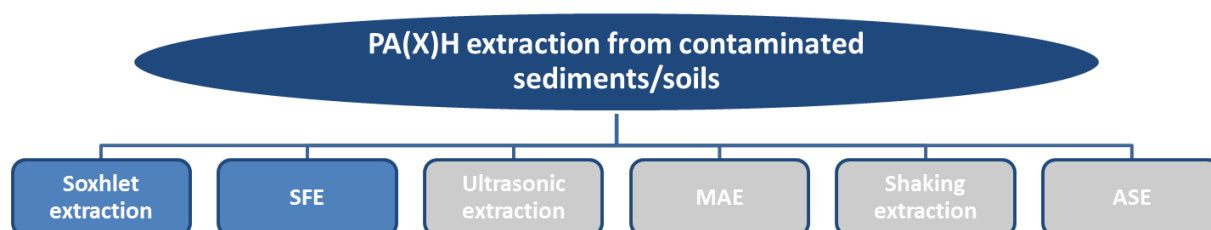


Figure 1-4. Extraction methods for PAH in contaminated sediments or soils. MAE: microwave-assisted extraction; ASE: accelerated-solvent extraction; SFE: supercritical fluid extraction. Methods in blue have been investigated in this work.

At a temperature above 31 °C and a pressure above 73 bar carbon dioxide becomes supercritical, leading to a higher diffusion coefficient and lower viscosity compared to common liquids.²² This increases the solubility of PAH in the supercritical CO₂. To further increase the extraction efficiency, especially of higher molecular weight PAH, small amount of co-solvent will be added into the system. Although SFE is a relatively fast method and requires no or little organic solvent, its acquisition cost is relatively high. In the past, the main focus of the research was to determine optimized conditions regarding temperature, pressure and co-solvent for the extraction of the 16 EPA PAH from contaminated sediments or soils.³⁵⁻⁴⁷ Fewer investigations have dealt with the extraction of other PA(X)H.⁴⁸

1.1.3. Targeted analysis of soils contaminated with PA(X)H

Soil represents the biggest reservoir of PAH, as they ubiquitous in sediments and soils worldwide^{2, 49} This is supported by studies of the 16 EPA PAH, that shows varying concentrations depending on the location. In rural areas their concentration is usually around 500 µg kg⁻¹, whereas their concentration in soil from industrial sites, such as manufactured gas plants, coking plants and wood preservation factories, can easily exceed 1,000 mg kg⁻¹.⁵⁰⁻⁵³

The targeted, often quantitative analysis of 16 EPA PAH has since the release of the U.S. EPA list of priority pollutants around forty years ago, mostly been performed using gas chromatographic separation of the corresponding samples. At that time, the resolving power of gas chromatography (GC) with packed column was not able to separate some isomeric signals of these 16 EPA PAH, such as anthracene and phenanthrene; benzo[*a*]pyrene and chrysene; benzo[*b*]fluoranthene and benzo[*k*]fluoranthene; dibenz[*a,h*]anthracene and indeno[*1,2,3-cd*]pyrene.⁵⁴ Detection and quantification of the analytes after chromatographic separation is often carried out by using a flame ionization detector (FID), which still is one of the most popular and universal GC detectors (Figure 1-5).⁵⁵ Also single (Q) or triple (QqQ) mass spectrometers with electron ionization (EI) are frequently used to gain a more sensitive and mass selective detection.⁵⁶ Besides GC related techniques, high performance liquid chromatography (HPLC) with fluorescence detector (FLD) or diode array detector (DAD) detector have been recommended by EPA and ISO for the quantification of PAH in 76 soils.⁵⁷ Many of the early investigations on the extraction efficiency of PAH from contaminated soil discussed in the above section have used one of these analytical methods, especially GC-EI-Q MS.

Lately, the awareness has been increased that polycyclic aromatic compounds other than the 16 EPA PAH occur in heavily contaminated soils.¹⁸ These compounds include (alkylated) PA(X)H, oxygen-containing PAH (oxy-PAH and hydroxyl-PAH) or nitrated PAH.⁵⁸ Some of these alkylated and high molecular weight PAH, such as dibenzopyrene, 5-methylchrysene and 1-methylpyrene, have an even higher toxicological impact on the environment and human beings.⁵⁹ Some other oxygenated PAHs or azaarenes are more polar, more water soluble, and can be considered having a higher impact on the toxicity.^{60, 61} More detailed information about the appearance and concentration of these compounds in the environment will help to:

- have a better assessment of the contaminated sites
- gain a deeper understanding of the chemical and biological transformation processes of the contaminants
- have an improved evaluation of remediation techniques for contaminated soils

A targeted analysis of PA(X)H other than the 16 EPA PAH in contaminated soils started only lately, since neither regulations nor standardized methods exist for these compounds. Earlier trials were through the transfer of the know-how from targeted analysis of the 16 EPA PAH to these compounds. This means for the identification and quantification of PA(X)H, mostly standard instrumentation, such as GC-FID, GC-EI-Q MS or HPLC-DAD, are utilized^{58, 60-68} However, the application of advanced mass spectrometric techniques, for instance tandem mass spectrometry and high resolution mass spectrometry (HRMS), have contributed to an improved detection, which reduces the probability of false positive assignments for the analytes of interest.^{21, 69, 70} Additionally, the development of new atmospheric pressure ionization (API) methods, such as atmospheric pressure photoionization (APPI) and atmospheric pressure laser ionization (APLI), has greatly increased the sensitivity towards PA(X)H.⁵⁹

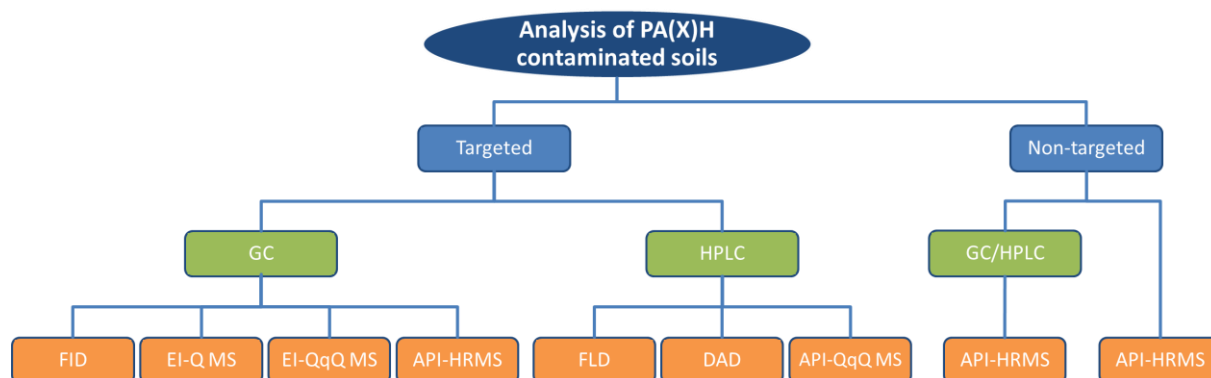


Figure 1-5. Analytical methods for the targeted and non-targeted analysis of PA(X)H in contaminated soils. Green: separation techniques; orange: detection methods.

1.1.4. Non-targeted analysis of soils contaminated with PA(X)H

While the number of published studies on the targeted analysis of PA(X)H in contaminated soils from industrial contaminated sites is limited as shown above, the number of studies using a non-targeted analysis is even fewer. This is due to the fact that a characterization of unknowns (contaminants) from a complex environmental matrix (soil) is an extremely challenging task. In order to minimize interference, to gain a broad overview and an accurate detection, state-of-the-art analytical instrumentation, including separation techniques and mass spectrometric analysis, are of essential importance here (Figure 1-5).⁷¹⁻⁷³

Here, the most powerful approach is Fourier transform (FT) MS.⁷⁴⁻⁷⁷ By its ultrahigh mass resolving power and accuracy signals of unknowns can be assigned unambiguously with the elemental composition of the corresponding analyte. However, even in this case, one analytical tool can usually not cover all analytes of interest, simply because of the extraordinary complexity of contaminated soil samples. A combination of different analytical techniques can offer a more comprehensive view of PA(X)H in contaminated soils.⁷⁷ This can help addressing contaminants and more important appraising the remediation efficiency for these contaminants on a non-targeted approach.^{74, 75}

1.2. Remediation techniques for PA(X)H contaminated soils

Industrial sites, such as manufactured gas plants, wood preserving and treatment sites, coking plants and petrochemical plants, are associated with PA(X)H contaminations.⁷⁸ Because of their environmental impact and potential risk to human beings, a range of remediation technologies, including physical, thermal, chemical, biological and integrated methods, are widely applied (Figure 1-6). Among them bioremediation is one of the most frequently implemented methods due to its inexpensive and easy handling characteristics as well as environmental friendliness. However, the duration of bioremediation processes usually is quite long.⁷⁴ Additionally, bioremediation alone is not suitable for “hot-spot” zones from industrial areas, where a concentration of the 16 EPA PAH exceeds 10,000 mg kg⁻¹,

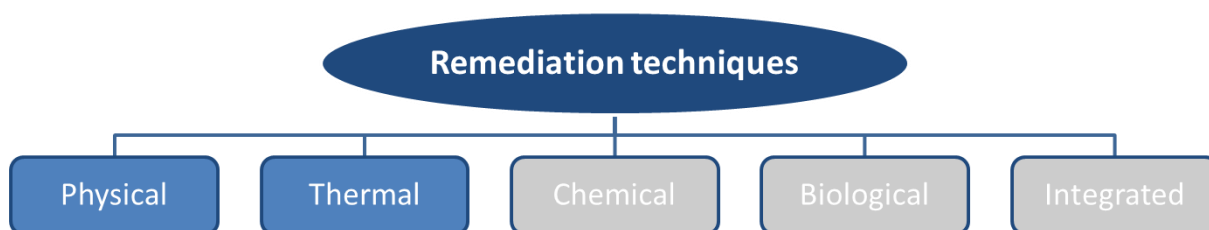


Figure 1-6. Different remediation techniques for PAXH contaminated soils. Methods in blue are investigated in this work.

since the growth of bacteria is inhibited by such a high PAH concentration.⁷⁹ Therefore, for these industrial “hot-spots” an integrated approach is commonly preferred, which means the application of more than one remediation technique, one after another, for instance: chemical + biological treatment,^{74, 75} physical + biological treatment, physical + chemical treatment,⁸⁰ or physical + chemical + biological treatment.⁸¹

During this study, effectivity of physical and thermal treatments has been investigated, by means of non-targeted analysis of a heavily contaminated soil before and after the corresponding treatment.

1.2.1. Physical treatments and the following PA(X)H analysis

Physical treatments involve density or particle size based separation and solvent extraction/soil washing. The advantages of physical techniques are:

- relatively fast and easy to implement
- suitable for large quantity of soils
- little change of the soil properties
- can be combined with other remediation techniques

Density or particle size based separations for PAH contaminated soils have been used in studies of Ghosh and co-workers.⁸²⁻⁸⁴ They were able to show, that most PAH were associated with the lighter fraction of contaminated sediment samples, especially with the coal tar pitch in this fraction. However, this assumption was based on the targeted analysis of the 16 EPA PAH using either GC-FID or GC-EI-Q MS. Richardson and Aitken utilized the same density separation method and could also determine a higher PAH concentration in the light fraction of a sample from a former manufactured gas plant. In addition, these PAH were less biodegradable than the PAH in the heavy fraction. For this conclusion only 13 from the 16 EPA PAH were quantitatively analyzed using HPLC-FLD.⁸⁵ It was not until recently, that a density separation using only water was applied for various industrial contaminated sites.⁵³ The targeted analysis of 16 EPA PAH for these contaminated soils and their fractions showed that the black particles involved in the light fraction were the main source of PAH. However, a detailed chemical characterization of these particles, which is referred to as coal tar pitches, is still missing.

Solvent extraction/washing appertains to one of the most commonly implemented remediation techniques for PAH contaminated soils.^{78, 80, 81} For the extraction two main parameters are

essential: The desorption kinetics and partitioning thermodynamics.⁸⁶ Typical solvents applied for the solvent extraction/washing are:

- water added with organic solvents or surfactants
- cyclodextrins
- supercritical fluids, such as supercritical carbon dioxide/water
- vegetable oils or fatty acid methyl esters (FAMES)

Vegetable oils, such as sunflower oil, rapeseed oil, or soybean oil, appear to be quite suitable as extraction solvent for PAH contaminated soils. This is mainly due to their cost-effective and non-toxic properties as well as their possibility to be regenerated and reused.⁸¹ Another benefit of using vegetable oils as extraction solvent is, that it is very convenient to combine with bioremediation, since such oils are biodegradable. However, the regeneration of large quantities of oils requires an additional treatment step, which causes higher remediation costs. On the other hand, the PAH are just transferred to the oil not really destroyed.⁸⁰ FAMES, in comparison to vegetable oils, can be produced from used cooking oils from the food industry, represent a more environmental friendly extraction solvent.⁵²

The assessment of remediation efficiency using different vegetable oils or FAMES was achieved through the quantification of the 16 EPA PAH using GC-FID, GC-EI-Q MS, HPLC-FLD or HPLC-DAD.^{52, 80} However, no detailed information is available yet, on how other PA(X)H respond to these methods. Here, results obtained from the non-targeted analysis might answer allow new conclusions.

1.2.2. Thermal treatments and the following PA(X)H analysis

During thermal treatments PA(X)H in contaminated soils are either volatilized or destroyed under elevated temperature. Depending on which thermal treatment technique is used, the temperature can range from 100-350 °C for low-temperature desorption, over 350-500 °C for pyrolysis, to 600-1200 °C for incineration.^{87, 88} Thermal treatments show an effective removal of PAH from highly contaminated soils.⁸⁹ The main drawbacks of thermal treatments are the destruction of the soil's fertility and a relatively high energy demand.⁹⁰

Recently, pyrolysis is gaining more attention as a reliable technique for the removal of PAH or hydrocarbons from contaminated soil, while keeping soil fertility high, due to the lower operation temperature.⁹⁰⁻⁹³ Here, temperature and operation duration are the parameters, which need to be optimized for the remediation. However, one important parameter, which can greatly influence the remediation efficiency, was neglected in previous studies. This is the

role of pressure during pyrolysis. Efforts have been made to evaluate the pyrolytic treatment using either chemical parameters, such as the concentrations of 16 EPA PAH or the content of total petroleum hydrocarbons (TPH), as well as biological parameters, such as plant growth. In this work, a detailed chemical investigation for the pyrolysis remediation on a non-targeted approach is provided.

1.3. Introduction to instrumentation

As shown in the chapter 1.2., the state-of-the-art approach for assessing remediation efficiency for PAH contaminated soils is still the quantitative analysis of 16 EPA PAH or TPH.^{52, 53, 80-85, 90-93} However, following questions remain unanswered:

- How complex are PAH contaminated soils from industrial sites?
- How do contaminants other than 16 EPA PAH behave under different remediation conditions?

Such questions can only be solved when the contaminated soil is analyzed in a non-targeted approach using Fourier transform (FT) based ultrahigh resolution mass spectrometers.⁷⁴⁻⁷⁷ These include FT-ion cyclotron resonance (ICR) and -Orbitrap mass spectrometers.^{94, 95} In combination with various API methods such instruments can lead to a more comprehensive view of what is really present in the contaminated sample and, ultimately to a deeper understanding of the mechanisms of different remediation processes.⁹⁶

1.3.1. Ionization techniques

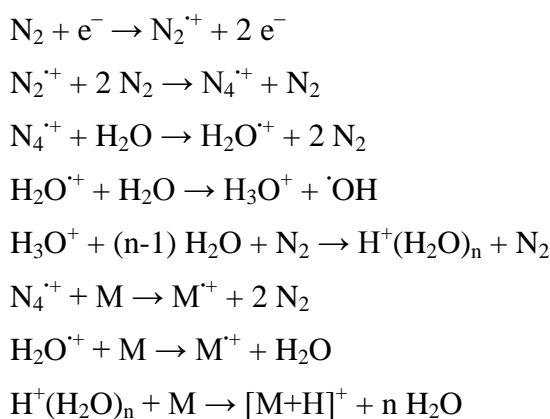
API are soft ionization techniques, which result little or no fragmentation of parent ions. These include electrospray ionization (ESI), atmospheric pressure chemical ionization (APCI), and atmospheric pressure photoionization (APPI). They found increasingly use for the non-targeted analysis of complex environmental samples.^{74-77, 97-102} Because of the sample complexity, a cross comparison of different API methods in both polarities can offer often comparable but more importantly also complementary data, which help characterize the entire sample.⁹⁶

ESI is probably the most versatile and frequently used API method. Different research areas, including proteomics, lipidomics, metabelomics, etc. find use of this ionization technique. During ESI, charged droplets are firstly released from the Taylor cone, which is formed at the tip of the sprayer as the result of increasing field strength. Two models describe the formation of gas-phase ions from the charged droplets. One is the charged-residue model, by which desolvated ions are what remains after the complete evaporation of solvent molecules from

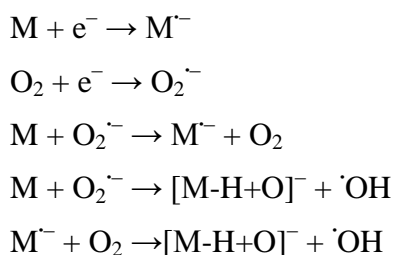
the droplet.¹⁰³ By the other model (ion evaporation model) it is assumed, that analyte ions directly evaporate from the surface of highly charged microdroplets.¹⁰⁴

ESI is a selective ionization method, which is predominantly suitable for polar to ionic analytes. By switching the polarity, analytes with different functional groups can be selectively ionized. For example, PANH containing a basic nitrogen atom, which is embedded in a six-membered aromatic ring, such as pyridine, are preferably ionized in positive mode ESI. In contrast to this, PANH with a neutral nitrogen atom, which is embedded in a five-membered aromatic ring, such as pyrrole, can be more easily deprotonated and therefore appear in negative mode ESI.^{105, 106} Thus, some valuable structural information of analytes can be gained already using ESI during the non-targeted analysis of contaminated soil samples. Additionally, analytes containing acidic functional groups, such as carboxylic acids, tend to lose one proton in negative mode ESI. Hence, oxygenated compounds produced by chemical or biological remediation processes can be determined well in negative mode ESI. This can lead to a better mechanistic understanding of degradation processes.^{74, 75}

APCI is the first API method, which replaced the radioactive ⁶³Ni with a corona discharge as source of ionization. In the positive mode and in the presence of nitrogen and water vapor, reactive species, such as N₄⁺, H₂O⁺ and H⁺(H₂O)_n, produced in the source chamber can further react with analyte molecules producing radical cations or protonated molecules (Scheme 1-1).¹⁰⁷⁻¹⁰⁹ In the negative mode, M⁻ can be directly formed through electron capture or through charge transfer from O₂⁻, which is produced primarily from traces of oxygen in the carrier gas (Scheme 1-2).¹¹⁰ Also, the formation of phenoxide ions especially for halogenated aromatic compounds can be observed.^{111, 112} In comparison to ESI, APCI can ionize more nonpolar compounds, such as pure hydrocarbons. This can provide a more comprehensive view of a soil contaminated with hydrocarbons including PAXH.

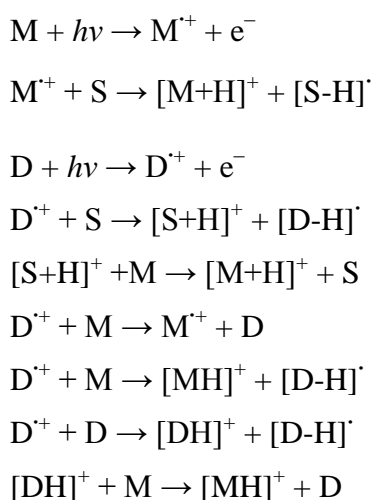


Scheme 1-1. Gas phase reactions leading to the formation of radical cations and protonated molecules of the analyte (M) by positive mode APCI.



Scheme 1-2. Gas phase reactions leading to the formation of radical anions and even-electron ions of analyte (M) by negative mode APCI.

APPI is a relatively new technique compared to ESI and APCI. It is also a soft ionization method, which was firstly introduced independently to the API family around the beginning of the 2000s by Syage and co-workers¹¹³ and Robb and co-workers.¹¹⁴ The light source for APPI can be a hydrogen discharge lamp, a krypton discharge lamp or a argon discharge lamp, which emit photons with an energy of 10.2 eV, 10.0 and 10.6 eV, or 11.2 eV, respectively.^{114, 115} During direct APPI, analytes are ionized by the vacuum ultraviolet light, by secondary ionization or through proton transfer. During dopant (D) assisted APPI, analytes ions are generated with the help of a UV-absorbing dopant (e.g. toluene) through charge exchange or proton transfer (Scheme 1-3).^{116, 117} The roll of a dopant, whose ionization energy lower than the photon energy provided from the lamp, is to increase the ionization efficiency analytes of interest. This can result in the formation of radical cations and protonated molecules of the analyte. APPI is similar to APCI and can ionize compounds with low polarity and nonpolar character. It has a high selectivity towards compounds containing double bonds or lone pairs, especially conjugated π systems, which makes it an useful tool for the non-targeted analysis of PAXH in contaminated soil.⁷⁷



Scheme 1-3. Gas phase reactions leading to the formation of radical cations and protonated molecules of the analyte (M) through positive mode normal APPI and dopant-assisted APPI (S: solvent, D: dopant).

1.3.2. Mass analyzers

Orbitrap analyzers are the newest members to the family of high-resolution mass analyzers and were invented by Makarov and co-workers at the end of last century.¹¹⁸ They are based on the physical principle of a Kingdon trap and quadrupole ion trap, and compete directly to FT-ICR in regard to mass resolution and accuracy.¹¹⁹

Figure 1-7 shows the schematic view of an Orbitrap Elite, a hybrid mass spectrometer from Thermo Fisher Scientific, as was used for this work. It consists of a Velos Pro linear quadrupole ion trap (LTQ) and a high-field Orbitrap mass spectrometer. The Orbitrap analyzer consists of a spindle-like central electrode that is held at a constant potential, and two mirrored bowl-shaped outer electrodes at ground potential. Ions injected through the C-trap are rotating around the central electrode (rotational frequency), while oscillating along the central electrode (z-axis), axial frequency, of the Orbitrap cell (Figure 1-7).

Ions in the cell are trapped neither in a magnetic field nor by radio frequency, but in an electrostatic field. The electric field is a combination of a logarithmic field of a cylindrical capacitor and a quadrupole field of a three-dimensional ion trap.¹¹⁸ Three frequencies can be determined in this electrostatic field: The frequency of radial oscillation, the rotational frequency and the axial frequency. Unlike the other two frequencies, the axial frequency is independent of the initial properties of the ions, such as their kinetic energy or spatial spread. This harmonic frequency (ω_z) is only dependent on the field curvature (k) and the inverse mass-to-charge ratio (Equation 1-1). It can be accurately determined for all present ions at the same time by detecting the induced image current as a function of time and subsequent fast FT.¹¹⁸

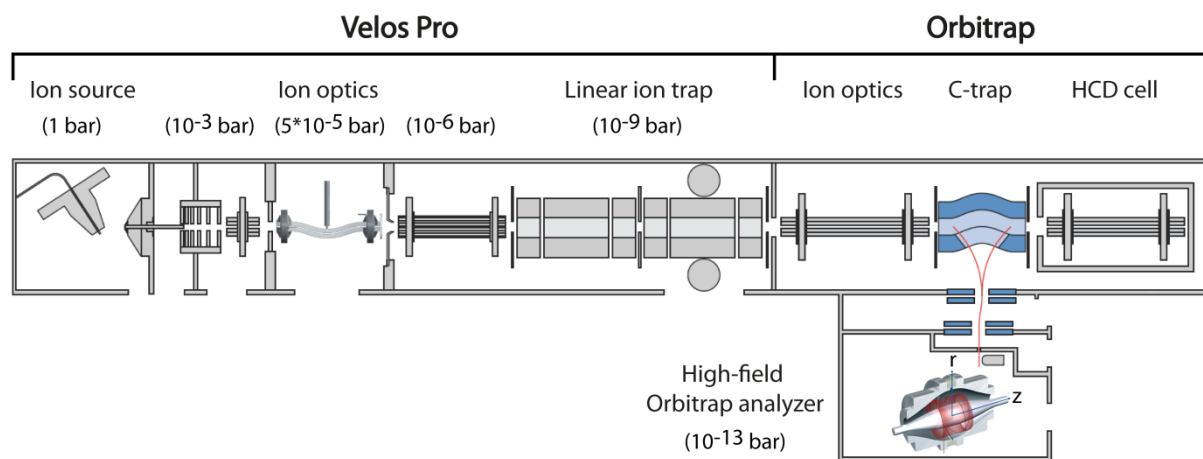


Figure 1-7. Schematic view of Thermo Fisher Scientific Orbitrap Elite, adapted from Scigelova and Makarov.¹²⁰

$$\omega_z = \sqrt{\frac{k}{m/z}} \quad (\text{Equation 1-1})$$

$$k = \sqrt{\frac{2Ur}{R_m^2 \ln\left(\frac{R_2}{R_1}\right) - \frac{1}{2}(R_2^2 - R_1^2)}} \quad (\text{Equation 1-2})$$

The mass resolution and accuracy of the Orbitrap mass analyzer have been improved over the years. This includes the development of a high-field trap and utilization of an improved signal processing by enhanced FT.

As can be seen in Equation 1-1, the frequency is a function of mass-to-charge ratio and the field curvature. The field curvature (k) is a function of the voltage applied to the central electrode and the scaling of the trap (Equation 1-2). With increasing frequency (ω_z) the maximum resolving power of the mass analyzer increases. The straightforward ways to improve the performance of an Orbitrap mass analyzer are therefore the increase of applied voltage or the down-scaling of the trap.¹²¹ The original Orbitrap mass analyzer had an inner electrode radius (R_1) of 6 mm and an outer electrode radius (R_2) of 15 mm (Figure 1-8). In the first version of a high-field mass analyzer the inner electrode radius was enlarged to 9 mm while keeping the outer electrode radius unchanged.¹²¹ At the same time the applied voltage was raised from 3.5 to 5.0 kV. This increases the frequency by a factor of 1.7. Another option was to scale down the whole mass analyzer. This was achieved in the second version high-field mass analyzer, which had a $R_1 = 5$ mm and $R_2 = 10$ mm, keeping the voltage at 3.5 kV. This leads to a 1.8-fold increase in frequency.¹²²

Another means to enhance resolving power is to use absorption rather than magnitude mode Fourier transform. Thus either the acquisition speed can be doubled with constant resolution or mass resolution can be doubled. In this case, enhanced FT is used, which combines the magnitude spectrum with the absorption spectrum. These two factors were weighted, so that for the top of a peak the absorption spectrum predominates, whereas at the base of the peak

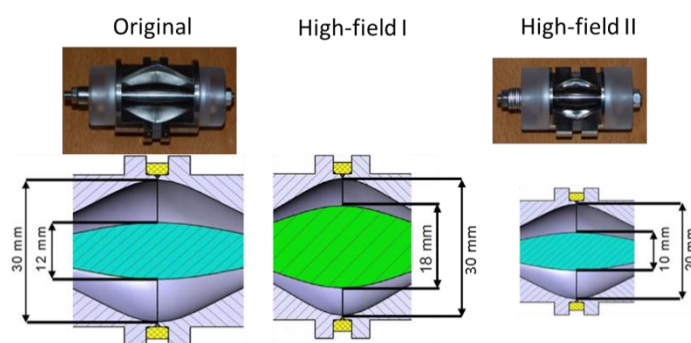


Figure 1-8. Original and high-field Orbitrap mass analyzers, adapted from Makarov et al..¹²¹⁻¹²³

the magnitude spectrum predominates.¹²⁴

Figure 1-9 compares the m/z dependent resolving power for the high-field Orbitrap mass analyzer in enhanced FT mode with a 7 T FT-ICR MS in magnitude mode. At m/z 400, the Orbitrap mass analyzer with an acquisition time of 1.5 s offers a mass resolving power greater of 480,000, which is higher than the resolving power provided from 7 T FT-ICR MS with an transient acquisition time of 3 s. While the resolving power is inversely proportional to the square root of the m/z for the Orbitrap mass analyzer (Equation 1-1), for the FT-ICR MS it is inversely proportional to the m/z . This means, that for Orbitrap mass analyzers the loss of resolving power at high m/z is less pronounced (Figure 1-9, comparing red solid line with red dashed line). By doubling the acquisition time from 1.5 s to 3 s, a resolving power of around 960,000 at m/z 400 can be achieved by Orbitrap, which is comparable to the resolving power provided from 7 T FT ICR MS with a 12 s transient. The better resolution at higher mass range and increased sensitivity of the Orbitrap MS make it a promising tool for analyzing complex environmental samples, such as soil. In addition, the relatively short acquisition time needed for a given resolution allows the coupling of Orbitrap to chromatographic separation techniques, such as GC,¹²⁵ HPLC¹²⁶ or ion mobility¹²⁷.

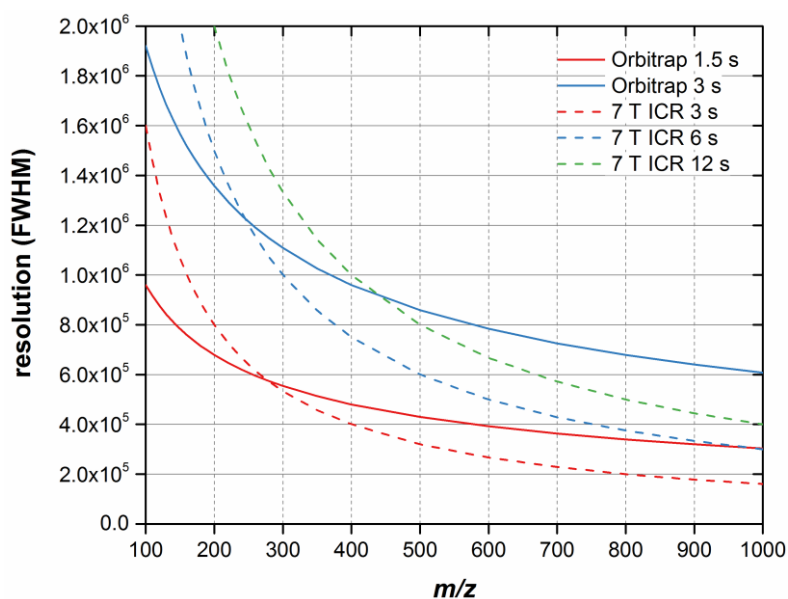


Figure 1-9. Resolving power dependency on m/z for the high-field Orbitrap mass analyzer with enhanced FT (solid lines), compared to the 7 T FT ICR MS in magnitude mode (dashed lines), adapted from Vetere and Schrader.⁹⁵

While FTMS with its resolving power and mass accuracy is a powerful analytical tool for the non-targeted analysis of complex environmental samples, the limited dynamic range of a trapping device leads to different problems. As analytes of interest are typically present in very different amounts, detecting them all can be a difficult task. This can be overcome by

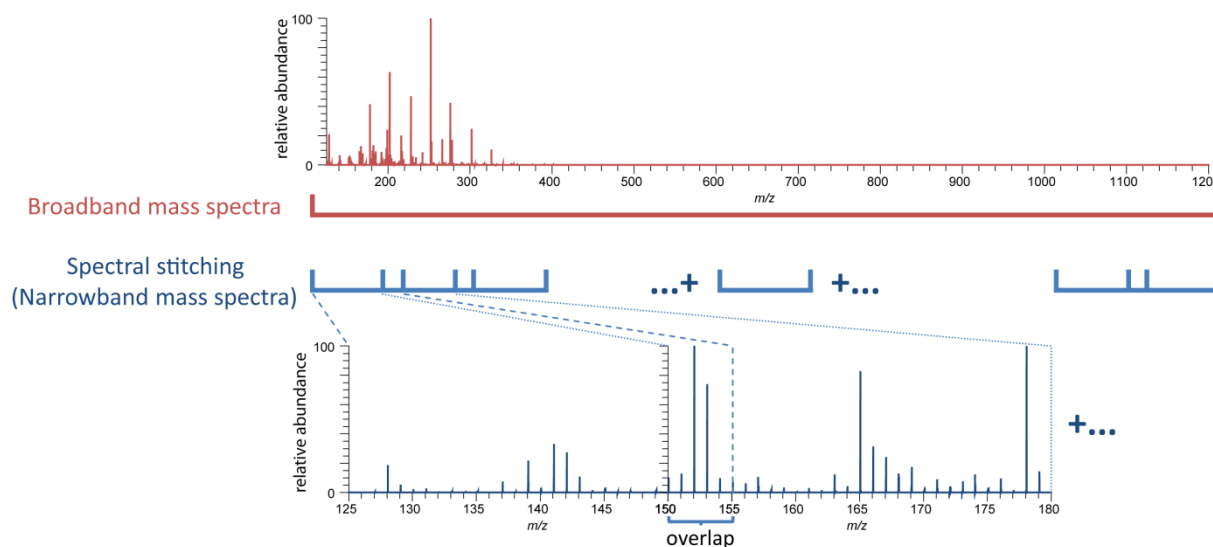


Figure 1-10. broadband (top) vs. spectral stitching (narrowband, bottom) measurement.

stitching the narrowband mass spectra together for the mass range of interest (Figure 1-10). Here, narrowband mass spectra with a 30 Da mass window are recorded. Segments of adjacent mass windows along the mass range are stitched together with an overlap of 5 Da which results a single recombined mass spectrum. By doing so, the dynamic range of the mass analyzer can be increased. At the same time, space-charge effects are reduced. These can in the end lead to a higher sensitivity and better mass accuracy.^{95, 128, 129}

1.4. Scope of the study

PAH are omnipresent in the environment. This is a result of complex geobiochemical processes as well as anthropogenic activities. Although the concentration of the selected 16 EPA PAH has been monitored for over 40 years, the non-targeted analysis of PAXH from industrial contaminated sites remains challenging. This is because of the complexity of soil matrices and the contamination source itself. The scope of this study is to develop analytical methods for the non-targeted characterization of PAXH in industrial contaminated soils. The application of the developed method for PAXH contaminated soils opens a comprehensive view of the contaminants. In the following, the remediation efficiency of conventional treatment techniques, including physical and thermal methods, are assessed on a non-targeted approach.

For this purpose, the extraction methods, which were developed and optimized for the extraction of the 16 EPA PAH from contaminated soils, need to be extended to the non-targeted analysis of petroleum hydrocarbon contaminated soils. In the Chapter 2, the extraction efficiency of conventional Soxhlet extraction and supercritical CO₂ extraction for

petroleum hydrocarbons is investigated. Different API methods were utilized in order to examine all compounds from different classes with different polarities.

In Chapter 3, a highly PAXH contaminated soil was subjected to a comprehensive analysis on a non-targeted approach. Here, FT Orbitrap MS in combination with multiple API methods (including ESI, APCI and APPI in positive and negative mode) showed its ability to characterize complex environmental samples. This is done by comparing the contaminated soil with a potting soil, as a non-contaminated reference sample, and a sand sample spiked with petroleum hydrocarbons.

After the characterization of this highly PAXH contaminated soil, it is further subjected to different remediation techniques, which include physical and thermal treatments. The remediation efficiency is then again assessed using a non-targeted approach.

Chapter 4 is focused on the physical pre-separation of the contaminated soil prior to other remediation techniques. During the optical examination for the contaminated soil, black solid aggregates (BSA), which differ from typical soil minerals, drew attention. One characteristic of these BSA is that they are lighter than other soil minerals. This makes them easy to be separated from soil using an aqueous system, which has a density lower than that of soil minerals but higher than that of BSA. Different approaches were tested for the separation. Afterwards, the BSA was characterized and compared to the original contaminated soil on a non-targeted approach.

In the Chapter 5 an environmental friendly and economically favorable approach for the removal of PAXH from the contaminated soil was investigated. Here, a mixture of methyl esters of waste cooking oil was used for the solvent extraction of PAXH. The efficiency of this method is examined using direct injection APPI FT Orbitrap MS and GC-APPI-FT Orbitrap MS is performed.

Pyrolysis is one of the thermal treatment techniques, which arises attention recently because of its relative low cost and possibility to maintenance soil fertility after treatment. In Chapter 6 the pyrolysis and the following analysis of highly PAXH contaminated soil under different temperature and pressure conditions are investigated. Also here, the contaminated soil before and after pyrolysis is analyzed using direct injection APPI FT Orbitrap MS and GC-APPI-FT Orbitrap MS.

Finally in Chapter 7 a summary of all results is presented.

1.5. References

1. Achten, C.; Andersson, J. T., Overview of Polycyclic Aromatic Compounds (PAC). *Polycycl. Aromat. Comp.* **2015**, *35*, (2-4), 177-186.
2. Stout, S. A.; Emsbo-Mattingly, S. D.; Douglas, G. S.; Uhler, A. D.; McCarthy, K. J., Beyond 16 Priority Pollutant PAHs: A Review of PACs used in Environmental Forensic Chemistry. *Polycycl. Aromat. Comp.* **2015**, *35*, (2-4), 285-315.
3. Gocht, T.; Barth, J. A. C.; Epp, M.; Jochmann, M.; Blessing, M.; Schmidt, T. C.; Grathwohl, P., Indications for pedogenic formation of perylene in a terrestrial soil profile: Depth distribution and first results from stable carbon isotope ratios. *Appl. Geochem.* **2007**, *22*, (12), 2652-2663.
4. Wang, Z.; Yang, C.; Parrott, J. L.; Frank, R. A.; Yang, Z.; Brown, C. E.; Hollebhone, B. P.; Landriault, M.; Fieldhouse, B.; Liu, Y.; Zhang, G.; Hewitt, L. M., Forensic source differentiation of petrogenic, pyrogenic, and biogenic hydrocarbons in Canadian oil sands environmental samples. *J. Hazard. Mater.* **2014**, *271*, 166-177.
5. Manzetti, S., Polycyclic Aromatic Hydrocarbons in the Environment: Environmental Fate and Transformation. *Polycycl. Aromat. Comp.* **2013**, *33*, (4), 311-330.
6. Zhang, Y.; Tao, S., Global atmospheric emission inventory of polycyclic aromatic hydrocarbons (PAHs) for 2004. *Atmos. Environ.* **2009**, *43*, (4), 812-819.
7. Keyte, I. J.; Harrison, R. M.; Lammel, G., Chemical reactivity and long-range transport potential of polycyclic aromatic hydrocarbons – a review. *Chem. Soc. Rev.* **2013**, *42*, (24), 9333-9391.
8. Dat, N.-D.; Chang, M. B., Review on characteristics of PAHs in atmosphere, anthropogenic sources and control technologies. *Sci. Total Environ.* **2017**, *609*, 682-693.
9. Lai, I. C.; Lee, C.-L.; Zeng, K.-Y.; Huang, H.-C., Seasonal variation of atmospheric polycyclic aromatic hydrocarbons along the Kaohsiung coast. *J. Environ. Manage.* **2011**, *92*, (8), 2029-2037.
10. Zhong, Y.; Zhu, L., Distribution, input pathway and soil–air exchange of polycyclic aromatic hydrocarbons in Banshan Industry Park, China. *Sci. Total Environ.* **2013**, *444*, 177-182.
11. Schwarzenbach, R. P.; Gschwend, P. M.; Imboden, D. M., *Environmental organic chemistry*. Third edition ed.; Wiley: Hoboken, New Jersey, 2017.
12. Nadarajah, N.; Van Hamme, J.; Pannu, J.; Singh, A.; Ward, O., Enhanced transformation of polycyclic aromatic hydrocarbons using a combined Fenton's reagent, microbial treatment and surfactants. *Appl. Microbiol. Biotechnol.* **2002**, *59*, (4-5), 540-544.
13. Qu, C.; Li, B.; Wu, H.; Wang, S.; Giesy, J. P., Multi-pathway assessment of human health risk posed by polycyclic aromatic hydrocarbons. *Environ Geochem Hlth* **2015**, *37*, (3), 587-601.
14. Varjani, S. J.; Gnansounou, E.; Pandey, A., Comprehensive review on toxicity of persistent organic pollutants from petroleum refinery waste and their degradation by microorganisms. *Chemosphere* **2017**, *188*, 280-291.
15. Moorthy, B.; Chu, C.; Carlin, D. J., Polycyclic Aromatic Hydrocarbons: From Metabolism to Lung Cancer. *Toxicol. Sci.* **2015**, *145*, (1), 5-15.
16. Keith, L.; Telliard, W., ES&T Special Report: Priority pollutants: I-a perspective view. *Environ. Sci. Technol.* **1979**, *13*, (4), 416-423.
17. Keith, L. H., The source of U.S. EPA's sixteen PAH priority pollutants. *Polycycl. Aromat. Comp.* **2015**, *35*, (2-4), 147-160.
18. Andersson, J. T.; Achten, C., Time to say goodbye to the 16 EPA PAHs? Toward an up-to-date use of PACs for environmental purposes. *Polycycl. Aromat. Comp.* **2015**, *35*, (2-4), 330-354.

19. Greim, H., Gesundheitsschädliche Arbeitsstoffe; Toxikologisch-arbeitsmedizinische Begründungen von MAK-Werten und Einstufungen.(534) Weinheim, DFG, Deutsche Forschungsgemeinschaft. In Wiley-VCH Verlag: 2008.
20. Blumer, M., Polycyclic Aromatic Compounds in Nature. *Sci.Am.* **1976**, 234, (3), 34-45.
21. Zeigler, C. D.; Robbat, A., Comprehensive Profiling of Coal Tar and Crude Oil to Obtain Mass Spectra and Retention Indices for Alkylated PAH Shows Why Current Methods Err. *Environ. Sci. Technol.* **2012**, 46, (7), 3935-3942.
22. Lopez-Avila, V., Sample preparation for environmental analysis. *Crit. Rev. Anal. Chem.* **1999**, 29, (3), 195-230.
23. U.S. EPA, SW-846 test methods for evaluating solid waste, Method 3540C: Soxhlet extraction. **1996**.
24. U.S. EPA, SW-846 Test Method 3561: Supercritical Fluid Extraction of Polynuclear Aromatic Hydrocarbons (PAHs). **1996**.
25. U.S. EPA, SW-846 Test Method 3550C: Ultrasonic Extraction. **2007**.
26. U.S. EPA, SW-846 Test Method 3546: Microwave Extraction. **2007**.
27. ISO 13859, Soil quality determination of polycyclic aromatic hydrocarbons (PAH) by gas chromatography (GC) and high performance liquid chromatography (HPLC). **2014**.
28. Song, Y. F.; Jing, X.; Fleischmann, S.; Wilke, B. M., Comparative study of extraction methods for the determination of PAHs from contaminated soils and sediments. *Chemosphere* **2002**, 48, (9), 993-1001.
29. Hollender, J.; Koch, B.; Lutermann, C.; Dott, W., Efficiency of different methods and solvents for the extraction of polycyclic aromatic hydrocarbons from soils. *Intern. J. Environ. Anal. Chem.* **2003**, 83, (1), 21-32.
30. Wang, W.; Meng, B.; Lu, X.; Liu, Y.; Tao, S., Extraction of polycyclic aromatic hydrocarbons and organochlorine pesticides from soils: A comparison between Soxhlet extraction, microwave-assisted extraction and accelerated solvent extraction techniques. *Anal. Chim. Acta* **2007**, 602, (2), 211-222.
31. Itoh, N.; Numata, M.; Aoyagi, Y.; Yarita, T., Comparison of low-level polycyclic aromatic hydrocarbons in sediment revealed by Soxhlet extraction, microwave-assisted extraction, and pressurized liquid extraction. *Anal. Chim. Acta* **2008**, 612, (1), 44-52.
32. Luque de Castro, M. D.; García-Ayuso, L. E., Soxhlet extraction of solid materials: an outdated technique with a promising innovative future. *Anal. Chim. Acta* **1998**, 369, (1), 1-10.
33. Szolar, O. H. J.; Rost, H.; Braun, R.; Loibner, A. P., Analysis of polycyclic aromatic hydrocarbons in soil: Minimizing sample pretreatment using automated Soxhlet with ethyl acetate as extraction solvent. *Anal. Chem.* **2002**, 74, (10), 2379-2385.
34. Chester, T. L.; Pinkston, J. D.; Raynie, D. E., Supercritical Fluid Chromatography and Extraction. *Anal. Chem.* **1996**, 68, (12), 487-514.
35. Hawthorne, S. B.; Miller, D. J., Extraction and recovery of polycyclic aromatic hydrocarbons from environmental solids using supercritical fluids. *Anal. Chem.* **1987**, 59, (13), 1705-1708.
36. Dankers, J.; Groenenboom, M.; Scholtis, L. H. A.; van der Heiden, C., High-speed supercritical fluid extraction method for routine measurement of polycyclic aromatic hydrocarbons in environmental soils with dichloromethane as a static modifier. *J. Chromatogr. A.* **1993**, 641, (2), 357-362.
37. Langenfeld, J. J.; Hawthorne, S. B.; Miller, D. J.; Pawliszyn, J., Effects of temperature and pressure on supercritical fluid extraction efficiencies of polycyclic aromatic hydrocarbons and polychlorinated biphenyls. *Anal. Chem.* **1993**, 65, (4), 338-344.

38. Lee, H.-B.; Peart, T. E.; Hong-You, R. L.; Gere, D. R., Supercritical carbon dioxide extraction of polycyclic aromatic hydrocarbons from sediments. *J. Chromatogr. A* **1993**, *653*, (1), 83-91.
39. Meyer, A.; Kleiböhmer, W., Supercritical fluid extraction of polycyclic aromatic hydrocarbons from a marine sediment and analyte collection via liquid—solid trapping. *J. Chromatogr. A* **1993**, *657*, (2), 327-335.
40. Hawthorne, S. B.; Miller, D. J., Direct comparison of Soxhlet and low- and high-temperature supercritical CO₂ extraction efficiencies of organics from environmental solids. *Anal. Chem.* **1994**, *66*, (22), 4005-4012.
41. Lopez-Avila, V.; Young, R.; Tehrani, J.; Damian, J.; Hawthorne, S.; Dankers, J.; van der Heiden, C., Mini-round-robin study of a supercritical fluid extraction method for polynuclear aromatic hydrocarbons in soils with dichloromethane as a static modifier. *J. Chromatogr. A* **1994**, *672*, (1), 167-175.
42. Barnabas, I. J.; Dean, J. R.; Tomlinson, W. R.; Owen, S. P., Experimental Design Approach for the Extraction of Polycyclic Aromatic Hydrocarbons from Soil Using Supercritical Carbon Dioxide. *Anal. Chem.* **1995**, *67*, (13), 2064-2069.
43. Dean, J. R.; Barnabas, I. J.; Fowlis, I. A., Extraction of polycyclic aromatic hydrocarbons from highly contaminated soils: a comparison between Soxhlet, microwave and supercritical fluid extraction techniques. *Anal. Proc.* **1995**, *32*, (8), 305-308.
44. Reimer, G.; Suarez, A., Comparison of supercritical fluid extraction and Soxhlet extraction for the analysis of native polycyclic aromatic hydrocarbons in soils. *J. Chromatogr. A* **1995**, *699*, (1), 253-263.
45. Saim, N. a.; Dean, J. R.; Abdullah, M. P.; Zakaria, Z., Extraction of polycyclic aromatic hydrocarbons from contaminated soil using Soxhlet extraction, pressurised and atmospheric microwave-assisted extraction, supercritical fluid extraction and accelerated solvent extraction. *J. Chromatogr. A* **1997**, *791*, (1), 361-366.
46. Berset, J. D.; Ejem, M.; Holzer, R.; Lischer, P., Comparison of different drying, extraction and detection techniques for the determination of priority polycyclic aromatic hydrocarbons in background contaminated soil samples. *Anal. Chim. Acta* **1999**, *383*, (3), 263-275.
47. Becnel, J. M.; Dooley, K. M., Supercritical fluid extraction of polycyclic aromatic hydrocarbon mixtures from contaminated soils. *Ind. Eng. Chem. Res.* **1998**, *37*, (2), 584-594.
48. Lopez-Avila, V.; Beckert, W. F., Supercritical Fluid Extraction in Environmental Analysis. In *Supercritical Fluid Technology*, American Chemical Society: 1992; Vol. 488, pp 179-205.
49. Wild, S. R.; Jones, K. C., Polynuclear aromatic hydrocarbons in the United Kingdom environment: A preliminary source inventory and budget. *Environ. Pollut.* **1995**, *88*, (1), 91-108.
50. Malawska, M.; Wiołkomirski, B., An analysis of soil and plant (*Taraxacum Officinale*) contamination with heavy metals and polycyclic aromatic hydrocarbons (PAHs) in the area of the railway junction Iława Główna, Poland. *Water Air Soil Poll.* **2001**, *127*, (1), 339-349.
51. Wilcke, W., Global patterns of polycyclic aromatic hydrocarbons (PAHs) in soil. *Geoderma* **2007**, *141*, (3), 157-166.
52. Gong, Z.; Wang, X.; Tu, Y.; Wu, J.; Sun, Y.; Li, P., Polycyclic aromatic hydrocarbon removal from contaminated soils using fatty acid methyl esters. *Chemosphere* **2010**, *79*, (2), 138-143.
53. Trellu, C.; Miltner, A.; Gallo, R.; Huguenot, D.; van Hullebusch, E. D.; Esposito, G.; Oturan, M. A.; Kästner, M., Characteristics of PAH tar oil contaminated soils—Black

- particles, resins and implications for treatment strategies. *J. Hazard. Mater.* **2017**, *327*, 206-215.
54. U.S. EPA, SW-846 Test Method 8100: Polynuclear Aromatic Hydrocarbons. **1986**.
55. Li, D.-X.; Gan, L.; Bronja, A.; Schmitz, O. J., Gas chromatography coupled to atmospheric pressure ionization mass spectrometry (GC-API-MS): Review. *Anal. Chim. Acta* **2015**, *891*, 43-61.
56. U.S. EPA, SW-846 Test Method 8270D: Semivolatile Organic Compounds by Gas Chromatography/Mass Spectrometry (GC/MS). **1998**.
57. U.S. EPA, SW-846 Test Method 8310: Polynuclear Aromatic Hydrocarbons. **1986**.
58. Bandowe, B. A. M.; Lueso, M. G.; Wilcke, W., Oxygenated polycyclic aromatic hydrocarbons and azaarenes in urban soils: A comparison of a tropical city (Bangkok) with two temperate cities (Bratislava and Gothenburg). *Chemosphere* **2014**, *107*, 407-414.
59. Richter-Brockmann, S.; Achten, C., Analysis and toxicity of 59 PAH in petrogenic and pyrogenic environmental samples including dibenzopyrenes, 7H-benzo[c]fluorene, 5-methylchrysene and 1-methylpyrene. *Chemosphere* **2018**, *200*, 495-503.
60. Lemieux, C. L.; Lambert, A. B.; Lundstedt, S.; Tysklind, M.; White, P. A., Mutagenic hazards of complex polycyclic aromatic hydrocarbon mixtures in contaminated soil. *Environ. Toxicol. Chem.* **2008**, *27*, (4), 978-990.
61. Lundstedt, S.; Bandowe, B. A. M.; Wilcke, W.; Boll, E.; Christensen, J. H.; Vila, J.; Grifoll, M.; Faure, P.; Biache, C.; Lorgeoux, C.; Larsson, M.; Frech Irgum, K.; Ivarsson, P.; Ricci, M., First intercomparison study on the analysis of oxygenated polycyclic aromatic hydrocarbons (oxy-PAHs) and nitrogen heterocyclic polycyclic aromatic compounds (N-PACs) in contaminated soil. *TrAC-Trend. Anal. Chem.* **2014**, *57*, 83-92.
62. Meyer, S.; Cartellieri, S.; Steinhart, H., Simultaneous Determination of PAHs, Hetero-PAHs (N, S, O), and Their Degradation Products in Creosote-Contaminated Soils. Method Development, Validation, and Application to Hazardous Waste Sites. *Anal. Chem.* **1999**, *71*, (18), 4023-4029.
63. Lundstedt, S.; Haglund, P.; Öberg, L., Degradation and formation of polycyclic aromatic compounds during bioslurry treatment of an aged gasworks soil. *Environ. Toxicol. Chem.* **2003**, *22*, (7), 1413-1420.
64. Lundstedt, S.; Haglund, P.; Öberg, L., Simultaneous Extraction and Fractionation of Polycyclic Aromatic Hydrocarbons and Their Oxygenated Derivatives in Soil Using Selective Pressurized Liquid Extraction. *Anal. Chem.* **2006**, *78*, (9), 2993-3000.
65. Biache, C.; Mansuy-Huault, L.; Faure, P.; Munier-Lamy, C.; Leyval, C., Effects of thermal desorption on the composition of two coking plant soils: Impact on solvent extractable organic compounds and metal bioavailability. *Environ. Pollut.* **2008**, *156*, (3), 671-677.
66. Bandowe, B. A. M.; Shukurov, N.; Kersten, M.; Wilcke, W., Polycyclic aromatic hydrocarbons (PAHs) and their oxygen-containing derivatives (OPAHs) in soils from the Angren industrial area, Uzbekistan. *Environ. Pollut.* **2010**, *158*, (9), 2888-2899.
67. Bandowe, B. A. M.; Wilcke, W., Analysis of polycyclic aromatic hydrocarbons and their oxygen-containing derivatives and metabolites in soils. *J. Environ. Qual.* **2010**, *39*, (4), 1349-1358.
68. Biache, C.; Ghislain, T.; Faure, P.; Mansuy-Huault, L., Low temperature oxidation of a coking plant soil organic matter and its major constituents: An experimental approach to simulate a long term evolution. *J. Hazard. Mater.* **2011**, *188*, (1), 221-230.
69. Avagyan, R.; Nyström, R.; Boman, C.; Westerholm, R., Determination of hydroxylated polycyclic aromatic hydrocarbons by HPLC-photoionization tandem

- mass spectrometry in wood smoke particles and soil samples. *Anal. Bioanal. Chem.* **2015**, *407*, (16), 4523-4534.
70. Arp, H. P. H.; Lundstedt, S.; Josefsson, S.; Cornelissen, G.; Enell, A.; Allard, A.-S.; Kleja, D. B., Native Oxy-PAHs, N-PACs, and PAHs in Historically Contaminated Soils from Sweden, Belgium, and France: Their Soil-Porewater Partitioning Behavior, Bioaccumulation in *Enchytraeus crypticus*, and Bioavailability. *Environ. Sci. Technol.* **2014**, *48*, (19), 11187-11195.
 71. Chibwe, L.; Davie-Martin, C. L.; Aitken, M. D.; Hoh, E.; Massey Simonich, S. L., Identification of polar transformation products and high molecular weight polycyclic aromatic hydrocarbons (PAHs) in contaminated soil following bioremediation. *Sci. Total Environ.* **2017**, *599*, 1099-1107.
 72. Manzano, C. A.; Marvin, C.; Muir, D.; Harner, T.; Martin, J.; Zhang, Y., Heterocyclic Aromatics in Petroleum Coke, Snow, Lake Sediments, and Air Samples from the Athabasca Oil Sands Region. *Environ. Sci. Technol.* **2017**, *51*, (10), 5445-5453.
 73. Tian, Z.; Vila, J.; Wang, H.; Bodnar, W.; Aitken, M. D., Diversity and Abundance of High-Molecular-Weight Azaarenes in PAH-Contaminated Environmental Samples. *Environ. Sci. Technol.* **2017**, *51*, (24), 14047-14054.
 74. Lu, M.; Zhang, Z.; Qiao, W.; Guan, Y.; Xiao, M.; Peng, C., Removal of residual contaminants in petroleum-contaminated soil by Fenton-like oxidation. *J. Hazard. Mater.* **2010**, *179*, (1-3), 604-611.
 75. Lu, M.; Zhang, Z.; Qiao, W.; Wei, X.; Guan, Y.; Ma, Q.; Guan, Y., Remediation of petroleum-contaminated soil after composting by sequential treatment with Fenton-like oxidation and biodegradation. *Bioresour. Technol.* **2010**, *101*, (7), 2106-2113.
 76. Noah, M.; Poetz, S.; Vieth-Hillebrand, A.; Wilkes, H., Detection of Residual Oil-Sand-Derived Organic Material in Developing Soils of Reclamation Sites by Ultra-High-Resolution Mass Spectrometry. *Environ. Sci. Technol.* **2015**, *49*, (11), 6466-6473.
 77. Thomas, M. J.; Collinge, E.; Witt, M.; Palacio Lozano, D. C.; Vane, C. H.; Moss-Hayes, V.; Barrow, M. P., Petroleum depth profiling of Staten Island salt marsh soil: 2 ω detection FTICR MS offers a new solution for the analysis of environmental contaminants. *Sci. Total Environ.* **2019**, *662*, 852-862.
 78. Kuppusamy, S.; Thavamani, P.; Venkateswarlu, K.; Lee, Y. B.; Naidu, R.; Megharaj, M., Remediation approaches for polycyclic aromatic hydrocarbons (PAHs) contaminated soils: Technological constraints, emerging trends and future directions. *Chemosphere* **2017**, *168*, 944-968.
 79. Khodadoust, A. P.; Bagchi, R.; Suidan, M. T.; Brenner, R. C.; Sellers, N. G., Removal of PAHs from highly contaminated soils found at prior manufactured gas operations. *J. Hazard. Mater.* **2000**, *80*, (1), 159-174.
 80. Yap, C. L.; Gan, S.; Ng, H. K., Application of vegetable oils in the treatment of polycyclic aromatic hydrocarbons-contaminated soils. *J. Hazard. Mater.* **2010**, *177*, (1), 28-41.
 81. Gan, S.; Lau, E. V.; Ng, H. K., Remediation of soils contaminated with polycyclic aromatic hydrocarbons (PAHs). *J. Hazard. Mater.* **2009**, *172*, (2), 532-549.
 82. Ghosh, U.; Gillette, J. S.; Luthy, R. G.; Zare, R. N., Microscale location, characterization, and association of polycyclic aromatic hydrocarbons on harbor sediment particles. *Environ. Sci. Technol.* **2000**, *34*, (9), 1729-1736.
 83. Ghosh, U.; Zimmerman, J. R.; Luthy, R. G., PCB and PAH speciation among particle types in contaminated harbor sediments and effects on PAH bioavailability. *Environ. Sci. Technol.* **2003**, *37*, (10), 2209-2217.

84. Khalil, M. F.; Ghosh, U.; Kreitinger, J. P., Role of weathered coal tar pitch in the partitioning of polycyclic aromatic hydrocarbons in manufactured gas plant site sediments. *Environ. Sci. Technol.* **2006**, *40*, (18), 5681-5687.
85. Richardson, S. D.; Aitken, M. D., Desorption and bioavailability of polycyclic aromatic hydrocarbons in contaminated soil subjected to long-term in situ biostimulation. *Environ. Toxicol. Chem.* **2011**, *30*, (12), 2674-2681.
86. Kubátová, A.; Jansen, B.; Vaudoisot, J.-F.; Hawthorne, S. B., Thermodynamic and kinetic models for the extraction of essential oil from savory and polycyclic aromatic hydrocarbons from soil with hot (subcritical) water and supercritical CO₂. *J. Chromatogr. A* **2002**, *975*, (1), 175-188.
87. Yi, Y. M.; Park, S.; Munster, C.; Kim, G.; Sung, K., Changes in Ecological Properties of Petroleum Oil-Contaminated Soil After Low-Temperature Thermal Desorption Treatment. *Water Air Soil Poll.* **2016**, *227*, (4), 108.
88. O'Brien, P. L.; DeSutter, T. M.; Casey, F. X. M.; Khan, E.; Wick, A. F., Thermal remediation alters soil properties – a review. *J. Environ. Manage.* **2018**, *206*, 826-835.
89. Vidonish, J. E.; Zygourakis, K.; Masiello, C. A.; Sabadell, G.; Alvarez, P. J. J., Thermal Treatment of Hydrocarbon-Impacted Soils: A Review of Technology Innovation for Sustainable Remediation. *Engineering* **2016**, *2*, (4), 426-437.
90. Vidonish, J. E.; Zygourakis, K.; Masiello, C. A.; Gao, X.; Mathieu, J.; Alvarez, P. J. J., Pyrolytic Treatment and Fertility Enhancement of Soils Contaminated with Heavy Hydrocarbons. *Environ. Sci. Technol.* **2016**, *50*, (5), 2498-2506.
91. Li, D.-C.; Xu, W.-F.; Mu, Y.; Yu, H.-Q.; Jiang, H.; Crittenden, J. C., Remediation of Petroleum-Contaminated Soil and Simultaneous Recovery of Oil by Fast Pyrolysis. *Environ. Sci. Technol.* **2018**, *52*, (9), 5330-5338.
92. Vidonish, J. E.; Alvarez, P. J. J.; Zygourakis, K., Pyrolytic Remediation of Oil-Contaminated Soils: Reaction Mechanisms, Soil Changes, and Implications for Treated Soil Fertility. *Ind. Eng. Chem. Res.* **2018**, *57*, (10), 3489-3500.
93. Song, W.; Vidonish, J. E.; Kamath, R.; Yu, P.; Chu, C.; Moorthy, B.; Gao, B.; Zygourakis, K.; Alvarez, P. J. J., Pilot-Scale Pyrolytic Remediation of Crude-Oil-Contaminated Soil in a Continuously-Fed Reactor: Treatment Intensity Trade-Offs. *Environ. Sci. Technol.* **2019**, *53*, (4), 2045-2053.
94. Panda, S. K.; Andersson, J. T.; Schrader, W., Characterization of Supercomplex Crude Oil Mixtures: What Is Really in There? *Angew. Chem. Int. Edit* **2009**, *48*, (10), 1788-1791.
95. Vetere, A.; Schrader, W., Mass Spectrometric Coverage of Complex Mixtures: Exploring the Carbon Space of Crude Oil. *ChemistrySelect* **2017**, *2*, (3), 849-853.
96. Gaspar, A.; Zellermann, E.; Lababidi, S.; Reece, J.; Schrader, W., Impact of Different Ionization Methods on the Molecular Assignments of Asphaltenes by FT-ICR Mass Spectrometry. *Anal. Chem.* **2012**, *84*, (12), 5257-5267.
97. Tfaily, M. M.; Chu, R. K.; Tolić, N.; Roscioli, K. M.; Anderton, C. R.; Paša-Tolić, L.; Robinson, E. W.; Hess, N. J., Advanced Solvent Based Methods for Molecular Characterization of Soil Organic Matter by High-Resolution Mass Spectrometry. *Anal. Chem.* **2015**, *87*, (10), 5206-5215.
98. Guigue, J.; Harir, M.; Mathieu, O.; Lucio, M.; Ranjard, L.; Lévêque, J.; Schmitt-Kopplin, P., Ultrahigh-resolution FT-ICR mass spectrometry for molecular characterisation of pressurised hot water-extractable organic matter in soils. *Biogeochemistry* **2016**, *128*, (3), 307-326.
99. Fleury, G.; Del Nero, M.; Barillon, R., Effect of mineral surface properties (alumina, kaolinite) on the sorptive fractionation mechanisms of soil fulvic acids: Molecular-scale ESI-MS studies. *Geochim. Cosmochim. Ac.* **2017**, *196*, 1-17.

100. Tfaily, M. M.; Chu, R. K.; Toyoda, J.; Tolic, N.; Robinson, E. W.; Pasa-Tolic, L.; Hess, N. J., Sequential extraction protocol for organic matter from soils and sediments using high resolution mass spectrometry. *Anal. Chim. Acta* **2017**, *972*, 54-61.
101. Headley, J. V.; Peru, K. M.; Barrow, M. P., Advances in mass spectrometric characterization of naphthenic acids fraction compounds in oil sands environmental samples and crude oil—A review. *Mass Spectrom. Rev.* **2016**, *35*, (2), 311-328.
102. Barrow, M. P.; Peru, K. M.; Headley, J. V., An Added Dimension: GC Atmospheric Pressure Chemical Ionization FTICR MS and the Athabasca Oil Sands. *Anal. Chem.* **2014**, *86*, (16), 8281-8288.
103. Mack, L. L.; Kralik, P.; Rheude, A.; Dole, M., Molecular Beams of Macroions. II. *J. Chem. Physics* **1970**, *52*, (10), 4977-4986.
104. Labowsky, M.; Fenn, J. B.; Fernandez de la Mora, J., A continuum model for ion evaporation from a drop: effect of curvature and charge on ion solvation energy. *Anal. Chim. Acta* **2000**, *406*, (1), 105-118.
105. Purcell, J.; Rodgers, R.; Hendrickson, C.; Marshall, A., Speciation of nitrogen containing aromatics by atmospheric pressure photoionization or electrospray ionization fourier transform ion cyclotron resonance mass spectrometry. *J Am Soc Mass Spectrom* **2007**, *18*, (7), 1265-1273.
106. Tong, J.; Liu, J.; Han, X.; Wang, S.; Jiang, X., Characterization of nitrogen-containing species in Huadian shale oil by electrospray ionization Fourier transform ion cyclotron resonance mass spectrometry. *Fuel* **2013**, *104*, (0), 365-371.
107. Horning, E. C.; Carroll, D. I.; Dzidic, I.; Haegele, K. D.; Horning, M. G.; Stillwell, R. N., Atmospheric Pressure Ionization (API) Mass Spectrometry. Solvent-Mediated Ionization of Samples Introduced in Solution and in a Liquid Chromatograph Effluent Stream. *J. Chromatogr. Sci.* **1974**, *12*, (11), 725-729.
108. Carroll, D. I.; Dzidic, I.; Stillwell, R. N.; Haegele, K. D.; Horning, E. C., Atmospheric pressure ionization mass spectrometry. Corona discharge ion source for use in a liquid chromatograph-mass spectrometer-computer analytical system. *Anal. Chem.* **1975**, *47*, (14), 2369-2373.
109. Dzidic, I.; Carroll, D. I.; Stillwell, R. N.; Horning, E. C., Comparison of positive ions formed in nickel-63 and corona discharge ion sources using nitrogen, argon, isobutane, ammonia and nitric oxide as reagents in atmospheric pressure ionization mass spectrometry. *Anal. Chem.* **1976**, *48*, (12), 1763-1768.
110. Horning, E. C.; Carroll, D. I.; Dzidic, I.; Lin, S. N.; Stillwell, R. N.; Thenot, J. P., Atmospheric pressure ionization mass spectrometry: Studies of negative ion formation for detection and quantification purposes. *J. Chromatogr. A.* **1977**, *142*, 481-495.
111. Dzidic, I.; Carroll, D. I.; Stillwell, R. N.; Horning, E. C., Atmospheric pressure ionization (API) mass spectrometry. Formation of phenoxide ions from chlorinated aromatic compounds. *Anal. Chem.* **1975**, *47*, (8), 1308-1312.
112. Mitchum, R. K.; Moler, G. F.; Korfmacher, W. A., Combined capillary gas chromatography/atmospheric pressure negative chemical ionization/mass spectrometry for the determination of 2,3,7,8-tetrachlorodibenzo-p-dioxin in tissue. *Anal. Chem.* **1980**, *52*, (14), 2278-2282.
113. Syage, J. A.; Evans, M. D., Photoionization Mass Spectrometry. *Spectroscopy* **2001**, *16*, (11), 14-21.
114. Robb, D. B.; Covey, T. R.; Bruins, A. P., Atmospheric Pressure Photoionization: An Ionization Method for Liquid Chromatography–Mass Spectrometry. *Anal. Chem.* **2000**, *72*, (15), 3653-3659.
115. Raffaelli, A.; Saba, A., Atmospheric pressure photoionization mass spectrometry. *Mass Spectrom. Rev.* **2003**, *22*, (5), 318-331.

116. Kauppila, T. J.; Kuuranne, T.; Meurer, E. C.; Eberlin, M. N.; Kotiaho, T.; Kostianen, R., Atmospheric Pressure Photoionization Mass Spectrometry. Ionization Mechanism and the Effect of Solvent on the Ionization of Naphthalenes. *Anal. Chem.* **2002**, *74*, (21), 5470-5479.
117. Kauppila, T. J.; Kersten, H.; Benter, T., The Ionization Mechanisms in Direct and Dopant-Assisted Atmospheric Pressure Photoionization and Atmospheric Pressure Laser Ionization. *J Am Soc Mass Spectrom* **2014**, *25*, (11), 1870-1881.
118. Makarov, A., Electrostatic Axially Harmonic Orbital Trapping: A High-Performance Technique of Mass Analysis. *Anal. Chem.* **2000**, *72*, (6), 1156-1162.
119. Maher, S.; Jjunju, F. P. M.; Taylor, S., 100 years of mass spectrometry: Perspectives and future trends. *Rev. Mod. Phys.* **2015**, *87*, (1), 113-135.
120. Scigelova, M.; Makarov, A., Orbitrap Mass Analyzer – Overview and Applications in Proteomics. *Proteomics* **2006**, *6*, (S2), 16-21.
121. Makarov, A.; Denisov, E.; Lange, O., Performance Evaluation of a High-field Orbitrap Mass Analyzer. *J Am Soc Mass Spectrom* **2009**, *20*, (8), 1391-1396.
122. Michalski, A.; Damoc, E.; Lange, O.; Denisov, E.; Nolting, D.; Müller, M.; Viner, R.; Schwartz, J.; Remes, P.; Belford, M.; Dunyach, J.-J.; Cox, J.; Horning, S.; Mann, M.; Makarov, A., Ultra High Resolution Linear Ion Trap Orbitrap Mass Spectrometer (Orbitrap Elite) Facilitates Top Down LC MS/MS and Versatile Peptide Fragmentation Modes. *Mol Cell Proteomics* **2012**, *11*, (3), O111.013698.
123. Zubarev, R. A.; Makarov, A., Orbitrap Mass Spectrometry. *Anal. Chem.* **2013**, *85*, (11), 5288-5296.
124. Lange, O.; Damoc, E.; Wiegand, A.; Makarov, A., Enhanced Fourier transform for Orbitrap mass spectrometry. *Int. J. Mass Spectrom.* **2014**, *369*, 16-22.
125. Kondyli, A.; Schrader, W., High-resolution GC/MS studies of a light crude oil fraction. *J. Mass Spectrom.* **2019**, *54*, (1), 47-54.
126. Molnárné Guricza, L.; Schrader, W., New Separation Approach for Asphaltene Investigation: Argentation Chromatography Coupled with Ultrahigh-Resolution Mass Spectrometry. *Energy Fuel* **2015**, *29*, (10), 6224-6230.
127. Vetere, A.; Schrader, W., 1- and 2-Photon Ionization for Online FAIMS-FTMS Coupling Allows New Insights into the Constitution of Crude Oils. *Anal. Chem.* **2015**, *87*, (17), 8874-8879.
128. Southam, A. D.; Payne, T. G.; Cooper, H. J.; Arvanitis, T. N.; Viant, M. R., Dynamic range and mass accuracy of wide-scan direct infusion nanoelectrospray Fourier transform ion cyclotron resonance mass spectrometry-based metabolomics increased by the spectral stitching method. *Anal. Chem.* **2007**, *79*, (12), 4595-4602.
129. Gaspar, A.; Schrader, W., Expanding the data depth for the analysis of complex crude oil samples by Fourier transform ion cyclotron resonance mass spectrometry using the spectral stitching method. *Rapid Commun. Mass Spectrom.* **2012**, *26*, (9), 1047-1052.

Chapter 2. Development of a Non-Targeted Method to Study Petroleum Polyaromatic Hydrocarbons in Soil by Ultrahigh Resolution Mass Spectrometry Using Multiple Ionization Methods

Redrafted from “Luo, R.; Schrader, W., Development of a Non-Targeted Method to Study Petroleum Polyaromatic Hydrocarbons in Soil by Ultrahigh Resolution Mass Spectrometry Using Multiple Ionization Methods. *Polycycl. Aromat. Comp.* **2020**, 1-16”

2.1. Abstract

A non-targeted method for analyzing petroleum hydrocarbons in soil was established by extracting a wide range of PAC compounds using a model system. Here, sand was spiked with a heavy crude oil, which simulated a hydrocarbons contaminated soil with low soil organic matter (SOM). Soxhlet and supercritical fluid extraction (SFE) was optimized for PAXHs analysis in soil. A concept of using multidimensional ionization for ultrahigh resolution mass spectrometry was employed for detection using electrospray ionization (ESI), atmospheric pressure chemical ionization (APCI) and atmospheric pressure photo ionization (APPI) for the analysis of polycyclic aromatic hydrocarbons (PAHs) and polycyclic aromatic heterocycles. Fourier transform mass spectrometry (FT MS) with its ultrahigh mass resolution and high mass accuracy enables an unambiguous assignment of the detected ions obtained from different ionization methods, which provides a secure and comprehensive view of contaminants in soil on a molecular level. Over 95% of the spiked crude oil could be recovered by Soxhlet extraction using toluene, dichloromethane and acetone:*n*-hexane (1:1, *v*:*v*). In comparison, when using SFE with supercritical CO₂ the recovery was only about 50 % but showed more polar compounds. Detailed analyses showed that besides 16 PAHs, a wide range with more than 10,000 PAXHs could also be successfully extracted.

2.2. Introduction

Polycyclic aromatic hydrocarbons (PAHs) originated from petrogenic, pyrogenic or biogenic sources are omnipresent contaminants in soils.¹ Alone in Europe over half a million contamination sites have been identified as results of hundred years of industrialization. Annual clean-up cost ranging from 2 to 17 billion were estimated for these contamination sites.² Among others, PAHs produced from coking and manufactured gas plants are of great concern because of their carcinogenic, mutagenic and ecotoxicological effects.³

PAHs in soil are mostly analyzed in a targeted approach, where only 16 PAHs were selected, which belong to the priority pollutant list from the U.S. Environmental Protection Agency (EPA), and monitored for over four decades.⁴ Concerns have been arisen for an extension of this list of PAHs, since high-molecular-weight PAHs, alkylated derivatives (alkyl-PAHs) and polycyclic aromatic heterocycles containing N, S or O (PAXH, X = N, S, O), which co-occur with those 16 PAHs as contaminants and might have higher toxicity, are not included.⁵

Recently targeted analyses of selected alkyl-PAHs and PAXHs have been reported using a combination of gas chromatography and mass spectrometry (GC-MS).⁶⁻⁸ Inductively coupled plasma mass spectrometry (ICP-MS) is another powerful tool for the quantification of priority compounds or emerging contaminants, such as sulfur compounds in crude oil.^{9, 10} In addition, a non-targeted approach for PAH contaminated soils was enabled by coupling time-of-flight mass spectrometry (ToF MS) with high performance liquid chromatography (HPLC) or two-dimensional gas chromatography (GC x GC).¹¹⁻¹³ However, GC related techniques are restricted to volatile and semi-volatile compounds. Furthermore, using HPLC-ToF MS both the separation and mass resolving power could be challenged as the sample complexity and molecular weight of analytes increases.

Fourier transform ion cyclotron resonance (FT-ICR) and Orbitrap mass spectrometry with their ultrahigh mass resolution and mass accuracy ensure an unambiguous assignment of each detected signal in complex mixtures such as crude oil, bio oils, tar oils or lignin derivatives.¹⁴⁻²⁰ A combination of various atmospheric pressure ionization (API) methods, such as electrospray ionization (ESI), atmospheric pressure chemical and photo ionization (APCI/APPI), enables a comprehensive view of the sample.²¹ Negative mode ESI coupled to FT MS opens the possibility for detailed characterization of acidic compounds especially oxygenated classes. This combination is already applied for the analysis of naphthenic acids from environmental samples²²⁻²⁴, natural organic matter (NOM)²⁵⁻²⁸, oil-sand-derived organic material²⁹ and soil organic matters (SOM)³⁰⁻³². In contrast to these, basic compounds for

instance pyridine-containing molecules are favored under positive mode ESI.³³ Both APCI and APPI are suitable for ionizing nonpolar compounds especially PAXHs, which provide complementary data to the ESI measurements for the same sample.^{21, 34}

In the environmental analysis sample preparation especially extraction is the crucial step.³⁵ Around the beginning of this century various extraction methods such as Soxhlet extraction,³⁶ mechanic shaking,³⁷ ultrasonic extraction,³⁸ accelerated solvent extraction³⁹ or supercritical fluid extraction (SFE),⁴⁰ for extracting PAHs from soil were investigated and compared.⁴¹⁻⁴⁴ Despite the long extraction duration and large solvent consumption, the conventional Soxhlet extraction with its continuous and inexpensive character still serves as a standard method for PAHs extraction.⁴⁵ Its extraction efficiency was usually compared with other newer techniques. Among them SFE using inert, reusable CO₂ with/without addition of few organic solvents as modifier offers a more environmental friendly way of extracting contaminants in soil.⁴⁶⁻⁴⁸

Analyzing different chemical compounds in a matrix such as soil is not easy. Different parameters play a role, such as how the compounds can be fully removed from the soil for a whole determination and characterization. This is followed by answers to the question which analytical method gives the best information. And doing this for an extremely complex analyte mixture such as tar oils makes matters worse. In this study, we perform a non-target analysis of a spiked sand sample with heavy crude oil, which simulates a soil sample contaminated with petroleum hydrocarbons and low SOM to better understand and optimize the extraction procedures and ionization conditions. FT Orbitrap MS coupled with Different API methods including ESI, APCI and APPI in both polarities were applied in order to gain a panorama of the contaminants in the sample. Afterwards the extraction efficiency of Soxhlet extraction with different solvents for petroleum hydrocarbons in this model sample was investigated. Finally SFE using CO₂ was compared to Soxhlet extraction in detail on a molecular level.

2.3. Material and Methods

2.3.1. Model sample

Pure sand (50-70 mesh, Sigma-Aldrich, Germany) was spiked with a heavy crude oil (5%, w/w), which was firstly diluted in dichloromethane. Afterwards the remaining dichloromethane was rotary-evaporated the spiked sand sample.

2.3.2. Sample preparation

The Soxhlet extractions were performed using 5.00 g of spiked sand and additionally 5.00 g of anhydrous sodium sulfate (99.5%, Acros Organics) with 100 mL of toluene (Tol), dichloromethane (DCM), acetone:*n*-hexane (1:1, *v*:*v*, AceHex) or methanol (MeOH) at the boiling point of the solvents for around 300 cycles. All solvents used were HPLC-grade and purchased from Sigma-Aldrich (Germany) or Acros Organics (Germany). The extracts were concentrated in a rotary evaporator and dried under gentle argon stream.

The SFE experiments were performed using a lab-built SFE system (detailed description see Figure A2-1). 5.00 g of spiked sand were added into a stainless steel column and heated to 40 °C. Then samples were extracted at 180 bar and 40 °C with supercritical CO₂ (99.995%, Air Liquide, Germany) at a flow rate of 2 mL min⁻¹ for 4 h. The SFE extracts were rotary-evaporated and dried under gentle argon stream. The SFE residues were Soxhlet extracted using dichloromethane with the procedure described above.

2.3.3. Mass spectrometric and data analysis

Mass analysis was performed on a research type linear quadrupole ion-trap (LTQ) FT Orbitrap MS (Thermo Fisher, Bremen, Germany) with LTQ Tune Plus 2.7.0 data processing system (Thermo Fisher, Bremen, Germany). The mass spectra were collected from 200 to 1200 Da using the spectral stitching method with 30 Da mass windows with 5 Da overlap.^{15, 49, 50} Additionally positive/negative mode ESI or positive mode APCI/APPI with a mass resolution of 960,000 at *m/z* 400 was applied. For ESI measurements samples were diluted to 250 µg mL⁻¹ in toluene:methanol (1:1, *v*:*v*), and injected at a flow rate of 5 µL min⁻¹ with a spray voltage of 4/-3.5 kV for the positive/negative mode. Sheath, auxiliary and sweep gases were set to 5, 2 and 1 arbitrary unit for both polarities. Samples for APCI or APPI were diluted to 250 µg mL⁻¹ in toluene and ionized under the following conditions: flow rate = 20 µL min⁻¹, vaporizer temperature = 350 °C, sheath gas = 20 arbitrary unit, auxiliary gas = 5 and sweep gas = 2. The corona discharge for the APCI was set to 5 µA and a Krypton VUV lamp (10.0 and 10.6 eV, Syagen, Tustin, CA, U.S.A.) was used for the APPI.

Data were exported into Composer64 v1.5.3. (Sierra Analytics, Modesto, CA, U.S.A.) and processed with the following chemical constraints: 0 < C < 200, 0 < H < 1000, 0 < N < 4, 0 < S < 5, 0 < O < 11, 0 < double bond equivalent (DBE) < 100. A maximum mass error of 1 ppm was accepted and only classes with a relative abundance higher than 1% were compared and discussed.

The DBE value for a given elemental composition $C_cH_hN_nS_sO_o$ was calculated with the following equation: $DBE = c - h/2 + n/2 + 1$

2.4. Results and Discussion

2.4.1. Recovery of crude oil in spiked sand

A non-targeted analysis of petroleum hydrocarbons in soil is an adventure due to the high complexity of compounds present in such a sophisticated system. As one of the most important sample preparation steps, the extraction of petroleum based contaminants from soil should be firstly investigated in detail.

Therefore, pure sand spiked with a heavy crude oil was served as a model sample for a better understanding of the extraction step. Here, we compared the traditional Soxhlet extraction using different solvents with supercritical CO_2 extraction. Toluene, dichloromethane and a 1:1 (v:v) mixture of acetone and *n*-hexane are commonly used solvents for the Soxhlet extraction of 16 EPA PAHs in soils on a routine scale.^{36, 41-44, 51}

Using these three solvent systems a recovery of over 95% for crude oil in the spiked sand was carried out (Figure 2-1), where dichloromethane with $97\% \pm 1\%$ recovery delivered the highest extraction efficiency. Methanol was applied as a mild extraction solvent to study the solubility in polar solvents and therefore, the bioavailability of hydrocarbons in soil.⁵² Here, a lower recovery of $73\% \pm 4\%$ compared to other Soxhlet extraction solvents was obtained. This implies the complex character of the heavy crude oil.

When using supercritical CO_2 extraction $47\% \pm 1\%$ of petroleum components were extracted.

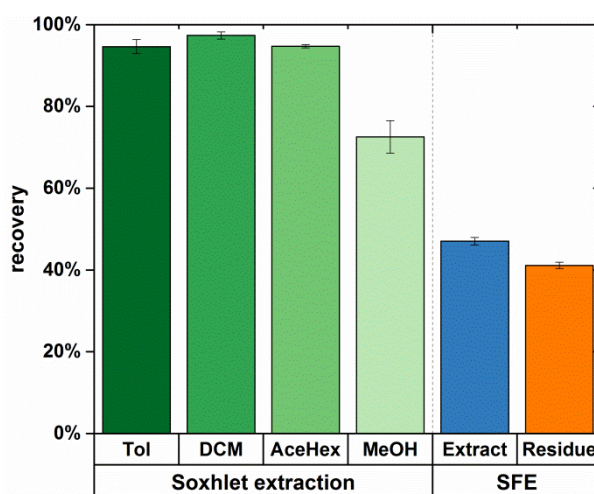


Figure 2-1. Recovery of heavy crude oil in the spiked sand using Soxhlet extraction (in green) with toluene (Tol), dichloromethane (DCM), acetone:*n*-hexane (1:1, v:v) (AceHex), methanol (MeOH) and supercritical CO_2 extraction (extract in blue, residue in brown).

Reports in the literature showed a wide range of results for the extraction using SFE. A good recovery of over 80% was reported for lighter jet-diesel oil and fuel oil from spiked sand after the SFE at 65 °C and 400 bar.⁴⁶ However, Hawthorne and Miller showed that at a comparable extraction temperature of 50 °C and accelerated pressure of 405 bar, lower extraction efficiency was found for higher molecular weight and heteroatom containing PAHs.⁴⁷ This explained the lower extraction efficiency gained in our study, thus the heavy crude oil contained to a proper portion high molecular weight and heteroatom such containing PAXHs.

Although SFE is more environmental friendly and time saving, it cannot extract all contaminants from the soil, especially compounds with higher molecular weight. In contrast to that, the traditionally Soxhlet extraction with dichloromethane offers a simple and feasible way to extract petroleum hydrocarbons from the soil for the non-targeted analysis, albeit the large volume and long extraction time needed.

2.4.2. Mass spectra

Because of the sample complexity, the selectivity of different ionization methods and polarities can be used to provide a comprehensive view of the sample.²¹ This is presented in the recombined mass spectra, which was recorded using spectral stitching method,^{15, 49, 50} for the original crude oil (Figure 2-2, left column). For all ionization methods applied ions were detected throughout the whole mass range starting from 200 to 1200 Da. In the zoomed in mass spectra between m/z 400.00 and 400.50 (Figure 2-2, right column) up to 42 elemental compositions were detected, which was depended on the selected ionization method. Compounds containing basic nitrogen dominated in the ESI(+) spectrum. Acidic oxygenated

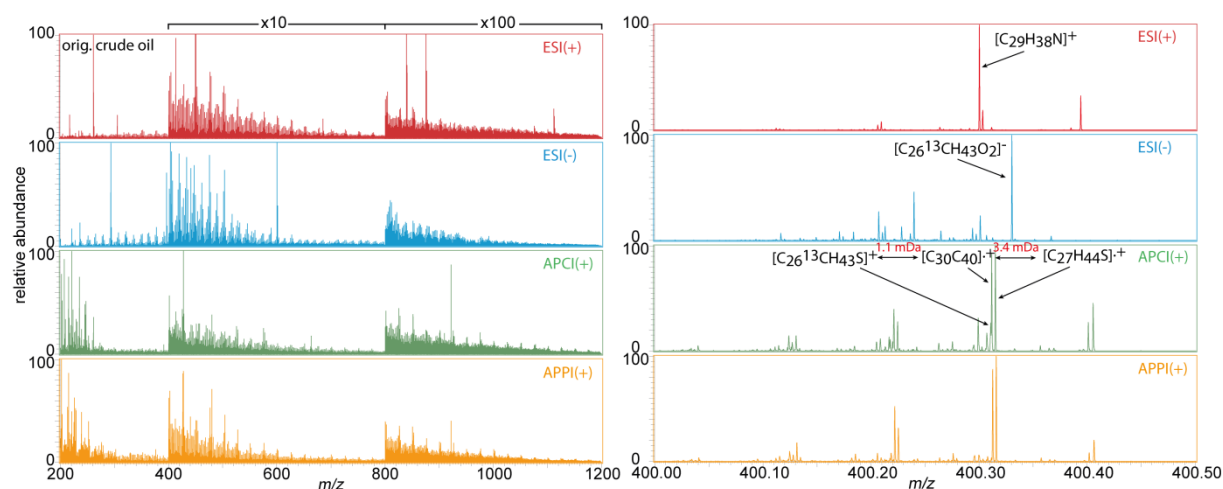


Figure 2-2. Recombined (left column) and zoomed in mass spectra at m/z 400 (right column) for the original crude oil sample, analyzed by FT Orbitrap MS using positive mode ESI (red), negative mode ESI (blue), positive mode APCI (green) and APPI (orange), respectively.

classes and neutral nitrogen containing components are well ionizable in ESI(-).

Nonpolar classes such as pure hydrocarbons and sulfur containing PAHs appear in both APCI and APPI measurements. In order to resolve isobaric peaks of $C_{26}^{13}CH_{43}S^+$ (m/z 400.31135) and $C_{30}H_{40}^+$ (m/z 400.31245) with a $\Delta m = 0.00110$ Da, a resolving power higher than 400,000 is needed. The result shows the necessity of combining different ionization methods with ultrahigh resolution MS for a non-targeted analysis of complex petroleum hydrocarbons.

In Figure 2-3, the zoomed in positive mode APPI mass spectra between m/z 400.00 and 400.50 for the original crude oil, Soxhlet extract of the spiked sand using dichloromethane, SFE extract and residue of the spiked sand were compared. In total 42 elemental compositions were found at this mass range for the original crude oil (Table A2-1). Here, radical cations of pure hydrocarbons and PASHs dominated in the mass spectra. $C_{30}H_{40}$ and $C_{27}H_{44}S$ with a double bond equivalent (DBE) of 11 and 6 were the first and second highest signal detected in mass spectra for the original crude oil, Soxhlet and SFE extracts. By decreasing m/z value the DBE value of isobaric pure hydrocarbon ions ($C_{29}H_{52}^+$, $C_{30}H_{40}^+$, $C_{31}H_{28}^+$, $C_{32}H_{16}^+$, highlighted in red from right to left in Figure 2-3), which have a $\Delta m = 0.09390$ Da between each other, increases from 4 to 25. The extraction efficiency of SFE decreases the higher the aromaticity is. As can be seen in the spectra, $C_{29}H_{52}^+$ (DBE = 4) and $C_{30}H_{40}^+$ (DBE = 11) were to a great degree extracted using SFE, while $C_{31}H_{28}^+$ and $C_{32}H_{16}^+$ with a DBE of 18 and

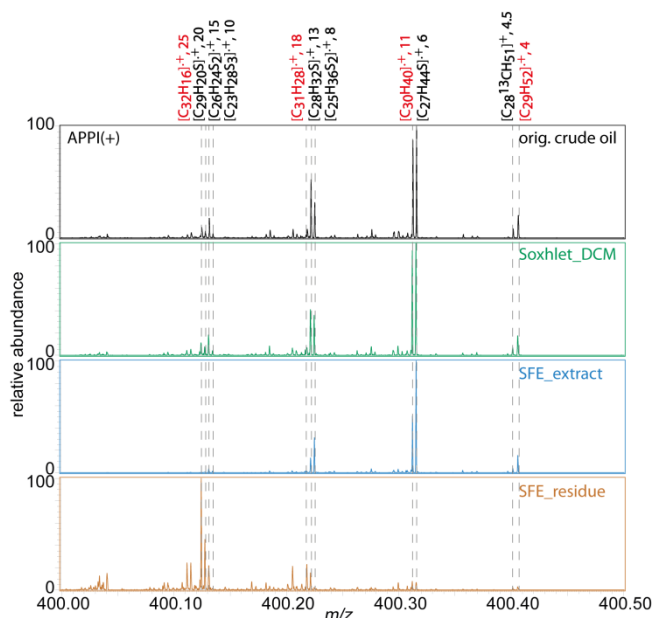


Figure 2-3. Zoomed in mass spectra at m/z 400 for the original crude oil (black), Soxhlet extract using dichloromethane (green), SFE extract (blue) and SFE residue (brown) using positive mode APPI FT Orbitrap MS. Some signals are highlighted with calculated elemental compositions and double bond equivalent (DBE) values, separated with a comma.

25 remained mainly in the residue. This is also applicable for S class compositions shown in Figure 2-3.

Furthermore, positive and negative mode ESI mass spectra for the original crude oil, the extract and residue after SFE reveal that basic and acidic crude oil related contaminants could also be extracted from the spiked sand (Figures AFigure A2-2 to AFigure A2-4). Compounds with lower DBE were preferentially extracted than compounds with higher DBE. Using API-FT MS a detailed comparison between Soxhlet and SFE on a molecular level can be fulfilled.

2.4.3. Class distribution

Due to the high data load obtained from the non-targeted analysis using ultrahigh resolution FT MS, a suitable, concise and explicit data interpretation is obligatory. This can be done by sorting each signal from the mass spectrum into elemental compositions, which then can be categorized into classes according to their counts of heteroatoms. Different classes such as pure hydrocarbon or heteroatom (N, S, and O) containing classes from different ionization techniques or samples can be compared in a bar chart with their corresponding relative abundances or numbers of assigned compositions.

In Figure 2-4 a summary of intensity based class distributions for the Soxhlet extract using

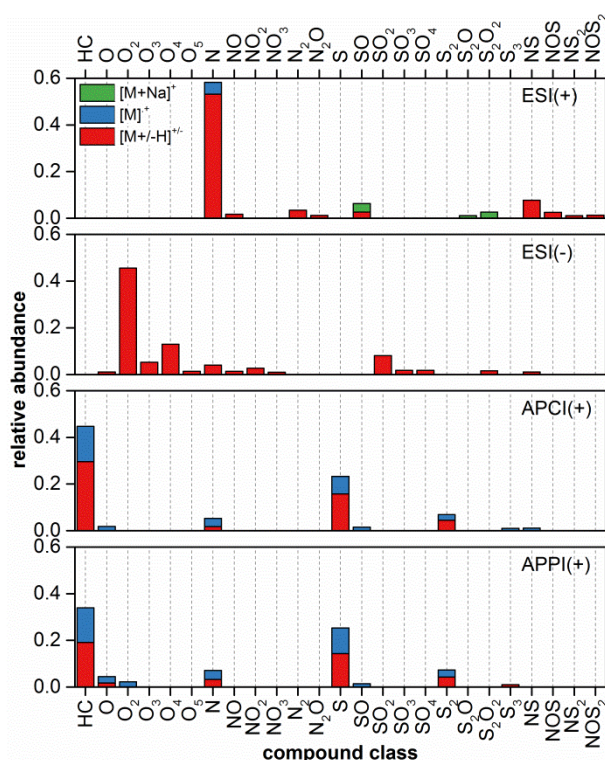


Figure 2-4. Intensity based class distributions for the Soxhlet extracted sample using dichloromethane, analyzed by positive/negative mode ESI, positive mode APCI/APPI (top to bottom) FT Orbitrap MS with protonated/deprotonated molecules in red, radical cations in blue and molecules with sodium adduct in green.

dichloromethane is shown. Protonated basic nitrogen containing classes such as N, N₂, NS and NS₂ dominate the ESI(+) spectrum with few compounds form radical ions as well as oxygenated sulfur containing class ionized with sodium adduct. In ESI(-) the mass spectrum consists of mainly oxygenated classes especially O₂ and O₄, which can correspond to molecules contain one or two carboxylic acids.⁵³ Other oxidized heteroatom containing classes such as NO_x and SO_x were also present with a lower intensity. The selective ionization of acidic components in the sample makes it a perfect method for examining polar transformation products, which are created during the chemical/biological oxidation of PAHs contaminated soil.⁵⁴⁻⁵⁶

Both APCI and APPI form radical cations [M]⁺ and protonated molecules [M+H]⁺ of predominantly nonpolar pure hydrocarbons (HC), S_x and N classes. In particular APPI by exciting the double bonds in a molecule which suits the best for the targeted and non-targeted analyses of pure PAHs and PAXHs (X = S, N, O).^{21, 57} Results show how complex such a system, which is simulating a petroleum hydrocarbon contaminated soil, can be. Additionally, when analyzing petroleum hydrocarbons in soil in a non-targeted way, ion suppression and discrimination effects can occur.⁵⁸ This consolidates the need of multidimensional ionization techniques for the deep and comprehensive analysis of petroleum hydrocarbon contaminated soils.

For the targeted analysis, only the 16 EPA PAHs are of interest. But by using positive mode APPI FT MS other high molecular weight and heteroatom containing PAHs present as contaminants can be efficiently ionized and analyzed as well.²¹ For the original crude oil the highest number of assigned compositions was detected by APPI(+) (25,943), followed by APCI(+) (22,802), ESI(+) (15,264) and finally ESI(-) (12,221) (Figure 2-5 to Figure 2-7). Results confirmed the nonpolar character of the spiked contamination source. For a comparison the extraction efficiency of Soxhlet extraction using different solvents and SFE is summarized in left column of Figure 2-5. Here, both the relative abundance and the number of assigned compositions for each detected class were considered.

Among these 25,943 assigned compositions by APPI(+) around 4000 were detected as either protonated or radical hydrocarbons in the mass spectrum, which display a relative intensity of around 35%. With an increase in polarity from toluene to methanol, the number of assigned compositions in the HC class decreases from 4082 to 3629. For the polycyclic aromatic heterocycles, such as compounds in S, S₂ and N classes, over 95% of the assigned compositions from the original crude oil could be found in the Soxhlet extracts using toluene,

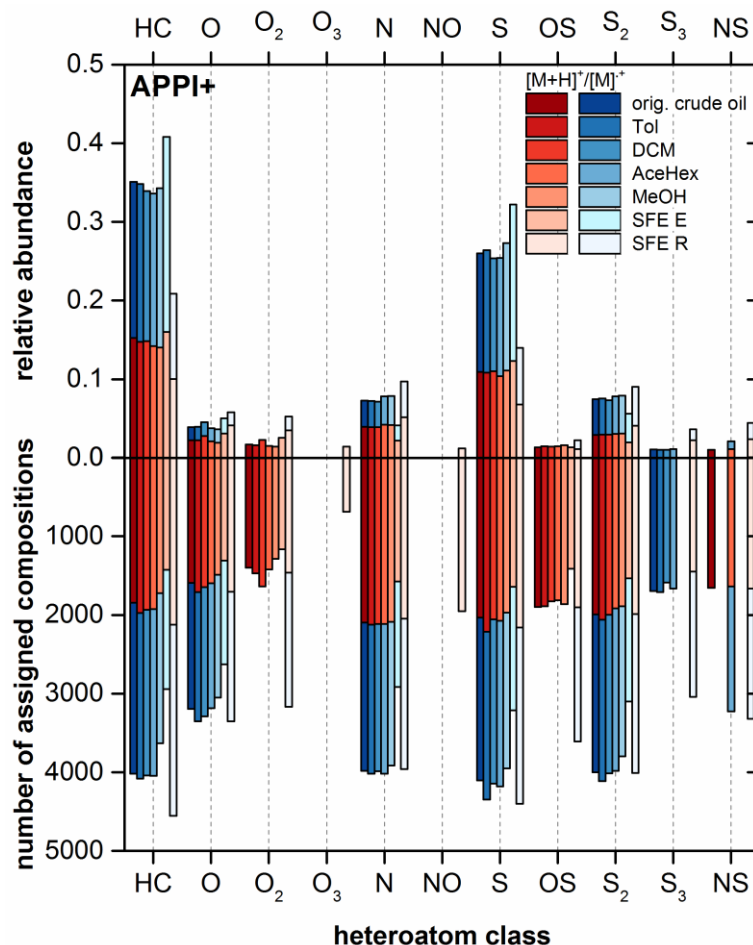


Figure 2-5. Intensity (top) and population (bottom) based class distributions for the original crude oil, spiked sand Soxhlet extracted using Tol, DCM, AceHex or MeOH and its SFE extract (SFE E) and residue (SFE R), analyzed by positive mode APPI FT Orbitrap MS. Protonated molecules and radical cations are denoted in red and blue, respectively.

dichloromethane and acetone/*n*-hexane solvent mixture. For methanol as extraction solvent a recovery of over 90% of the assigned compositions was observed.

In comparison, less than 67% (17367 out of 25943 compositions from the original crude oil) were present in the SFE extract, which consisted of predominantly pure hydrocarbons (41%), followed by S (32%), S₂ (6%), O (5%) and N (4%) classes. As a result of extraction, the relative intensities of HC and S classes found in the SFE residue decreased dramatically to 21% and 14%, respectively.

However, the numbers of assigned compositions between the original crude oil and SFE residue did not differ too much, which indicates lower extraction efficiency for the complex sample when SFE was applied. The slightly higher amount of HC class compounds and new classes found in the SFE residue could be explained, as there was discrimination and ion suppression occurred during ionization for the original crude oil.⁵⁸ Additionally, SFE separated the sample into two fractions which led to an increasing analysis depth.⁵⁹ Similar

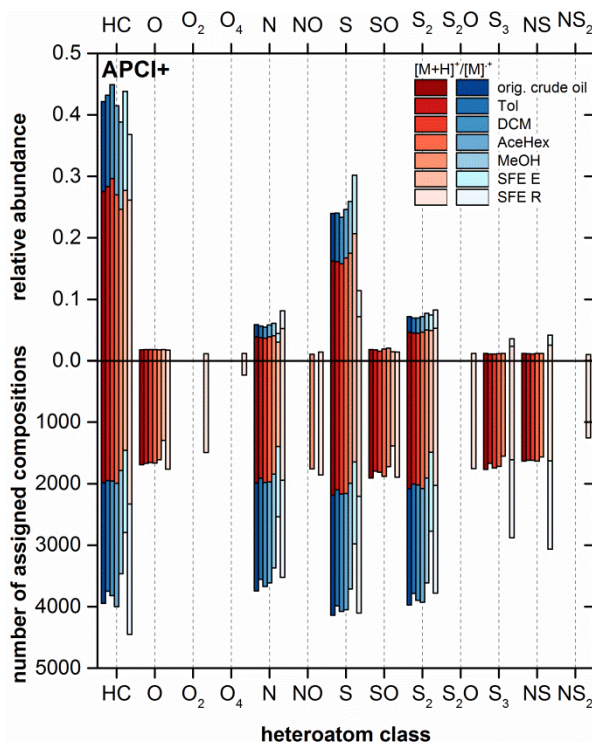


Figure 2-6. Intensity (top) and population (bottom) based class distributions for the original crude oil, spiked sand Soxhlet extracted using Tol, DCM, AceHex or MeOH and its SFE extract (SFE E) and residue (SFE R), analyzed by positive mode APCI FT Orbitrap MS.

results were observed by APCI(+) studies (see Figure 2-6). There, compositions from pure hydrocarbon and heteroatom containing classes such as S, S₂ and N could be extracted well by Soxhlet extraction using toluene, dichloromethane and acetone/*n*-hexane solvent mixture. Only a portion ($\approx 70\%$) of the compositions in the above mentioned classes could be extracted using SFE.

Results from APPI(+) and APCI(+) were mutually supportive and implied a better extraction efficiency for nonpolar compounds by Soxhlet extraction using toluene, dichloromethane and acetone/*n*-hexane solvent mixture than SFE. In ESI(+) the N class with the highest intensity of 60% in the original crude oil consists of mainly basic pyridine-like azaarenes (see Figure 2-7, left).¹³ Out of 2701 assigned compositions as either protonated or radical cations for the N class in original crude oil 1951, 2002, 1569 and 2259 compositions were recovered using toluene, dichloromethane and acetone/*n*-hexane solvent mixture and methanol, respectively. For the second and third highest intensity classes in the original crude oil, namely NS and N₂, same trend was observed. As the most polar solvent investigated methanol could extract over 80% of the assigned compositions for these two classes, whereas for other solvent systems the recovery was between 60% and 70%. The appearance of [SO+Na]⁺ class with relative high intensity for the Soxhlet extracts was probably as a result of sodium salt

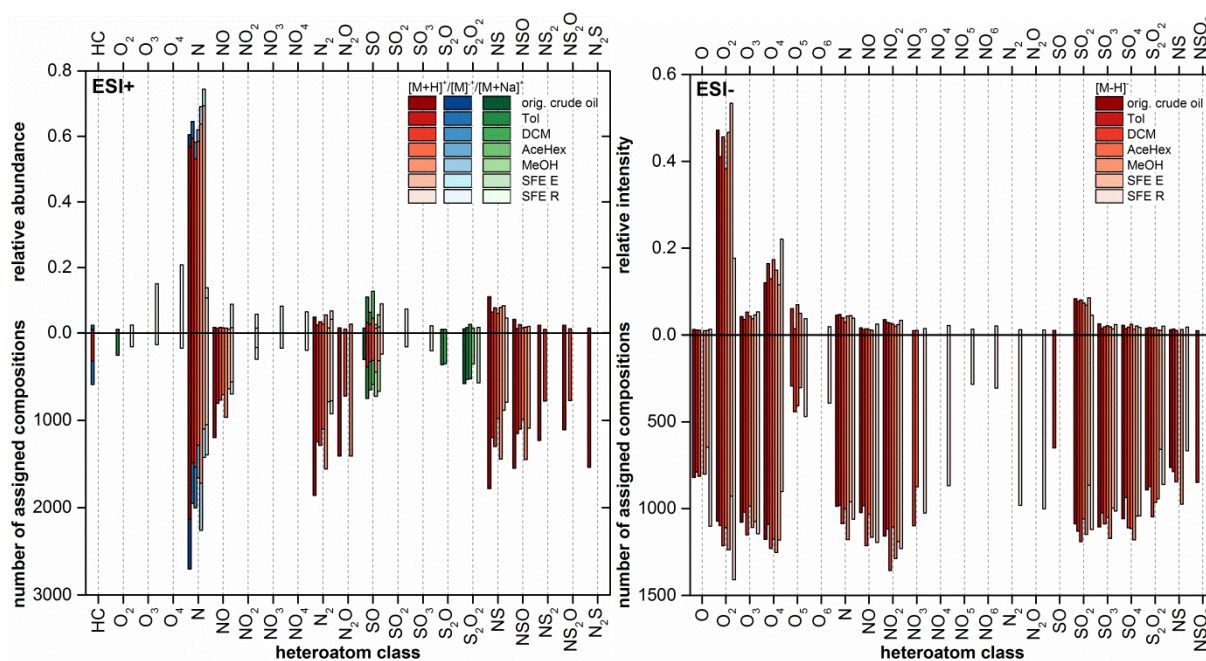


Figure 2-7. Intensity (top) and population (bottom) based class distributions for the original crude oil, spiked sand Soxhlet extracted using Tol, DCM, AceHex or MeOH and its SFE extract (SFE E) and residue (SFE R), analyzed by positive (left) and negative (right) mode-ESI FT Orbitrap MS. Protonated molecules and radical cations are denoted in red and blue, respectively.

added for the removal of water.⁶⁰ Compared to the Soxhlet extraction also a good extraction of polar N class compounds from the spiked sand was achieved when supercritical CO₂ was used. Here, a decrease of relative abundance from 74% (SFE E) to 14% (SFE R) was observed.

Compared to ESI(+) with 15,264 assignments, in ESI(-) 12,221 compositions were detected for the original crude oil, which comprise polar compounds containing acidic functional groups (Figure 2-7, right). Unlike in the positive mode the assigned compositions in ESI(-) were distributed to O₂₋₄, N₀₋₂ and S₂₋₄ quite equally. A comparable high recovery was achieved by Soxhlet extraction using dichloromethane and methanol. In comparison to this, SFE could only partially extract polar compositions in each class.

These findings obtained from each ionization method showed, Soxhlet extraction is an easy and efficient method, which can be applied prior to the non-targeted analysis of crude oil related contaminants in soil and gives the best representation of the sample.

2.4.4. DBE distribution

The absolute intensity within a given DBE was plotted against compound classes for the APPI(+) measurement of the samples (Figure 2-8). The radical cation and protonated molecule classes are denoted as M and M[H], respectively.

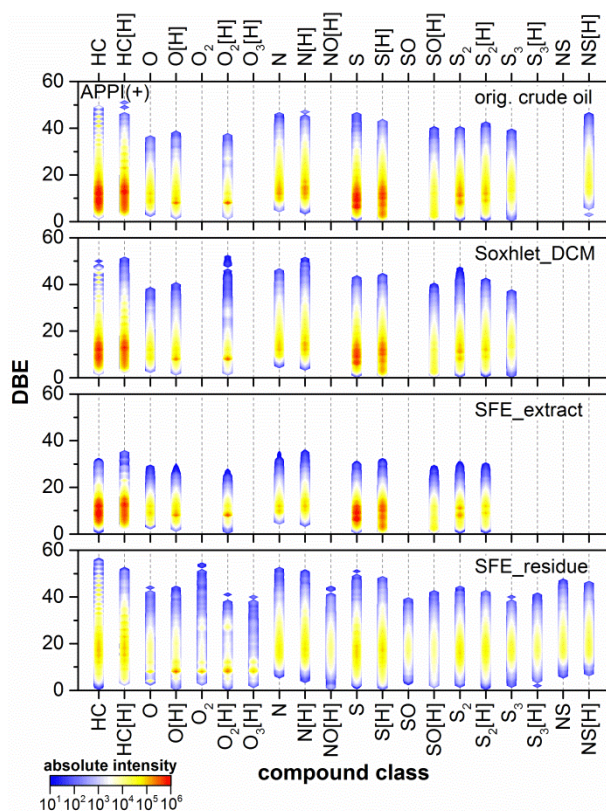


Figure 2-8. Intensity based DBE vs. class distributions for the original crude oil, Soxhlet extract using DCM, SFE extract and residue (from top to bottom) using positive mode APPI FT Orbitrap MS (radical cations: M, protonated molecules: M[H]).

A DBE range of 1 to 50 was observed for the pure hydrocarbon and heteroatom containing classes, such as S_{1-3} and N, found in the original crude oil, Soxhlet extract and SFE residue. However, in the SFE extract compounds with DBE only up to 37 were detected. Considering a benzene ring has a DBE value of 4 and by adding another aromatic ring into the system to form naphthalene, anthracene and so on, the DBE increases by 3 every time with up to 12 aromatic rings. Similar results were observed using APCI(+) as shown in Figure A2-5. Since predominant compounds with lower DBE could be extracted using SFE, this reduces the sample complexity and increases the intensity of compounds with lower abundance (Figure 2-5),⁵⁹ which explains the additional classes found in the SFE residue.

As summarized in Table 2-1, the mean m/z value for the SFE extract was shifted to the lower mass range compared to the original crude oil sample. Besides, the DBE value decreased from 19 to 15 while H/C increased from 1.23 to 1.38. Accordingly for the SFE residue the mean DBE value increased to 20 while H/C decreased to 1.17. These indicate that SFE favors low aromatized hydrocarbons, which is in agreement with previous studies.⁴⁰

Table 2-1. Calculated mean values of m/z , DBE, number of carbon atoms and X/C for the samples, analyzed using APPI(+) FT Orbitrap MS.

samples	mean values						
	m/z	DBE	#C	H/C	N/C	O/C	S/C
orig. crude oil	703	19	50	1.23	0.005	0.008	0.019
Soxhlet_DCM	700	19	50	1.23	0.004	0.008	0.019
SFE_extract	677	15	48	1.38	0.004	0.010	0.016
SFE_residue	703	20	50	1.17	0.006	0.012	0.019

Moreover, polar compounds such as basic pyridine-like or neutral pyrrole-like nitrogen containing compounds and oxygenated classes, analyzed using ESI(+/-), could also be extracted with a maximum DBE of 35 (Figure A2-6 and 2-7).

2.4.5. DBE vs. carbon count/intensity plot

A closer look into the radical HC class on a molecular level is shown in left column of Figure 2-9 using the so-called Kendrick plot.¹⁴ Here, each detected composition was visualized by its DBE value and number of carbon atoms per molecule. In addition, the total monoisotopic abundance as a sum of all compositions within one given DBE was displayed in line.

2107 and 1515 out of in total 2173 radical cations found in the original crude oil could be fully or partially extracted using Soxhlet or SFE, respectively. For the original crude oil, Soxhlet and SFE extracts pure hydrocarbons with DBE of 12 exhibited the highest intensity, which correspond to PAHs containing 4 rings, such as pyrene or fluoranthene with different length of side chains. Instead, in the SFE residue the maximum intensity of DBE shifted to 15, indicating PAHs involving 5 aromatic rings, such as benzo[*a*]anthracene, benzo[*b*]fluoranthene or benzo[*k*]fluoranthene, were dominant in the mass spectrum. Furthermore, the maximum intensity at DBE 15 in the SFE residue (10^5) was reduced by one order of magnitude compared to the value in the extract (10^6).

The PASHs in the original crude oil, Soxhlet and SFE extracts showed a maximum intensity at DBE of 9, which correspond to mostly dibenzothiophene and its alkylated derivatives (Figure A2-8, left column).⁶¹ However, in the SFE residue compounds with DBE = 19 gained the highest intensity. Also for PANHs a shift of the maximum intensity from DBE = 12 to DBE = 17 was observed after SFE (Figure A2-8, right column). Overall the results from APPI(+) measurements showed that SFE as compared to Soxhlet extracts only contains

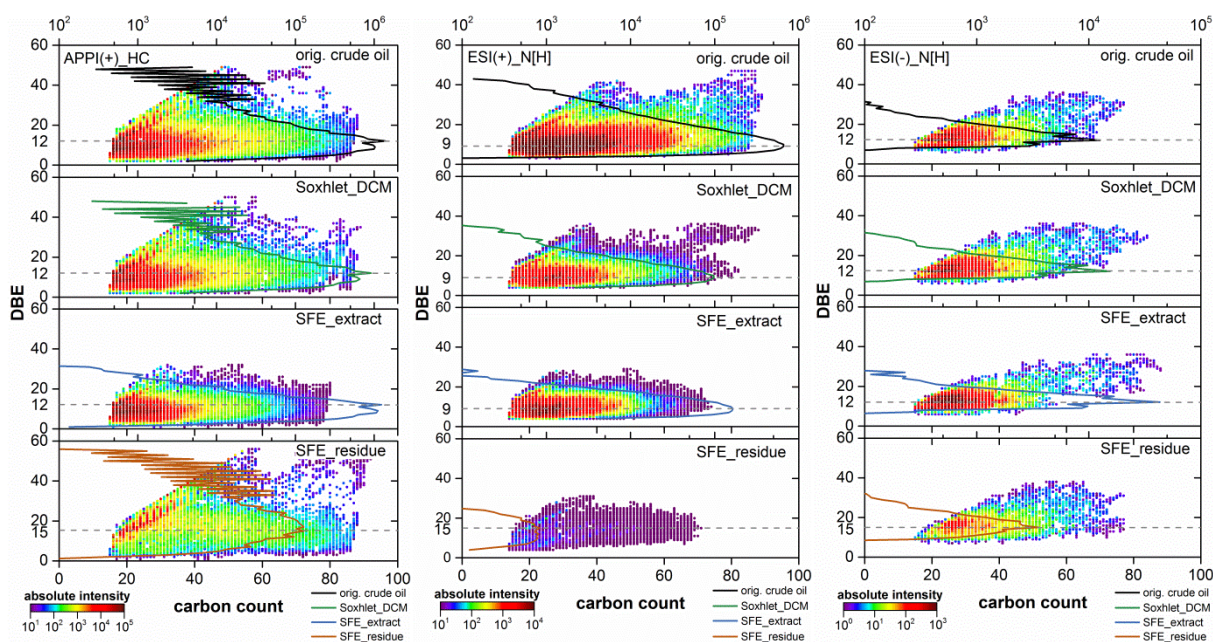


Figure 2-9. DBE vs. carbon count/intensity (Kendrick) plots for the radical HC (left column), [N+H]⁺ (middle column) and [N-H]⁻ (right column) classes in the original crude oil, Soxhlet extract using DCM, SFE extract and residue (from top to bottom) using positive mode APPI or positive/negative mode ESI FT Orbitrap MS. Upper abscissa for the absolute intensity in a given DBE and lower abscissa for the number of carbon atoms in a assigned composition.

nonpolar PAHs and PAXHs with DBE below 35 and carbon number below 90.

As an example for ESI(+) measurements, basic nitrogen containing compounds are shown in the middle column of Figure 2-9. From 2134 polar pyridine-like compounds 1538 and 1101 could be extracted using Soxhlet and SFE, which contains mainly 1 to 5 aromatic rings. However, as the length of alkyl side chains increases, the extraction efficiency decreases. The neutral pyrrole-like nitrogen containing compounds were analyzed using ESI(-) (Figure 2-9, right column). Since in the original crude oil N class compounds with only DBE up to 36 were detected, they can all be extracted to a certain extent using both methods. Comparing the SFE extract with its corresponding residue, neutral PANHs could be largely (about 90%) extracted through SFE.

2.5. Conclusion

In this work, different organic solvents, which are commonly used for the quantitative analysis of 16 EPA PAHs by Soxhlet extraction, were extended to extract other PAHs and PAXHs containing N or S and their alkylated or oxygenated derivatives. The analysis on a molecular level showed that nonpolar compounds could be extracted quite well by the solvents applied, whereas for polar compounds the sample extracted using dichloromethane and methanol exhibited the highest recovery. Results demonstrated that prior to the mass

spectrometric analysis the Soxhlet extraction could be used for extracting a large variety of hydrocarbon related contaminants from the soil, which are co-occurring with these 16 PAHs.

Additionally, the SFE using CO₂, which is usually referred to as a green extraction method, was studied in detail for extracting petroleum hydrocarbons from spiked sand. Compared to the standard Soxhlet extraction SFE could extract a range of compounds from nonpolar to polar hydrocarbons with a DBE and carbon count lower than 35 and 90, respectively.

In our study, a non-targeted method was developed to examine oil contamination in soil by using ultrahigh resolution mass spectrometry with different ionization methods. A heavy crude soil sample was spiked into pure sand to produce a simple model simulating a hydrocarbon contaminated soil sample with low organic content. Results showed that the selectivity of ionization methods applied offers sometime comparable but more importantly complementary data, each of which reflects only a part of the real sample. Therefore, for the non-targeted analysis of petroleum hydrocarbons in soil, a multidimensional ionization is indispensable. In addition, the coupling to FT MS instrument after ionization ensures a distinct assignment of the signals for such a complex sample.

2.6. References

1. Stout, S. A.; Emsbo-Mattingly, S. D.; Douglas, G. S.; Uhler, A. D.; McCarthy, K. J., Beyond 16 priority pollutant PAHs: A review of PACs used in environmental forensic chemistry. *Polycycl. Aromat. Comp.* **2015**, *35*, (2-4), 285-315.
2. SEC(2006)1165, Commission staff working document, accompany document to the communication from the commission to the council, the European parliament, the European economic and social committee and the committee of the regions, thematic strategy for soil protection, summary of the impact assessment; COMMISSION OF THE EUROPEAN COMMUNITIES: 2006.
3. Ranc, B.; Faure, P.; Croze, V.; Simonnot, M. O., Selection of oxidant doses for in situ chemical oxidation of soils contaminated by polycyclic aromatic hydrocarbons (PAHs): A review. *J. Hazard. Mater.* **2016**, *312*, 280-297.
4. Keith, L. H., The source of U.S. EPA's sixteen PAH priority pollutants. *Polycycl. Aromat. Comp.* **2015**, *35*, (2-4), 147-160.
5. Andersson, J. T.; Achten, C., Time to say goodbye to the 16 EPA PAHs? Toward an up-to-date use of PACs for environmental purposes. *Polycycl. Aromat. Comp.* **2015**, *35*, (2-4), 330-354.
6. Lundstedt, S.; Bandowe, B. A. M.; Wilcke, W.; Boll, E.; Christensen, J. H.; Vila, J.; Grifoll, M.; Faure, P.; Biache, C.; Lorgeoux, C.; Larsson, M.; Frech Irgum, K.; Ivarsson, P.; Ricci, M., First intercomparison study on the analysis of oxygenated polycyclic aromatic hydrocarbons (oxy-PAHs) and nitrogen heterocyclic polycyclic aromatic compounds (N-PACs) in contaminated soil. *TrAC-Trend. Anal. Chem.* **2014**, *57*, 83-92.
7. Wilcke, W.; Bandowe, B. A. M.; Lueso, M. G.; Ruppenthal, M.; del Valle, H.; Oelmann, Y., Polycyclic aromatic hydrocarbons (PAHs) and their polar derivatives

- (oxygenated PAHs, azaarenes) in soils along a climosequence in Argentina. *Sci. Total Environ.* **2014**, *473*, 317-325.
8. Bandowe, B. A. M.; Lueso, M. G.; Wilcke, W., Oxygenated polycyclic aromatic hydrocarbons and azaarenes in urban soils: A comparison of a tropical city (Bangkok) with two temperate cities (Bratislava and Gothenburg). *Chemosphere* **2014**, *107*, 407-414.
 9. Pröfrock, D.; Prange, A., Inductively Coupled Plasma–Mass Spectrometry (ICP-MS) for Quantitative Analysis in Environmental and Life Sciences: A Review of Challenges, Solutions, and Trends. *Applied Spectroscopy* **2012**, *66*, (8), 843-868.
 10. Vetere, A.; Profrock, D.; Schrader, W., Quantitative and Qualitative Analysis of Three Classes of Sulfur Compounds in Crude Oil. *Angew. Chem. Int. Edit* **2017**, *56*, (36), 10933-10937.
 11. Chibwe, L.; Davie-Martin, C. L.; Aitken, M. D.; Hoh, E.; Massey Simonich, S. L., Identification of polar transformation products and high molecular weight polycyclic aromatic hydrocarbons (PAHs) in contaminated soil following bioremediation. *Sci. Total Environ.* **2017**, *599*, 1099-1107.
 12. Manzano, C. A.; Marvin, C.; Muir, D.; Harner, T.; Martin, J.; Zhang, Y., Heterocyclic aromatics in petroleum coke, snow, lake sediments, and air samples from the athabasca oil sands region. *Environ. Sci. Technol.* **2017**, *51*, (10), 5445-5453.
 13. Tian, Z.; Vila, J.; Wang, H.; Bodnar, W.; Aitken, M. D., Diversity and abundance of high-molecular-weight azaarenes in PAH-contaminated environmental samples. *Environ. Sci. Technol.* **2017**, *51*, (24), 14047-14054.
 14. Panda, S. K.; Andersson, J. T.; Schrader, W., Characterization of supercomplex crude oil mixtures: What is really in there? *Angew. Chem. Int. Edit* **2009**, *48*, (10), 1788-1791.
 15. Vetere, A.; Schrader, W., Mass spectrometric coverage of complex mixtures: Exploring the carbon space of crude oil. *ChemistrySelect* **2017**, *2*, (3), 849-853.
 16. Palacio Lozano, D. C.; Gavard, R.; Arenas-Diaz, J. P.; Thomas, M. J.; Stranz, D. D.; Mejía-Ospino, E.; Guzman, A.; Spencer, S. E. F.; Rossell, D.; Barrow, M. P., Pushing the analytical limits: new insights into complex mixtures using mass spectra segments of constant ultrahigh resolving power. *Chem. Sci.* **2019**, *10*, (29), 6966-6978.
 17. Owen, B. C.; Hauptert, L. J.; Jarrell, T. M.; Marcum, C. L.; Parsell, T. H.; Abu-Omar, M. M.; Bozell, J. J.; Black, S. K.; Kenttämaa, H. I., High-Performance Liquid Chromatography/High-Resolution Multiple Stage Tandem Mass Spectrometry Using Negative-Ion-Mode Hydroxide-Doped Electrospray Ionization for the Characterization of Lignin Degradation Products. *Anal. Chem.* **2012**, *84*, (14), 6000-6007.
 18. Qi, Y.; Hempelmann, R.; Volmer, D. A., Shedding light on the structures of lignin compounds: photo-oxidation under artificial UV light and characterization by high resolution mass spectrometry. *Anal. Bioanal. Chem.* **2016**, *408*, (28), 8203-8210.
 19. Qi, Y.; Luo, R.; Schrader, W.; Volmer, D. A., Application of phase correction to improve the characterization of photooxidation products of lignin using 7 Tesla Fourier-transform ion cyclotron resonance mass spectrometry. *FACETS* **2017**, *2*, (1), 461-475.
 20. Rüger, C. P.; Sklorz, M.; Schwemer, T.; Zimmermann, R., Characterisation of ship diesel primary particulate matter at the molecular level by means of ultra-high-resolution mass spectrometry coupled to laser desorption ionisation—comparison of feed fuel, filter extracts and direct particle measurements. *Anal. Bioanal. Chem.* **2015**, *407*, (20), 5923-5937.

21. Gaspar, A.; Zellermann, E.; Lababidi, S.; Reece, J.; Schrader, W., Impact of different ionization methods on the molecular assignments of asphaltenes by FT-ICR mass spectrometry. *Anal. Chem.* **2012**, *84*, (12), 5257-5267.
22. Headley, J. V.; Peru, K. M.; Barrow, M. P., Mass spectrometric characterization of naphthenic acids in environmental samples: A review. *Mass Spectrom. Rev.* **2009**, *28*, (1), 121-134.
23. Headley, J. V.; Barrow, M. P.; Peru, K. M.; Derrick, P. J., Salting-out effects on the characterization of naphthenic acids from Athabasca oil sands using electrospray ionization. *Journal of Environmental Science and Health, Part A* **2011**, *46*, (8), 844-854.
24. Headley, J. V.; Peru, K. M.; Barrow, M. P., Advances in mass spectrometric characterization of naphthenic acids fraction compounds in oil sands environmental samples and crude oil—A review. *Mass Spectrom. Rev.* **2016**, *35*, (2), 311-328.
25. Reemtsma, T.; These, A.; Linscheid, M.; Leenheer, J.; Spitzzy, A., Molecular and Structural Characterization of Dissolved Organic Matter from the Deep Ocean by FTICR-MS, Including Hydrophilic Nitrogenous Organic Molecules. *Environ. Sci. Technol.* **2008**, *42*, (5), 1430-1437.
26. Reemtsma, T.; These, A.; Springer, A.; Linscheid, M., Differences in the molecular composition of fulvic acid size fractions detected by size-exclusion chromatography—on line Fourier transform ion cyclotron resonance (FTICR-) mass spectrometry. *Water Res.* **2008**, *42*, (1), 63-72.
27. Reemtsma, T., Determination of molecular formulas of natural organic matter molecules by (ultra-) high-resolution mass spectrometry: Status and needs. *J. Chromatogr. A* **2009**, *1216*, (18), 3687-3701.
28. Raeke, J.; Lechtenfeld, O. J.; Wagner, M.; Herzsprung, P.; Reemtsma, T., Selectivity of solid phase extraction of freshwater dissolved organic matter and its effect on ultrahigh resolution mass spectra. *Environ. Sci. -Proc. Imp.* **2016**, *18*, (7), 918-927.
29. Noah, M.; Poetz, S.; Vieth-Hillebrand, A.; Wilkes, H., Detection of residual oil-sand-derived organic material in developing soils of reclamation sites by ultra-high-resolution mass spectrometry. *Environ. Sci. Technol.* **2015**, *49*, (11), 6466-6473.
30. Guigue, J.; Harir, M.; Mathieu, O.; Lucio, M.; Ranjard, L.; Lévêque, J.; Schmitt-Kopplin, P., Ultrahigh-resolution FT-ICR mass spectrometry for molecular characterisation of pressurised hot water-extractable organic matter in soils. *Biogeochemistry* **2016**, *128*, (3), 307-326.
31. Fleury, G.; Del Nero, M.; Barillon, R., Effect of mineral surface properties (alumina, kaolinite) on the sorptive fractionation mechanisms of soil fulvic acids: Molecular-scale ESI-MS studies. *Geochim. Cosmochim. Ac.* **2017**, *196*, 1-17.
32. Tfaily, M. M.; Chu, R. K.; Toyoda, J.; Tolic, N.; Robinson, E. W.; Pasa-Tolic, L.; Hess, N. J., Sequential extraction protocol for organic matter from soils and sediments using high resolution mass spectrometry. *Anal. Chim. Acta* **2017**, *972*, 54-61.
33. Ohno, T.; Sleighter, R. L.; Hatcher, P. G., Comparative study of organic matter chemical characterization using negative and positive mode electrospray ionization ultrahigh-resolution mass spectrometry. *Anal. Bioanal. Chem.* **2016**, *408*, (10), 2497-2504.
34. Rüger, C. P.; Miersch, T.; Schwemer, T.; Sklorz, M.; Zimmermann, R., Hyphenation of Thermal Analysis to Ultrahigh-Resolution Mass Spectrometry (Fourier Transform Ion Cyclotron Resonance Mass Spectrometry) Using Atmospheric Pressure Chemical Ionization For Studying Composition and Thermal Degradation of Complex Materials. *Anal. Chem.* **2015**, *87*, (13), 6493-6499.
35. Lopez-Avila, V., Sample preparation for environmental analysis. *Crit. Rev. Anal. Chem.* **1999**, *29*, (3), 195-230.

36. Szolar, O. H. J.; Rost, H.; Braun, R.; Loibner, A. P., Analysis of polycyclic aromatic hydrocarbons in soil: Minimizing sample pretreatment using automated Soxhlet with ethyl acetate as extraction solvent. *Anal. Chem.* **2002**, *74*, (10), 2379-2385.
37. Schwab, A. P.; Su, J.; Wetzell, S.; Pekarek, S.; Banks, M. K., Extraction of petroleum hydrocarbons from soil by mechanical shaking. *Environ. Sci. Technol.* **1999**, *33*, (11), 1940-1945.
38. Sun, F.; Littlejohn, D.; David Gibson, M., Ultrasonication extraction and solid phase extraction clean-up for determination of US EPA 16 priority pollutant polycyclic aromatic hydrocarbons in soils by reversed-phase liquid chromatography with ultraviolet absorption detection1. *Anal. Chim. Acta* **1998**, *364*, (1-3), 1-11.
39. Richter, B. E.; Jones, B. A.; Ezzell, J. L.; Porter, N. L.; Avdalovic, N.; Pohl, C., Accelerated solvent extraction: A technique for sample preparation. *Anal. Chem.* **1996**, *68*, (6), 1033-1039.
40. Becnel, J. M.; Dooley, K. M., Supercritical Fluid Extraction of Polycyclic Aromatic Hydrocarbon Mixtures from Contaminated Soils. *Ind. Eng. Chem. Res.* **1998**, *37*, (2), 584-594.
41. Song, Y. F.; Jing, X.; Fleischmann, S.; Wilke, B. M., Comparative study of extraction methods for the determination of PAHs from contaminated soils and sediments. *Chemosphere* **2002**, *48*, (9), 993-1001.
42. Hollender, J.; Koch, B.; Lutermann, C.; Dott, W., Efficiency of different methods and solvents for the extraction of polycyclic aromatic hydrocarbons from soils. *Intern. J. Environ. Anal. Chem.* **2003**, *83*, (1), 21-32.
43. Wang, W.; Meng, B.; Lu, X.; Liu, Y.; Tao, S., Extraction of polycyclic aromatic hydrocarbons and organochlorine pesticides from soils: A comparison between Soxhlet extraction, microwave-assisted extraction and accelerated solvent extraction techniques. *Anal. Chim. Acta* **2007**, *602*, (2), 211-222.
44. Itoh, N.; Numata, M.; Aoyagi, Y.; Yarita, T., Comparison of low-level polycyclic aromatic hydrocarbons in sediment revealed by Soxhlet extraction, microwave-assisted extraction, and pressurized liquid extraction. *Anal. Chim. Acta* **2008**, *612*, (1), 44-52.
45. Luque de Castro, M. D.; García-Ayuso, L. E., Soxhlet extraction of solid materials: an outdated technique with a promising innovative future. *Anal. Chim. Acta* **1998**, *369*, (1), 1-10.
46. Eckert-Tilotta, S. E.; Hawthorne, S. B.; Miller, D. J., Supercritical fluid extraction with carbon dioxide for the determination of total petroleum hydrocarbons in soil. *Fuel* **1993**, *72*, (7), 1015-1023.
47. Hawthorne, S. B.; Miller, D. J., Direct comparison of Soxhlet and low- and high-temperature supercritical CO₂ extraction efficiencies of organics from environmental solids. *Anal. Chem.* **1994**, *66*, (22), 4005-4012.
48. Tena, M. T.; Luque de Castro, M. D.; Valcárcel, M., Screening of polycyclic aromatic hydrocarbons in soil by on-line fiber-optic-interfaced supercritical fluid extraction spectrofluorometry. *Anal. Chem.* **1996**, *68*, (14), 2386-2391.
49. Southam, A. D.; Payne, T. G.; Cooper, H. J.; Arvanitis, T. N.; Viant, M. R., Dynamic range and mass accuracy of wide-scan direct infusion nanoelectrospray Fourier transform ion cyclotron resonance mass spectrometry-based metabolomics increased by the spectral stitching method. *Anal. Chem.* **2007**, *79*, (12), 4595-4602.
50. Gaspar, A.; Schrader, W., Expanding the data depth for the analysis of complex crude oil samples by Fourier transform ion cyclotron resonance mass spectrometry using the spectral stitching method. *Rapid Commun. Mass Spectrom.* **2012**, *26*, (9), 1047-1052.
51. U.S. Environmental Protection Agency (U.S. EPA), SW-846 test methods for evaluating solid waste, Method 3540C: Soxhlet extraction. In 1996.

52. Kelsey, J. W.; Kottler, B. D.; Alexander, M., Selective chemical extractants to predict bioavailability of soil-aged organic chemicals. *Environ. Sci. Technol.* **1997**, *31*, (1), 214-217.
53. Stanford, L. A.; Kim, S.; Klein, G. C.; Smith, D. F.; Rodgers, R. P.; Marshall, A. G., Identification of water-soluble heavy crude oil organic-acids, bases, and neutrals by electrospray ionization and field desorption ionization Fourier transform ion cyclotron resonance mass spectrometry. *Environ. Sci. Technol.* **2007**, *41*, (8), 2696-2702.
54. Lu, M.; Zhang, Z.; Qiao, W.; Guan, Y.; Xiao, M.; Peng, C., Removal of residual contaminants in petroleum-contaminated soil by Fenton-like oxidation. *J. Hazard. Mater.* **2010**, *179*, (1-3), 604-611.
55. Lu, M.; Zhang, Z.; Qiao, W.; Wei, X.; Guan, Y.; Ma, Q.; Guan, Y., Remediation of petroleum-contaminated soil after composting by sequential treatment with Fenton-like oxidation and biodegradation. *Bioresource Technol.* **2010**, *101*, (7), 2106-2113.
56. Wang, J.; Zhang, X.; Li, G., Detailed characterization of polar compounds of residual oil in contaminated soil revealed by Fourier transform ion cyclotron resonance mass spectrometry. *Chemosphere* **2011**, *85*, (4), 609-615.
57. Cai, S.-S.; Syage, J. A.; Hanold, K. A.; Balogh, M. P., Ultra performance liquid chromatography-atmospheric pressure photoionization-tandem mass spectrometry for high-sensitivity and high-throughput analysis of U.S. Environmental Protection Agency 16 priority pollutants polynuclear aromatic hydrocarbons. *Anal. Chem.* **2009**, *81*, (6), 2123-2128.
58. Schmitt-Kopplin, P.; Englmann, M.; Rossello-Mora, R.; Schiewek, R.; Brockmann, K. J.; Benter, T.; Schmitz, O. J., Combining chip-ESI with APLI (cESILI) as a multimode source for analysis of complex mixtures with ultrahigh-resolution mass spectrometry. *Anal. Bioanal. Chem.* **2008**, *391*, (8), 2803-2809.
59. Gaspar, A.; Zellermann, E.; Lababidi, S.; Reece, J.; Schrader, W., Characterization of saturates, aromatics, resins, and asphaltenes heavy crude oil fractions by atmospheric pressure laser ionization Fourier transform ion cyclotron resonance mass spectrometry. *Energy Fuel* **2012**, *26*, (6), 3481-3487.
60. Krueve, A.; Kaupmees, K.; Liigand, J.; Oss, M.; Leito, I., Sodium adduct formation efficiency in ESI source. *J. Mass Spectrom.* **2013**, *48*, (6), 695-702.
61. Hegazi, A. H.; Fathalla, E. M.; Panda, S. K.; Schrader, W.; Andersson, J. T., High-molecular weight sulfur-containing aromatics refractory to weathering as determined by Fourier transform ion cyclotron resonance mass spectrometry. *Chemosphere* **2012**, *89*, (3), 205-212.

Appendix for Chapter 2

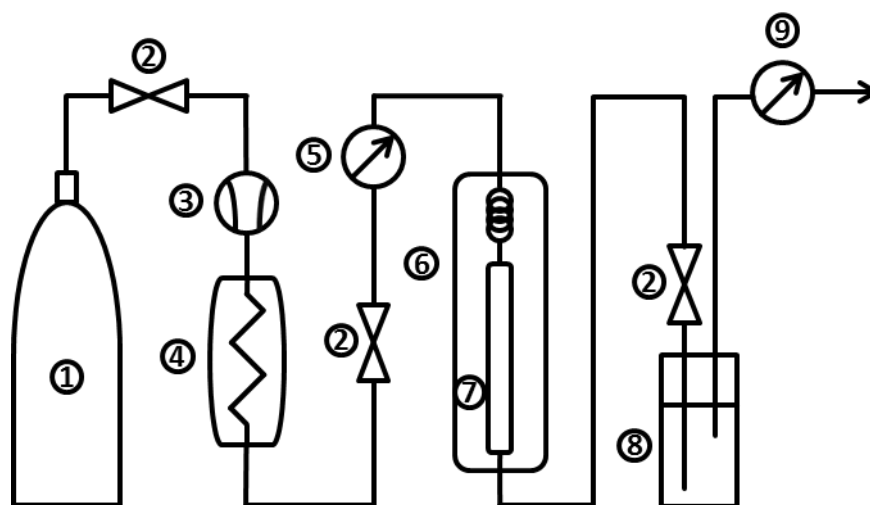


Figure A2-1. Schematic representation of the SFE system. 1. CO₂ supply 2. Valve 3. Compressor 4: temperature controlled capillary 5. Pressure gauge 6. Heated Oven 7. Stainless steel column for the sample 8. Cool trap with toluene 9. Gas meter

Table A2-1. The experimental m/z , calculated ion formula, double bond equivalent (DBE) and mass error for identified major ions at m/z 400 with absolute intensity higher than 500 found in the original crude oil, measured by APPI(+)-FT Orbitrap mass spectrometry.

theoretical m/z	ion formula	DBE
400.03412	$C_{30}H_8S^+$	27
400.04086	$C_{24}H_{16}S_3^+$	17
400.09501	$C_{25}H_{20}OS_2^+$	16
400.09503	$C_{29}^{13}CH_{11}N_2^+$	26.5
400.11208	$C_{31}H_{14}N^+$	25.5
400.11545	$C_{28}H_{18}NS^+$	20.5
400.12355	$C_{28}^{13}CH_{19}S^+$	20.5
400.12465	$C_{32}H_{16}^+$	25
400.12802	$C_{29}H_{20}S^+$	20
400.13139	$C_{26}H_{24}S_2^+$	15
400.13476	$C_{23}H_{28}S_3^+$	10
400.16959	$C_{29}H_{22}ON^+$	19.5
400.18217	$C_{30}H_{24}O^+$	19
400.18554	$C_{27}H_{28}OS^+$	14
400.18893	$C_{28}^{13}CH_{23}N_2^+$	19.5
400.20151	$C_{29}^{13}CH_{25}N^+$	19
400.20598	$C_{30}H_{26}N^+$	18.5
400.20935	$C_{27}H_{30}NS^+$	13.5
400.21272	$C_{24}H_{34}NS_2^+$	8.5
400.21745	$C_{27}^{13}CH_{31}S^+$	13.5
400.21855	$C_{31}H_{28}^+$	18
400.22082	$C_{24}^{13}CH_{35}S_2^+$	8.5
400.22192	$C_{28}H_{32}S^+$	13
400.22529	$C_{25}H_{36}S_2^+$	8
400.23968	$C_{28}H_{32}O_2^+$	13
400.24305	$C_{25}H_{36}O_2S^+$	8
400.26349	$C_{28}H_{34}ON^+$	12.5
400.2716	$C_{28}^{13}CH_{35}O^+$	12.5
400.27607	$C_{29}H_{36}O^+$	12
400.27944	$C_{26}H_{40}OS^+$	7
400.29541	$C_{28}^{13}CH_{37}N^+$	12
400.2961	$C_{22}^{13}CH_{43}O_3S^+$	2.5
400.29988	$C_{29}H_{38}N^+$	11.5
400.30325	$C_{26}H_{42}NS^+$	6.5
400.30798	$C_{29}^{13}CH_{39}^+$	11.5
400.31135	$C_{26}^{13}CH_{43}S^+$	6.5
400.31245	$C_{30}H_{40}^+$	11
400.31582	$C_{27}H_{44}S^+$	6
400.35739	$C_{27}H_{46}ON^+$	5.5
400.3655	$C_{27}^{13}CH_{47}O^+$	5.5
400.40188	$C_{28}^{13}CH_{51}^+$	4.5
400.40635	$C_{29}H_{52}^+$	4

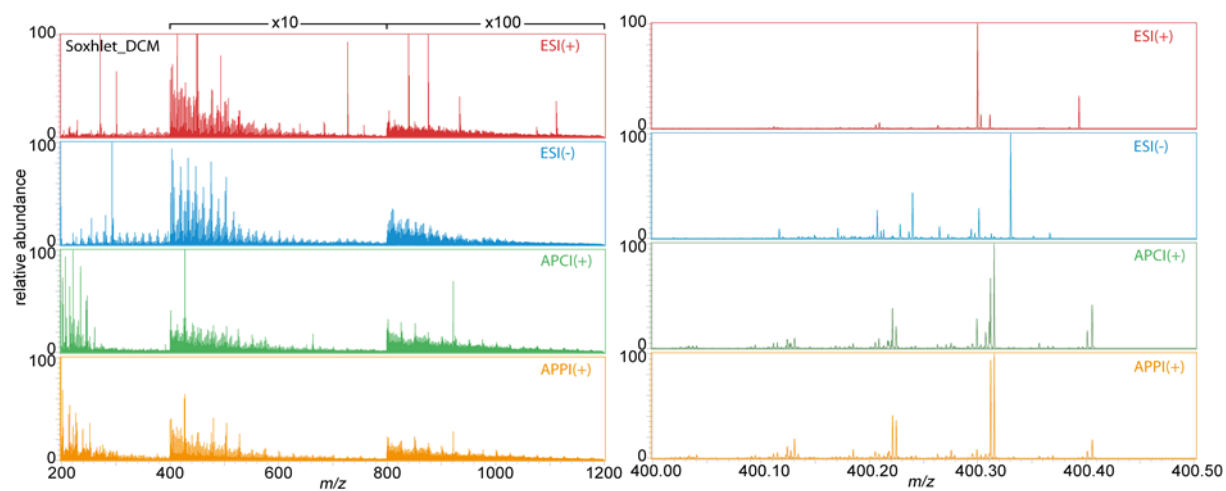


Figure A2-2. Recombined (left) and zoomed in mass spectra at 400 m/z (right) for the spiked sand sample Soxhlet extracted using dichloromethane, analyzed by FT Orbitrap MS using positive mode ESI (red), negative mode ESI (blue), positive mode APCI (green) and APPI (orange), respectively.

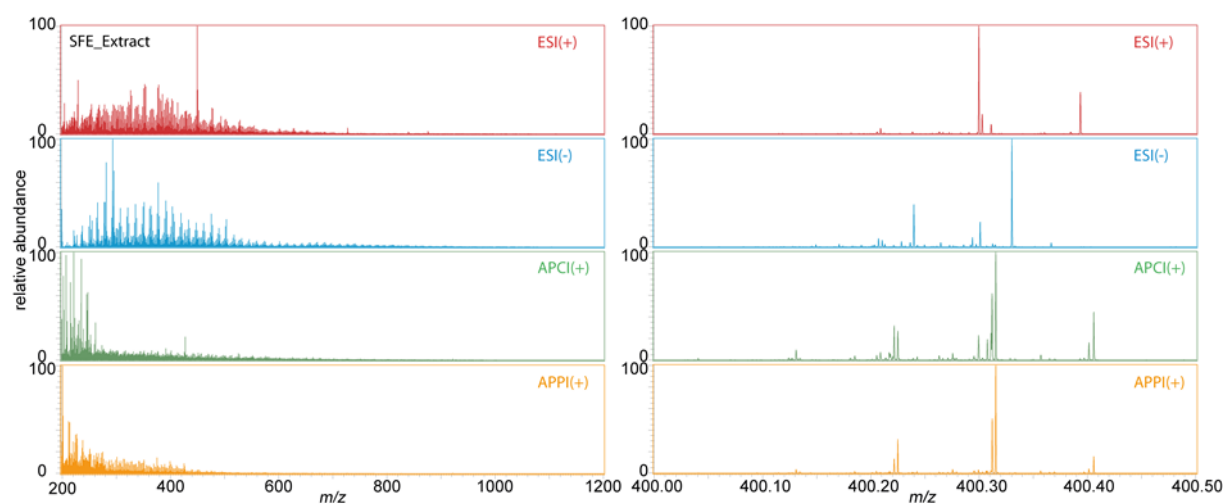


Figure A2-3. Recombined (left) and zoomed in mass spectra at 400 m/z (right) for SFE extract of spiked sand, analyzed by FT Orbitrap MS using positive mode ESI (red), negative mode ESI (blue), positive mode APCI (green) and APPI (orange), respectively.

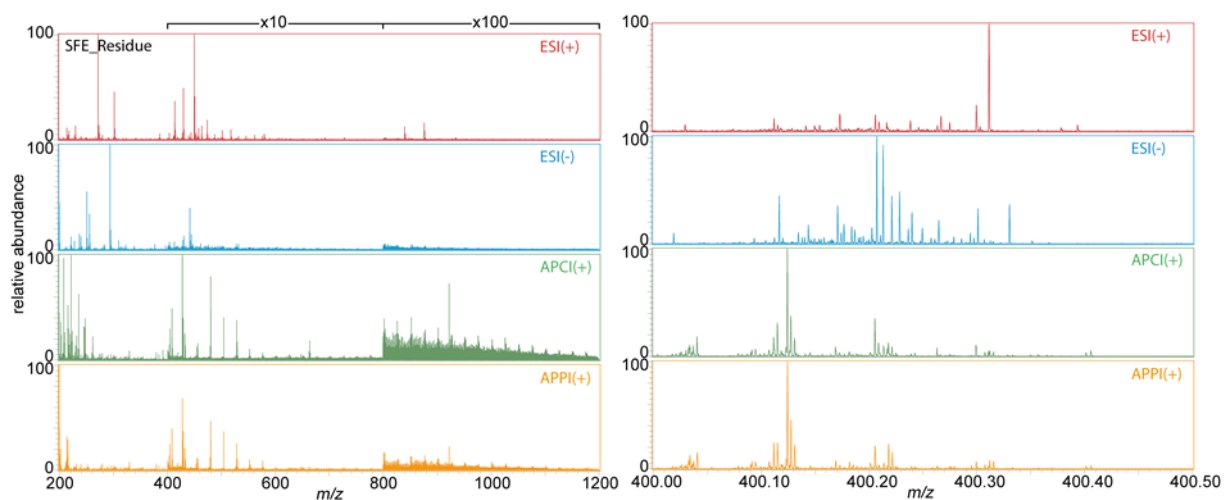


Figure A2-4. Recombined (left) and zoomed in mass spectra at 400 m/z (right) for SFE residue of spiked sand, analyzed by FT Orbitrap MS using positive mode ESI (red), negative mode ESI (blue), positive mode APCI (green) and APPI (orange), respectively.

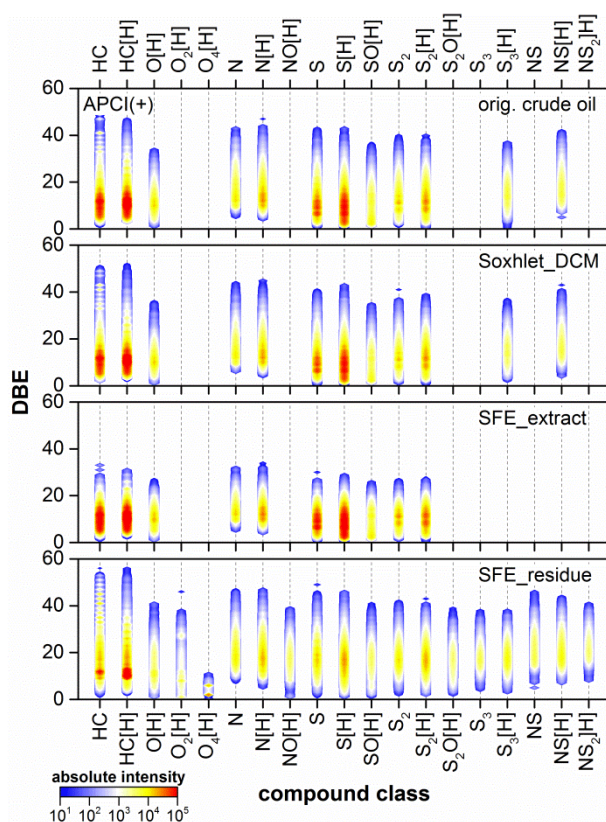


Figure A2-5. Intensity based DBE vs. class distributions for the original crude oil, Soxhlet extract using DCM, SFE extract and residue (from top to bottom) using positive mode-APCI FT Orbitrap MS (radical cations: M, protonated molecules: M[H]).

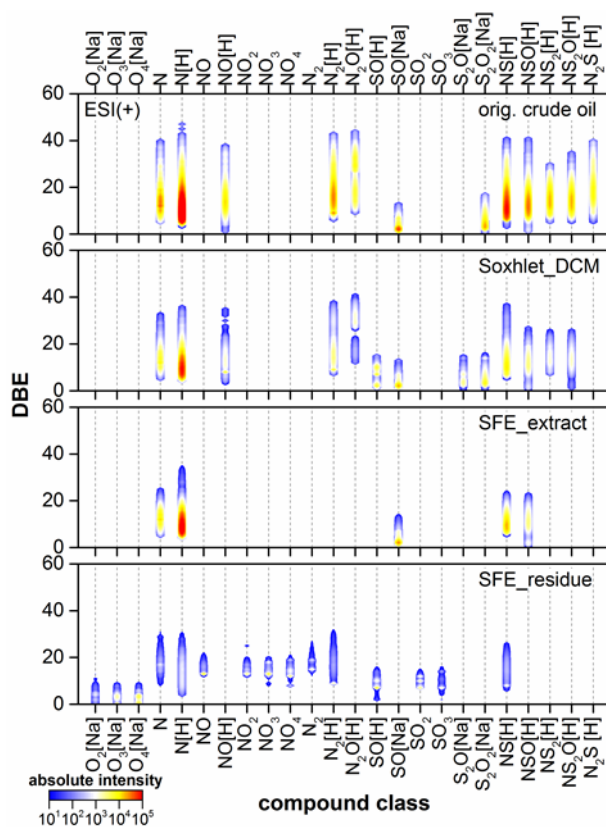


Figure A2-6. Intensity based DBE vs. class distributions for the original crude oil, Soxhlet extract using DCM, SFE extract and residue (from top to bottom) using positive mode-ESI FT Orbitrap MS (radical cations: M, protonated molecules: M[H], molecules with sodium adduct M[Na]).

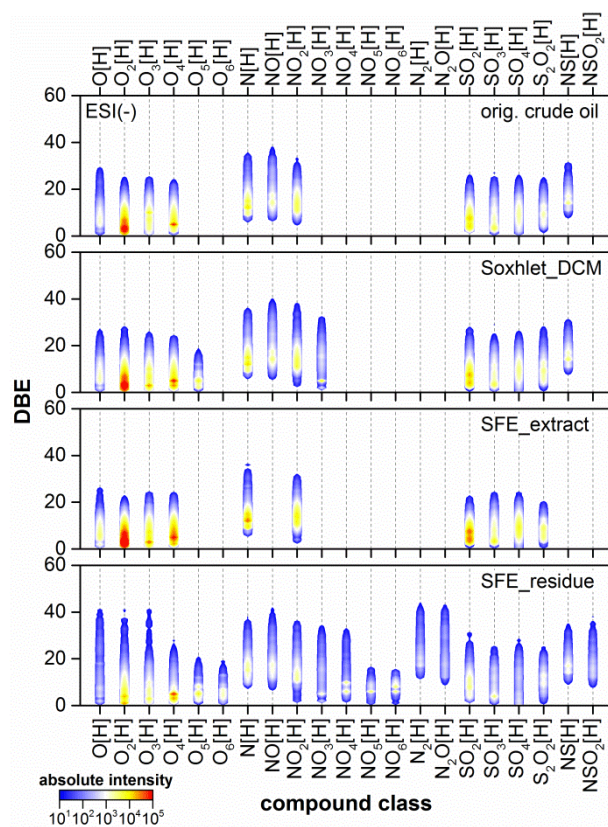


Figure A2-7. Intensity based DBE vs. class distributions for the original crude oil, Soxhlet extract using DCM, SFE extract and residue (from top to bottom) using negative mode-ESI FT Orbitrap MS (deprotonated molecules: M[H]).

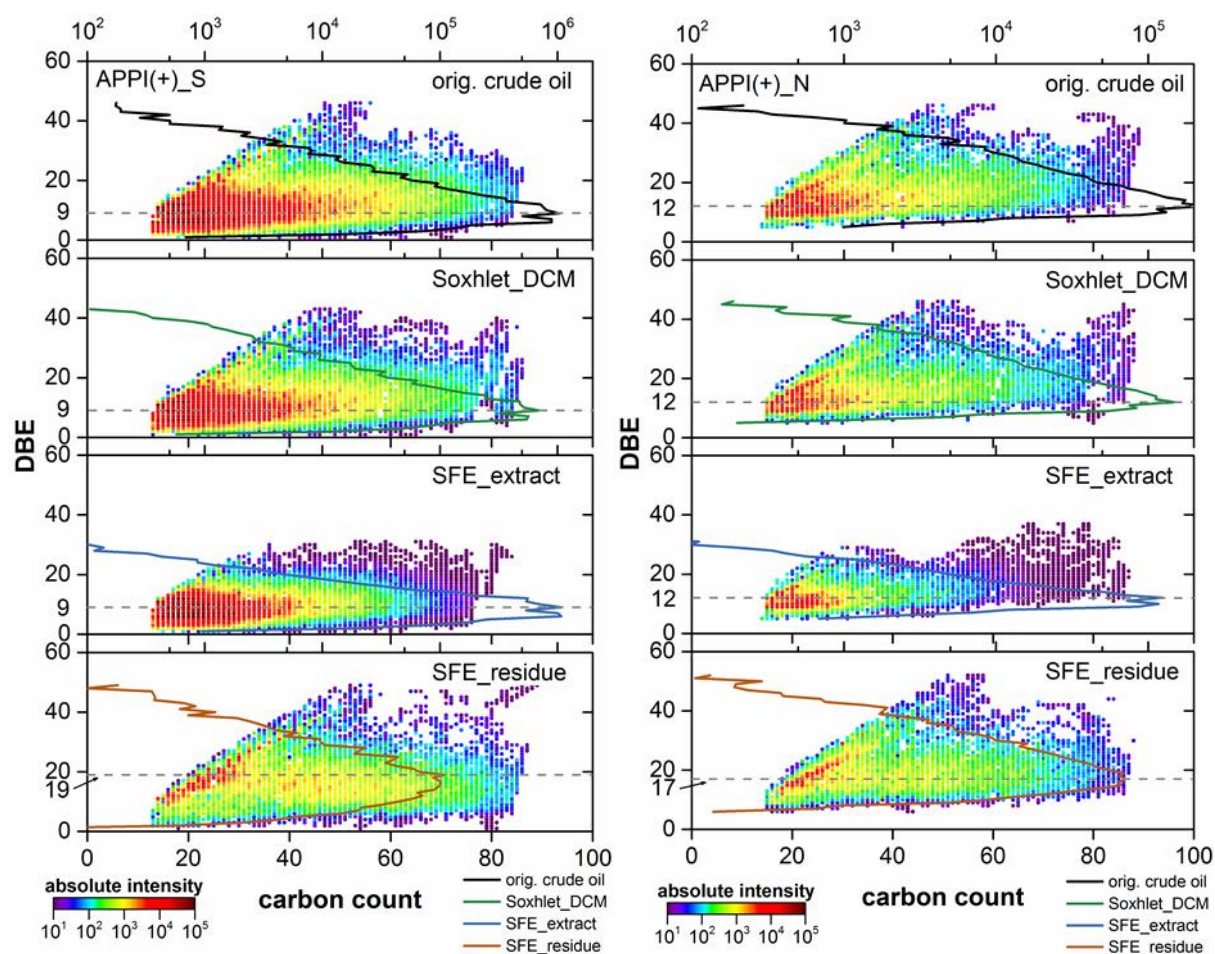


Figure A2-8. DBE vs. carbon number/intensity plots for the radical S (left column) and N (right column) class in the original crude oil, Soxhlet extract using DCM, SFE extract and residue (from top to bottom) using positive mode-APPI FT Orbitrap MS.

Chapter 3. Getting a Better Overview of a Highly PAH Contaminated Soil: a Non-Targeted Approach Assessing the Real Environmental Risk

Redrafted from “Luo, R.; Schrader, W., Getting a Better Overview of a Highly PAH Contaminated Soil: a Non-Targeted Approach Assessing the Real Environmental Risk”, submitted to Environmental Science & Technology.

3.1. Abstract

Over 40 years, soils contaminated with polycyclic aromatic hydrocarbons (PAH) were monitored according to a list of 16 PAH, established by the U.S. Environmental Protection Agency (EPA). This, however, is underestimating the danger to the environment and humanity because other high molecular weight PAHs, heterocycles (PAXH, X = N, O, S) and alkylated derivatives can also occur at the contaminated site. Here, a new non-targeted approach is introduced where ultrahigh resolution mass spectrometry is combined with multiple ionization methods to get a better overview of anthropogenic contamination at a former industrial site. In total, 21,958 elemental compositions were assigned for positive and negative mode measurements. The approach is strongly increasing the amount of data that can be obtained from a single contaminated soil, making an assessment of the real environmental risk possible. In addition to highly aromatized and (alkylated) high molecular weight PAH, other PAXH especially basic and neutral PANH with very high aromaticity were also detected. This shows that while regulations and routine analysis are still stuck in the 1960s, modern analytical methods are present in the 21st century.

3.2. Introduction

The type and number of emerging environmental contaminants are increasing the more better and more powerful analytical methods are being used to detect them.¹ Polycyclic aromatic compounds including pure polycyclic aromatic hydrocarbons (PAH) and polycyclic aromatic heterocycles containing sulfur, nitrogen or oxygen (PAXH, X = S, N, O) are a group of compounds, many of which are considered to be mutagenic and/or carcinogenic.² They are generated through either petrogenic, pyrogenic or biogenic processes and can be found with enhanced concentration in sites contaminated with crude oil, coal tar or creosote.^{3, 4} It is estimated that in the European Union alone the annual cost for the soil remediation from PAH can reach up to two billion Euros.⁵

The 16 PAH first introduced by the U.S. Environmental Protection Agency (EPA) in 1976 were selected as priority contaminants under consideration of the presence of commercially available standards as well as analytical techniques for their determination.⁶ This limited number of representatives reduced the analytical challenge, lowered costs, enabled qualitative and quantitative measurements, and ensured worldwide comparability.⁷ Nevertheless, the 16 PAH list has its limitations. A major one being a possible underestimation of the effect of a contamination since other, high molecular weight parent PAH, the heteroatom containing PAXH and alkylated PA(X)H are not considered at all.⁸

With the additional information of alkylated PA(X)H or their derivatives, the source of contamination, which means either pyrogenic or petrogenic or biogenic, could be determined.^{3, 9-15} For example, Richter-Brockmann and Achten have analyzed 59 (alkylated) PAH by gas chromatography coupled with (low resolution) mass spectrometry (GC-MS), which is the standard method for the targeted analysis of the 16 EPA PAH. They also assessed the toxicity of these compounds and found out, that dibenzopyrenes and 7*H*-benzo[*c*]fluorene, found in pyrogenic and petrogenic materials, respectively, are responsible for a large portion of the samples toxicity.¹⁶ Also relatively polar and therefore more leachable oxidized PAH and PANH were investigated by different researchers using GC-MS.¹⁷⁻¹⁹ Recently, non-targeted analysis of PAH related contaminants in soils was performed using advanced instrumentations such as two-dimensional GC (GC x GC) or high performance liquid chromatography (HPLC) coupled with time-of-flight mass spectrometry (TOF MS).^{15, 20, 21} By using this approach a more comprehensive view into PAH especially high molecular weight PAH and PAXH as well as their transformation products in soil can be achieved.

One of the most powerful instrumentations for the non-targeted analysis of complex environmental samples are Fourier transform Ion Cyclotron Resonance (FTICR)^{22, 23} and Orbitrap^{24, 25} mass spectrometers. Their (ultra)high mass resolution and accuracy allow an unambiguous assignment of an elemental composition to each detected signal within a complex system. Negative mode electrospray ionization (-)-ESI-FTICR-MS was often used to examine compounds in soil organic matter (SOM) or contaminated environmental samples, such as oil sand. Highly oxidized compounds²⁶⁻²⁹ and naphthenic acids^{30, 31} can be well studied using this method. Other atmospheric pressure ionization (API) methods such as atmospheric pressure chemical ionization (APCI) and atmospheric pressure photo ionization (APPI) found few applications for the non-targeted analysis of soil samples.^{32, 33} A cross comparison of different API methods can offer comparable but more important complementary data, which help characterize the sample.³⁴⁻³⁶

Here we present a non-targeted analysis of a highly PAXH contaminated soil using FT Orbitrap MS with multiple API methods including ESI, APCI and APPI. Results from the contaminated soil are compared with a sand sample spiked with crude oil and a non-contaminated potting soil sample. The aim of the study is to have a comprehensive view of the contaminated soil sample and try to link the big data generated to the origin of contamination.

3.3. Materials and Methods

3.3.1. Sample Preparation

All solvents used were HPLC-grade and purchased from Sigma-Aldrich or Acros Organics.

An already contaminated soil (CS) from an industrial site and potting soil (PS, Bauhaus, Germany) were air dried at room temperature, sieved through a 2 mm sieve and after homogenization stored in the fridge at 4°C for further treatment. A heavy crude oil was diluted in dichloromethane and then spiked into the contaminated soil, potting soil as well as pure sand (50-70 mesh, Sigma-Aldrich, Germany). The remaining dichloromethane for dilution was removed through rotary-evaporation. The final concentration of spiked heavy crude oil in each solid matrix was 50.0 g kg⁻¹ (w/w). Pure sand was used during this study to simulate a soil environment with low SOM.³⁷

5.00 g of each sample were placed into a glass fiber thimble (type 603G, Whatman, VWR) with addition of 5.00 g anhydrous sodium sulfate (99.5%, Acros Organics) and Soxhlet extracted using 100 mL dichloromethane for around 300 cycles.³⁷ After extraction solvents

were rotary-evaporated to a volume of 2 mL and then dried under a gentle argon gas stream. The amount of solvent extractable organics was determined by dividing the amount of extracts by the amount of sample used (w/w). Extracts were stored in the fridge at 4°C prior to mass spectrometric analysis.

3.3.2. Mass Spectrometric and Data Analysis

Extracts were analyzed using a research type FT Orbitrap MS (Thermo Fisher Scientific, Bremen, Germany). For ESI measurements samples were diluted to 250 $\mu\text{g mL}^{-1}$ in toluene:methanol (1:1, $v:v$). For both APCI and APPI measurements samples were diluted to the same concentration in chlorobenzene to reduce interfering signals in the lower mass range as compared to using the more common toluene as solvent. For ESI measurements samples were injected with a flow rate of 5 $\mu\text{L min}^{-1}$ with 5, 2 and 1 a.u. (arbitrary units) of sheath, auxiliary and sweep gas, respectively. The spray voltage was set to +/-4 kV for positive/negative mode measurements. For both APCI and APPI measurements samples were injected with a flow rate of 20 $\mu\text{L min}^{-1}$ at a vaporizer temperature of 350 °C. Sheath, auxiliary and sweep gases were set to 20, 5 and 2 a.u., respectively. The discharge current for APCI was set to 5 μA . For APPI measurement a Krypton VUV lamp (Syagen, Tustin, CA, U.S.A.) with a photon emission at 10.0 and 10.6 eV was used. A whole mass range between 125 and 1200 was recorded using spectral stitching,^{24, 38, 39} meaning 30 Da mass windows with 5 Da overlap, using a 3s transient (mass resolution of 960,000 at m/z 400).

Individual mass windows were recombined to one mass spectrum in Xcalibur 2.2 (Thermo Fisher Scientific, Bremen, Germany) and further processed using Composer64 v1.5.3. (Sierra Analytics, Modesto, CA, U.S.A.) with the following chemical constraints: $0 < C < 200$, $0 < H < 1000$, $0 < N < 4$, $0 < S < 5$, $0 < O < 11$, $0 < P < 2$ and a maximum mass error of 1 ppm. The double bond equivalent (DBE) value used in the results and discussion section was calculated for an elemental composition $\text{C}_c\text{H}_h\text{N}_n\text{O}_o\text{S}_s\text{P}_p$ by the following equation:

$$\text{DBE} = c - h/2 + n/2 + 1$$

3.4. Results and Discussion

3.4.1. Solvent Extractable Organics

Soxhlet extraction as one of the oldest conventional extraction techniques has been successfully applied for the quantitative analysis of the 16 EPA PAH in soils.^{37, 40-42} Despite its relatively high extraction duration compared to other newly developed techniques such as supercritical fluid extraction and accelerated solvent extraction, its simple setup and unlimited

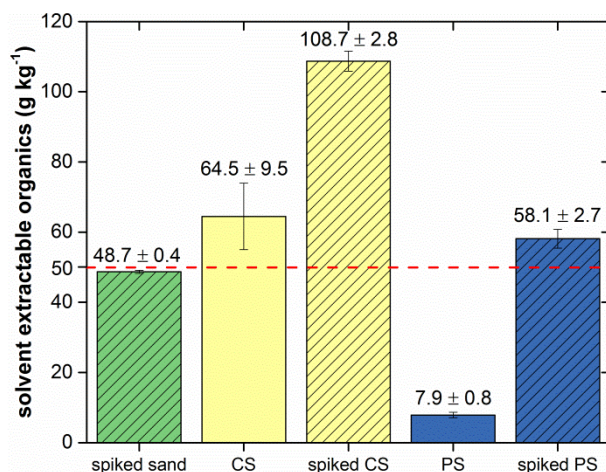


Figure 3-1. The amount of solvent extractable organics in spiked sand, contaminated soil (CS), spiked contaminated soil, potting soil (PS) and spiked potting soil (from left to right) after Soxhlet extraction, spiked samples (with 50 g kg⁻¹ heavy crude oil per solid matrix) are denoted with oblique lines in the column (n = 3).

extraction capacity present an ideal extraction method for non-targeted soil analysis. The amounts of solvent extractable organics in original soils and spiked samples are summarized in Figure 3-1. The results show a good recovery of crude oil related contaminants from the model sample (sand, which simulates soil with low organic content) and the real samples (potting soil and contaminated soil) with recovery rates of 97±1%, 88±14%, 100±6%, respectively. The high amount of solvent extractable organics found in the contaminated soil (64.5 ± 9.5 g kg⁻¹) compared to potting soil (7.9 ± 0.8 g kg⁻¹) indicates that the contaminated soil was enriched with organic matter.

3.4.2. Mass Spectra

Discrimination effects can occur by analyzing complex environmental samples using mass spectrometry, especially with only one ionization method. This has been discussed in detail for crude oil^{22,35} and organic matter.²⁷

In order to gain a more comprehensive dataset for the sample of interest, the utilization of multiple ionization methods using both polarities is required. This is exemplarily shown in Figure 3-2 for the extract from contaminated soil. Full scan spectra recorded in positive and negative mode using the different ionization methods are shown on the left and right side, respectively. In both cases results from APPI and APCI show a very similar overall pattern, with the ESI spectrum being more different (comparing the most abundant signals for different ionization methods shown in Table A3-1 to A3-6). The center panel shows a zoomed-in section around m/z 400 for the positive mode measurements. The ESI spectrum predominately shows basic nitrogen containing species and, to a lesser extent, pure hydrocarbons, such as C₃₂H₁₆^{•+}.⁴³ This radical ion ($m/z = 400.12465$) with a double bond

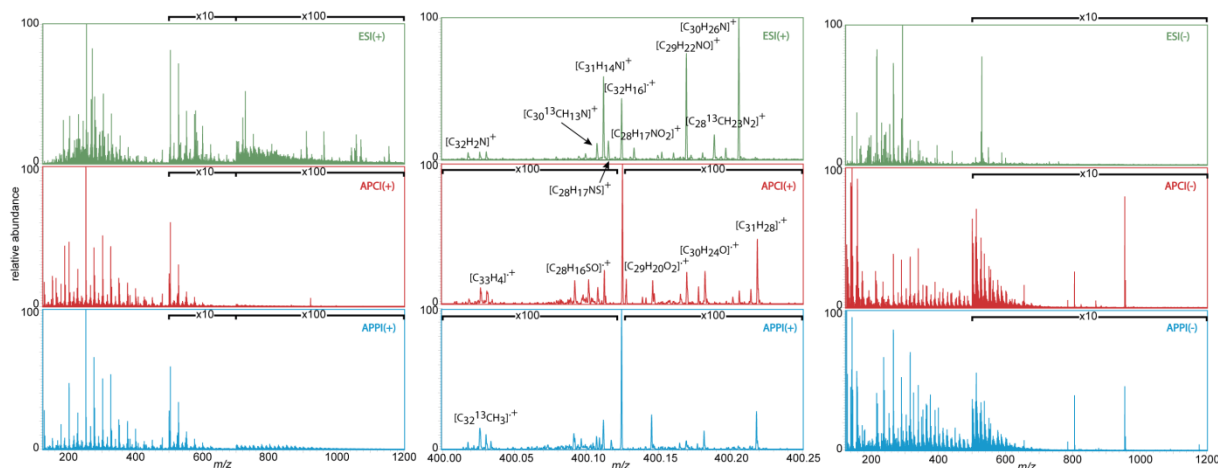


Figure 3-2. Recombined positive mode (left column), zoomed-in section at m/z 400 (middle column) and negative (right column) mode mass spectra for the contaminated soil extract using ESI (green), APCI (red) and APPI (blue) FT Orbitrap MS. The magnification factor of the m/z signals is indicated above each mass spectrum.

equivalent (DBE) of 25 is the most abundant signal detected for both the APCI and the APPI spectra. Its DBE value and molecular mass both exceed the values for the largest members from the 16 EPA PAH list benzo[*ghi*]perylene and indeno[*1,2,3-cd*]pyrene (DBE = 17, MW = 276 Da) (supporting information Table A3-7). In addition to this radical ion other fourteen molecular compositions were assigned within this 0.25 Da mass window, which represents the complexity of the contaminated soil sample.

Among the different ionization methods APPI showed the highest average m/z values (also resulting in the highest number of carbon atoms per molecule) for the original contaminated soil. Especially in positive mode APPI also resulted in the highest observed DBE and lowest H/C values, i.e. it favors compounds with extended aromatic moieties, as is to be expected by the ionization mechanism (Table 3-1). For all six modes the mean m/z values found for the extracts from the contaminated soil sample are lower than values for the extracts from spiked sand and potting soil samples (Table A3-8 and A3-9). Furthermore, relative high mean DBE and low H/C values determined for the contaminated soil imply that the contamination contains highly condensed aromatic structures. Detected H/C values fall into the range for the 16 EPA PAHs (0.55 to 0.83, Table A3-7) for all six ionization modes except for negative mode ESI. The relatively high H/C (1.0710) and O/C (0.1555) values imply a strong preference of negative mode ESI for the ionization of naphthenic acids or SOM,²⁶⁻²⁸ as can be expected. Positive mode ESI on the other hand shows a relatively high value for the N/C ratio (0.0338), implying a preference for basic nitrogen containing compounds. In the spiked sand and potting soil the values of N/C ratio (0.0257 and 0.0202) were significantly lower than in the contaminated soil. These results indicate that the contaminants in the soil

Table 3-1. Mean values of m/z , DBE, number of carbon atoms per molecule and X/C for the original contaminated soil extract, analyzed using different API-FT Orbitrap MS. Values were calculated using all assigned elemental compositions with on weighting of their absolute intensity.

Contaminated soil	mean values						
	m/z	DBE	#C	H/C	N/C	O/C	S/C
ESI+	505.1	27	37	0.6501	0.0338	0.0206	0.0063
APCI+	490.6	25	37	0.7100	0.0137	0.0223	0.0030
APPI+	598.2	33	45	0.6177	0.0156	0.0271	0.0031
ESI-	431.2	15	28	1.0710	0.0270	0.1555	0.0068
APCI-	463.0	24	34	0.6995	0.0170	0.0735	0.0000
APPI-	484.0	24	34	0.7226	0.0199	0.0907	0.0060

sample consist of mainly condensed pure hydrocarbons and partially nitrogen-containing hydrocarbons (see also Figure 3-2).

3.4.3. Venn Diagram

The extent of discrimination effects among the ionization methods is shown in Figure 3-3 using scaled Venn diagrams.⁴⁴ In total 12,520 and 16,101 different elemental compositions were assigned for positive and negative mode measurements with 4,714; 5,557 and 9,702 found for positive ESI, APCI and APPI, 8,860; 3,092 and 12,058 found for negative ESI, APCI, and APPI, respectively. In both polarities APPI delivered the highest number of assignments, which implies that a majority of compounds extracted from the contaminated soil are of aromatic nature. While there is a high overlap between APPI and APCI (4,935 and 3,025 compositions) ESI shows a very distinct behavior with 2,196 and 3,976 detected uniquely by this method. Overall, only 15% and 13% (1,833; 2,062 out of 12,520; 16,101) compositions were detected simultaneously by all methods in positive and negative mode measurements.

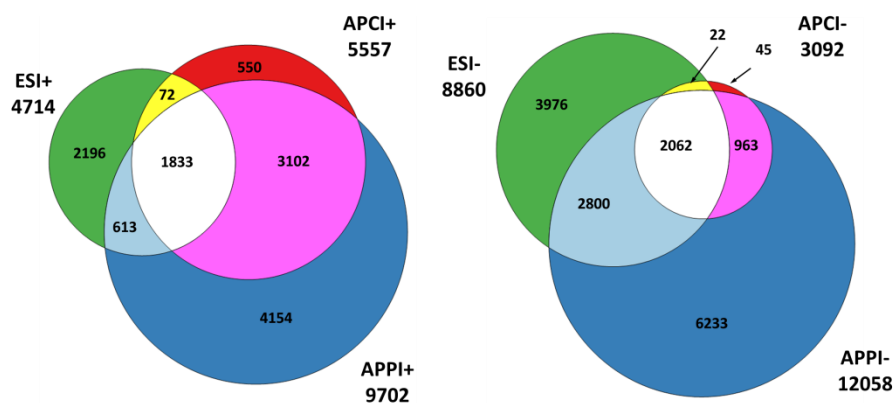


Figure 3-3. Venn diagrams for numbers of assigned compositions obtained from the extract of original contaminated soil using multiple ionization methods in positive (left) and negative (right) mode.

Similar allocations for the different ionization methods were found for the extract from the spiked sand sample with a total of 37,628 and 46,922 assignments in positive and negative mode (Figure A3-1). Also here, only around 5 to 10% of these compositions were common between the three API methods. For the potting soil extract the APCI mass spectrum contained the highest number of assignments in the positive mode (Figure A3-2), which might refer to a larger relative amount of natural organic matter (NOM) compounds.⁴⁵ Here, less than 3% (8% in negative mode) of the compositions could be found by all three methods. The small proportion of common assignments points out the necessity of using multiple ionization methods for examining complex environmental samples.

3.4.4. Class Distribution

More detailed information for assigned compositions from the contaminated soil extract is displayed in Figure 3-4 as population and intensity based class distribution plots. Considering the benefits and drawbacks of population and intensity plots we decided to show both plots.^{31,35} In order to simplify the graph only classes with a relative intensity higher than 1% are shown. The overall plot can be seen in Figure A3-3. Here, the tremendous number of

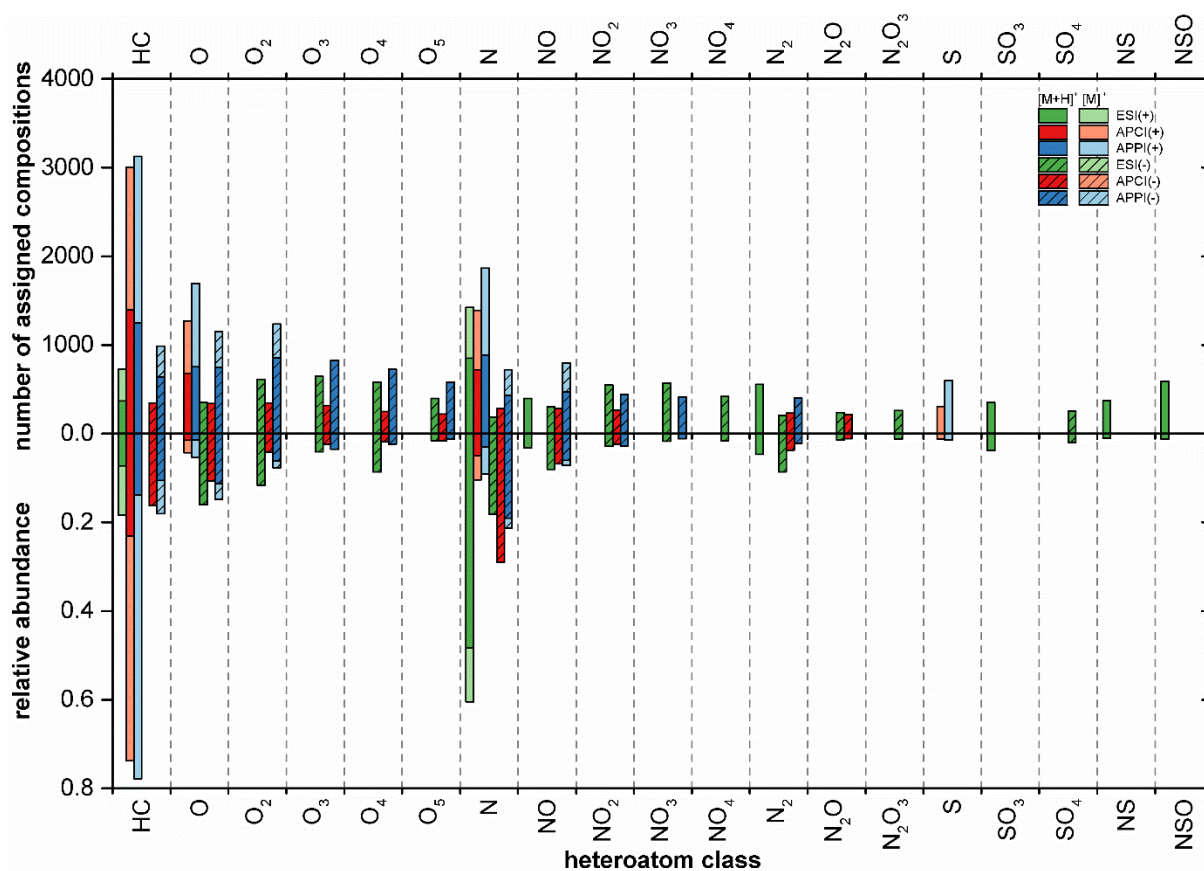


Figure 3-4. Population (top) and intensity (bottom) based class distributions for the original contaminated soil, analyzed by positive and negative mode ESI (green), APCI (red) and APPI (blue) FT Orbitrap MS, only classes with relative abundance higher than 1% are shown.

compositions detected by ultrahigh resolution FTMS was sorted based on their chemical formulas. In both plots elemental compositions were grouped according to their heteroatom content with pure hydrocarbons forming the HC class. Depending on the ionization methods utilized (shown in individual colors), both, protonated molecules $[M+H]^+$ and radical ions $[M]^+$ can be formed. This is commonly observed in APCI and APPI mass spectra but sometimes also in ESI spectra radical ions can appear.^{35, 43} Radical ions are differentiated from protonated molecules in the same class by applying slightly lighter colors. Additionally, results from negative mode measurements are depicted as shaded bars.

As already indicated by the Venn diagrams, in the positive measurements APCI offered similar results compared to APPI. In both methods pure hydrocarbons with around 3,000 compositions including protonated molecules and radical ions presented the most abundant class (around 75%), followed by N (9-10%), O (4-5%) and finally S (1%) classes with around 1,400, 1,300 and 300 detected compositions in APCI(+) and 1,900, 1,700 and 600 in APPI+, respectively. ESI(+) provided a similar number of assignments for the N class (1,400). However, the N class was already the most abundant class in the spectrum with over 60% relative intensity.

The N class, also showed the highest intensity in the negative mode mass spectra for all ionization methods (ESI(-) (18%), APCI(-) (29%), APPI(-) (21%)). However, the compounds detected in positive and in negative mode differ from each other, especially when ESI is used. Unlike the N species detected in the positive mode, which are supposed to be mainly basic nitrogen compounds, such as pyridine, the N species in the negative mode comprise pyrrole-like neutral compounds.^{46, 47}

Besides, acidic oxygenated classes could also be ionized easily in the negative mode. For oxidized hydrocarbons (O_x) and nitrogen containing compounds (NO_x) APPI(-) delivered the highest number of assignments, followed by ESI(-) then APCI(-). Few SO_x compounds were found, which is in line with the overall low sulfur content found in the contaminated soil extract.³¹

Overall, the results show that the organic extract from the contaminated soil is highly enriched in pure and nitrogen containing hydrocarbons in addition to their oxidized derivatives.

3.4.5. ESI Measurements

The class distributions shown in Figure 3-4 reveal a wide array of different classes and a large number of assigned molecular compositions within each class. One way that allows a deeper

understanding of the details of one class is the representation in a Kendrick plot as shown in Figure 3-5, where the DBE of a detected composition is plotted against its number of carbon atoms in the molecule.

A detailed look at the N-class obtained from ESI measurements reveals that the results from the contaminated soil extract (first column) present a large but narrow distribution for both negative and positive mode measurements. At a given DBE the distribution is only 5 (ESI(-)) to 10 (ESI(+)) C-atoms wide, indicating the presence of only short aliphatic side chains attached to the aromatic cores. Most compositions have a DBE higher than 7 while reaching values above 50 in ESI(+), which implies highly aromatized PANH being present in the contaminated soil.^{46,47}

The data from the crude oil spiked sand sample on the other hand show a different distribution. Here, lower DBE values are detected while having much broader distributions at a given DBE (over 30 C-atoms) than the ones from the contaminated soil sample. This difference in pattern directly refers to differences in the origin of the PAH contamination, which, in the case of the contaminated soil sample, is obviously not caused by crude oil.

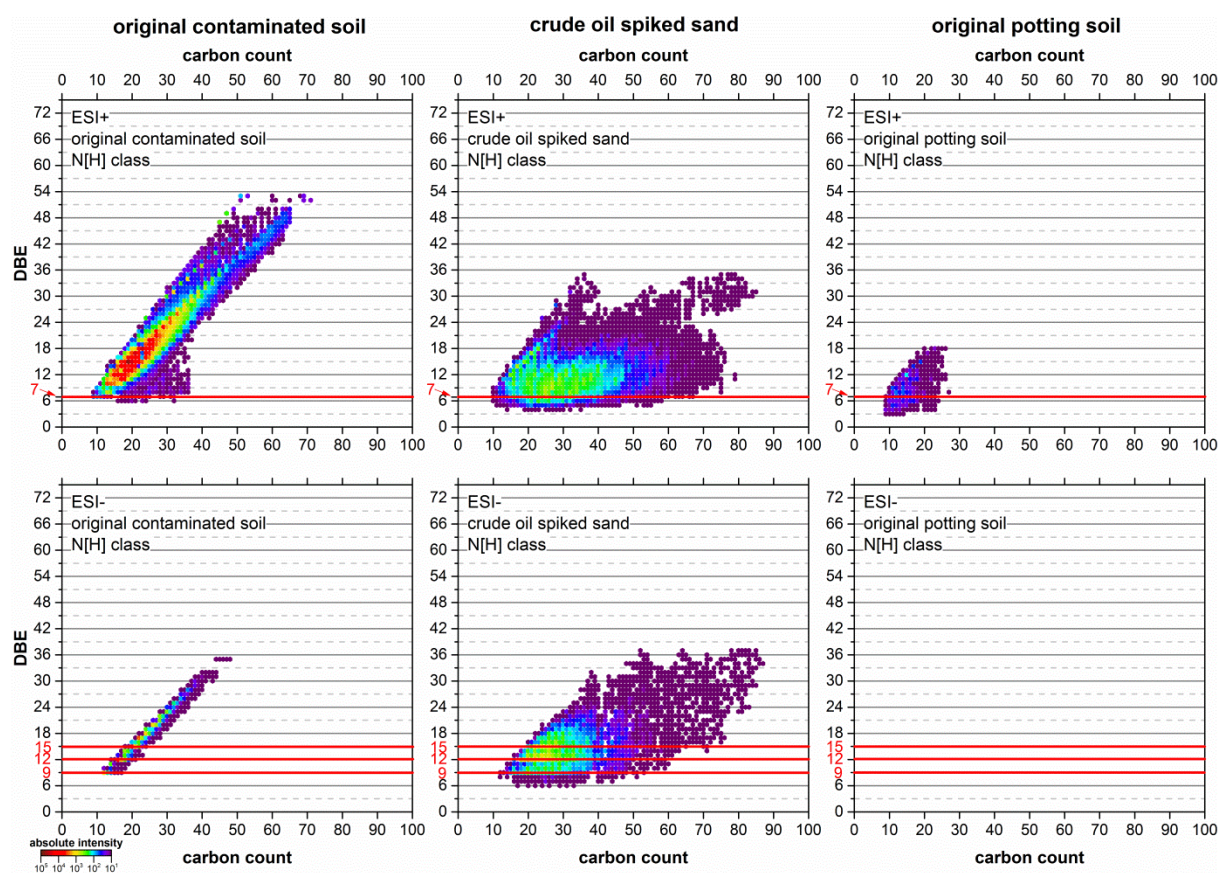


Figure 3-5. Kendrick plots for protonated/deprotonated N class after positive (top) and negative (bottom) mode multiple ionization methods.

In the potting soil extract, almost no nitrogen containing compounds were found, as can be expected for an uncontaminated sample. The few detected compounds can be attributed to natural soil organic material.

3.4.6. APPI Measurements

The broadest datasets have been obtained by APPI measurements. Figure 3-6 shows DBE distributions of all classes observed with an intensity higher than 1%. Highly condensed compositions with DBE values up to 70 were found in the contaminated soil extract. Such extremely high values are, to the best of our knowledge, reported here for the first time for a non-targeted soil analysis. In comparison, the extract from the crude oil spiked sand only shows DBE values up to 50 (Figure A3-4), which is in good agreement with earlier data obtained by APPI Orbitrap MS.²⁴ This also indicates the very high aromaticity of the compounds detected in the extract from the contaminated soil.

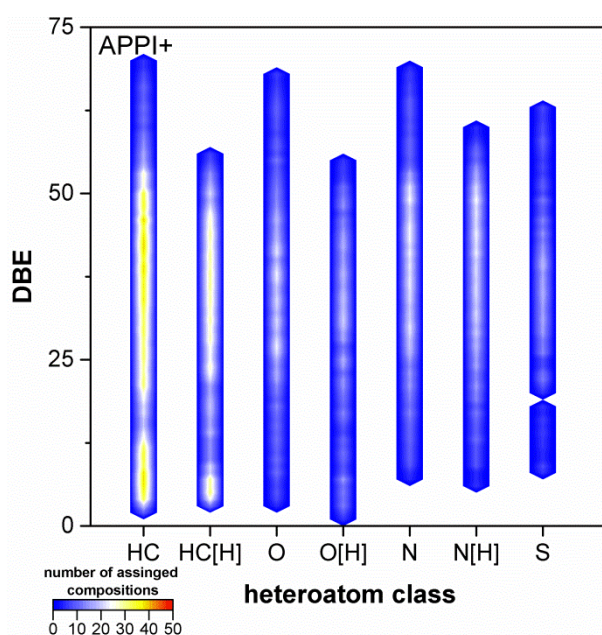


Figure 3-6. Population based DBE vs. class distribution for the original contaminated soil extract. Only classes with relative abundance higher than 1% are shown.

For all heteroatom classes a broad distribution of compounds with high amounts of assignments between approximately DBE 20 to 55 is observed. In case of pure hydrocarbons (HC and HC[H]), however, an additional distribution is present that ranges from DBE 2 to 12. Compositions from the spiked sand sample or the uncontaminated potting soil sample on the other hand only covered lower DBE ranges of 2 to 30 and 2 to 15, respectively (Figure A3-4).

The Kendrick plot shown in Figure 3-7 (DBE vs number of carbon atoms per molecule⁴⁸) provides more detailed information on the pure hydrocarbons on a molecular level since every

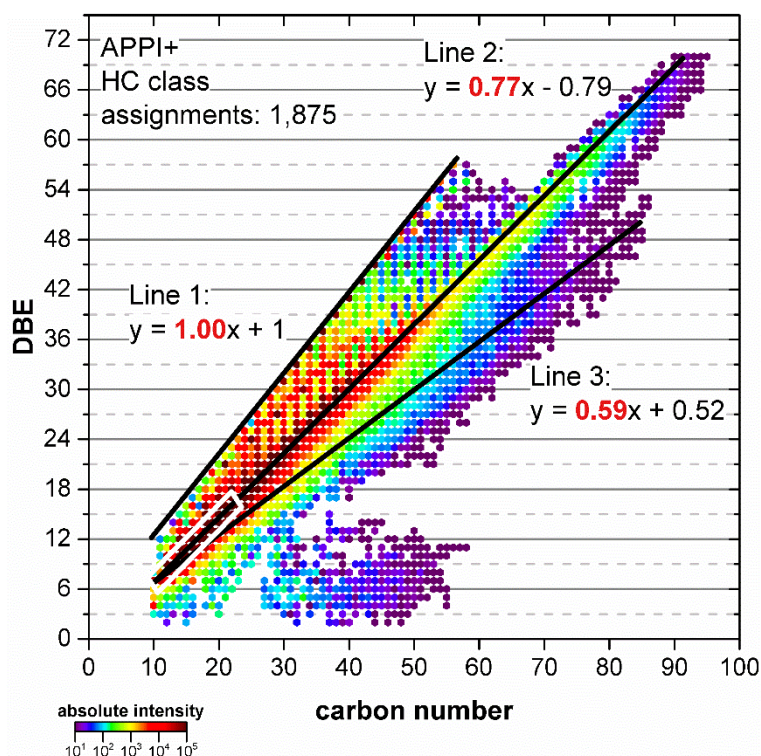


Figure 3-7. Kendrick plot for HC class from the original contaminated soil extract, analyzed using positive mode APPI FTMS.

detected composition is represented by a single data point. The 16 EPA PAHs (in total 10 elemental compositions), all fall into the region which is highlighted by the white rectangle. Additionally, other 1,865 elemental compositions have been found as radical hydrocarbons. The number of detected compounds will be multiple times higher, since the possible isomers for a single composition cannot be distinguished here. An indication of the isomeric variance might be obtained from MS/MS measurements.⁴⁸

When studying the Kendrick plot in Figure 3-7 several trends of local intensity maxima can be noticed that can be connected by a straight line. Three such trend lines have been recognized, from which the individual slope can be calculated.

The first one (line 1) with a slope of 1 is the so-called planar limit, which defines the maximum DBE value for a given carbon number.⁴⁹ The same planar limit was also observed for the radical HC class from the spiked sand and potting soil extracts (Figure A3-5). The compositions with the highest intensity at a given carbon are covered by line 2 with a slope of 0.77. Additionally, the 16 EPA PAHs, indicated by a white box are located around this line. A different series of hydrocarbons is distributed around another line with a more shallow slope of 0.59 (line 3).

Figure 3-8A shows how to correlate the slope information to structural details. Structures and their associated chemical formulas are summarized in Figure 3-8B. Starting with anthracene (DBE of 10 and 14 carbon atoms), the prolongation of saturated side chains e.g. by insertion of C_4H_8 will not change the DBE value of the molecule, which leads to a slope of 0 (Line I). When adding saturated rings with a C_4H_6 unit this will result in a slope of 0.25 (Line II). By incorporating an unsaturation into the ring, the slope increases further from 0.5 (Line III) over 0.63 (line IV) to 0.75 (line V), which corresponds to the linear or bent addition of aromatic rings (C_4H_2), thus leading to catacondensed compounds, i.e. compounds where only two rings share common carbon atoms.⁵⁰ Adding unsaturated rings (addition of C_2) into armchair configured catacondensed aromatized systems, for example benzo[*c*]picene as in Figure 3-8B, generates the highest slope of 1 (line VI). This leads to pericondensed compounds, where three (or more) ring systems share common carbon atoms.

Coming back to the hydrocarbons found in the contaminated soil extract (Figure 3-7), these show a major intensity along line 2 with a slope of 0.77. This implies the catacondensation of aromatic rings to different core-compounds, such as the 16 EPA PAH. The hydrocarbons along line 3 with a slope of 0.59 contain not fully aromatized rings. A possible way to achieve this is to alternately add benzene and cyclohexene, which results a slope of 0.63 (Figure 3-8A and B). This procedure allows summarizing the data of an extremely complex contamination of unknown compounds and can give an idea of the correlation among the different structural entities present.

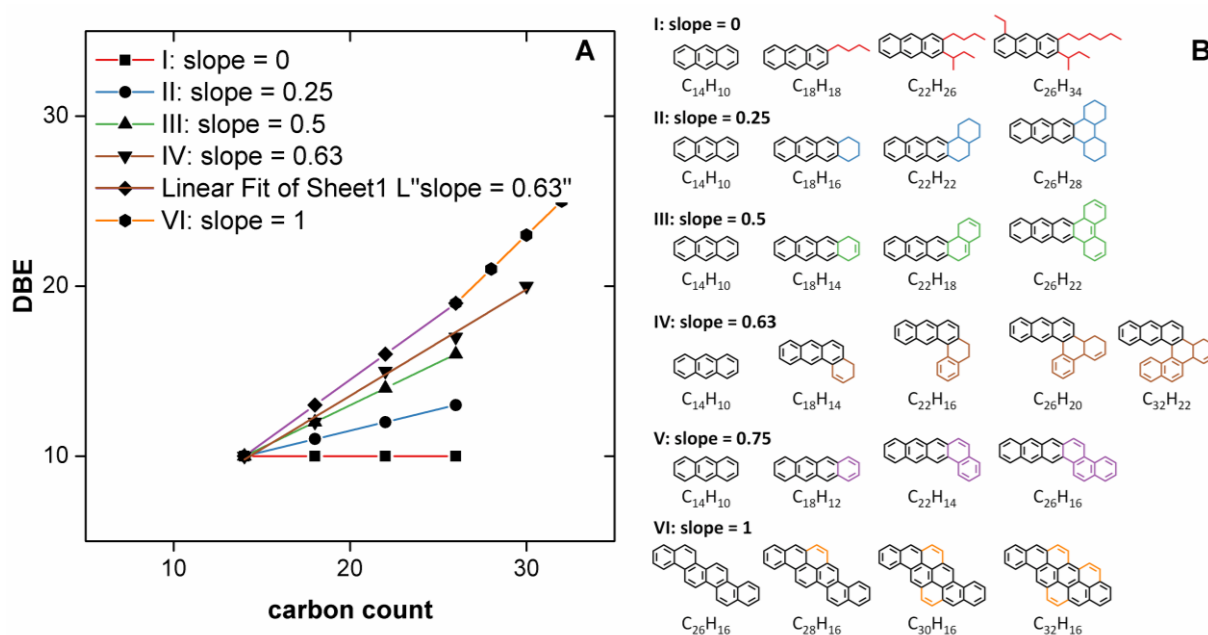


Figure 3-8. Kendrick plot for the slope calculation (A) with the corresponding proposed possible structures (B).

All the data summarized here show that a large variety of PAXH can present in the environment. Anthropogenic contaminations have increased the overall level of PAH in any soil sample.^{3,51,52} This means, that the contaminations are a constant threat due to the toxicity and mutagenicity of the different compounds. But since the regulations are 50 years behind the development of science, the contaminations are more complex than actually considered. There are little toxicological or ecotoxicological data available, especially for PAXH with more than 7 rings.²

New regulations need to be developed that are in agreement with the real contaminations. Ecotoxicologists need to be able to assess the danger of what is really present in the contaminated sites.

3.5. Conclusion

As the results have shown here, the number of PAH is much higher than what is routinely covered. We could demonstrate that besides the 16 EPA PAH a large quantity of other PAH can be found in the contaminated soil. An analytical method is presented here that instead of the standard 16 PAH compounds reveals about 1,000 times more elemental compositions of PAH contaminants. Considering the fact, that isomeric compounds are excluded, this reveals that the complexity of PAH contamination is much bigger than generally discussed. Although it is very difficult to study detailed compound structures in complex systems,⁴⁸ the utilization of the trend line approach in Kendrick plots shown here allows the characterization of the basic structures in PAH contaminations in an extremely complex sample.

The short length of sidechains (from 0 to 10 carbon atoms) indicates that the origin of the contamination is pyrogenic rather than petrogenic or biogenic, meaning that the contaminants were generated through rapid combustion or pyrolysis of organic matter.³ These results fit well to our suggestion that the soil originates from a former coking site, where it has been contaminated with high amounts of tar oil residues.

3.6. References

1. Richardson, S. D.; Kimura, S. Y., Emerging environmental contaminants: Challenges facing our next generation and potential engineering solutions. *Environ. Technol. Innov* **2017**, *8*, 40-56.
2. Achten, C.; Andersson, J. T., Overview of Polycyclic Aromatic Compounds (PAC). *Polycycl. Aromat. Comp.* **2015**, *35*, (2-4), 177-186.
3. Stout, S. A.; Emsbo-Mattingly, S. D.; Douglas, G. S.; Uhler, A. D.; McCarthy, K. J., Beyond 16 Priority Pollutant PAHs: A Review of PACs used in Environmental Forensic Chemistry. *Polycycl. Aromat. Comp.* **2015**, *35*, (2-4), 285-315.

4. Manzetti, S., Polycyclic Aromatic Hydrocarbons in the Environment: Environmental Fate and Transformation. *Polycycl. Aromat. Comp.* **2013**, *33*, (4), 311-330.
5. SEC(2006)1165, Commission staff working document, accompany document to the communication from the commission to the council, the European parliament, the European economic and social committee and the committee of the regions, thematic strategy for soil protection, summary of the impact assessment; COMMISSION OF THE EUROPEAN COMMUNITIES: 2006.
6. Keith, L.; Telliard, W., ES&T Special Report: Priority pollutants: I-a perspective view. *Environ. Sci. Technol.* **1979**, *13*, (4), 416-423.
7. Keith, L. H., The Source of U.S. EPA's Sixteen PAH Priority Pollutants. *Polycycl. Aromat. Comp.* **2015**, *35*, (2-4), 147-160.
8. Andersson, J. T.; Achten, C., Time to Say Goodbye to the 16 EPA PAHs? Toward an Up-to-Date Use of PACs for Environmental Purposes. *Polycycl. Aromat. Comp.* **2015**, *35*, (2-4), 330-354.
9. Achten, C.; Hofmann, T., Native polycyclic aromatic hydrocarbons (PAH) in coals – A hardly recognized source of environmental contamination. *Sci. Total Environ.* **2009**, *407*, (8), 2461-2473.
10. Saha, M.; Togo, A.; Mizukawa, K.; Murakami, M.; Takada, H.; Zakaria, M. P.; Chiem, N. H.; Tuyen, B. C.; Prudente, M.; Boonyatumanond, R.; Sarkar, S. K.; Bhattacharya, B.; Mishra, P.; Tana, T. S., Sources of sedimentary PAHs in tropical Asian waters: Differentiation between pyrogenic and petrogenic sources by alkyl homolog abundance. *Mar. Pollut. Bull.* **2009**, *58*, (2), 189-200.
11. McGregor, L. A.; Gauchotte-Lindsay, C.; Nic Daéid, N.; Thomas, R.; Kalin, R. M., Multivariate Statistical Methods for the Environmental Forensic Classification of Coal Tars from Former Manufactured Gas Plants. *Environ. Sci. Technol.* **2012**, *46*, (7), 3744-3752.
12. Hindersmann, B.; Achten, C., Accelerated benzene polycarboxylic acid analysis by liquid chromatography–time-of-flight–mass spectrometry for the determination of petrogenic and pyrogenic carbon. *J. Chromatogr. A.* **2017**, *1510*, 57-65.
13. Hindersmann, B.; Förster, A.; Achten, C., Novel and specific source identification of PAH in urban soils: Alk-PAH-BPCA index and “V”-shape distribution pattern. *Environ. Pollut.* **2020**, *257*, 113594.
14. Jautzy, J. J.; Ahad, J. M. E.; Hall, R. I.; Wiklund, J. A.; Wolfe, B. B.; Gobeil, C.; Savard, M. M., Source Apportionment of Background PAHs in the Peace-Athabasca Delta (Alberta, Canada) Using Molecular Level Radiocarbon Analysis. *Environ. Sci. Technol.* **2015**, *49*, (15), 9056-9063.
15. Chibwe, L.; Davie-Martin, C. L.; Aitken, M. D.; Hoh, E.; Massey Simonich, S. L., Identification of polar transformation products and high molecular weight polycyclic aromatic hydrocarbons (PAHs) in contaminated soil following bioremediation. *Sci. Total Environ.* **2017**, *599*, 1099-1107.
16. Richter-Brockmann, S.; Achten, C., Analysis and toxicity of 59 PAH in petrogenic and pyrogenic environmental samples including dibenzopyrenes, 7H-benzo[c]fluorene, 5-methylchrysene and 1-methylpyrene. *Chemosphere* **2018**, *200*, 495-503.
17. Lundstedt, S.; Bandowe, B. A. M.; Wilcke, W.; Boll, E.; Christensen, J. H.; Vila, J.; Grifoll, M.; Faure, P.; Biache, C.; Lorgeoux, C.; Larsson, M.; Frech Irgum, K.; Ivarsson, P.; Ricci, M., First intercomparison study on the analysis of oxygenated polycyclic aromatic hydrocarbons (oxy-PAHs) and nitrogen heterocyclic polycyclic aromatic compounds (N-PACs) in contaminated soil. *TrAC-Trend. Anal. Chem.* **2014**, *57*, 83-92.
18. Bandowe, B. A. M.; Lueso, M. G.; Wilcke, W., Oxygenated polycyclic aromatic hydrocarbons and azaarenes in urban soils: A comparison of a tropical city (Bangkok)

- with two temperate cities (Bratislava and Gothenburg). *Chemosphere* **2014**, *107*, 407-414.
19. Wilcke, W.; Bandowe, B. A. M.; Lueso, M. G.; Ruppenthal, M.; del Valle, H.; Oelmann, Y., Polycyclic aromatic hydrocarbons (PAHs) and their polar derivatives (oxygenated PAHs, azaarenes) in soils along a climosequence in Argentina. *Sci. Total Environ.* **2014**, *473*, 317-325.
 20. Manzano, C. A.; Marvin, C.; Muir, D.; Harner, T.; Martin, J.; Zhang, Y., Heterocyclic Aromatics in Petroleum Coke, Snow, Lake Sediments, and Air Samples from the Athabasca Oil Sands Region. *Environ. Sci. Technol.* **2017**, *51*, (10), 5445-5453.
 21. Tian, Z.; Vila, J.; Wang, H.; Bodnar, W.; Aitken, M. D., Diversity and Abundance of High-Molecular-Weight Azaarenes in PAH-Contaminated Environmental Samples. *Environ. Sci. Technol.* **2017**, *51*, (24), 14047-14054.
 22. Panda, S. K.; Andersson, J. T.; Schrader, W., Characterization of Supercomplex Crude Oil Mixtures: What Is Really in There? *Angew. Chem. Int. Edit* **2009**, *48*, (10), 1788-1791.
 23. Stanford, L. A.; Kim, S.; Klein, G. C.; Smith, D. F.; Rodgers, R. P.; Marshall, A. G., Identification of water-soluble heavy crude oil organic-acids, bases, and neutrals by electrospray ionization and field desorption ionization Fourier transform ion cyclotron resonance mass spectrometry. *Environ. Sci. Technol.* **2007**, *41*, (8), 2696-2702.
 24. Vetere, A.; Schrader, W., Mass Spectrometric Coverage of Complex Mixtures: Exploring the Carbon Space of Crude Oil. *ChemistrySelect* **2017**, *2*, (3), 849-853.
 25. Vetere, A.; Profrock, D.; Schrader, W., Quantitative and Qualitative Analysis of Three Classes of Sulfur Compounds in Crude Oil. *Angew. Chem. Int. Edit* **2017**, *56*, (36), 10933-10937.
 26. Tfaily, M. M.; Chu, R. K.; Tolić, N.; Roscioli, K. M.; Anderton, C. R.; Paša-Tolić, L.; Robinson, E. W.; Hess, N. J., Advanced Solvent Based Methods for Molecular Characterization of Soil Organic Matter by High-Resolution Mass Spectrometry. *Anal. Chem.* **2015**, *87*, (10), 5206-5215.
 27. Guigue, J.; Harir, M.; Mathieu, O.; Lucio, M.; Ranjard, L.; Lévêque, J.; Schmitt-Kopplin, P., Ultrahigh-resolution FT-ICR mass spectrometry for molecular characterisation of pressurised hot water-extractable organic matter in soils. *Biogeochemistry* **2016**, *128*, (3), 307-326.
 28. Fleury, G.; Del Nero, M.; Barillon, R., Effect of mineral surface properties (alumina, kaolinite) on the sorptive fractionation mechanisms of soil fulvic acids: Molecular-scale ESI-MS studies. *Geochim. Cosmochim. Ac.* **2017**, *196*, 1-17.
 29. Tfaily, M. M.; Chu, R. K.; Toyoda, J.; Tolic, N.; Robinson, E. W.; Pasa-Tolic, L.; Hess, N. J., Sequential extraction protocol for organic matter from soils and sediments using high resolution mass spectrometry. *Anal. Chim. Acta* **2017**, *972*, 54-61.
 30. Headley, J. V.; Peru, K. M.; Barrow, M. P., Advances in mass spectrometric characterization of naphthenic acids fraction compounds in oil sands environmental samples and crude oil—A review. *Mass Spectrom. Rev.* **2016**, *35*, (2), 311-328.
 31. Noah, M.; Poetz, S.; Vieth-Hillebrand, A.; Wilkes, H., Detection of Residual Oil-Sand-Derived Organic Material in Developing Soils of Reclamation Sites by Ultra-High-Resolution Mass Spectrometry. *Environ. Sci. Technol.* **2015**, *49*, (11), 6466-6473.
 32. Barrow, M. P.; Peru, K. M.; Headley, J. V., An Added Dimension: GC Atmospheric Pressure Chemical Ionization FTICR MS and the Athabasca Oil Sands. *Anal. Chem.* **2014**, *86*, (16), 8281-8288.
 33. Thomas, M. J.; Collinge, E.; Witt, M.; Palacio Lozano, D. C.; Vane, C. H.; Moss-Hayes, V.; Barrow, M. P., Petroleomic depth profiling of Staten Island salt marsh soil:

- 2 ω detection FTICR MS offers a new solution for the analysis of environmental contaminants. *Sci. Total Environ.* **2019**, *662*, 852-862.
34. Hertkorn, N.; Frommberger, M.; Witt, M.; Koch, B. P.; Schmitt-Kopplin, P.; Perdue, E. M., Natural Organic Matter and the Event Horizon of Mass Spectrometry. *Anal. Chem.* **2008**, *80*, (23), 8908-8919.
 35. Gaspar, A.; Zellermann, E.; Lababidi, S.; Reece, J.; Schrader, W., Impact of Different Ionization Methods on the Molecular Assignments of Asphaltenes by FT-ICR Mass Spectrometry. *Anal. Chem.* **2012**, *84*, (12), 5257-5267.
 36. Ohno, T.; Sleighter, R. L.; Hatcher, P. G., Comparative study of organic matter chemical characterization using negative and positive mode electrospray ionization ultrahigh-resolution mass spectrometry. *Anal. Bioanal. Chem.* **2016**, *408*, (10), 2497-2504.
 37. Luo, R.; Schrader, W., Development of a Non-Targeted Method to Study Petroleum Polyaromatic Hydrocarbons in Soil by Ultrahigh Resolution Mass Spectrometry Using Multiple Ionization Methods. *Polycycl. Aromat. Comp.* **2020**, 1-16.
 38. Southam, A. D.; Payne, T. G.; Cooper, H. J.; Arvanitis, T. N.; Viant, M. R., Dynamic range and mass accuracy of wide-scan direct infusion nanoelectrospray Fourier transform ion cyclotron resonance mass spectrometry-based metabolomics increased by the spectral stitching method. *Anal. Chem.* **2007**, *79*, (12), 4595-4602.
 39. Gaspar, A.; Schrader, W., Expanding the data depth for the analysis of complex crude oil samples by Fourier transform ion cyclotron resonance mass spectrometry using the spectral stitching method. *Rapid Commun. Mass Spectrom.* **2012**, *26*, (9), 1047-1052.
 40. Hollender, J.; Koch, B.; Lutermann, C.; Dott, W., Efficiency of different methods and solvents for the extraction of polycyclic aromatic hydrocarbons from soils. *Intern. J. Environ. Anal. Chem.* **2003**, *83*, (1), 21-32.
 41. Wang, W.; Meng, B.; Lu, X.; Liu, Y.; Tao, S., Extraction of polycyclic aromatic hydrocarbons and organochlorine pesticides from soils: A comparison between Soxhlet extraction, microwave-assisted extraction and accelerated solvent extraction techniques. *Anal. Chim. Acta* **2007**, *602*, (2), 211-222.
 42. Itoh, N.; Numata, M.; Aoyagi, Y.; Yarita, T., Comparison of low-level polycyclic aromatic hydrocarbons in sediment revealed by Soxhlet extraction, microwave-assisted extraction, and pressurized liquid extraction. *Anal. Chim. Acta* **2008**, *612*, (1), 44-52.
 43. Molnárné Guricza, L.; Schrader, W., Electrospray ionization for determination of non - polar polyaromatic hydrocarbons and polyaromatic heterocycles in heavy crude oil asphaltenes. *J. Mass Spectrom.* **2015**, *50*, (3), 549-557.
 44. Hulsen, T.; de Vlieg, J.; Alkema, W., BioVenn – a web application for the comparison and visualization of biological lists using area-proportional Venn diagrams. *BMC Genomics* **2008**, *9*, (1), 488.
 45. Vecchiato, M.; Bonato, T.; Bertin, A.; Argiriadis, E.; Barbante, C.; Piazza, R., Plant residues as direct and indirect sources of hydrocarbons in soils: current issues and legal implications. *Environ. Sci. Tech. Let.* **2017**, *4*, (12), 512-517.
 46. Purcell, J.; Rodgers, R.; Hendrickson, C.; Marshall, A., Speciation of nitrogen containing aromatics by atmospheric pressure photoionization or electrospray ionization fourier transform ion cyclotron resonance mass spectrometry. *J Am Soc Mass Spectrom* **2007**, *18*, (7), 1265-1273.
 47. Tong, J.; Liu, J.; Han, X.; Wang, S.; Jiang, X., Characterization of nitrogen-containing species in Huadian shale oil by electrospray ionization Fourier transform ion cyclotron resonance mass spectrometry. *Fuel* **2013**, *104*, (0), 365-371.

48. Vetere, A.; Alachraf, W.; Panda, S. K.; Andersson, J. T.; Schrader, W., Studying the fragmentation mechanism of selected components present in crude oil by CID mass spectrometry. *Rapid Commun. Mass Spectrom.* **2018**, *32*, (24), 2141-2151.
49. Cho, Y.; Kim, Y. H.; Kim, S., Planar Limit-Assisted Structural Interpretation of Saturates/Aromatics/Resins/Asphaltenes Fractionated Crude Oil Compounds Observed by Fourier Transform Ion Cyclotron Resonance Mass Spectrometry. *Anal. Chem.* **2011**, *83*, (15), 6068-6073.
50. Balaban, A. T.; Brunvoll, J.; Cioslowski, J.; Cyvin, B. N.; Cyvin, S. J.; Gutman, I.; He, W.; He, W.; Knop, J. V.; Kovačević, M.; Müller, W. R.; Szymanski, K.; Tošić, R.; Trinajstić, N., Enumeration of Benzenoid and Coronoid Hydrocarbons. *Z. Naturforsch. A* **1987**, *42*, (8), 863-870.
51. Wilcke, W., Global patterns of polycyclic aromatic hydrocarbons (PAHs) in soil. *Geoderma* **2007**, *141*, (3), 157-166.
52. Kuppusamy, S.; Thavamani, P.; Venkateswarlu, K.; Lee, Y. B.; Naidu, R.; Megharaj, M., Remediation approaches for polycyclic aromatic hydrocarbons (PAHs) contaminated soils: Technological constraints, emerging trends and future directions. *Chemosphere* **2017**, *168*, 944-968.

Appendix for Chapter 3

Table A3-1. Suggested molecular structures of 10 most abundant signals for the original contaminated soil extract, analyzed by positive mode ESI FT Orbitrap MS.

chemical formula	formula of detected ions	monoisotopic mass of detected ions	DBE	H/C	possible compounds	literature
C19H11N	[C19H11N+H] ⁺	254.096426	15	0.5789	azabenz[<i>a</i>]pyrene	1
C23H13N	[C23H13N+H] ⁺	304.112076	18	0.5652	Benzo[1,10]phenanthro[2,3,4- <i>de</i>]quinoline	4
C21H11N	[C21H11N+H] ⁺	278.096426	17	0.5238	7-Azabenz[<i>ghi</i>]perylene	5
C20H13N	[C20H13N+H] ⁺	268.112076	15	0.65	C1-azabenz[<i>a</i>]pyrene	1
C25H13N	[C25H13N+H] ⁺	328.112076	20	0.52	Diacenaphtho[1,2- <i>b</i> :1',2'- <i>e</i>]pyridine	6
C17H11N	[C17H11N+H] ⁺	230.096426	13	0.6471	benzo[<i>a</i>]acridine	1
C15H9N	[C15H9N+H] ⁺	204.080776	12	0.6	azapyrene	1
C21H13N	[C21H13N+H] ⁺	280.112076	16	0.619	Dibenz[<i>a,h</i>]acridine	1,2
C18H13N	[C18H13N+H] ⁺	244.112076	13	0.7222	C1-benzo[<i>a</i>]acridine	1
C21H15N	[C21H15N+H] ⁺	282.127726	15	0.7143	C2-azabenz[<i>a</i>]pyrene	1

Table A3-2. Suggested molecular structures of 10 most abundant signals for the original contaminated soil extract, analyzed by positive mode APCI FT Orbitrap MS.

chemical formula	formula of detected ions	monoisotopic mass of detected ions	DBE	H/C	possible compounds	literature
C20H12	[C20H12] ⁺	252.093352	15	0.6	Benzo[<i>a</i>]pyrene, Benzo[<i>b</i>]fluoranthene, Benzo[<i>k</i>]fluoranthene	16 EPA PAH
C24H14	[C24H14] ⁺	302.109002	18	0.5833	benzo[<i>b</i>]perylene	2,3
C16H10	[C16H10] ⁺	202.077702	12	0.625	Fluoranthene, Pyrene	16 EPA PAH
C26H14	[C26H14] ⁺	326.109002	20	0.5385	Dibenzo[<i>cd,lm</i>]perylene	2,3
C22H12	[C22H12] ⁺	276.093352	17	0.5455	Benzo[<i>ghi</i>]perylene, Indeno[1,2,3- <i>cd</i>]pyrene	16 EPA PAH
C18H12	[C18H12] ⁺	228.093352	13	0.6667	Benz[<i>a</i>]anthracene, Chrysene	16 EPA PAH
C22H14	[C22H14] ⁺	278.109002	16	0.6364	Dibenz[<i>a,h</i>]anthracene	16 EPA PAH
C12H8	[C12H8] ⁺	152.062052	9	0.6667	Acenaphthylene	16 EPA PAH
C28H14	[C28H14] ⁺	350.109002	22	0.5	Benzocoronene	2,3
C26H14	[C26H14+H] ⁺	327.116827	19.5	0.5385	Dibenzo[<i>cd,lm</i>]perylene	2,3

Table A3-3. Suggested molecular structures of 10 most abundant signals for the original contaminated soil extract, analyzed by positive mode APPI FT Orbitrap MS.

chemical formula	formula of detected ions	monoisotopic mass of detected ions	DBE	H/C	possible compounds	literature
C20H12	[C20H12] ⁺	252.093352	15	0.6	Benzo[<i>a</i>]pyrene, Benzo[<i>b</i>]fluoranthene, Benzo[<i>k</i>]fluoranthene	16 EPA PAH
C22H12	[C22H12] ⁺	276.093352	17	0.5455	Benzo[<i>ghi</i>]perylene, Indeno[1,2,3- <i>cd</i>]pyrene	16 EPA PAH
C26H14	[C26H14] ⁺	326.109002	20	0.5385	Dibenzo[<i>cd,lm</i>]perylene	2,3
C24H14	[C24H14] ⁺	302.109002	18	0.5833	benzo[<i>b</i>]perylene	2,3
C16H10	[C16H10] ⁺	202.077702	12	0.625	Fluoranthene, Pyrene	16 EPA PAH
C22H14	[C22H14] ⁺	278.109002	16	0.6364	Dibenz[<i>a,h</i>]anthracene	16 EPA PAH
C18H12	[C18H12] ⁺	228.093352	13	0.6667	Benz[<i>a</i>]anthracene, Chrysene	16 EPA PAH
C28H14	[C28H14] ⁺	350.109002	22	0.5	Benzocoronene	2,3
C30H16	[C30H16] ⁺	376.124652	23	0.5333	1,2,7,8-dibenzanthrene	2,3
C14H10	[C14H10] ⁺	178.077702	10	0.7143	Anthracene, Phenanthrene	16 EPA PAH

Table A3-4. Suggested molecular structures of 10 most abundant signals for the original contaminated soil extract, analyzed by negative mode ESI FT Orbitrap MS.

chemical formula	formula of detected ions	monoisotopic mass of detected ions	DBE	H/C	possible compounds	literature
C17H26O4	[C17H26O4-H] ⁻	293.175833	5	1.5294	4-[(10-Hydroxydecyl)oxy]benzoic acid	7
C16H10O	[C16H10O-H] ⁻	217.065888	12	0.625	1-Hydroxypyrene	2
C16H11N	[C16H11N-H] ⁻	216.081873	12	0.6875	7H-benzo[c]carbazole	8
C20H13N	[C20H13N-H] ⁻	266.097523	15	0.65	Dibenzo[<i>c,g</i>]carbazole	2
C20H12O	[C20H12O-H] ⁻	267.081539	15	0.6	3-Hydroxybenzo[<i>a</i>]pyrene	2
C9H18O2	[C9H18O2-H] ⁻	157.123403	1	2	1-nonanoic acid	9
C22H13N	[C22H13N-H] ⁻	290.097523	17	0.5909	4H-Benzo[<i>def</i>]naphtho[2,3- <i>b</i>]carbazole	10
C17H12O	[C17H12O-H] ⁻	231.081539	12	0.7059	2-Benzoylnaphthalene	11
C18H12N2	[C18H12N2-H] ⁻	255.092772	14	0.6667	5,11-Dihydroindolo[3,2- <i>b</i>]carbazole	12
C17H11NO	[C17H11NO-H] ⁻	244.076788	13	0.6471	3-Amino-7H-benzo[<i>de</i>]anthracen-7-one	2

Table A3-5. Suggested molecular structures of 10 most abundant signals for the original contaminated soil extract, analyzed by negative mode APCI FT Orbitrap MS.

chemical formula	formula of detected ions	monoisotopic mass of detected ions	DBE	H/C	possible compounds	literature
C26H15N	[C26H15N-H] ⁻	340.113173	20	0.5769	5H-Diindeno[2,1- <i>a</i> :2',1'- <i>c</i>]carbazole	13
C20H13N	[C20H13N-H] ⁻	266.097523	15	0.65	Dibenzo[<i>c,g</i>]carbazole	2
C24H15N	[C24H15N-H] ⁻	316.113173	18	0.625	Anthra[2,3- <i>c</i>]carbazole	14
C22H13N	[C22H13N-H] ⁻	290.097523	17	0.5909	4H-Benzo[<i>def</i>]naphtho[2,3- <i>b</i>]carbazole	10
C30H17N	[C30H17N-H] ⁻	390.128823	23	0.5667	Pyranthren-1-amine	17
C16H11N	[C16H11N-H] ⁻	216.081873	12	0.6875	7H-benzo[c]carbazole	8
C27H17N	[C27H17N-H] ⁻	354.128823	20	0.6296	10-Phenyldibenzo[<i>a,c</i>]phenanthridine	15
C28H15N	[C28H15N-H] ⁻	364.113173	22	0.5357	8-methylbenzo[6,7]perylene[1,12- <i>fg</i>]quinoline	Chemdraw
C28H17N	[C28H17N-H] ⁻	366.128823	21	0.6071	8H-Dinaphtho[2,3- <i>c</i> :2',3'- <i>g</i>]carbazole	16
C32H17N	[C32H17N-H] ⁻	414.128823	25	0.5312	Bispyrenopyrrole	18

Table A3-6. Suggested molecular structures of 10 most abundant signals for the original contaminated soil extract, analyzed by negative mode APPI FT Orbitrap MS.

chemical formula	formula of detected ions	monoisotopic mass of detected ions	DBE	H/C	possible compounds	literature
C20H13N	[C20H13N-H] ⁻	266.097523	15	0.5789	Dibenzo[<i>c,g</i>]carbazole	2
C24H15N	[C24H15N-H] ⁻	316.113173	18	0.5652	Anthra[2,3- <i>c</i>]carbazole	14
C22H13N	[C22H13N-H] ⁻	290.097523	17	0.5238	4H-Benzo[<i>def</i>]naphtho[2,3- <i>b</i>]carbazole	10
C26H15N	[C26H15N-H] ⁻	340.113173	15	0.65	5H-Diindeno[2,1- <i>a</i> :2',1'- <i>c</i>]carbazole	13
C26H14	[C26H14] ⁻	326.110099	20	0.52	Dibenzo[<i>cd,lm</i>]perylene	2,3
C16H11N	[C16H11N-H] ⁻	216.081873	13	0.6471	7H-benzo[c]carbazole	8
C30H16	[C30H16] ⁻	376.125749	12	0.6	1,2,7,8-dibenzanthrene	2,3
C28H15N	[C28H15N-H] ⁻	364.113173	16	0.619	8-methylbenzo[6,7]perylene[1,12- <i>fg</i>]quinoline	Chemdraw
C28H17N	[C28H17N-H] ⁻	366.128823	13	0.7222	8H-Dinaphtho[2,3- <i>c</i> :2',3'- <i>g</i>]carbazole	16
C32H16	[C32H16] ⁻	400.125749	15	0.7143	Dibenzo[<i>a,g</i>]coronene	2,3

Table A3-7. Properties of 16 EPA PAHs.

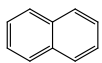
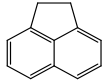
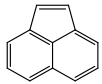
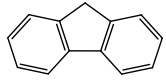
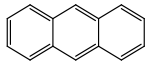
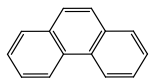
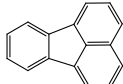
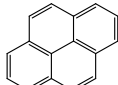
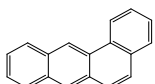
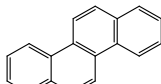
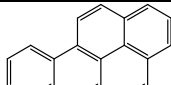
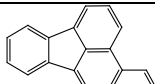
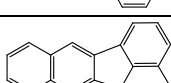
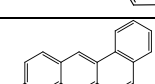
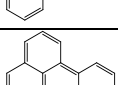
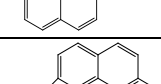
Compound name	chemical formula	CAS	monoisotopic mass	DBE	H/C	Structure
Naphthalene	C ₁₀ H ₈	91-20-3	128.06260	7	0.80	
Acenaphthene	C ₁₂ H ₁₀	83-32-9	154.07825	8	0.83	
Acenaphthylene	C ₁₂ H ₈	208-96-8	152.06260	9	0.67	
Fluorene	C ₁₃ H ₁₀	86-73-7	166.07825	9	0.77	
Anthracene	C ₁₄ H ₁₀	120-12-7	178.07825	10	0.71	
Phenanthrene	C ₁₄ H ₁₀	85-01-8	178.07825	10	0.71	
Fluoranthene	C ₁₆ H ₁₀	206-44-0	202.07825	12	0.63	
Pyrene	C ₁₆ H ₁₀	129-00-0	202.07825	12	0.63	
Benz[a]anthracene	C ₁₈ H ₁₂	56-55-3	228.09390	13	0.67	
Chrysene	C ₁₈ H ₁₂	218-01-9	228.09390	13	0.67	
Benzo[a]pyrene	C ₂₀ H ₁₂	50-32-8	252.09390	15	0.60	
Benzo[b]fluoranthene	C ₂₀ H ₁₂	205-99-2	252.09390	15	0.60	
Benzo[k]fluoranthene	C ₂₀ H ₁₂	207-08-9	252.09390	15	0.60	
Dibenz[a,h]anthracene	C ₂₂ H ₁₄	53-70-3	278.10955	16	0.64	
Benzo[ghi]perylene	C ₂₂ H ₁₂	191-24-2	276.09390	17	0.55	
Indeno[1,2,3-cd]pyrene	C ₂₂ H ₁₂	193-39-5	276.09390	17	0.55	

Table A3-8. Calculated mean values of m/z , DBE, number of carbon atoms and X/C for the spiked sand sample, analysed using different API-FT Orbitrap MS.

spiked sand	mean values						
	m/z	DBE	#C	H/C	N/C	O/C	S/C
ESI+	707.2	18	49	1.2886	0.0257	0.0154	0.0166
APCI+	568.9	15	39	1.2113	0.0101	0.0185	0.0295
APPI+	661.7	18	46	1.2003	0.0095	0.0287	0.0235
ESI-	464.8	8	29	1.4793	0.0118	0.1678	0.0129
APCI-	483.3	13	33	1.2269	0.0125	0.0927	0.0083
APPI-	635.2	20	43	1.1075	0.0185	0.0637	0.0238

Table A3-9. Calculated mean values of m/z , DBE, number of carbon atoms and X/C for the potting soil, analysed using different API-FT Orbitrap MS.

potting soil	mean values						
	m/z	DBE	#C	H/C	N/C	O/C	S/C
ESI+	731.8	20	51	1.2845	0.0202	0.0421	0.0080
APCI+	550.7	12	37	1.3146	0.0092	0.0759	0.0116
APPI+	507.8	12	34	1.3027	0.0099	0.0944	0.0104
ESI-	563.7	9	34	1.5061	0.0118	0.2081	0.0049
APCI-	682.0	17	46	1.3021	0.0140	0.0897	0.0077
APPI-	675.1	19	46	1.1930	0.0231	0.0849	0.0174

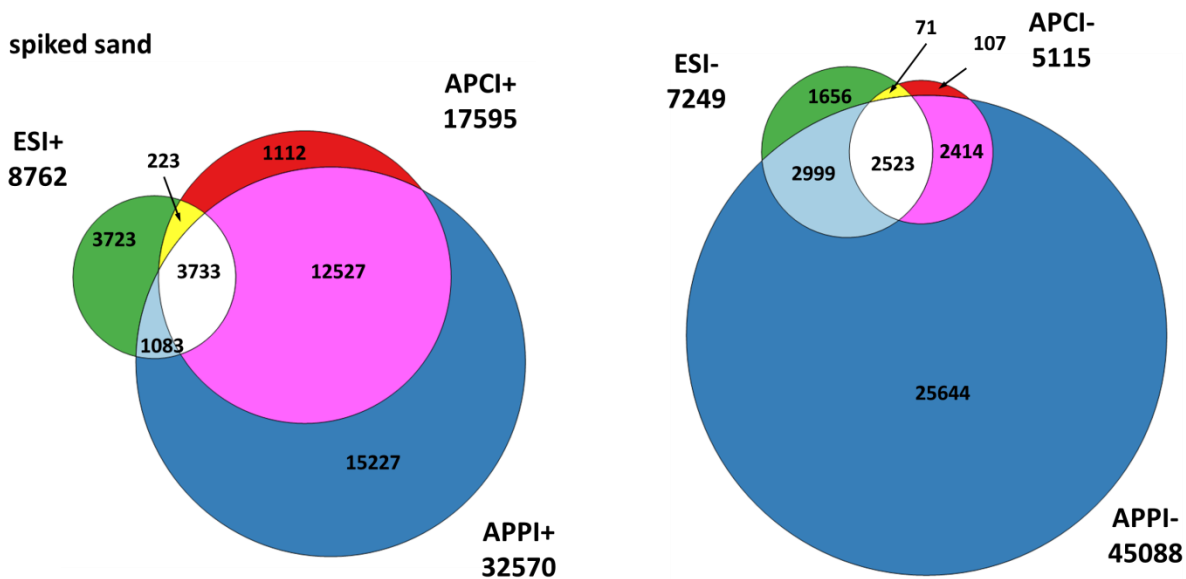


Figure A3-1. Venn diagrams for numbers of assigned compositions obtained using positive (left) and negative mode multiple ionization methods in the spiked sand.

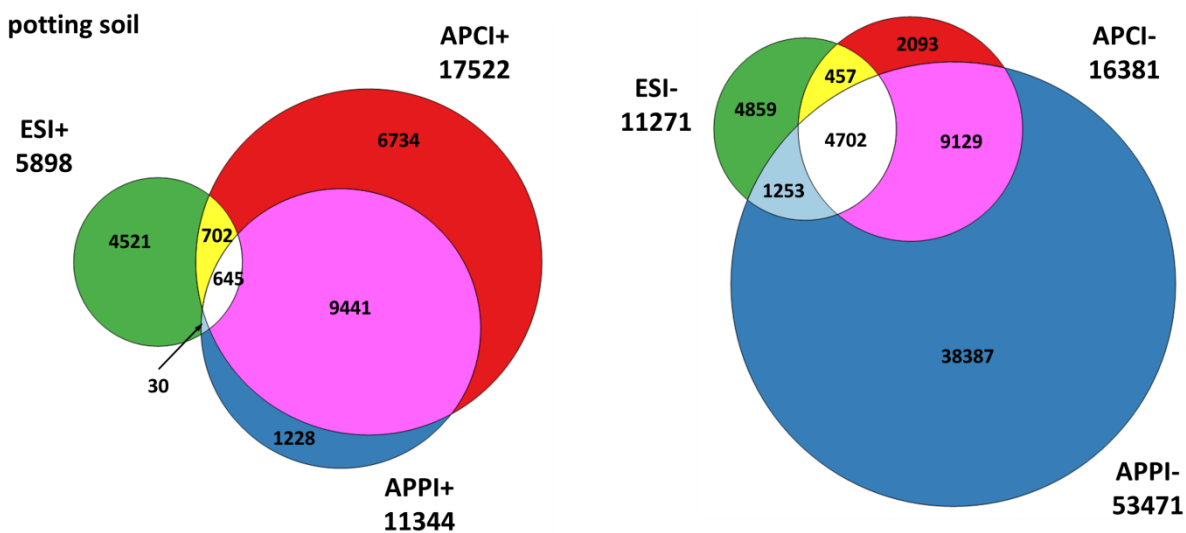


Figure A3-2. Venn diagrams for numbers of assigned compositions obtained using positive (left) and negative mode multiple ionization methods in the potting soil.

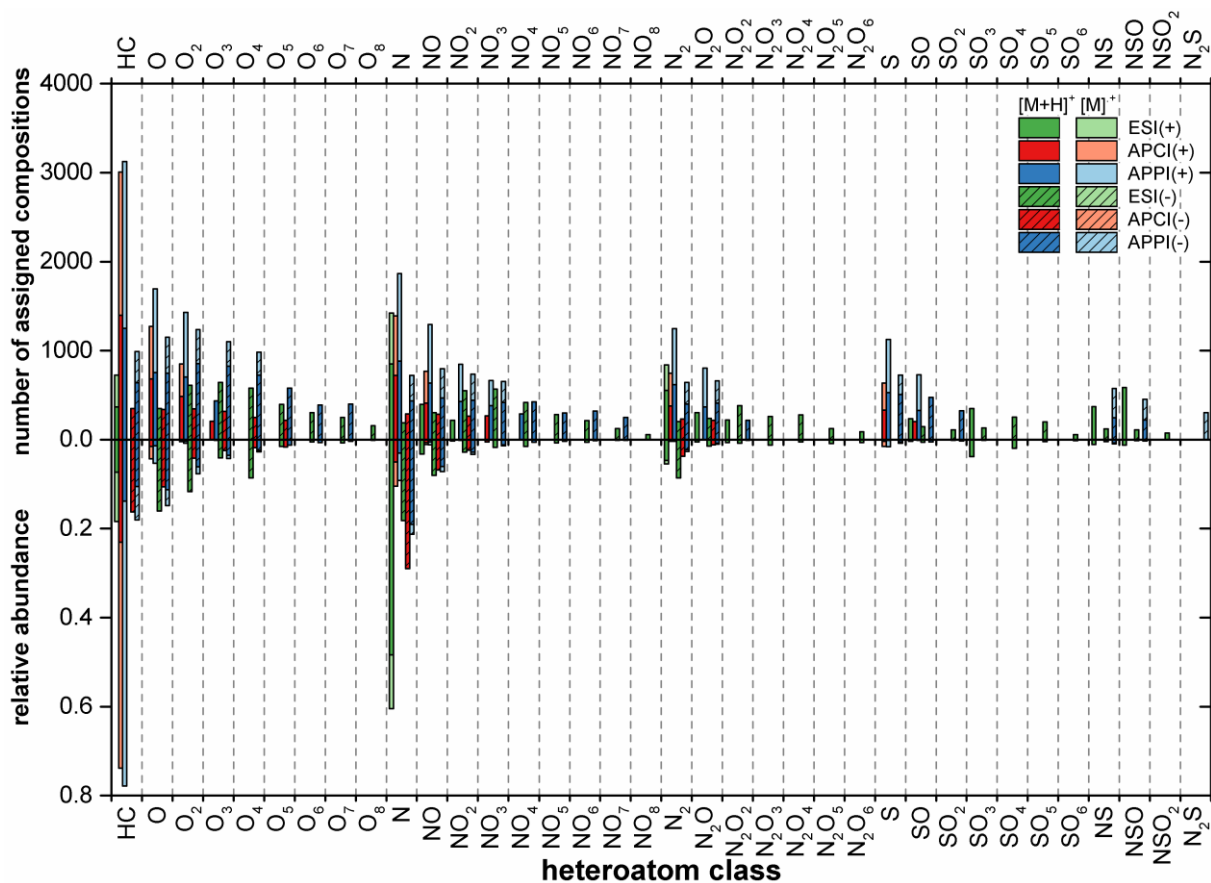


Figure A3-3. Population (top) and intensity (bottom) based class distributions for the contaminated soil, analysed by positive and negative mode ESI (green), APCI (red) and APPI (blue) FT Orbitrap MS.

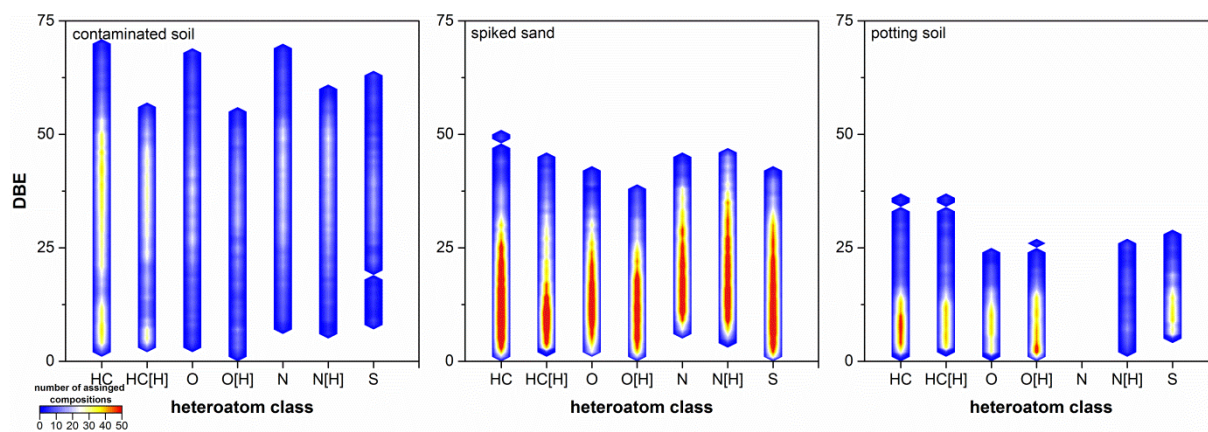


Figure A3-4. Population based DBE vs. class distribution for selected classes from contaminated soil (left), spiked sand (middle) and potting soil.

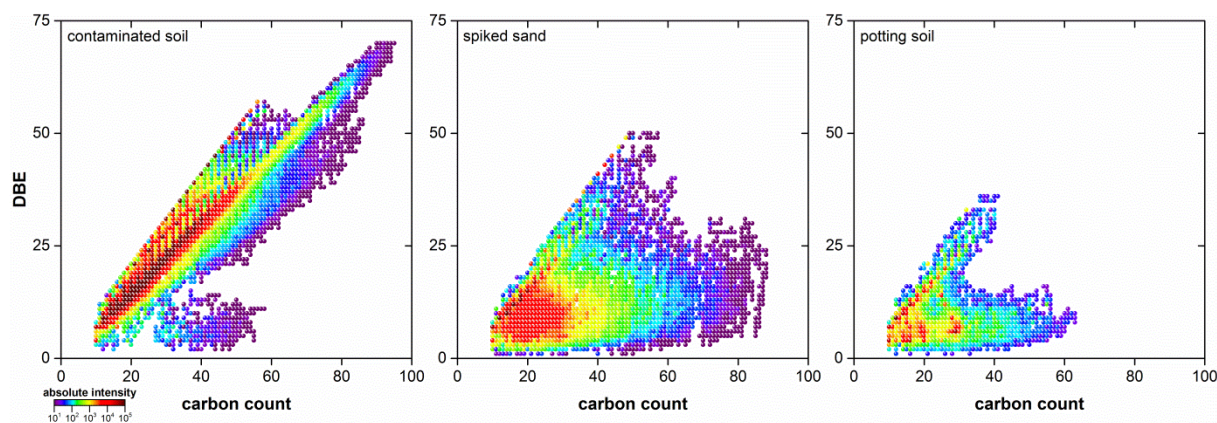


Figure A3-5. Kendrick plots for HC class from contaminated soil (left), spiked sand (middle) and potting soil.

References for the Appendix

1. Tian, Z.; Vila, J.; Wang, H.; Bodnar, W.; Aitken, M. D., Diversity and Abundance of High-Molecular-Weight Azaarenes in PAH-Contaminated Environmental Samples. *Environ. Sci. Technol.* **2017**, *51*, (24), 14047-14054.
2. Achten, C.; Andersson, J. T., Overview of Polycyclic Aromatic Compounds (PAC). *Polycycl. Aromat. Comp.* **2015**, *35*, (2-4), 177-186.
3. Zimmermann, R.; Vaeck, L. V.; Davidovic, M.; Beckmann, M.; Adams, F., Analysis of Polycyclic Aromatic Hydrocarbons (PAH) Adsorbed on Soot Particles by Fourier Transform Laser Microprobe Mass Spectrometry (FT LMMS): Variation of the PAH Patterns at Different Positions in the Combustion Chamber of an Incineration Plant. *Environ. Sci. Technol.* **2000**, *34*, (22), 4780-4788.
4. CSID:28706005, <http://www.chemspider.com/Chemical-Structure.28706005.html> (accessed 15:44, Jul 5, 2020)
5. CSID:9360089, <http://www.chemspider.com/Chemical-Structure.9360089.html> (accessed 15:48, Jul 5, 2020)
6. CSID:9407728, <http://www.chemspider.com/Chemical-Structure.9407728.html> (accessed 15:49, Jul 5, 2020)
7. CSID:14410459, <http://www.chemspider.com/Chemical-Structure.14410459.html> (accessed 15:51, Jul 5, 2020)
8. CSID:60784, <http://www.chemspider.com/Chemical-Structure.60784.html> (accessed 16:04, Jul 5, 2020)
9. CSID:7866, <http://www.chemspider.com/Chemical-Structure.7866.html> (accessed 16:03, Jul 5, 2020)
10. CSID:543789, <http://www.chemspider.com/Chemical-Structure.543789.html> (accessed 16:05, Jul 5, 2020)
11. CSID:62721, <http://www.chemspider.com/Chemical-Structure.62721.html> (accessed 16:07, Jul 5, 2020)

12. CSID:86517, <http://www.chemspider.com/Chemical-Structure.86517.html> (accessed 16:08, Jul 5, 2020)
13. CSID:25947775, <http://www.chemspider.com/Chemical-Structure.25947775.html> (accessed 16:10, Jul 5, 2020)
14. CSID:119932, <http://www.chemspider.com/Chemical-Structure.119932.html> (accessed 16:11, Jul 5, 2020)
15. CSID:4335923, <http://www.chemspider.com/Chemical-Structure.4335923.html> (accessed 16:25, Jul 5, 2020)
16. CSID:549302, <http://www.chemspider.com/Chemical-Structure.549302.html> (accessed 16:27, Jul 5, 2020)
17. National Center for Biotechnology Information. PubChem Database. Pyranthren-1-amine, CID=22349134, <https://pubchem.ncbi.nlm.nih.gov/compound/pyranthren-1-amine> (accessed on July 5, 2020)
18. National Center for Biotechnology Information. PubChem Database. Bispyrenopyrrole, CID=129859836, <https://pubchem.ncbi.nlm.nih.gov/compound/Bispyrenopyrrole> (accessed on July 5, 2020)

Chapter 4. Physical Separation of Highly PAXH Contaminated Soil as Well as Analysis of Its Fractions and Corresponding Water Phase Using Fourier Transform Mass Spectrometry

Redrafted from “Luo, R.; Schrader, W., Physical Separation of Highly PAXH Contaminated Soil as Well as Analysis of Its Fractions and Corresponding Water Phase Using Fourier Transform Mass Spectrometry”, will be submitted to Environment International.

4.1. Abstract

Contaminated soils from industrial sites, such as for coal mining or manufactured gas production, can contain polycyclic aromatic hydrocarbons (PAHs) with a concentration higher than 10,000 mg kg⁻¹, require an integrated approach for the remediation. A physical treatment by separating organic contaminants from soil materials using the density difference could lower the cost for the upcoming chemical and/or biological treatment. In our study, a highly PAH contaminated soil was separated in a 39% (w/w) calcium chloride solution ($\rho = 1.4 \text{ g/cm}^3$) via stirring, aeration or ultrasonication. Both first and second methods could separate soil materials from organic particles efficiency. The light fraction from them comprised around 10% of the total soil weight but 80% of solvent extractable organics (SEO). Optical and transmission electron microscopic analysis showed the light fraction, which consisted of mainly black solid aggregates (BSA), differed strongly from soil materials. Additionally, the original contaminated soil, its light and heavy fractions and the corresponding water phase together with the manually separated BSA were analyzed on the molecular level using ultrahigh resolution mass spectrometry (HRMS) with different atmospheric pressure ionization (API) methods, such as electrospray (ESI) and atmospheric pressure photo ionization (APPI). Results showed that SEO, which were primarily associated with BSA and successfully separated through physical method, contained mainly condensed aromatic ring structures of pure hydrocarbons and nitrogen heterocycles with low oxygen content.

4.2. Introduction

Polycyclic aromatic hydrocarbons (PAHs) are omnipresent contaminants in soils and sediments worldwide.¹ Their concentration varies widely from below $5 \mu\text{g kg}^{-1}$ in the rural area to over $1,000 \text{ mg kg}^{-1}$ in the industrial sites, such as for the coal mining or manufactured gas production.²⁻⁷ Considering their mutagenic and carcinogenic effects, 16 selected parent PAHs, which are involved in the priority contaminant list suggested by the United States Environmental Protection Agency (U.S. EPA), have been monitored over more than four decades.^{8,9}

Until 1990s, excavation and landfilling were recommended as a method to treat heavily PAH contaminated soils from manufactured gas plant sites.¹⁰ However, the PAHs were not really eliminated. During the years a wide range of remediation techniques such as thermal, physical, chemical, and biological treatments have been applied for PAH contaminated soil.^{10, 11} Among them, the bioremediation is the most commonly implemented method due to its safe, eco-friendly cost-effective character. The integrated approach, meaning a combination of more than one remediation techniques, presents the second most frequently used method for especially some highly contaminated soils.¹² For instance, soils in the “hot-spot” zones of industrial areas, where PAH concentrations higher than $10,000 \text{ mg kg}^{-1}$, are not amenable to most bioremediation.¹³ Accordingly, a thermal, physical or chemical pretreatment step was advised.

Physical treatments such as soil washing or using solvent extraction are feasible cleanup techniques for highly contaminated soils with PAHs.⁵ Besides, the usage of density difference as a physical parameter found quiet applications in soil analysis and treatment. For example, heavy metals with a density between 5 and 9 g mL^{-1} could be precipitated from soil minerals ($\rho \approx 2.5\text{-}3.0 \text{ g mL}^{-1}$) using a heavy liquid.^{14, 15} Quite the other way around, by applying a liquid with a proper density lighter organic materials could float and be separated from the soil minerals.¹⁶ Ghosh et al. separated PAHs contaminated sediment samples into light and heavy fractions using cesium chloride with a specific gravity of 1.8. Results showed that the light fraction consisting of mainly organic particles, which contributed 5-20% of the total mass but 60-95% of the PAHs.¹⁷⁻¹⁹ Using the same solution Richardson and Aitken could recover more than 50% of the PAHs in the light fraction separated from a manufactured gas plant soil, which constituted less than 2% of the total mass.⁶ Even by suspending contaminated soils into two-fold amount of water could lead to a separation of maximum 76% of the PAHs for tar oil contaminated soils.⁷ The higher removal rate of PAHs by the simple

density separation is very promising for highly PAH contaminated soils. However, in the previous studies conclusions were made based on the quantitative analysis of 16 EPA PAHs. Other alkylated and high molecular weight PAHs as well as polycyclic aromatic heterocycles containing N, S or O (PAXHs, X = N, S, O), which could co-occur with the 16 PAHs depending on their origin,²⁰ were not under consideration, thus limiting the method.

A versatile tool for the non-targeted soil analysis is the ultrahigh resolution Fourier transform mass spectrometry (FT MS).²¹ With a combination of different atmospheric pressure ionization (API) methods, such as electrospray ionization (ESI), atmospheric pressure chemical ionization (APCI), atmospheric pressure photo ionization (APPI) and atmospheric pressure laser ionization (APLI), in negative and positive polarities FT MS deliver multidimensional information about ultracomplex samples such as crude oil²² and soil. Negative mode electrospray ionization (ESI) FT MS analysis of dissolved organic matter (DOM)²³⁻²⁷ or soil organic matter (SOM)^{28, 29} helped to understand the soil biogeochemistry and global carbon cycling. However, a non-targeted analysis of PAH contaminated soil using FT MS was not frequently published.^{30, 31}

In this work we compared different physical separation methods through density difference for a highly PAXH contaminated soil and present a detailed analysis of the original soil, its fractions and corresponding water phase on the molecular level using ultrahigh resolution MS with different API methods.

4.3. Materials and Methods

4.3.1. Sample

One highly contaminated soil sample with PAXHs was air dried, grinded in mortar, sieved through 2 mm sieve, and stored in the fridge at 4 °C.

4.3.2. Physical Separation and Following Treatment

The contaminated soil was density separated using a calcium chloride (93%, Sigma-Aldrich, Germany) solution with a specific gravity of 1.4 by means of stirring, aeration or ultrasonication (Figure 4-1). 80 mL 39% (w/w) calcium chloride solution were poured into a 100 mL baker or filter funnel (pore size: 16-40 µm) containing 5 g of contaminated soil. Then the mixture was either stirred or aerated with gentle nitrogen gas from the bottom for 5 min, or ultrasonicated for 30 min. Afterwards the mixture was equilibrated overnight. Subsequently the light fraction floated on the top were decanted on a filter paper (0.5 µm particle retention, Macherey-Nagel, Germany) and washed with pure water five times to remove calcium

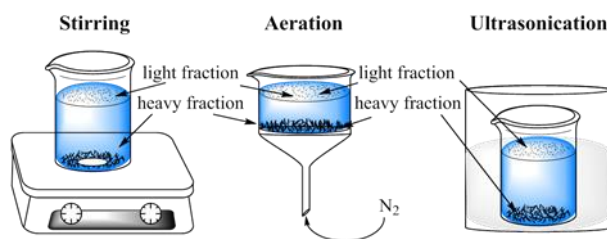


Figure 4-1. Physical separation of contaminated soil in calcium chloride solution using stirring, aeration or ultrasonication.

chloride. The calcium chloride solution was liquid-liquid extracted with 3 x 40 mL dichloromethane (DCM, 99%, Sigma-Aldrich, Germany). The heavy fraction was washed as the light fraction.

The original contaminated soil and the separated fractions were Soxhlet extracted using DCM for over 300 cycles. In addition the manually picked black solid aggregates (BSA) were extracted as described above. Furthermore, because of the low amount of organic matter found after the liquid-liquid extraction in the calcium chloride solution, a Soxhlet extraction of the original contaminated soil using pure water was performed. Eventually, solvents used for the liquid-liquid and Soxhlet extractions were rotary-evaporated and samples were store in the fridge at 4 °C prior to the analysis.

4.3.3. Spectrometric Analysis

The light and heavy fractions were characterized using Hitachi HF-2000 transmission electron microscopy (TEM) equipped with a cold-field emission gun and a Noran energy dispersive X-ray (EDX) detector.

4.3.4. Mass Spectrometric and Data Analysis

Mass spectrometric analysis was performed on a research type FT Orbitrap MS (Thermo Fisher Scientific, Bremen, Germany) with a LTQ Tune Plus 2.7.0 data processing system (Thermo Fisher Scientific, Bremen, Germany). Samples were diluted to 250 $\mu\text{g mL}^{-1}$ in toluene (99.8%, Arcos Organic, Belgium):methanol (99.8%, J.T. Baker, VWR, Germany) (1:1, v:v) or chlorobenzene (99%, Arcos Organic, Belgium) for ESI or APPI measurements, respectively. The sprayer voltage was set to +4/-4 kV for the positive and negative mode ESI. The diluted samples were infused with a flow rate of 5 $\mu\text{L min}^{-1}$ at 5, 2 and 1 a.u. (arbitrary unit) sheath, auxiliary and sweep gas flow for both polarities. For the positive mode APPI samples were infused with a flow rate of 20 $\mu\text{L min}^{-1}$ under the irradiation from a Krypton VUV lamp (Syagen, Tustin, CA, U.S.A.) with a photon emission at 10.0 and 10.6 eV. The vaporizer temperature, sheath, auxiliary and sweep gases were set to 350 °C, 20, 5 and 2 a.u.,

correspondingly. Mass spectra were recorded at a mass resolution of 480,000 at m/z 400 using spectra stitching^{32, 33} from 125 to 1200, meaning 30 Da mass windows with 5 Da overlap.

The data were recorded by Xcalibur 2.2 (Thermo Fisher Scientific, Bremen, Germany) and further processed using Composer v1.5.0 (Sierra Analytics, Modesto, CA, U.S.A) with the following chemical constraints: $0 < C < 200$, $0 < H < 1000$, $0 < N < 3$, $0 < S < 3$, $0 < O < 11$, $0 < \text{double bond equivalent (DBE)} < 100$, maximum mass error < 1.5 ppm.

4.4. Results and Discussion

4.4.1. Physical Separation

The contaminated soil was separated via density difference into light ($\rho < 1.4 \text{ g/cm}^3$) and heavy ($\rho > 1.4 \text{ g/cm}^3$) fractions. It is shown in Figure 4-2 that the light fractions from stirring, aeration and ultrasonication consist of only 10%, 11% and 4% of the total soil weight, whereas the majority (over 85%) of the soil constituents that comprise sand, silt, and clays remained in the heavy fraction. However, considering about the solvent extractable organics (SEO) the result was just reversed. Both the light fractions after stirring and aeration contained over 80% of the SEO, and the corresponding heavy fractions contributed the minor rest portion. This result is in good agreement with the data obtained from other researchers,¹⁷⁻¹⁹ who used cesium chloride with a specific gravity of 1.8 and centrifugation for the separation of PAH contaminated soil. Only after ultrasonication, the amount of SEO found in the heavy fraction was higher than in the light fraction. This was probably due to a compact layer of heavier soil formed initially, which entrained the lighter material, thus preventing

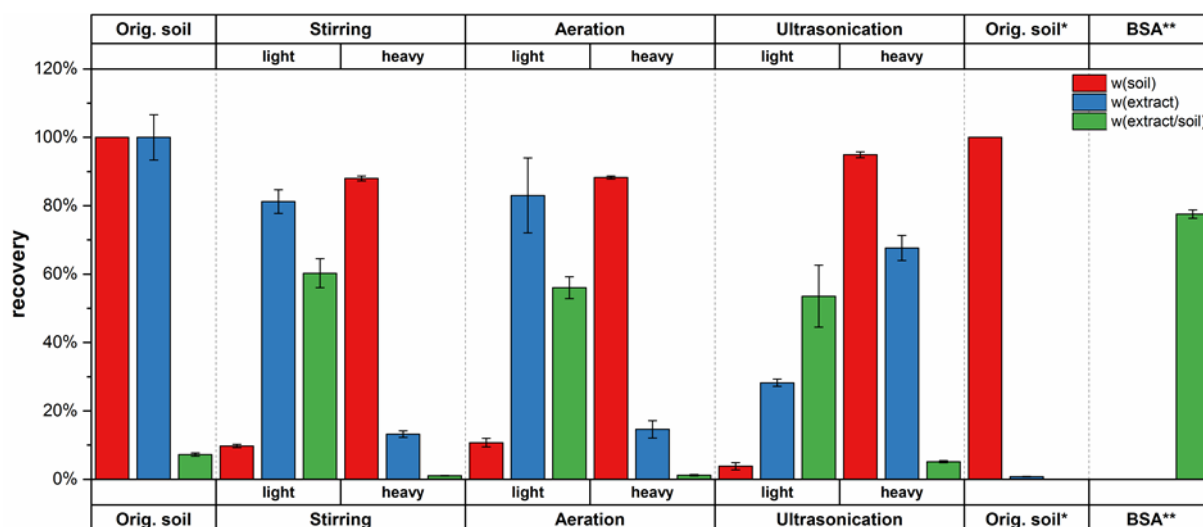


Figure 4-2. Mass and SEO distributions and weight proportion of SEO to the contaminated soil and its fractions after physical separation through stirring, aeration or ultrasonication in 39% CaCl_2 solution ($\rho = 1.40 \text{ g cm}^{-3}$). *: Soxhlet extracted using pure water. **: Black solid aggregates manually separated from the contaminated soil sample.

them from floating.

The amount of SEO transferred during the separation into the calcium chloride solution was negligible, so that it did not provide enough sample volume to complete the mass spectrometric measurement. Nonetheless it might be interesting to see what and which part from the contamination can be transferred into the water phase during the separation. Therefore the original contaminated soil was Soxhlet extracted using only water, which gained less than 1% of the total SEO (Figure 4-2, denoted as Orig. soil*). The result indicates a strong hydrophobic character of the SEO originated from the contaminated soil.

The original soil was highly contaminated with organic matter. This was presented in Figure 4-2 in green, thus around 7% of the total soil weight were extractable using DCM. The percentages were increased to 60% and 56% for the light fractions from stirring and aeration, respectively. In the meanwhile the weight ratios of the extract to the corresponding heavy fractions were decreased from 7% (compared to the original contaminated soil) to 1.1% and 1.2%. Although the light fraction after ultrasonication weighed less than after stirring or aeration, it consisted of comparable amount of SEO (56%). Additionally, the result of the Soxhlet extraction of manually selected pure BSA from the original contaminated soil showed, that up to 80% of BSA were DCM extractable. This implies that the main SEO was derived from BSA.

Results showed that a simple physical separation through stirring or aeration could lead to an efficient removal of organic matter, which aggregates and has a different density than soil materials. These two physical methods can easily be scaled up for the industrial use and compared to ultrasonication, which anyway showed lower separation efficiency, require less energy.

4.4.2. Soil Particle Characterization

As shown in Figure 4-3 (a and d), already from the optic view the heavy fraction differed strongly from the light fraction. The heavy fraction manifested a clay brown color. In contrast to that the light fraction was almost black. Furthermore, the TEM-EDX results revealed, that the heavy fraction contained primarily irregular Si-dominated, Si-Al or Ca natural mineral particles (Figure 4-3, c).

Instead, organic particles dominated in the light fraction (Figure 4-3, f). The signal for Cu was derived from the copper grid used for fixation of soil particles. The result further confirmed that the particles from the light fraction contained high amount of organic matters, which were

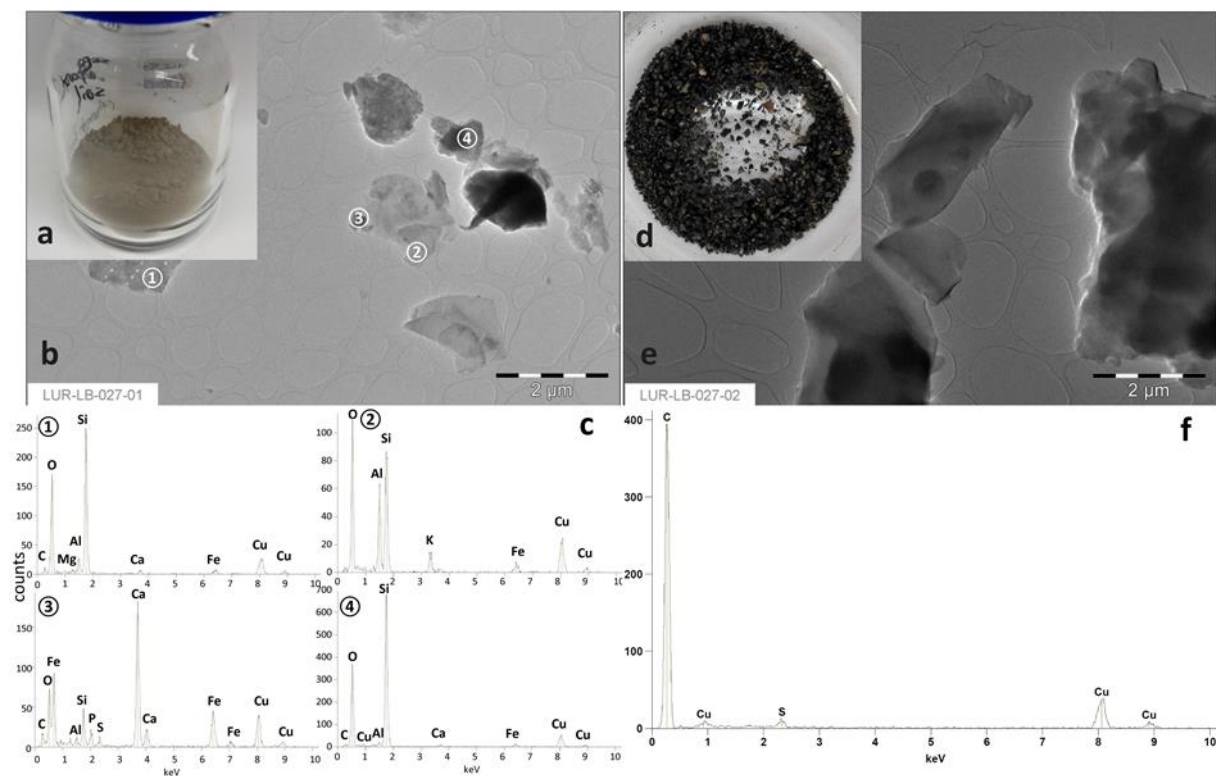


Figure 4-3. The separated heavy (a) and light (d) fractions from the original soil with their TEM images (b and e) and corresponding EDX results (c and f).

successfully removed from soil minerals through simple physical separation. This is in good accordance with the results obtained from Trellu et al.⁷ However, it needs deeper examinations on the molecular level to judge, whether the rest SEOs adsorbed on soil particles differ from the separated BSA.

4.4.3. FT Orbitrap Mass Spectra

Soil is a complex mixture consisting of inorganic, organic materials and macro- and microorganisms. A non-targeted analysis of the organic extract from soil is a sophisticated task. Depending highly on the location where the soil is coming from, its content of soil organic matter can vary widely. Their existence can influence the analysis of organic contaminants such as PAXHs in the non-targeted approach. The complexity can be deciphered using ultrahigh-resolution MS. In earlier investigations, negative mode ESI was frequently utilized for the study of organic matter in or derived from soil, which contain mostly polar constituents and high number of oxygen per molecule.²³⁻²⁹ However, it is difficult to completely analyze all compounds in soil by using single ionization method, especially when mostly nonpolar PAHs are of interest. Hence, it is essential to compare different ionization methods for encompassing all detectable classes.

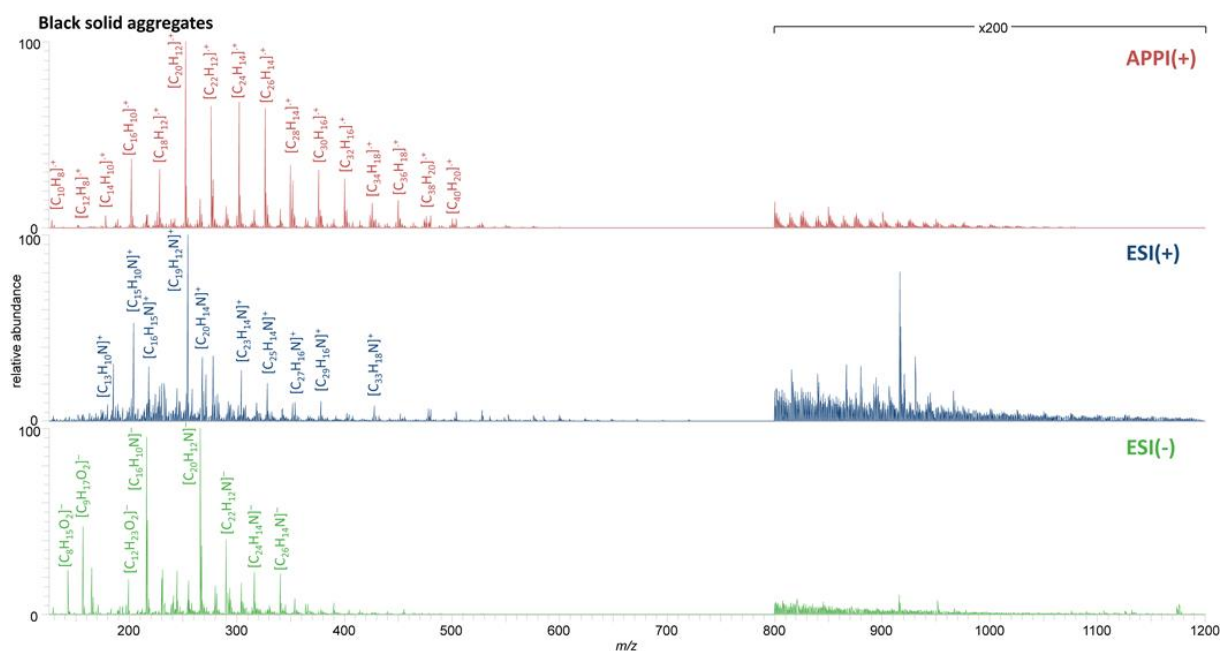


Figure 4-4. Recombined mass spectra for the Soxhlet extract from BSA, analyzed by FT Orbitrap MS using positive mode APPI (top), ESI (middle) and negative mode ESI (bottom).

Firstly shown in the top row of Figure 4-4 on the top is the mass spectrum of APPI(+) for BSA separated from the contaminated soil. Result distinguished strongly from the data obtained for the natural organic matter,³⁴ but comparable to the spectrum for organic-carbon rich particles analyzed by Ghosh et al.¹⁷ Here, radical hydrocarbon class compounds were predominated in the spectrum throughout the mass range between 125 and 1200 Da. Most of them have a high aromaticity including the 16 EPA PAHs in lower mass range. Analogous distributions were acquired for the original contaminated soil and its fractions (Figure A4-1), which illustrate that the soil was heavily contaminated with PAHs that were mainly associated with BSA.

Not only pure PAHs were identified as contaminants, results of positive and negative mode ESI (Figure 4-4, middle and bottom) demonstrate that also nitrogen containing PAHs co-occurred. Further, with both polarities applied the PANHs found in the contaminated soil can be categorized as basic pyridine-containing or neutral pyrrole-containing PAXHs.^{35, 36}

Although the proportion of water soluble organics to the total SEO using DCM was small (< 1%, Figure 4-2), it delivered valuable information about which contaminants can be transferred directly into the water phase, such as groundwater or surface water close to the contamination side, before any remediation techniques have been taken place. Differed from the DCM extracts of BSA, the contaminated soil and as well as its fractions, the water extract of contaminated soil contained more polar PANHs (Figure A4-2). Additionally, the signals

were shifted towards lower mass ranges (< 300 Da). Same trend was observed in the positive and negative mode ESI spectra, where low molecular weight basic pyridine-like PANHs and oxygenated PA(N)Hs were detected, respectively. Results revealed that by only targeted monitoring the 16 EPA PAHs might not be sufficient to examine the total risk of PAH contaminated sites, since higher molecular weight PAHs could coexist and other more polar heteroatom containing PAHs or transformation products could leach more easily.

4.4.4. Class Distribution

The elemental compositions detected using API FT MS were categorized into classes according to the number of heteroatoms (N, S and O) per molecule and summarized in a class distribution plot for each sample. Pure hydrocarbons without any heteroatoms were grouped in the HC class. In total of 20 compound classes were detected in the positive mode APPI for Soxhlet extracts of BSA, contaminated soil and its fractions after stirring using DCM (Figure 4-5). The number of classes for the water extract (Figure 4-5, orig. soil*) exceeded 20 classes. However, in order to compare the water extract with other samples, only classes were selected, which were found for the DCM extracts. APPI can ionize pure and heteroatom containing PAH efficiently and generate two types of ions: radical cations and protonated molecules.²²

The highest number of total assigned compositions was found for the heavy fraction after stirring, which was reduced from 22149, 16168 (orig. soil), 15161 (stirring_light) to 13377 (BSA). Even in the water extract a total number of 9093 chemical compositions were assigned. When comparing classes within one sample of the Soxhlet extracts using DCM, highest assignments were detected in the radical hydrocarbon (HC) class, followed by radical and protonated O, O₂, N, NO, NO₂, N₂ and S classes. When comparing same classes between DCM extracts, the number of assigned compositions in each class reduced gradually from the heavy fraction to original soil to light fraction and finally to BSA. This can be very clearly seen from the radical and protonated HC, O, O₂ classes. Similar observation was gained for the soil fractions after aeration (Figure A4-3). However, because of an insufficient separation through ultrasonication, the difference between the original soil and its fractions was not as prominent as from other two methods (Figure A4-4). Nevertheless, among the DCM extracts BSA always displayed lowest assignments in each class. This indicates that, with regard to the chemical composition BSA are simpler than the original soil and its fractions.

In the ESI(+) measurements the total number of assigned compositions was lower than in the APPI(+) measurements, even though more polar classes were detected (Figure A4-5 to 4-7).

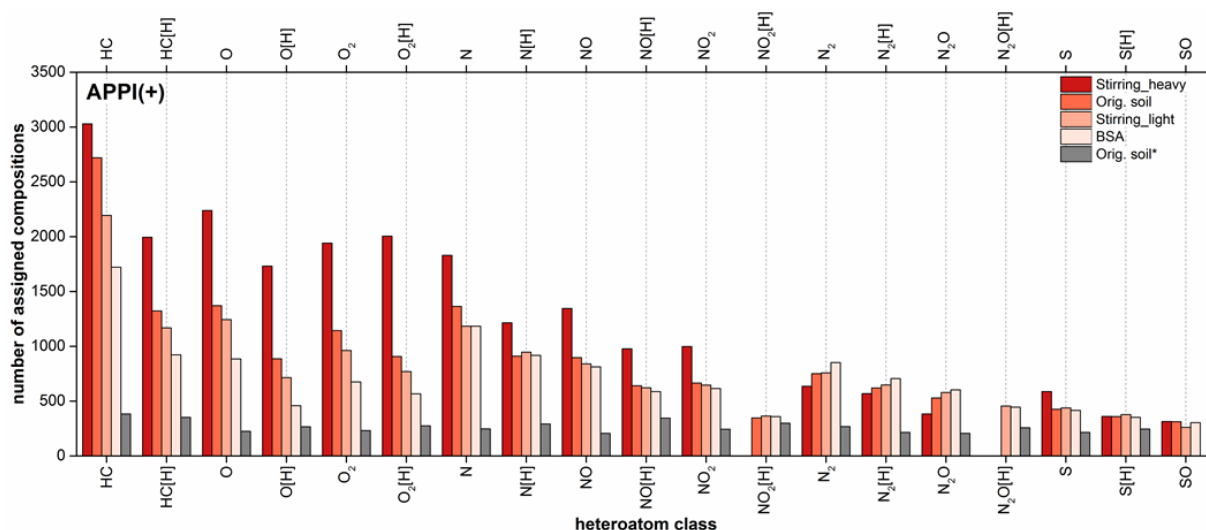


Figure 4-5. Class distributions for the heavy fraction after stirring, original soil, light fraction after stirring and BSA (from dark to light red) as well as the water extract (selected classes only) denoted as orig. soil*, analyzed using positive mode APPI FT Orbitrap MS.

Similar results were obtained compared to the APPI(+) measurements: the highest assignments were found for the heavy fractions, followed by the original soil, light fractions and lastly BSA. Here basic pyridine-like PANHs (N, N₂) and their oxygenated classes (NO, NO₂) with NSO_x and SO_x classes were the most abundant classes. Besides, protonated molecules radical ions were also detected for such as HC, N and N₂ classes, which implies on the other hand the presence of highly condensed aromatic structures in the sample.³⁷

In the ESI(-) measurements the total assignments was further reduced to around 10000 for the heavy fractions (Figure A4-8 to Figure A4-10). In spite of this, negative mode data allowed a better examination of 5-membered nitrogen containing heterocycles or acidic species such as carboxylic acids, which trace the influence of natural weathering or chemical/biological remediation processes.³⁸ Here, the difference between the heavy fraction and the original soil was minor, but the number of assigned compositions in each class was still higher than the corresponding light fraction and BSA. In the DCM extracts the most abundant classes were O₂₋₄, NO₂₋₃ and N₂O₂, but a clear shifting towards highly oxidized classes such as O₆₋₈ or NO₆ were observed in the water extract. Results indicate that because of better solubility highly weathered oxygen containing polar PAXHs could be easily transferred into the water phase.

4.4.5. Kendrick Plot

In Figure 4-6, the major compound classes, namely radical HC and protonated N classes, from the positive mode APPI and ESI measurements for the different samples were compared in Kendrick plots. Here, each composition from one class can be visualized by its DBE and number of carbon atoms per molecule. A maximum DBE of 70 with 95 carbon atoms per

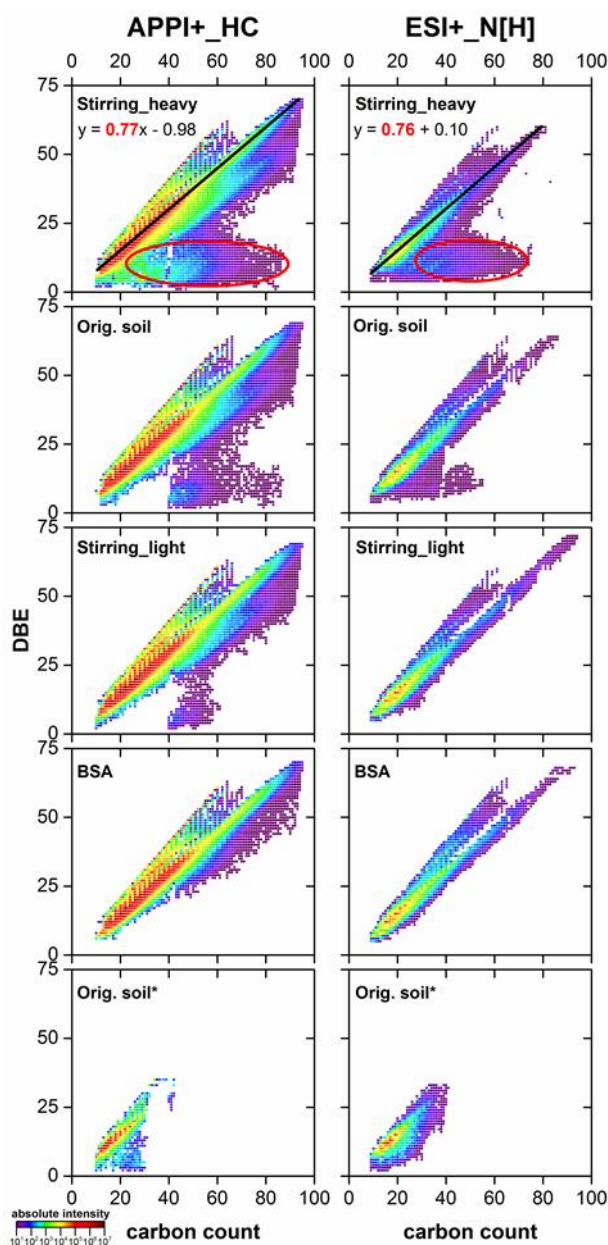


Figure 4-6. Kendrick plots for radical hydrocarbon (left column) and protonated nitrogen (right column) classes from the heavy fraction after stirring, original soil, light fraction after stirring, BSA and original soil after Soxhlet extraction with water (from top to bottom), analyzed using positive mode APPI and ESI Orbitrap MS.

molecule was detected in the radical HC class. In the N class high molecular weight azaarenes with a maximum DBE of 72 and 94 carbon atoms per molecule were discovered, which exceeded the largest azaarenes reported by Tian et al. for PAH contaminated soils.³⁹

In the HC and N classes for BSA only highly condensed aromatic hydrocarbons and N-heterocycles were detected, which represent the identity of the contaminants on a molecular level. From the light fraction to original soil and to the heavy fraction, increasing amount of additional compositions with relative lower DBE (< 25) showed up. Compared to the highly aromatized compositions e.g. 16 PAHs or quinolone (DBE = 7), acridine (DBE = 10), and benzo[*b*]acridine (DBE = 13), these compositions (highlighted in red cycles, Figure 4-6)

contained higher amount of carbon atoms per molecule. Likewise, in the heavy fractions after aeration and ultrasonication, where the main soil particles stayed, more compositions with high carbon number and low DBE were found in comparison to the corresponding light fractions (Figure A4-11). They were distinct from the chemical point of view from the real contaminants, suggesting their natural origin.

The occurrence of natural hydrocarbons of biogenic origin in soil was investigated by different researchers.^{40, 41} Here, because of the analytical technique used, results were restricted to volatile hydrocarbons using mainly sum parameters such as TPH and 16 EPA PAH related compounds. Using ultrahigh resolution FT MS with different API methods, more compositional information especially polar compounds can be gained.

Moreover, Kendrick plots for the water extract (orig. soil*, Figure 4-6) demonstrated that also low molecular weight parent PAXHs could be transferred into water phase easily.

4.4.6. Van Krevelen Plot

Another graphical method frequently used for the study of natural organic matter in the environment is the van Krevelen plot.^{42, 43} recently a new concept called aromaticity index (AI) is incorporated into the van Krevelen plot, which represents the density of C-C double bond in a molecule thereby its aromaticity.⁴⁴

In Figure 4-7 the Van Krevelen plots for BSA and the unique compositions in the heavy fraction as well as water extract after subtraction of common compositions from SBA were compared. The compositions in BSA existed largely in lower H/C and O/C ratio ranges. 2648 out of 3970 compositions of HC and O_x classes for BSA were below the gray line with AI greater than 0.5 (Table 4-1), which reflects the presence of aromatic cores in the compositions. On the top of this, around 60% of them (1530) possessed condensed aromatic ring structures (CARS), which exhibit below the black line with AI greater than 0.67. Highly CARS were also detected in volcanic ash soil,²³ DOM from boreal lakes²⁴ and paddy soils²⁷. There, CARS pervaded throughout the O/C range of 0 to 0.8 and mainly located between 0.2 and 0.6. Instead, results from our study showed that nearly 90% of the CARS (1370) detected in BSA had an O/C lower than 0.1 and they mainly belonged to pure HC as well as low oxygenated classes (O₁₋₃). The absolute number of compositions with AI > 0.5 or > 0.67 was slightly increased for the heavy fraction after stirring. However, due to the large increase in compositions with lower AI, the percentages of compositions with AI > 0.5 and > 0.67 reduced from 67% to 41% and from 38% to 21%, respectively. The percentages of aromatic

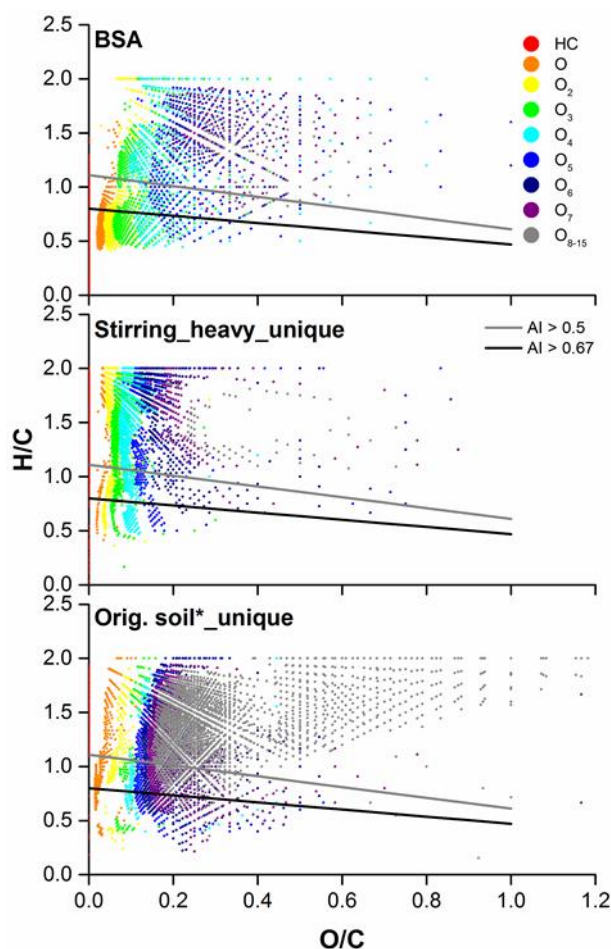


Figure 4-7. Van Krevelen plots for Soxhlet extract from BSA (top), the unique compositions from the heavy fraction after stirring (middle), and the original soil Soxhlet extracted using water (bottom, denoted as orig. soil*), compared with BSA, analyzed by both positive mode APPI (HC) and negative mode ESI (O_x) FT Orbitrap MS. Compositions below the gray or black line have a aromaticity index (AI) higher than 0.5 or 0.67, respectively.

Table 4-1. The number of HC and O_x class compositions detected in total, AI > 0.5 or > 0.67 (proportion to total number in parenthesis) for different samples.

HC+ O_x classes	Number of compositions in		
	total	AI > 0.5	AI > 0.67
BSA	3970	2648 (67%)	1530 (38%)
Stirring_heavy	7643	3125 (41%)	1633 (21%)
Orig. soil*	6523	2150 (33%)	928 (14%)

and condensed aromatic structures in the water extract were further reduced to 33% and 14%. Similar result was obtained for the NO_x classes (Figure A4-12 and Table A4-1).

Combined the results obtained from Figure 4-6 and Figure 4-7, we propose that BSA, which were characterized as the main contamination source containing highly amount of pure and nitrogen involved CARS with/without short side chains, could be separated from natural soil material quiet efficiently through physical methods. This simple and cheap separation step via

density difference is recommended to be implemented prior to other chemical or biological remediation techniques for soils highly contaminated with PAXHs, which present as BSA.

4.5. Conclusion

In this study we investigated different physical separation techniques for the removal of PAXHs from the heavily contaminated soil. Over 80% of SEO could be removed from the contaminated soil using stirring and aeration in a 39% (*w/w*) calcium chloride solution. Most of the SEO in the lighter fraction were associated with BSA. The BSA were then analyzed and compared to the original contaminated soil as well as soil fractions using FTMS with different API in a non-targeted approach. By combining the results obtained from positive mode APPI and positive/negative mode ESI the BSA were characterized as containing highly aromatized structures, which include pure PAHs and PAXHs (X = N, O and S). Around 67% of the assigned elemental compositions from HC and O_x classes and over 40% of N and NO_x class compounds comprise condensed aromatic structures. The short length of side chain for these PAXHs detected in the BSA indicates that the contamination has a pyrogenic origin.

Results show that by applying comprehensive non-targeted analysis using API-FTMS a deeper understanding of the soil contamination, including the source and determination of contaminants as well as the corresponding remediation efficiency, can be achieved.

4.6. References

1. Stout, S. A.; Emsbo-Mattingly, S. D.; Douglas, G. S.; Uhler, A. D.; McCarthy, K. J., Beyond 16 priority pollutant PAHs: A review of PACs used in environmental forensic chemistry. *Polycycl. Aromat. Comp.* **2015**, *35*, (2-4), 285-315.
2. Wilcke, W., Global patterns of polycyclic aromatic hydrocarbons (PAHs) in soil. *Geoderma* **2007**, *141*, (3), 157-166.
3. Jones, K. C.; Stratford, J. A.; Waterhouse, K. S.; Vogt, N. B., Organic contaminants in Welsh soils: polynuclear aromatic hydrocarbons. *Environ. Sci. Technol.* **1989**, *23*, (5), 540-550.
4. Morillo, E.; Romero, A. S.; Maqueda, C.; Madrid, L.; Ajmone-Marsan, F.; Grcman, H.; Davidson, C. M.; Hursthouse, A. S.; Villaverde, J., Soil pollution by PAHs in urban soils: a comparison of three European cities. *J. Environ. Monitor.* **2007**, *9*, (9), 1001-1008.
5. Gong, Z.; Wang, X.; Tu, Y.; Wu, J.; Sun, Y.; Li, P., Polycyclic aromatic hydrocarbon removal from contaminated soils using fatty acid methyl esters. *Chemosphere* **2010**, *79*, (2), 138-143.
6. Richardson, S. D.; Aitken, M. D., Desorption and bioavailability of polycyclic aromatic hydrocarbons in contaminated soil subjected to long-term in situ biostimulation. *Environ. Toxicol. Chem.* **2011**, *30*, (12), 2674-2681.
7. Trelu, C.; Miltner, A.; Gallo, R.; Huguenot, D.; van Hullebusch, E. D.; Esposito, G.; Oturan, M. A.; Kästner, M., Characteristics of PAH tar oil contaminated soils—Black particles, resins and implications for treatment strategies. *J. Hazard. Mater.* **2017**, *327*, 206-215.

8. Keith, L.; Telliard, W., ES&T special report: Priority pollutants: I-a perspective view. *Environ. Sci. Technol.* **1979**, *13*, (4), 416-423.
9. Keith, L. H., The source of U.S. EPA's sixteen PAH priority pollutants. *Polycycl. Aromat. Comp.* **2015**, *35*, (2-4), 147-160.
10. Kuppusamy, S.; Thavamani, P.; Venkateswarlu, K.; Lee, Y. B.; Naidu, R.; Megharaj, M., Remediation approaches for polycyclic aromatic hydrocarbons (PAHs) contaminated soils: Technological constraints, emerging trends and future directions. *Chemosphere* **2017**, *168*, 944-968.
11. Gan, S.; Lau, E. V.; Ng, H. K., Remediation of soils contaminated with polycyclic aromatic hydrocarbons (PAHs). *J. Hazard. Mater.* **2009**, *172*, (2), 532-549.
12. Mohan, S. V.; Kisa, T.; Ohkuma, T.; Kanaly, R. A.; Shimizu, Y., Bioremediation technologies for treatment of PAH-contaminated soil and strategies to enhance process efficiency. *Rev. Environ. Sci. Biotechnol.* **2006**, *5*, (4), 347-374.
13. Khodadoust, A. P.; Bagchi, R.; Suidan, M. T.; Brenner, R. C.; Sellers, N. G., Removal of PAHs from highly contaminated soils found at prior manufactured gas operations. *J. Hazard. Mater.* **2000**, *80*, (1), 159-174.
14. Henley, K. J., Improved heavy-liquid separation at fine particle sizes. *Am. Mineral.* **1977**, *62*, (3-4), 377-381.
15. Cotter-Howells, J., Separation of high density minerals from soil. *Sci. Total Environ.* **1993**, *132*, (1), 93-98.
16. Cerli, C.; Celi, L.; Kalbitz, K.; Guggenberger, G.; Kaiser, K., Separation of light and heavy organic matter fractions in soil — Testing for proper density cut-off and dispersion level. *Geoderma* **2012**, *170*, 403-416.
17. Ghosh, U.; Gillette, J. S.; Luthy, R. G.; Zare, R. N., Microscale location, characterization, and association of polycyclic aromatic hydrocarbons on harbor sediment particles. *Environ. Sci. Technol.* **2000**, *34*, (9), 1729-1736.
18. Ghosh, U.; Zimmerman, J. R.; Luthy, R. G., PCB and PAH speciation among particle types in contaminated harbor sediments and effects on PAH bioavailability. *Environ. Sci. Technol.* **2003**, *37*, (10), 2209-2217.
19. Khalil, M. F.; Ghosh, U.; Kreitinger, J. P., Role of weathered coal tar pitch in the partitioning of polycyclic aromatic hydrocarbons in manufactured gas plant site sediments. *Environ. Sci. Technol.* **2006**, *40*, (18), 5681-5687.
20. Andersson, J. T.; Achten, C., Time to say goodbye to the 16 EPA PAHs? Toward an up-to-date use of PACs for environmental purposes. *Polycycl. Aromat. Comp.* **2015**, *35*, (2-4), 330-354.
21. Panda, S. K.; Andersson, J. T.; Schrader, W., Characterization of supercomplex crude oil mixtures: What is really in there? *Angew. Chem. Int. Edit* **2009**, *48*, (10), 1788-1791.
22. Gaspar, A.; Zellermann, E.; Lababidi, S.; Reece, J.; Schrader, W., Impact of different ionization methods on the molecular assignments of asphaltenes by FT-ICR mass spectrometry. *Anal. Chem.* **2012**, *84*, (12), 5257-5267.
23. Kramer, R. W.; Kujawinski, E. B.; Hatcher, P. G., Identification of black carbon derived structures in a volcanic ash soil humic acid by Fourier transform ion cyclotron resonance mass spectrometry. *Environ. Sci. Technol.* **2004**, *38*, (12), 3387-3395.
24. Kellerman, A. M.; Dittmar, T.; Kothawala, D. N.; Tranvik, L. J., Chemodiversity of dissolved organic matter in lakes driven by climate and hydrology. *Nat. Commun.* **2014**, *5*, 3804.
25. Guigue, J.; Harir, M.; Mathieu, O.; Lucio, M.; Ranjard, L.; Lévêque, J.; Schmitt-Kopplin, P., Ultrahigh-resolution FT-ICR mass spectrometry for molecular characterisation of pressurised hot water-extractable organic matter in soils. *Biogeochemistry* **2016**, *128*, (3), 307-326.

26. Fleury, G.; Del Nero, M.; Barillon, R., Effect of mineral surface properties (alumina, kaolinite) on the sorptive fractionation mechanisms of soil fulvic acids: Molecular-scale ESI-MS studies. *Geochim. Cosmochim. Ac.* **2017**, *196*, 1-17.
27. Li, X.-M.; Sun, G.-X.; Chen, S.-C.; Fang, Z.; Yuan, H.-Y.; Shi, Q.; Zhu, Y.-G., Molecular chemodiversity of dissolved organic matter in paddy soils. *Environ. Sci. Technol.* **2018**, *52*, (3), 963-971.
28. Tfaily, M. M.; Chu, R. K.; Tolić, N.; Roscioli, K. M.; Anderton, C. R.; Paša-Tolić, L.; Robinson, E. W.; Hess, N. J., Advanced solvent based methods for molecular characterization of soil organic matter by high-resolution mass spectrometry. *Anal. Chem.* **2015**, *87*, (10), 5206-5215.
29. Tfaily, M. M.; Chu, R. K.; Toyoda, J.; Tolic, N.; Robinson, E. W.; Pasa-Tolic, L.; Hess, N. J., Sequential extraction protocol for organic matter from soils and sediments using high resolution mass spectrometry. *Anal. Chim. Acta* **2017**, *972*, 54-61.
30. Lu, M.; Zhang, Z.; Qiao, W.; Guan, Y.; Xiao, M.; Peng, C., Removal of residual contaminants in petroleum-contaminated soil by Fenton-like oxidation. *J. Harzard. Mater.* **2010**, *179*, (1-3), 604-611.
31. Lu, M.; Zhang, Z.; Qiao, W.; Wei, X.; Guan, Y.; Ma, Q.; Guan, Y., Remediation of petroleum-contaminated soil after composting by sequential treatment with Fenton-like oxidation and biodegradation. *Bioresource Technol.* **2010**, *101*, (7), 2106-2113.
32. Southam, A. D.; Payne, T. G.; Cooper, H. J.; Arvanitis, T. N.; Viant, M. R., Dynamic range and mass accuracy of wide-scan direct infusion nano-electrospray Fourier transform ion cyclotron resonance mass spectrometry-based metabolomics increased by the spectral stitching method. *Anal. Chem.* **2007**, *79*, (12), 4595-4602.
33. Vetere, A.; Schrader, W., Mass spectrometric coverage of complex mixtures: Exploring the carbon space of crude oil. *ChemistrySelect* **2017**, *2*, (3), 849-853.
34. Hertkorn, N.; Frommberger, M.; Witt, M.; Koch, B. P.; Schmitt-Kopplin, P.; Perdue, E. M., Natural organic matter and the event horizon of mass spectrometry. *Anal. Chem.* **2008**, *80*, (23), 8908-8919.
35. Chen, X.; Shen, B.; Sun, J.; Wang, C.; Shan, H.; Yang, C.; Li, C., Characterization and comparison of nitrogen compounds in hydrotreated and untreated shale oil by electrospray ionization (ESI) Fourier transform ion cyclotron resonance mass spectrometry (FT-ICR MS). *Energy Fuel* **2012**, *26*, (3), 1707-1714.
36. Tong, J.; Liu, J.; Han, X.; Wang, S.; Jiang, X., Characterization of nitrogen-containing species in Huadian shale oil by electrospray ionization Fourier transform ion cyclotron resonance mass spectrometry. *Fuel* **2013**, *104*, (0), 365-371.
37. Guricza, L. M.; Schrader, W., Electrospray ionization for determination of non-polar polyaromatic hydrocarbons and polyaromatic heterocycles in heavy crude oil asphaltenes. *J. Mass Spectrom.* **2015**, *50*, (3), 549-557.
38. Chen, H.; Hou, A.; Corilo, Y. E.; Lin, Q.; Lu, J.; Mendelssohn, I. A.; Zhang, R.; Rodgers, R. P.; McKenna, A. M., 4 years after the Deepwater Horizon spill: Molecular transformation of Macondo well oil in Louisiana salt marsh sediments revealed by FT-ICR mass spectrometry. *Environ. Sci. Technol.* **2016**, *50*, (17), 9061-9069.
39. Tian, Z.; Vila, J.; Wang, H.; Bodnar, W.; Aitken, M. D., Diversity and abundance of high-molecular-weight azaarenes in PAH-contaminated environmental samples. *Environ. Sci. Technol.* **2017**, *51*, (24), 14047-14054.
40. Wang, Z. D.; Yang, C.; Yang, Z.; Hollebhone, B.; Brown, C. E.; Landriault, M.; Sun, J.; Mudge, S. M.; Kelly-Hooper, F.; Dixon, D. G., Fingerprinting of petroleum hydrocarbons (PHC) and other biogenic organic compounds (BOC) in oil-contaminated and background soil samples. *J. Environ. Monitor.* **2012**, *14*, (9), 2367-2381.

41. Vecchiato, M.; Bonato, T.; Bertin, A.; Argiriadis, E.; Barbante, C.; Piazza, R., Plant residues as direct and indirect sources of hydrocarbons in soils: current issues and legal implications. *Environ. Sci. Tech. Let.* **2017**, *4*, (12), 512-517.
42. Visser, S. A., Application of Van Krevelen's graphical-statistical method for the study of aquatic humic material. *Environ. Sci. Technol.* **1983**, *17*, (7), 412-417.
43. Hockaday, W. C.; Grannas, A. M.; Kim, S.; Hatcher, P. G., The transformation and mobility of charcoal in a fire-impacted watershed. *Geochim. Cosmochim. Ac.* **2007**, *71*, (14), 3432-3445.
44. Koch, B. P.; Dittmar, T., From mass to structure: an aromaticity index for high-resolution mass data of natural organic matter. *Rapid Commun. Mass Spectrom.* **2006**, *20*, (5), 926-932.

Appendix for Chapter 4

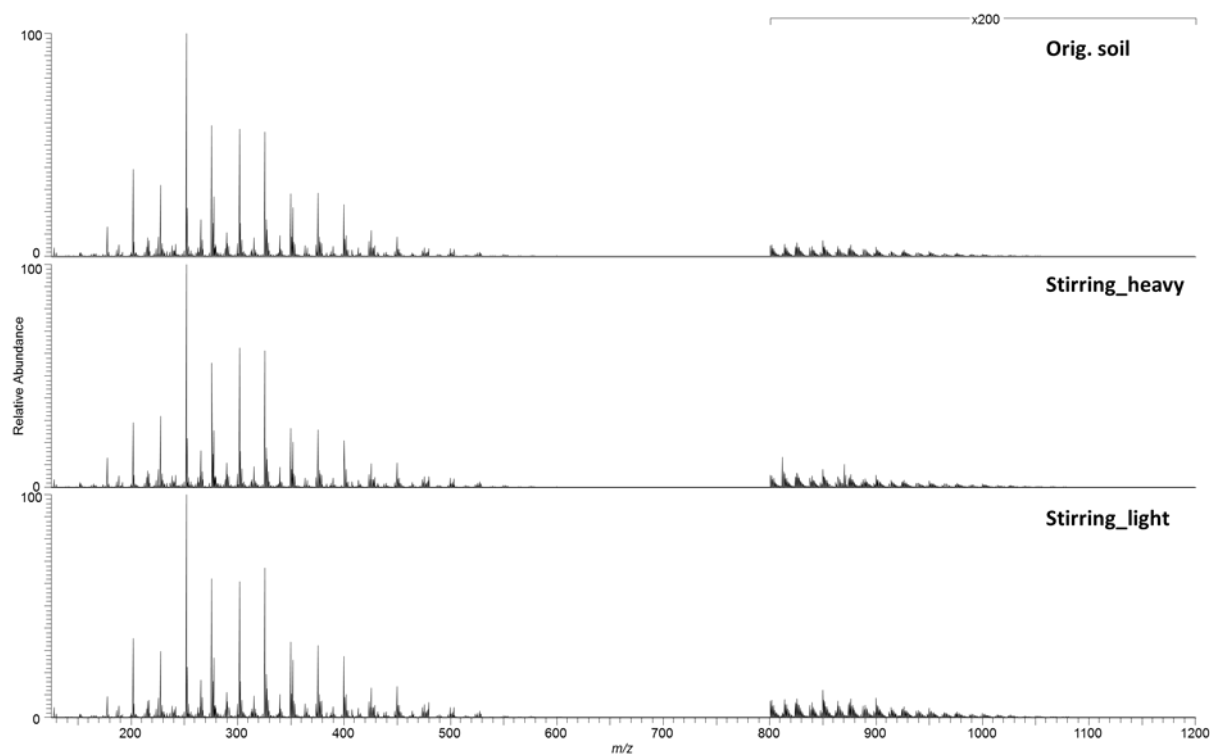


Figure A4-1. Recombined positive mode APPI mass spectra for original soil (top), its heavy (middle) and light (bottom) fractions after stirring.

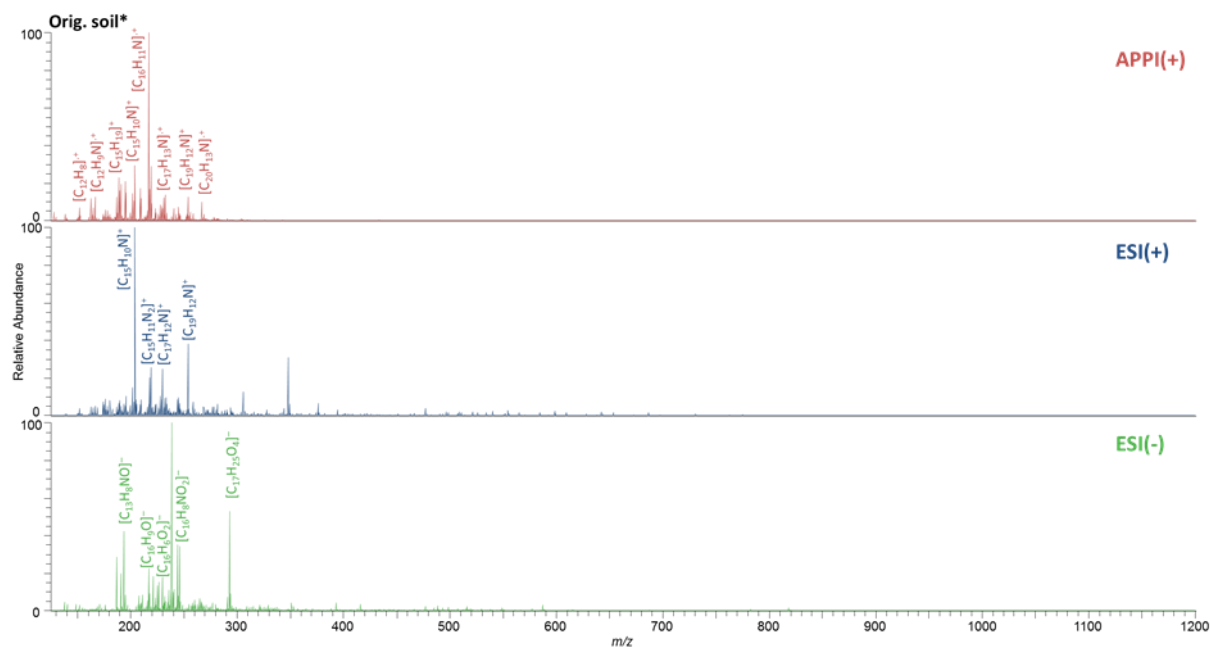


Figure A4-2. Recombined mass spectra for the original soil Soxhlet extracted using water, analyzed by FT Orbitrap MS using positive mode APPI (top), ESI (middle) and negative mode ESI (bottom).

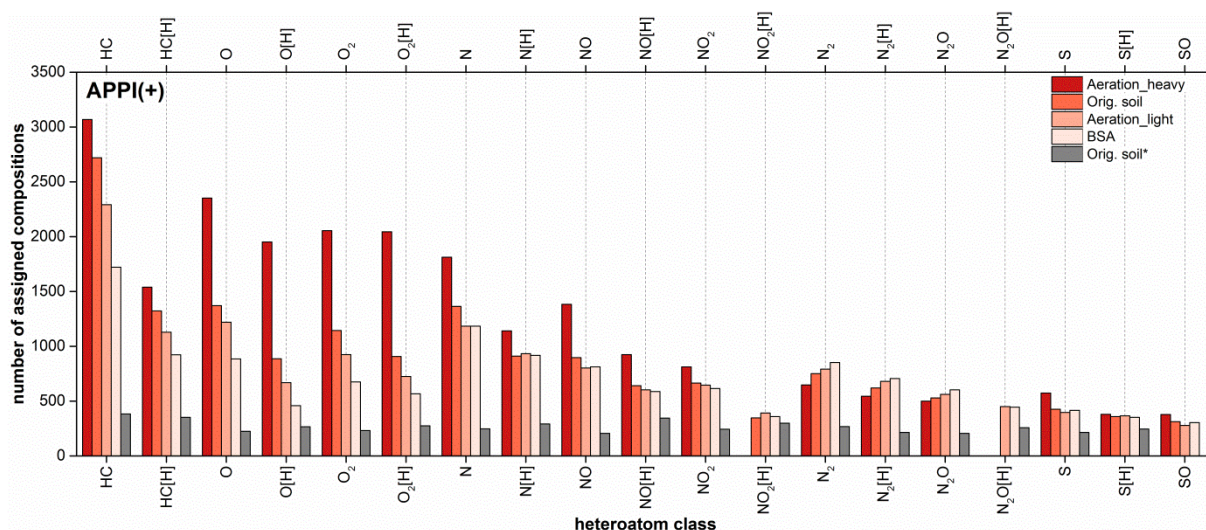


Figure A4-3. Class distributions for the heavy fraction after aeration, original soil, light fraction after aeration and the black solid aggregate (from dark to light red) as well as the water extract (selected classes only) denoted as orig. soil*, analyzed using positive mode APPI FT Orbitrap MS.

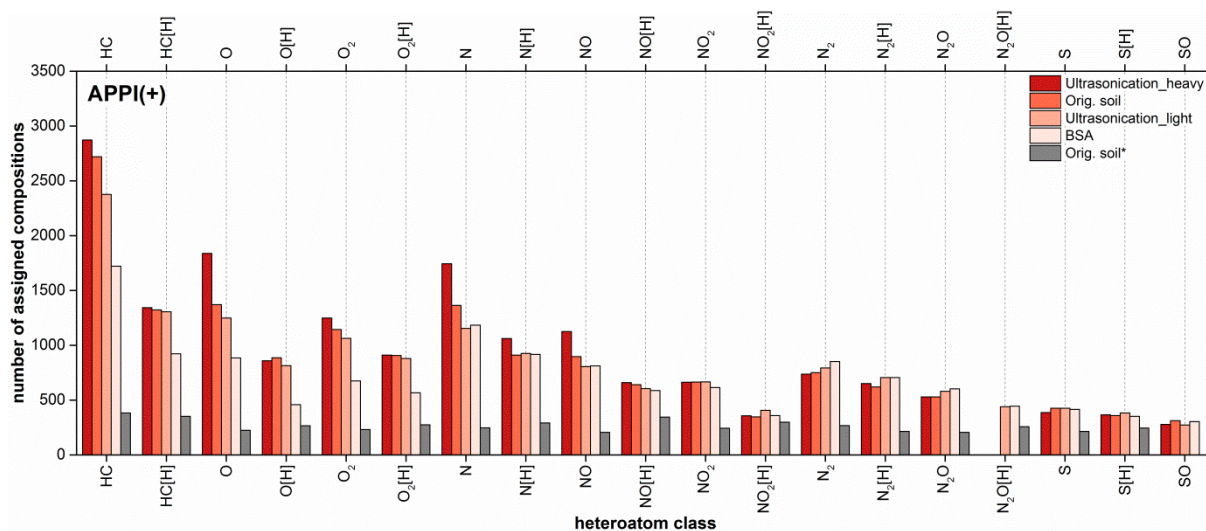


Figure A4-4. Class distributions for the heavy fraction after ultrasonication, original soil, light fraction after ultrasonication and the black solid aggregate (from dark to light red) as well as the water extract (selected classes only) denoted as orig. soil*, analyzed using positive mode APPI FT Orbitrap MS.

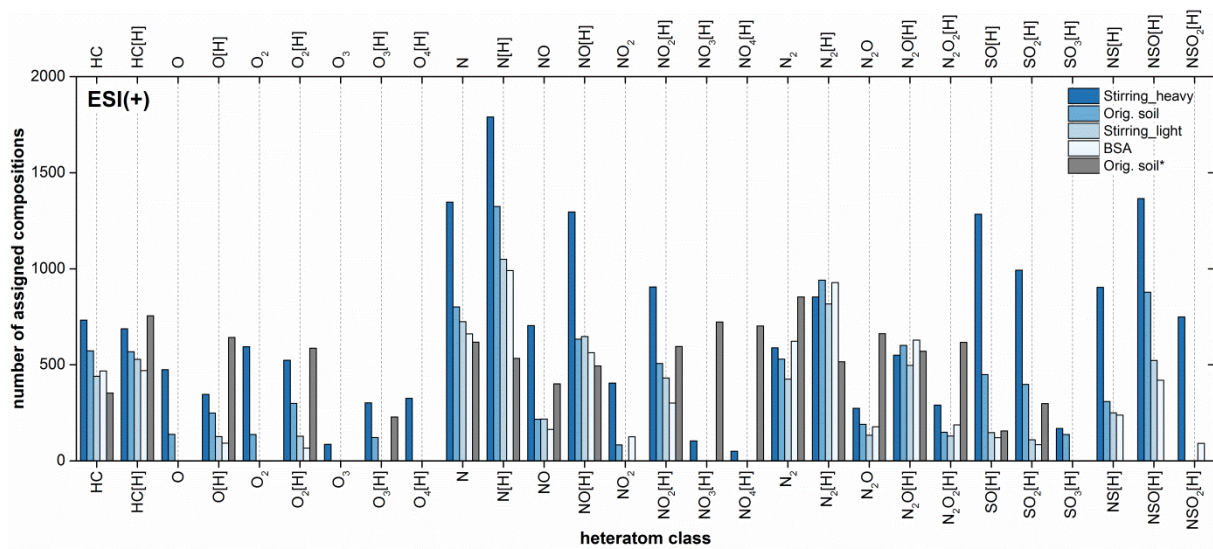


Figure A4-5. Class distributions for the heavy fraction after stirring, original soil, light fraction after stirring and the black solid aggregate (from dark to light blue) as well as the water extract (selected classes only) denoted as orig. soil*, analyzed using positive mode ESI FT Orbitrap MS.

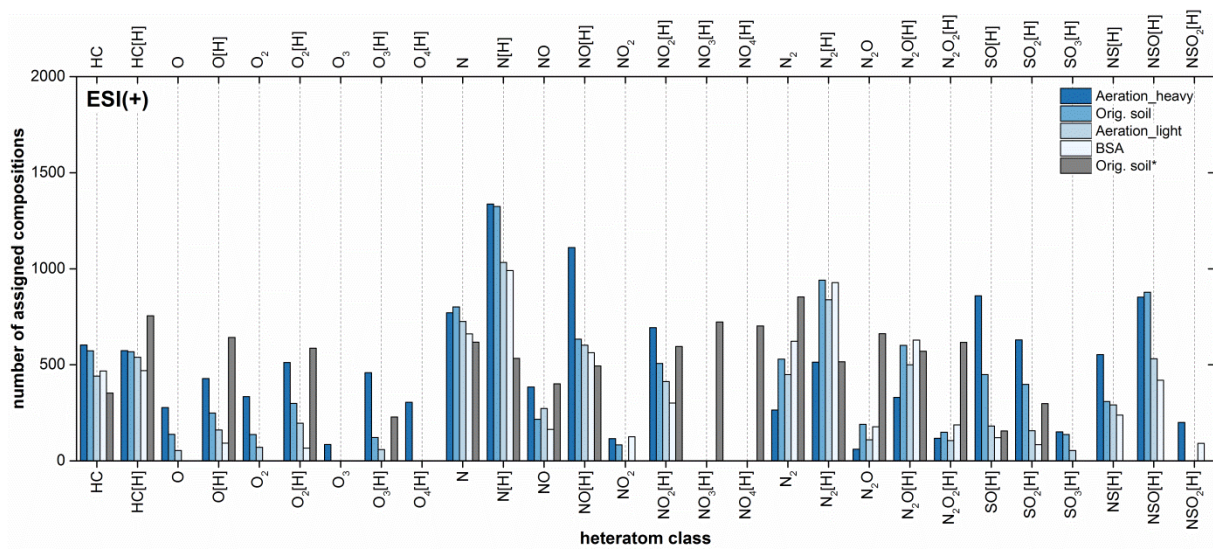


Figure A4-6. Class distributions for the heavy fraction after aeration, original soil, light fraction after aeration and the black solid aggregate (from dark to light red) as well as the water extract (selected classes only) denoted as orig. soil*, analyzed using positive mode ESI FT Orbitrap MS.

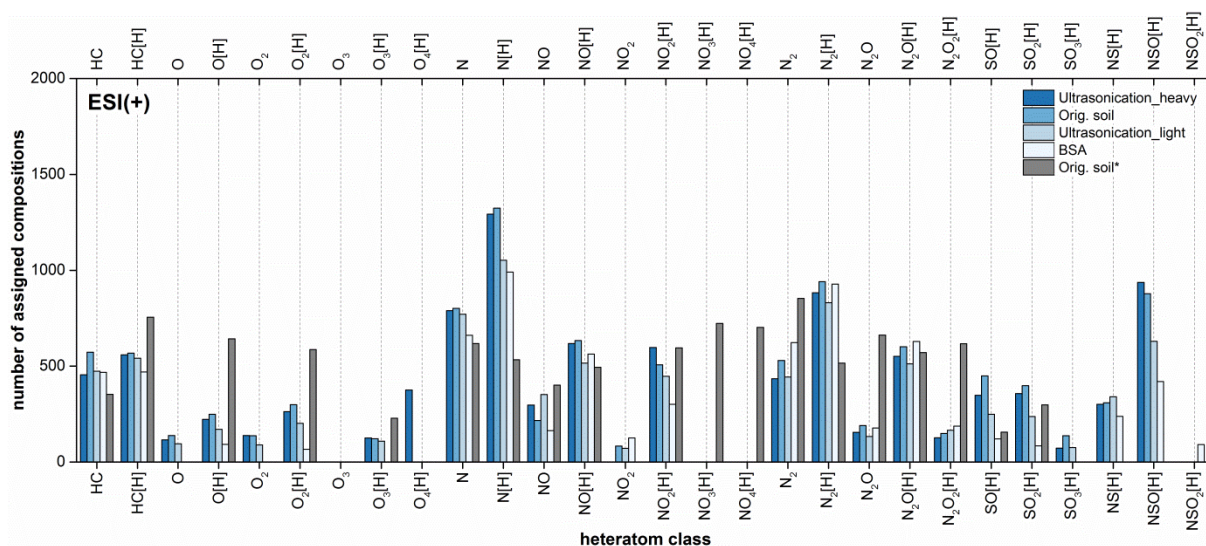


Figure A4-7. Class distributions for the heavy fraction after ultrasonication, original soil, light fraction after ultrasonication and the black solid aggregate (from dark to light red) as well as the water extract (selected classes only) denoted as orig. soil*, analyzed using positive mode ESI FT Orbitrap MS.

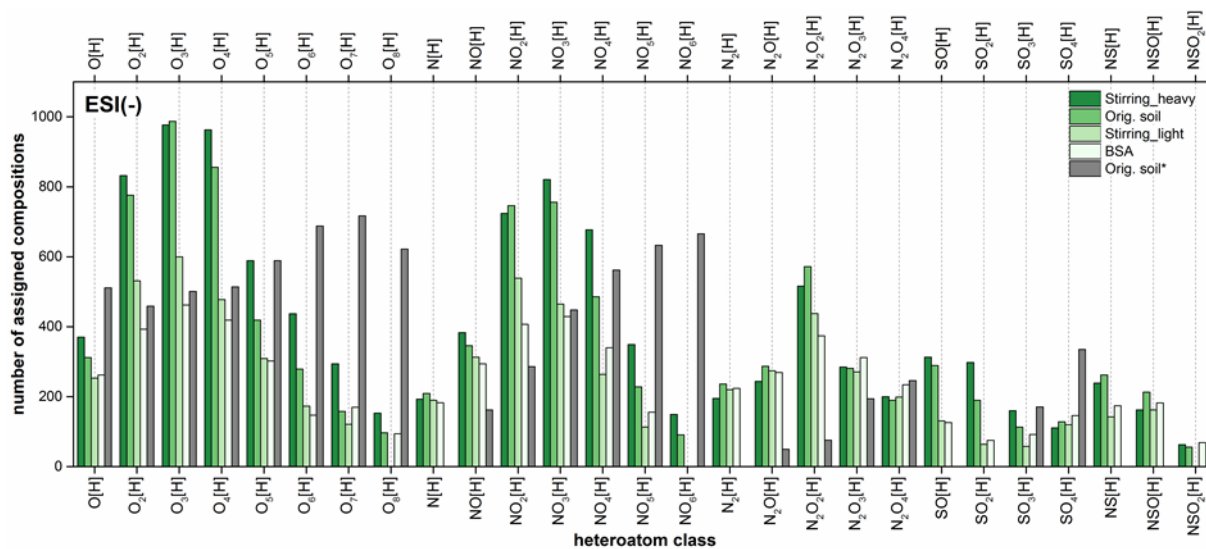


Figure A4-8. Class distributions for the heavy fraction after stirring, original soil, light fraction after stirring and the black solid aggregate (from dark to light red) as well as the water extract (selected classes only) denoted as orig. soil*, analyzed using negative mode ESI FT Orbitrap MS.

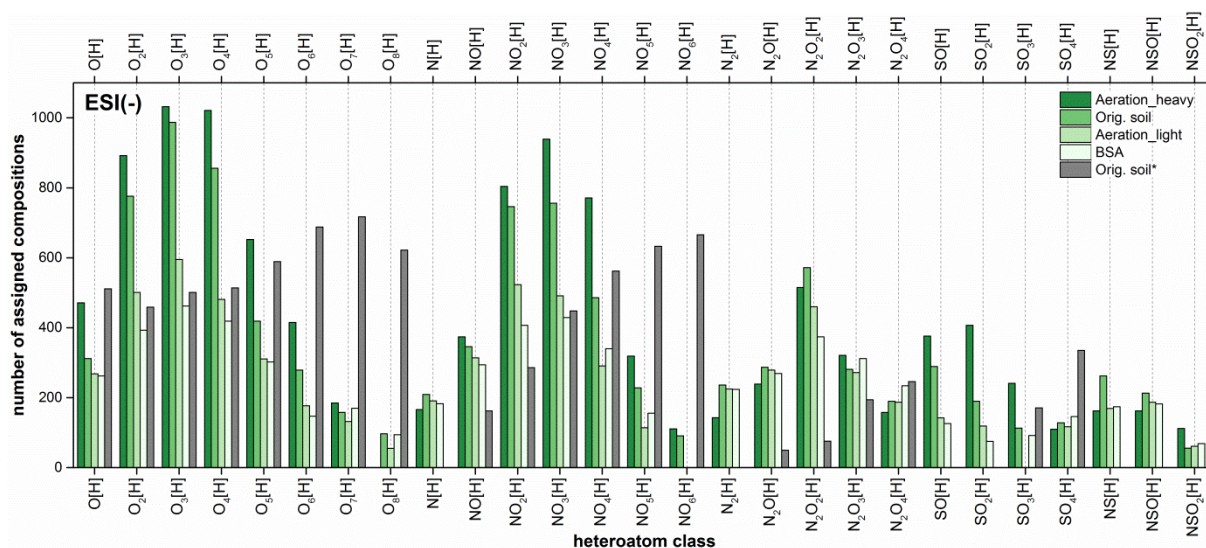


Figure A4-9. Class distributions for the heavy fraction after aeration, original soil, light fraction after aeration and the black solid aggregate (from dark to light red) as well as the water extract (selected classes only) denoted as orig. soil*, analyzed using negative mode ESI FT Orbitrap MS.

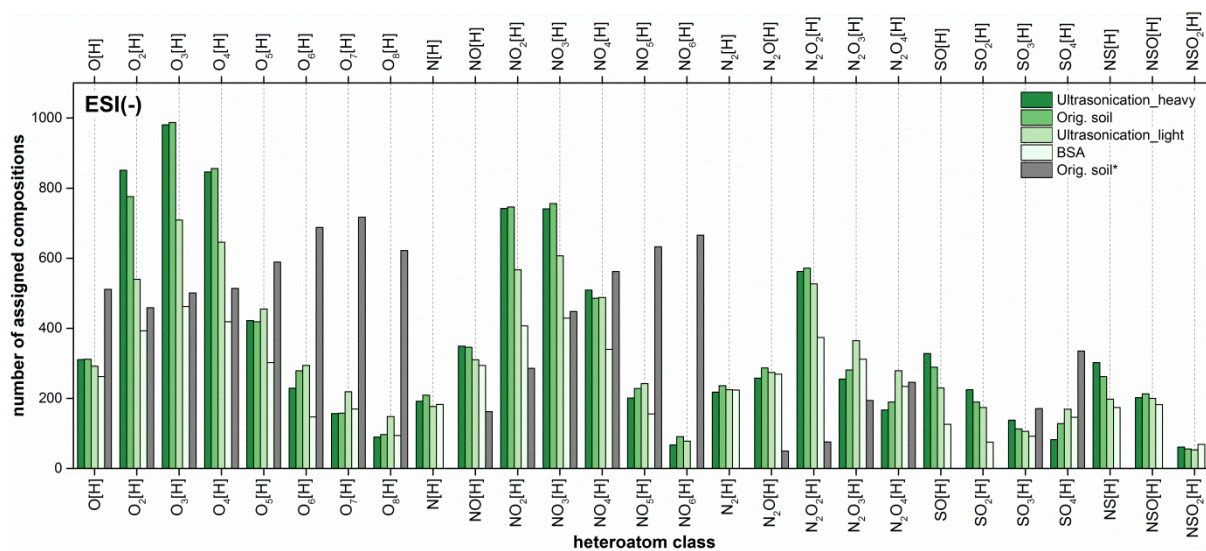


Figure A4-10. Class distributions for the heavy fraction after ultrasonication, original soil, light fraction after ultrasonication and the black solid aggregate (from dark to light red) as well as the water extract (selected classes only) denoted as orig. soil*, analyzed using negative mode ESI FT Orbitrap MS.

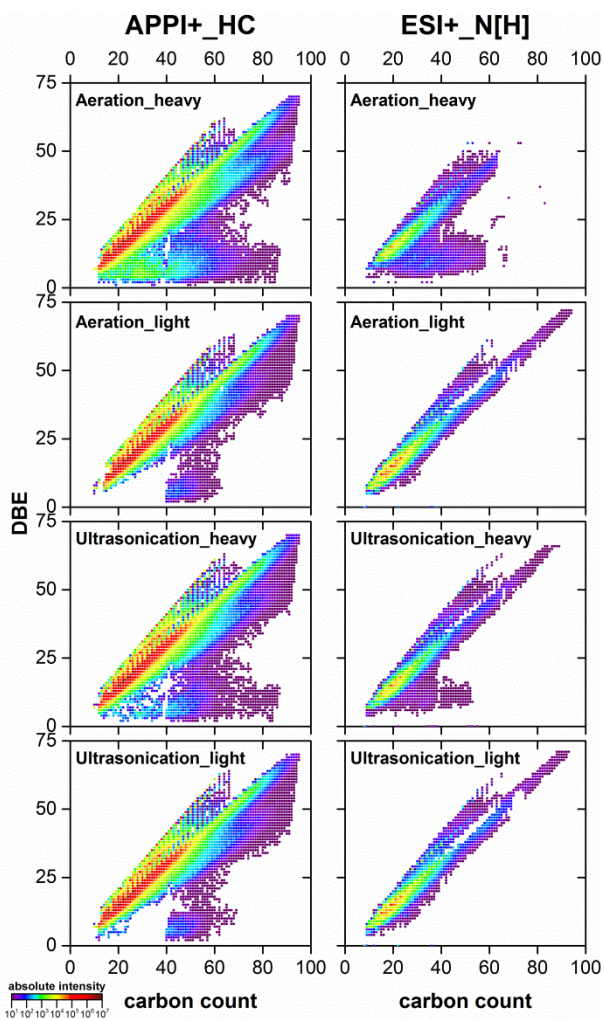


Figure A4-11. Kendrick plots for radical hydrocarbon (left column) and protonated nitrogen (right column) classes from the heavy and light fractions after aeration and ultrasonication (from top to bottom), analyzed using positive mode APP and ESI Orbitrap MS.

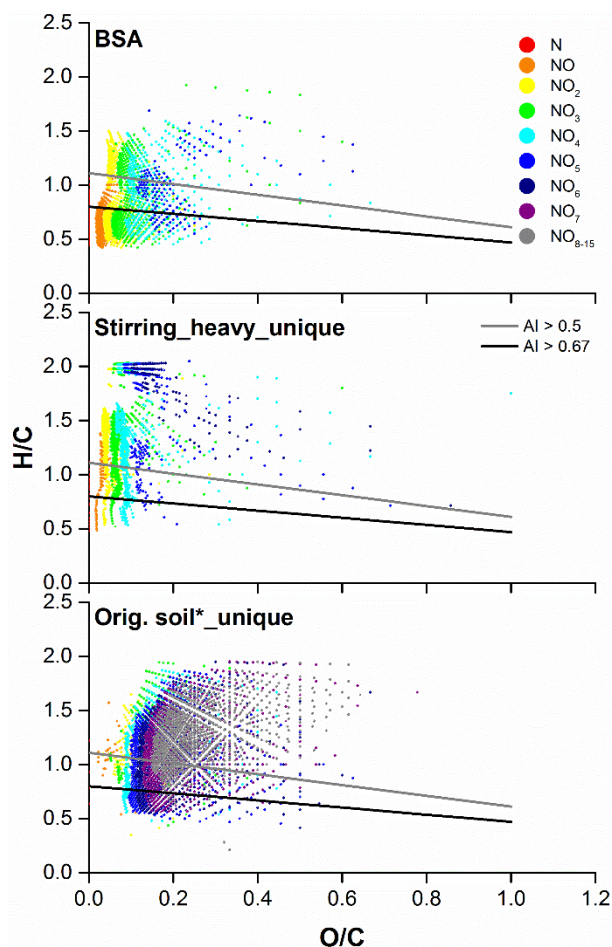


Figure A4-12. Van Krevelen plots for the black solid aggregate (top), the unique compositions from the heavy fraction after stirring (middle), and the original soil Soxhlet extracted using water (bottom, denoted as orig. soil*), compared with the black solid aggregate, analyzed by negative mode ESI FT Orbitrap MS. Compositions below the gray or black line have a AI higher than 0.5 or 0.67, respectively.

Table A4-1. The number of NO_x class compositions detected in total, AI > 0.5 or > 0.67 (proportion to total number in bracket) for different samples.

NO _x classes	Number of compositions in		
	total	AI > 0.5	AI > 0.67
BSA	1809	1298 (72%)	764 (42%)
Stirring_heavy	3296	1596 (48%)	787 (24%)
Orig. soil*	4531	1633 (36%)	567 (13%)

Chapter 5. Investigation of Solvent Extraction for Highly PAH Contaminated Soil Using Used Cooking Oil Methyl Ester

Redrafted from “Luo, R.; Schrader, W., Investigation of Solvent Extraction for Highly PAH Contaminated Soil Using Used Cooking Oil Methyl Ester”, will be submitted to International Journal of Environmental Research and Public Health.

5.1. Abstract

Industrial contaminated soils are associated with high concentration of polycyclic aromatic hydrocarbons (PAHs). Solvent extraction represents an easy, viable remediation technique for the removal of PAHs from highly contaminated soils. In contrast to standard organic solvents, vegetable oils and fatty acid methyl ester (FAME) provide an attractive solution for removing PAHs from the contaminated soil due to their non-toxic, cheap and biodegradable properties. In this study we introduce a waste (used cooking oil methyl ester (UCOME)) as extraction solvent for the removal of PAHs from the contaminated soil. In previous studies, the remediation efficiency was assessed by quantitatively analyzing 16 selected PAHs from the United States Environmental Protection Agency (U.S. EPA). Little effort has been put into understanding the behavior of polycyclic aromatic heterocycles containing nitrogen, sulfur or oxygen (PAXHs, X = N, S, O) under the treatment. For this purpose a non-targeted analysis using gas chromatography atmospheric pressure photoionization Fourier transform mass spectrometry (GC-APPI-FTMS) and direct injection (DI)-APPI-FTMS was performed. Results show at least three fourth of the contaminants were removed from the soil, which contain (high molecular weight and alkylated) PAXHs. Results also demonstrate the necessity of applying state-of-the-art analytical instrumentations for the assessment of remediation efficiency.

5.2. Introduction

Polycyclic aromatic hydrocarbons (PAHs) are a group of chemical compounds, which consist of conjugated aromatic rings.¹ They are considered to be omnipresent in the environment.² A relative high concentration of PAHs, which can be found in contaminated soils from industrial sites, such as manufactured gas plants, coking plants and wood preservation factories, poses a threat to the surrounding ecosystem.³ This is mainly due to their carcinogenic and mutagenic properties as well as their potential to bioaccumulate and persistence towards degradation.⁴ Thus, how to decontaminate the soil in an environmental friendly as well as cost-effective way is of particular importance.

During the years various remediation techniques have been developed for contaminated soils associated with PAHs. Among others, soil washing/solvent extraction belongs to one of the most common applied techniques, which is aimed to minimize disruption to the soil ecology. There are different extraction agents investigated, which include (bio)surfactants, microemulsions, humid acids, cyclodextrins and vegetable oils. Vegetable oils, whose main components are triglycerides, serve as an attractive extraction agent for the removal of PAHs in soil, because of their inexpensive, non-toxic and biodegradable characters.⁵ Recently, fatty acid methyl esters (FAME), which are the major constituents of biodiesel and can be produced from renewable agricultural materials, have shown to offer comparable or even higher removal rate of PAHs in the contaminated soil.⁶

From the analytical point of view, previous studies, which utilized vegetable oils or FAME as extraction solvent for PAH contaminated soil, were focused on the removal of some of the selected 16 PAHs, which are published in the list of priority pollutants from United States Environmental Protection Agency (U.S. EPA).⁷ The quantitative analyses were conducted using chromatographic separations including gas chromatography (GC) or high performance liquid chromatography (HPLC) with flame ionization detector (FID),^{8, 9} quadrupole mass analyzer,¹⁰⁻¹² ultraviolet (UV) detector¹³⁻¹⁵ or fluorescence detector.^{6, 16-18} Here, the research focus was on the optimization of extraction efficiency using vegetable oils or FAME as well as the investigation of integrated remediation including oil extraction with bioremediation or chemical remediation. However, little is known about the behavior of other contaminants in soil, especially high molecular weight PAH and polycyclic aromatic heterocycles containing sulfur, nitrogen or oxygen atom (PAXHs, X = S, N or O), since it is reported that they can occur in the same contaminated soil.^{2, 19} In order to assess the real remediation efficiency and understand the process of contaminant extraction, a more comprehensive analysis is required.

This can be done in a non-targeted approach by using Fourier transform mass spectrometry (FTMS). With its ultrahigh resolution and mass accuracy FTMS can unambiguously assign corresponding elemental compositions to any detected signal.²⁰ By using atmospheric pressure photoionization (APPI) the sensitivity towards PAXHs can be greatly increased.²¹ In addition to this a chromatographic separation, such as GC, can reveal differences in extraction efficiency for different isomeric structures.²²

During this study, we applied used cooking oil methyl ester (UCOME) as extraction solvent for a highly PAXH contaminated soil. The idea is to use a waste (UCOME) to fight another waste (PAXHs). Additionally, the remediation efficiency was examined in a non-targeted way using state-of-the-art instrumentations, which includes GC-APPI-FTMS and direct injection (DI)-APPI-FTMS.

5.3. Materials and Methods

5.3.1. Contaminated Soil Sample

One heavily contaminated soil with PAHs was investigated for this work. The sample was air dried, grinded in mortar and sieved through 2 mm sieve. Prior to the solvent extraction using used cooking oil methyl ester (UCOME) the contaminated soil was pre-separated from the black solid aggregated using a physical separation method, which was described in Chapter 4. Then, 5.00 g of the soil was extracted using dichloromethane (DCM, 99%, Sigma-Aldrich, Germany) for around 300 cycles, concentrated in a rotary evaporator and finally dried under gentle gas stream. The remaining solvent extractable organics (SEO) in the soil has a concentration of 1% (w/w).

5.3.2. Solvent Extraction Using UCOME

10.00 g of the contaminated soil were mixed with 10.00 g of UCOME. The mixture was ultrasonicated for 2 h and equilibrated in dark for 3 days. Subsequently, the mixture was filtered through a filter paper with 0.5 μm particle retention (Macherey-Nagel, Germany) using a water aspirator. The filtrate was denoted as oil phase after filtration, while the rest soil-UCOME mixture was subjected to supercritical fluid extraction (SFE) using CO_2 (99.995%, Air Liquide, Germany). For the SFE the mixture was placed in a stainless steel column, which is equilibrated in an oven with a temperature of 40 °C. The extraction was performed at 180 bar, 40 °C with a supercritical CO_2 flow rate of 2 mL min^{-1} for 4 and 8 h, respectively. The SFE extract from the system was washed out using DCM and rotary-

evaporated. Finally the treated soil was extracted in the same way as the contaminated soil, which is then designated as soil residue extract.

5.3.3. GC-APPI-FTMS Analysis

The original UCOME, contaminated soil extract, soil residue extract, oil phase after filtration and SFE extract were diluted in DCM to a concentration of 1000 ppm for the GC-APPI-FTMS analysis. 1 μL of each sample was injected in splitless mode into a Trace GC Ultra (Thermo Fisher Scientific, Bremen, Germany) coupled to a Q Exactive Plus mass spectrometer (Thermo Fisher Scientific, Bremen, Germany), which are connected through an APPI interface (MasCom, Bremen, Germany). The APPI interface contains a Krypton VUV lamp (photon emission at 10.0 and 10.6 eV, Syagen, Tustin, CA, U.S.A.). The transfer line temperature was set to 320 $^{\circ}\text{C}$. A ZB-5HT Inferno capillary column (30 m x 0.25 mm i.d. x 0.10 μm , Phenomenex, CA, U.S.A.) was used as stationary phase and Helium (purity 99.99999%, Air Liquide, Germany) as mobile phase for the chromatographic separation. The temperature of the oven was heated from 35 $^{\circ}\text{C}$ to 320 $^{\circ}\text{C}$ with a rate of 10 $^{\circ}\text{C min}^{-1}$ and held for 15 min. Mass spectra were acquired in full scan mode in the mass range m/z 60-900 with a resolution of 140,000 at m/z 200 and a scan rate of 1.5 Hz. The sheath gas was set to 8 arbitrary unit (a.u.).

5.3.4. Direct injection APPI FTMS Analysis

The same samples were analyzed using a research type FT Orbitrap MS (Thermo Fisher Scientific, Bremen, Germany) in positive mode APPI. Samples were injected directly at a concentration of 250 ppm in toluene (99.8%, Acros Organics, Germany) and flow rate of 20 mL min^{-1} into the instrument. The vaporizer temperature, sheath, auxiliary as well as sweep gas were set to 350 $^{\circ}\text{C}$, 20, 5 and 2 a.u., respectively. Mass spectra were recorded at a resolution of 480,000 at m/z 400 using spectral stitching,^{20, 23, 24} which means that a recombined mass spectrum for each sample was resulted in the end from small segments with 30 Da mass windows and 5 Da overlap.

5.3.5. Data Analysis

The data were recorded by Xcalibur 2.2 (Thermo Fisher Scientific, Bremen, Germany) and further processed using Composer v1.5.0 (Sierra Analytics, Modesto, CA, U.S.A) with the following chemical constraints: $0 < C < 200$, $0 < H < 1000$, $0 < N < 4$, $0 < S < 5$, $0 < O < 11$, $0 < \text{double bond equivalent (DBE)} < 100$, maximum mass error < 1 ppm.

5.4. Results and Discussion

5.4.1. UCOME extraction for contaminated soil

Investigations using vegetable oils, such as sunflower, rapeseed or peanut oil showed a promising extraction efficiency towards 16 EPA PAHs in contaminated soils.²⁵ However, additional steps must be involved in order to reuse the large amount of oil applied for the treatment. This is essential both from economic and environmental point of view. In comparison to vegetable oils, using FAMES generated from wastes (used cooking oil) or renewable agricultural materials as extraction solvent represent a more economic approach.

Figure 5-1 demonstrates the effect of solvent extraction using UCOME for highly PAH contaminated soil. From the 10.00 g UCOME applied for the extraction only around 70% could be separated from the contaminated soil through filtration. The rest 30% were adsorbed so strong on the soil material that they cannot be separated from soil using simple filtration. It is known that supercritical fluid extraction (SFE) using CO₂ is able to extract lipids from foods.²⁶ Depending on parameters applied for the extraction and the type of lipids to be extracted, mole fraction of lipids in supercritical CO₂ can range from below 0.001 to 0.6. According to this, the soil-UCOME-mixture was subsequently subjected to supercritical CO₂ extraction for separating soil from UCOME as complete as possible. Results show that almost all the rest of UCOME can be extracted from the contaminated soil. The amount SEO in the contaminated soil was reduced from 0.1 g to 0.046 g (4 h SFE) and 0.026 g (8 h SFE), respectively. It has to be noted, that during the SFE, PAHs or at least the 16 EPA PAHs can also be extracted from the contaminated soil.²⁷ This means that the achieved removal rate of

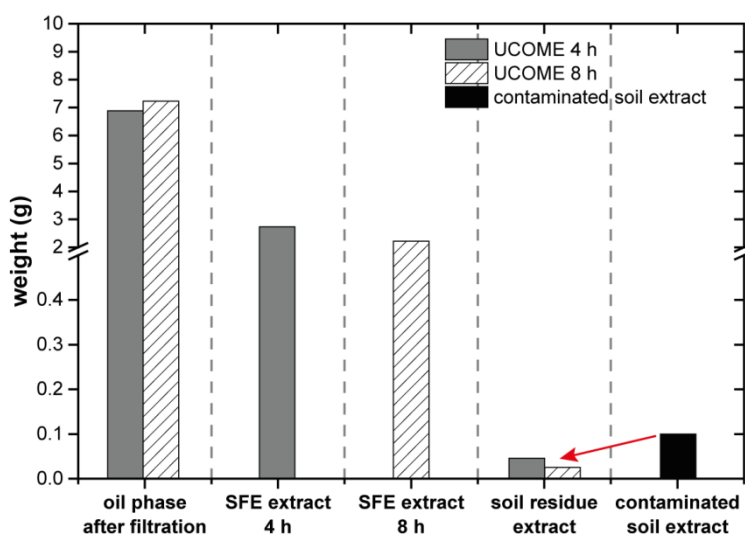


Figure 5-1. Efficiency of solvent extraction using UCOME for highly PAH contaminated soil. UCOME was removed from the contaminated soil through filtration and subsequent supercritical CO₂ extraction.

about 75% is a result of a combination of UCOME extraction and supercritical CO₂ extraction.

5.4.2. GC-APPI-FTMS analysis

The residual contamination in the soil after the treatment (UCOME extraction, subsequent filtration and supercritical CO₂ extraction) was Soxhlet extracted using DCM and analyzed using GC-APPI-FTMS, which was then compared with the UCOME and extract from the original contaminated soil.

Figure 5-2 shows the total ion chromatograms (TIC) for the UCOME, contaminated soil and soil residue extracts. While only few dominant peaks appear in the TIC for the UCOME, the TIC for the original contaminated soil is relative complex. Here, a range of PAHs and a few PANHs as well as PASHs can be detected. In the soil residue extract after the treatment however, most of the contaminants disappeared. Only at higher retention time, which corresponds to compounds with higher molecular weight, are traces of contaminants to be detected (highlighted in the rounded rectangle with green dashed line, Figure 5-2). The peaks with highest intensity found in the TIC for the soil residue extract represent the peaks from UCOME, regarding to the retention time and mass range. This indicates that even after SFE, UCOME was not fully removed from the contaminated soil. On the other hand, it also means, that the actual removal rate for the contaminants in soil should be even higher than 75%, since in the 0.026 g of SEO it still contains a small amount of UCOME.

During the GC-APPI-FTMS measurement mass spectra were recorded at a scan rate of 1.5 Hz.

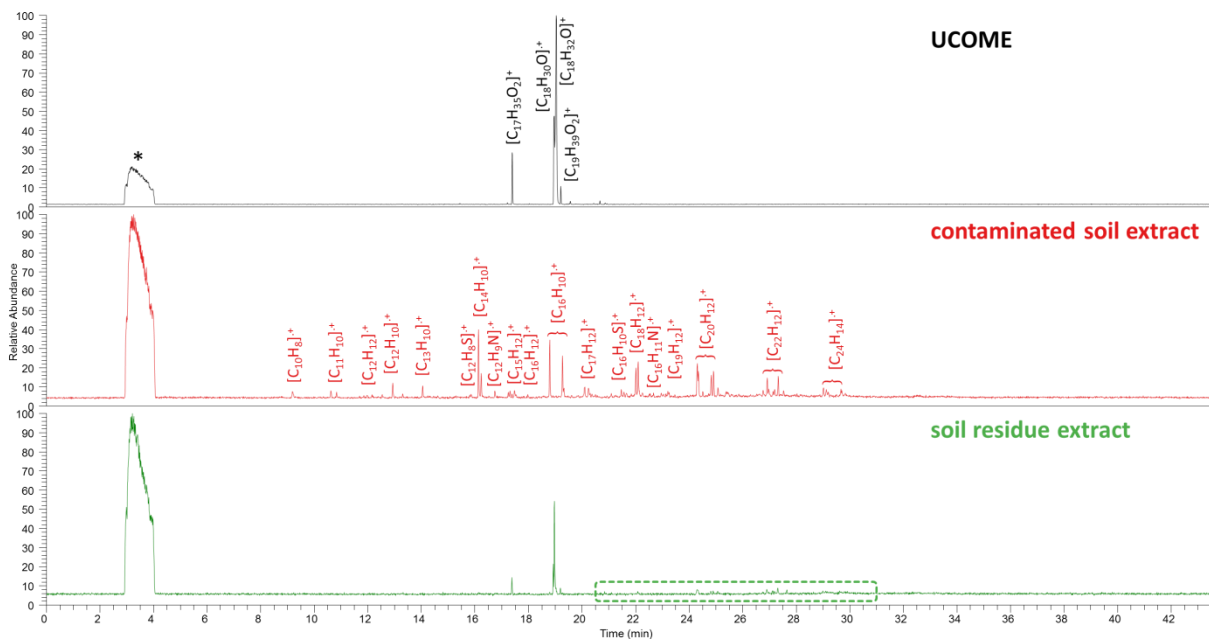


Figure 5-2. Total ion chromatogram for UCOME, contaminated soil and soil residue extracts, analyzed by GC-APPI-FT MS. *: solvent peak.

This means a total number of 3825 mass spectra were generated for only one sample. In order to reduce the data processing time, a recombined mass spectrum of all mass spectra recorded was created for each sample. The drawback of this simplification is that isomeric information was lost.

In the left column of Figure 5-3 the recombined mass spectra for the UCOME, contaminated soil and soil residue extracts, as well as oil phase after filtration (denoted as oil extract) and SFE extract are shown from top to bottom, respectively. Analog to the TIC, the mass spectra for UCOME, contaminated soil and soil residue extracts can be distinguished easily. For the UCOME, ions are mainly located in two mass regions. One region is between 60 and 200 Da and another between 200 and 350 Da. In the mass spectrum for the contaminated soil extract one distribution of m/z values between 150 and 400 with the maximum intensity at around 250 was observed. In comparison to this, fewer signals with lower intensity were detected for the soil residue extract. This consolidates the effectivity of solvent extraction using UCOME for the removal of contaminants from the soil. The mass spectra for oil extract and SFE extract have a high degree of similarity with the one for UCOME. It should be expectable, that the extracted contaminants showed up in both mass spectra for the oil extract as well as

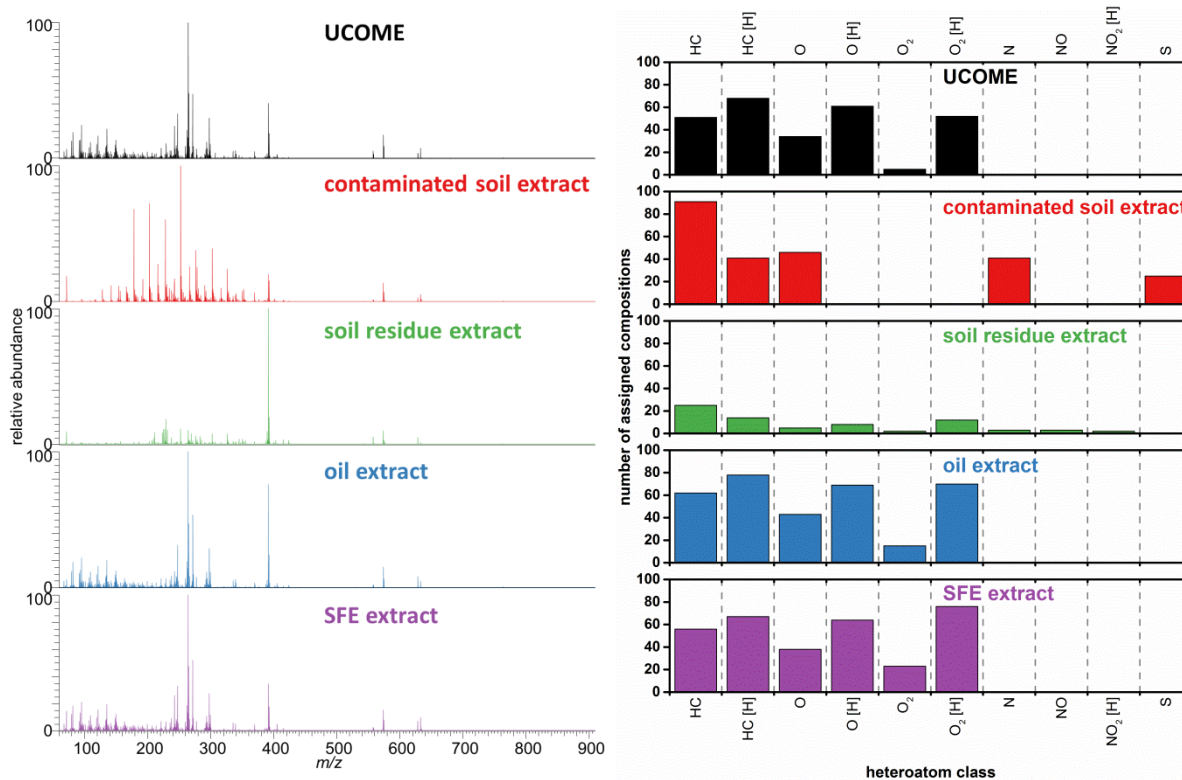


Figure 5-3. Recombined mass spectra (left column) and corresponding class distributions (right column) for UCOME (black), contaminated soil extract (red), soil residue extract (green), oil extract (blue) and SFE extract (purple) and, analyzed by GC-APPI-FT MS.

SFE extract. However, because of the low concentration of contaminants dissolved in UCOME, it is extremely difficult to detect them especially in a non-targeted approach.

The right column of Figure 5-3 summarizes class distributions for the corresponding samples from the left column. This so-called class distribution is done by grouping each detected signal from the mass spectrum according to its assigned elemental composition. For example, lipids from UCOME, such as $[C_{17}H_{34}O_2+H]^+$ (see Figure 5-2, first row), contain two oxygen atom per molecule, therefore they belong to the $O_2 [H]$ class, whereas radical ions of PAHs detected in the contaminated soil (Figure 5-2, second row) belong to the hydrocarbon HC class. Heteroatom classes containing protonated molecules are distinguished from classes containing radical ions with $[H]$ behind the class.

As can be seen in Figure 5-3, HC, O and O_2 class compounds in the UCOME are present predominantly as protonated molecules. These can also be found in the oil extract and SFE extract, since they consist to the largest extent of UCOME. In contrast to this, compounds in the contaminated soil extract are detected mostly as radical ions. Here, radical ions from not only HC class but also O, N and S classes are detectable, which implies the present of PAXH in the contaminated soil. A strong decrease in the number of assigned compositions for the just mentioned classes is observed for the soil residue extract. Results show the capability of using UCOME to extract PAXHs from contaminated soils.

5.4.3. DI-APPI-FTMS analysis

Figure 5-4 summarizes the mass spectra and corresponding class distributions for the same samples shown above, however measured by DI-APPI-FTMS. Here, a measurement technique called “spectral stitching” was implemented. It is done by “stitching” the narrowband mass spectra with a mass window of 30 Da and 5 Da overlap together to get the whole mass range. By doing so, space-charge effects in the mass analyzer are reduced, whereas the dynamic range is increased, which leads to a higher sensitivity and better accuracy.

For the UCOME, oil extract and SFE extract, ions detected in the mass spectra can be divided into two groups (Figure 5-4, left column). Signals below m/z 200 are dominantly produced by the solvent toluene, which was utilized to dissolve the contaminants for the measurement and act as a dopant for the APPI. Signals from the second group with m/z over 200 are originally from the UCOME. In the contaminated soil extract the measured mass range was covered with PAXH signals, and in the soil residue extract their intensities at the lower m/z range

(below m/z 250) are strongly reduced, so that the solvent peaks appeared as dominant signals. In the higher mass range however, contaminants are still detectable.

In the class distributions for UCOME, oil extract and SFE, highly oxidized compounds with up to six oxygen atoms per molecule are detected. These are impurities originally coming from UCOME. A detailed investigation on the structural information of these compounds is out the scope of this work. In the contaminated soil, more than 2500 elemental compositions are assigned to the HC class. These correspond mostly to (alkylated) PAHs. Besides, over 1000 elemental compositions could be assigned to heteroatom containing PAHs including O, N and S. These represent the extreme complexity of the contaminated soil. The class distribution for the soil residue extract looks like a combination of the original contaminated soil and UCOME. It consists of both PAXHs from the contaminated soil and highly oxidized species from UCOME. However, the number of elemental compositions for PAXHs, especially for PANHs and PASHs, is significantly reduced. Gong and co-workers showed, that using fatty acids methyl esters, even a total removal of selected PAHs from a manufactured gas plant soil is hardly to achieve.⁶ This explains why the number of assigned compositions for HC class in the soil residue extract is only slightly reduced in comparison to the value detected in the contaminated soil extract.

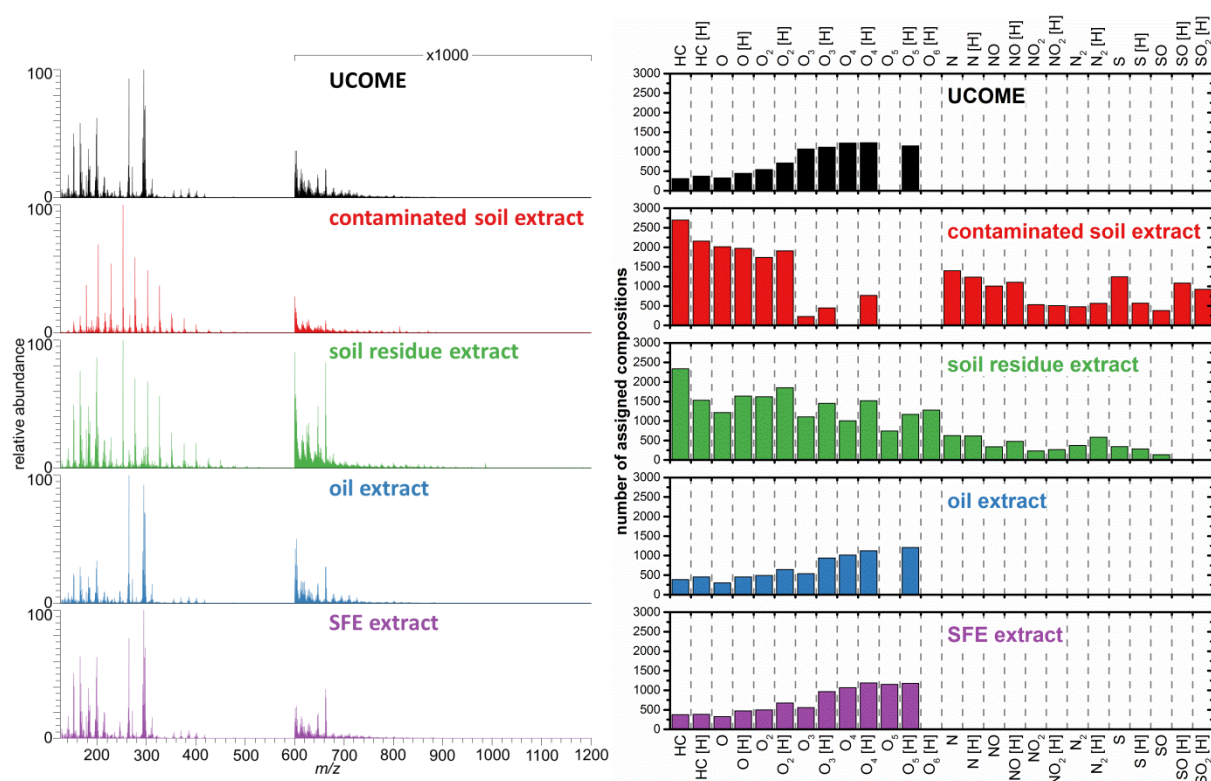


Figure 5-4. Recombined mass spectra (left column) and corresponding class distributions (right column) for UCOME (black), contaminated soil extract (red), soil residue extract (green), oil extract (blue), and SFE extract (purple), analyzed by DI APPI FT MS.

5.4.4. PAXH removal

One of the characteristics of PAXHs is their conjugated π system, which result in their high aromaticity. Taking the 16 selected PAHs from U.S. EPA as examples, their corresponding DBEs increase from 7 (for naphthalene) to 17 (for Benzo[*g,h,i*]perylene and Indeno[1,2,3-*cd*]pyrene). Higher DBE values indicate a higher aromaticity. The change of either number of assigned compositions or absolute intensity for a given DBE value between the soil before and after the treatment can therefore be used as a parameter to evaluate the remediation efficiency by the non-targeted analysis. In Figure 5-5 all assigned elemental compositions in the contaminated soil extract are categorized according to their DBE value and compared to the compositions in the soil residue extract. Here, both the number of assigned compositions (first row) and the absolute intensity (second row) for a given DBE value are summarized.

As can be seen in the GC-APPI-FTMS measurements (Figure 5-5, left column), the intensity based DBE distribution for compositions from the contaminated soil extract was not linear. Some DBE values have a higher absolute intensity in comparison to the values besides them, such as DBE of 10, 12, 15, 17/18 and 20. These represent PAXHs containing 3, 4, 5, 6, and 7 aromatic rings in the structure. Compositions with other DBE values may contain one or more double bonds on the side chain. Overall, reduced numbers of assigned compositions and absolute intensity can be observed for the DBE value between 5 and 25.

In the DI-APPI-FTMS measurements (Figure 5-5, right column), compounds with DBE up to 70 were detected, which is four times higher than the maximum DBE value for the 16 EPA PAHs. Similar to the results obtained from GC-APPI-FTMS measurements, a decrease in

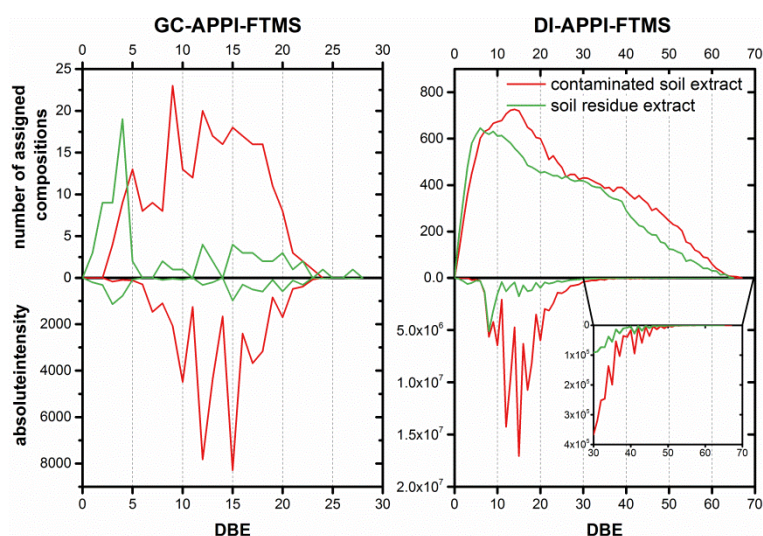


Figure 5-5. Population (top) and intensity (bottom) based DBE distribution for the contaminated soil (red) and soil residue extract (green), analyzed by GC APPI FT MS (left) or DI APPI FT MS (right), respectively.

numbers of assigned compositions with DBE between 5 and 25 can be observed for the treated soil. Additionally, the number of compositions with DBE between 35 and 70 was also decreased. Results from the intensity based DBE plot shows that significant removal of PAXHs with high aromaticity was achieved.

A more detailed view for the HC, N and S class compounds in the contaminated soil and soil residue extracts was presented in Figure 5-6. Here, the number of carbon atom in each detected elemental composition is plotted against its DBE value. By comparing the absolute intensity of each signal from the soil residue and contaminated soil extracts, it is able to assess the removal rate for every PAXH detected.

Already in the DBE vs. carbon count plot for the HC class compositions from the contaminated soil extracted (Figure 5-6, first row, left), which is measured using GC-APPI-

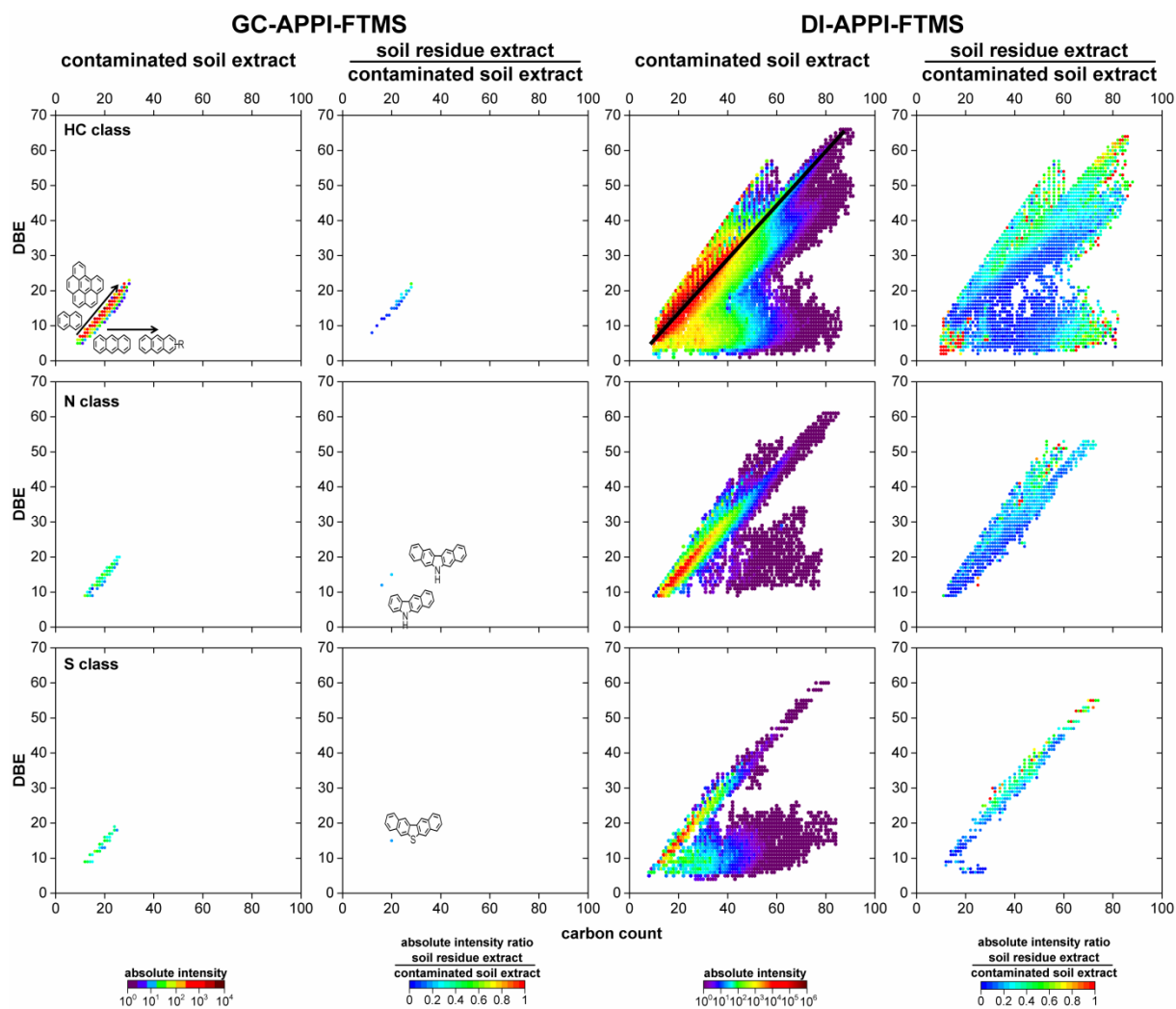


Figure 5-6. DBE vs. carbon count plots for HC (top), N (middle) and S (bottom) classes from the contaminated soil extract as well as soil residue extract compared to the contaminated soil extract, analyzed by GC- and DI-APPI-FTMS,

FTMS, it can be seen, that not only the 16 selected EPA PAHS, but also other high molecular weight PAHs as well as alkylated PAHs were present as contaminants in the soil. In addition to these (alkylated) PAHs, results from the GC-APPI-FTMS measurement also show that a few PANHs and PASHs are also detected in the contaminated soil. These can correspond to pyrrole, pyridine as well as thiophene containing PAHs.²⁸⁻³⁰

The DI-APPI-FTMS measurement for the contaminated soil (Figure 5-6, third column) revealed further that, the pattern of contaminants in the soil is far from simple. In total, 2697, 1399 and 1242 elemental compositions were assigned to the HC, N and S classes, respectively. Here, PAXHs with a DBE value up to 70 and carbon count above 90 can be detected. Compositions with higher absolute intensity are located on a line with a slope of 0.75, which represent PAXH core structures without side chains (detailed discussion in Chapter 3).

Results demonstrate clearly that assessing the remediation efficiency for contaminated soils using only 16 selected PAHs is far from enough. Only use non-targeted approach with state-of-the-art instrumentations a comprehensive view of contaminants in the soil can be gained, and their environmental impact together with remediation efficiency correctly evaluated. The efficiency of PAXH removal was examined by dividing the absolute intensity of each elemental composition in the soil residue extract by the corresponding intensity detected in the contaminated soil extract.

For the GC-APPI-FTMS measurements (Figure 5-6, second column), longer alkylated PAHs were removed totally, leaving few PAHs without or with maximum an ethyl side chain in the soil residue extract. The absolute intensity of the remaining PAHs was reduce to half ($C_{28}H_{14}$, DBE = 22) to below 5% ($C_{14}H_{10}$ DBE = 10, $C_{16}H_{10}$, or $C_{17}H_{12}$, DBE = 12) compared to the contaminated soil extract. A dramatic reduce of PAXHs indicate that UCOME is also applicable for the removal of PAXHs. Only $C_{16}H_{11}N$, $C_{20}H_{13}N$ and $C_{20}H_{12}S$, which can correspond to benzocarbazole, dibenzocarbazole and dinaphthothiophene as well as their structural isomers, are present in the soil residue extract, whose absolute intensity was reduced to 10% of the previous intensity.

For the DI-APPI-FTMS measurements (Figure 5-6, rightmost column) a clear decrease in the absolute intensity was observed for compositions at a DBE range between 4 and 40. A maximal removal for HC class compositions was found at DBE between 10 and 30 and carbon count between 10 and 60, where some of the compositions disappeared totally. With the increase in DBE and/or carbon count, the extraction efficiency decrease. Same trend was

also observed for N and S class compositions. Here, the entire PAXHs with longer side chains were removed and for the non-alkylated PAXHs a removal of higher than 60% was reached.

5.5. Conclusion

In this work we present an environmental friendly and economically favorable extraction solvent for the removal of PAXHs from contaminated soils. Here, the used cooking oil as a waste can be reused to treat another waste, in this case the contaminated soil. In addition to this, data from the non-targeted analysis using state-of-the-art instrumentations reveal the complexity of PAXHs in such contaminated soils. At the same time the data indicate that the remediation efficiencies assessed by using quantitative analysis of only 16 selected EPA PAHs should be questioned.

5.6. References

1. Achten, C.; Andersson, J. T., Overview of Polycyclic Aromatic Compounds (PAC). *Polycycl. Aromat. Comp.* **2015**, *35*, (2-4), 177-186.
2. Stout, S. A.; Emsbo-Mattingly, S. D.; Douglas, G. S.; Uhler, A. D.; McCarthy, K. J., Beyond 16 Priority Pollutant PAHs: A Review of PACs used in Environmental Forensic Chemistry. *Polycycl. Aromat. Comp.* **2015**, *35*, (2-4), 285-315.
3. Kuppusamy, S.; Thavamani, P.; Venkateswarlu, K.; Lee, Y. B.; Naidu, R.; Megharaj, M., Remediation approaches for polycyclic aromatic hydrocarbons (PAHs) contaminated soils: Technological constraints, emerging trends and future directions. *Chemosphere* **2017**, *168*, 944-968.
4. Qu, C.; Li, B.; Wu, H.; Wang, S.; Giesy, J. P., Multi-pathway assessment of human health risk posed by polycyclic aromatic hydrocarbons. *Environ Geochem Hlth* **2015**, *37*, (3), 587-601.
5. Lau, E. V.; Gan, S.; Ng, H. K.; Poh, P. E., Extraction agents for the removal of polycyclic aromatic hydrocarbons (PAHs) from soil in soil washing technologies. *Environ. Pollut.* **2014**, *184*, 640-649.
6. Gong, Z.; Wang, X.; Tu, Y.; Wu, J.; Sun, Y.; Li, P., Polycyclic aromatic hydrocarbon removal from contaminated soils using fatty acid methyl esters. *Chemosphere* **2010**, *79*, (2), 138-143.
7. Keith, L.; Telliard, W., ES&T Special Report: Priority pollutants: I-a perspective view. *Environ. Sci. Technol.* **1979**, *13*, (4), 416-423.
8. Pannu, J. K.; Singh, A.; Ward, O. P., Vegetable oil as a contaminated soil remediation amendment: application of peanut oil for extraction of polycyclic aromatic hydrocarbons from soil. *Process Biochem.* **2004**, *39*, (10), 1211-1216.
9. Lau, E. V.; Gan, S.; Ng, H. K., Extraction of phenanthrene and fluoranthene from contaminated sand using palm kernel and soybean oils. *J. Environ. Manage.* **2012**, *107*, 124-130.
10. Pizzul, L.; Pilar Castillo, M. d.; Stenström, J., Characterization of selected actinomycetes degrading polyaromatic hydrocarbons in liquid culture and spiked soil. *World J. Microb. Biot.* **2006**, *22*, (7), 745-752.
11. Pizzul, L.; Sjögren, Å.; Castillo, M. d. P.; Stenström, J., Degradation of polycyclic aromatic hydrocarbons in soil by a two-step sequential treatment. *Biodegradation* **2007**, *18*, (5), 607-616.

12. Pizzul, L.; Castillo, M. d. P.; Stenström, J., Effect of rapeseed oil on the degradation of polycyclic aromatic hydrocarbons in soil by *Rhodococcus wratislaviensis*. *Int. Biodeter. Biodegr.* **2007**, *59*, (2), 111-118.
13. Gong, Z.; Alef, K.; Wilke, B. M.; Li, P., Dissolution and removal of PAHs from a contaminated soil using sunflower oil. *Chemosphere* **2005**, *58*, (3), 291-298.
14. Leonardi, V.; Giubilei, M. A.; Federici, E.; Spaccapelo, R.; Šašek, V.; Novotny, C.; Petruccioli, M.; D'Annibale, A., Mobilizing agents enhance fungal degradation of polycyclic aromatic hydrocarbons and affect diversity of indigenous bacteria in soil. **2008**, *101*, (2), 273-285.
15. Bogan, B. W.; Trbovic, V.; Paterek, J. R., Inclusion of vegetable oils in Fenton's chemistry for remediation of PAH-contaminated soils. *Chemosphere* **2003**, *50*, (1), 15-21.
16. Gong, Z.; Wilke, B. M.; Alef, K.; Li, P., Influence of soil moisture on sunflower oil extraction of polycyclic aromatic hydrocarbons from a manufactured gas plant soil. *Sci. Total Environ.* **2005**, *343*, (1), 51-59.
17. Gong, Z.; Wilke, B. M.; Alef, K.; Li, P.; Zhou, Q., Removal of polycyclic aromatic hydrocarbons from manufactured gas plant-contaminated soils using sunflower oil: Laboratory column experiments. *Chemosphere* **2006**, *62*, (5), 780-787.
18. Scherr, K. E.; Hasinger, M.; Mayer, P.; Loibner, A. P., Effect of vegetable oil addition on bioaccessibility and biodegradation of polycyclic aromatic hydrocarbons in historically contaminated soils. *J. Chem. Technol. Biot.* **2009**, *84*, (6), 827-835.
19. Andersson, J. T.; Achten, C., Time to say goodbye to the 16 EPA PAHs? Toward an up-to-date use of PACs for environmental purposes. *Polycycl. Aromat. Comp.* **2015**, *35*, (2-4), 330-354.
20. Vetere, A.; Schrader, W., Mass spectrometric coverage of complex mixtures: Exploring the carbon space of crude oil. *ChemistrySelect* **2017**, *2*, (3), 849-853.
21. Gaspar, A.; Zellermann, E.; Lababidi, S.; Reece, J.; Schrader, W., Impact of Different Ionization Methods on the Molecular Assignments of Asphaltenes by FT-ICR Mass Spectrometry. *Anal. Chem.* **2012**, *84*, (12), 5257-5267.
22. Thomas, M. J.; Collinge, E.; Witt, M.; Palacio Lozano, D. C.; Vane, C. H.; Moss-Hayes, V.; Barrow, M. P., Petroleomic depth profiling of Staten Island salt marsh soil: 2 ω detection FTICR MS offers a new solution for the analysis of environmental contaminants. *Sci. Total Environ.* **2019**, *662*, 852-862.
23. Southam, A. D.; Payne, T. G.; Cooper, H. J.; Arvanitis, T. N.; Viant, M. R., Dynamic range and mass accuracy of wide-scan direct infusion nanoelectrospray Fourier transform ion cyclotron resonance mass spectrometry-based metabolomics increased by the spectral stitching method. *Anal. Chem.* **2007**, *79*, (12), 4595-4602.
24. Gaspar, A.; Schrader, W., Expanding the data depth for the analysis of complex crude oil samples by Fourier transform ion cyclotron resonance mass spectrometry using the spectral stitching method. *Rapid Commun. Mass Spectrom.* **2012**, *26*, (9), 1047-1052.
25. Yap, C. L.; Gan, S.; Ng, H. K., Application of vegetable oils in the treatment of polycyclic aromatic hydrocarbons-contaminated soils. *J. Hazard. Mater.* **2010**, *177*, (1), 28-41.
26. Güçlü, Ü.; Temelli, F., Correlating the Solubility Behavior of Fatty Acids, Mono-, Di-, and Triglycerides, and Fatty Acid Esters in Supercritical Carbon Dioxide. *Ind. Eng. Chem. Res.* **2000**, *39*, (12), 4756-4766.
27. Becnel, J. M.; Dooley, K. M., Supercritical fluid extraction of polycyclic aromatic hydrocarbon mixtures from contaminated soils. *Ind. Eng. Chem. Res.* **1998**, *37*, (2), 584-594.
28. Noah, M.; Poetz, S.; Vieth-Hillebrand, A.; Wilkes, H., Detection of Residual Oil-Sand-Derived Organic Material in Developing Soils of Reclamation Sites by Ultra-

- High-Resolution Mass Spectrometry. *Environ. Sci. Technol.* **2015**, *49*, (11), 6466-6473.
29. Manzano, C. A.; Marvin, C.; Muir, D.; Harner, T.; Martin, J.; Zhang, Y., Heterocyclic Aromatics in Petroleum Coke, Snow, Lake Sediments, and Air Samples from the Athabasca Oil Sands Region. *Environ. Sci. Technol.* **2017**, *51*, (10), 5445-5453.
 30. Tian, Z.; Vila, J.; Wang, H.; Bodnar, W.; Aitken, M. D., Diversity and Abundance of High-Molecular-Weight Azaarenes in PAH-Contaminated Environmental Samples. *Environ. Sci. Technol.* **2017**, *51*, (24), 14047-14054.

Chapter 6. Pyrolytic Remediation of Highly PAH Contaminated Soil, Analyzed Using Ultrahigh Resolution Atmospheric Pressure Photon Ionization (APPI) Fourier Transform Mass Spectrometry and Gas Chromatography-APPI-Mass Spectrometry

Redrafted from “Luo, R.; Schrader, W., Pyrolytic Remediation of Highly PAH Contaminated Soil, Analyzed Using Ultrahigh Resolution Atmospheric Pressure Photon Ionization (APPI) Fourier Transform Mass Spectrometry and Gas Chromatography-APPI-Mass Spectrometry”, will be submitted to Environmental Pollution.

6.1. Abstract

Soils from industrial sites, which are highly contaminated with polycyclic aromatic hydrocarbons (PAHs), are difficult to be cleaned up. Pyrolytic remediation presents a reliable approach for the removal of PAHs or other hydrocarbon based contaminants from contaminated soils, since lower energy is required in comparison to other thermal treatments and the soil fertility can be maintained or even enhanced. Its remediation efficiency is usually assessed by using non-specific gas chromatography flame ionization detector (GC-FID) analysis or quantitative analysis of the 16 PAHs from United States Environmental Protection Agency (U.S. EPA). However, in order to understand the chemistry for such an ultra-complex environmental system under pyrolytic remediation, which includes soil and diverse contaminants, advanced analytical techniques are needed. In our study, ultrahigh resolution data for the pyrolyzed samples are obtained by GC-atmospheric pressure photon ionization (APPI)-Fourier transform mass spectrometry (FTMS) and direct injection (DI) APPI FTMS. Results show a significant removal of PA(X)Hs (X = N, S, O) with double bond equivalent (DBE) up to 70 at a pyrolysis temperature of 450 °C. Low molecular weight (carbon count 10 to 40) and low DBE (with highest intensity around 10) compounds are generated and transferred into the oil fractions representing an usable fuel. By this application, especially the pyrolysis of highly PAH contaminated soil under vacuum condition, leads to a better remediation efficiency for PAXHs while the soil still stays viable. It is also possible to convert the contamination into a transportation fuel in the diesel range.

6.2. Introduction

Polycyclic aromatic hydrocarbons (PAHs) are omnipresent in the environment with ecotoxic and carcinogenic characters.¹ Extreme high concentration of PAHs can be found in the industrial sites, such as coal mining or manufactured gas plants.²⁻⁶ In these cases, the biological degradation, which is the most popular remediation technique, alone will not be amenable. Since the high toxicity suppresses the growth of bacteria in the contaminated soil.⁷ Also, higher amount of reagents are required for chemical treatments, which will directly result in higher remediation costs.

Among other remediation techniques, thermal treatments show an effective removal of PAHs from highly contaminated soils.⁸ The main drawbacks of thermal treatments are destruction of the soil's fertility and relative high energy demand.⁹ Recently, pyrolysis is gaining more attention as a reliable technique for the removal of PAHs or hydrocarbons from the contaminated soil while keeping the soil fertility due to the lower operation temperature.^{8, 10, 11} Efforts have been made to evaluate the pyrolytic treatment using either chemical parameters, such as PAH concentration or the content of total petroleum hydrocarbons (TPH), as well as biological parameters, such as plant growth. However, a detailed chemical investigation for the pyrolysis remediation on a non-targeted approach is missing.

This is just to the fact that environmental samples, especially those from contaminated industrial sites, are extremely complex. Recent targeted analyses have shown, that besides the 16 PAHs, which were selected as priority pollutants from United States Environmental Protection Agency (U.S. EPA), other high molecular weight PAHs, alkylated PAHs and heteroatom containing PAXHs (X = N, S, O) can co-occur in the contaminated soils.¹²⁻¹⁷ How do these compounds chemically behave, interact with each other as well as with the circumstance during the pyrolysis, this remains unresolved.

Because of the sample complexity advanced analytical techniques, such as two dimensional gas chromatography (GC x GC) and high resolution mass spectrometry including time-of flight mass spectrometry (ToF-MS), are applied for the non-targeted analysis of contaminated soils.^{18, 19} As one of the most versatile analytical instruments, Fourier transform ion cyclotron resonance (FT ICR) and FT Orbitrap mass spectrometry (MS) with their ultrahigh mass resolution and accuracy have proven to be able to unravel the chemistry of most complex environmental mixtures, such as crude oil.^{20, 21} The utilization of ultrahigh resolution MS for the soil analysis has been dedicated to its natural constituents, such as natural organic matters, in the first place.²²⁻²⁵ Fewer applications have addressed for contaminated soils from industrial

sites or samples after the remediation.²⁶⁻³⁰ The complexity of the soil itself and the contaminants as well as the remediation techniques applied makes it a challenging task.

In this study we applied state-of-the-art instrumentations, including atmospheric pressure photon ionization (APPI) FT Orbitrap MS and gas chromatography (GC) APPI FT MS for the non-targeted analysis of a highly PAH contaminated soil after pyrolysis. The detailed molecular characterization of the original and pyrolyzed samples allows a deeper chemical understanding of the pyrolytic remediation, which helps to assess the remediation efficiency. In addition to remediation, the contamination is a carbon precursor. This means that the liquid collected from the pyrolysis process are a fuel that depending on the conditions and precursor molecules can be used either as a diesel or gasoline surrogate.

6.3. Materials and Methods

6.3.1. Contaminated Soil Sample

One highly PAH contaminated soil sample was air dried, grinded in mortar, sieved through 2 mm sieve, and stored in the fridge at 4 °C. The soil was physically separated through density difference into light and heavy fractions. The light fraction ($\rho < 1.4 \text{ g cm}^{-3}$) consisted of high amount of solvent extractable organics, which were accumulated in the black solid aggregates. Only the heavy fraction ($\rho > 1.4 \text{ g cm}^{-3}$) was subjected to pyrolysis.

6.3.2. Thermogravimetric Analysis

The pre-separated contaminated soil ($\rho > 1.4 \text{ g/cm}^3$) and the black solid aggregates were analyzed thermal gravimetrically using a Mettler Toledo TGA/DSC 1 Star System from room temperature to 750 °C at 10 °C min⁻¹ under Argon atmosphere.

6.3.3. Pyrolysis

10 g of pre-separated contaminated soil were put into a quartz glass tube, which was placed vertically into a tube furnace (EVA 12/300/E301, Carbolite Gero, Germany). The sample was pyrolyzed at 450 °C or 300 °C under Argon gas flow, or at 300 °C under vacuum for 3 h. The resulting heavy and light volatile fractions during pyrolysis were collected at 0 °C and -78 °C, respectively. The soil residue after pyrolysis was Soxhlet extracted using dichloromethane (DCM, 99%, Sigma-Aldrich, Germany) for the determination of the amount of solvent extractable organics. The heavy and light volatile fractions were re-dissolved in dichloromethane and transferred into collecting vials. The solvent was evaporated under gentle nitrogen gas and the weight was determined. For comparison purposes, the pre-

separated contaminated soil was Soxhlet extracted as described for the soil residue after pyrolysis.

6.3.4. GC-APPI-FT MS Analysis

The Soxhlet extract of pre-separated contaminated soil, soil residue extracts and the corresponding heavy as well as light volatile fractions after pyrolysis under different conditions were diluted in DCM to a concentration of 1000 ppm. The samples were analyzed using a Trace GC Ultra (Thermo Fisher Scientific, Bremen, Germany) coupled to a Q Exactive Plus mass spectrometer (Thermo Fisher Scientific, Bremen, Germany) through an APPI interface. The APPI interface contains a Krypton VUV lamp (Syagen, Tustin, CA, U.S.A.) with a photon emission at 10.0 and 10.6 eV. The transfer line temperature was set to 320 °C. A ZB-5HT Inferno capillary column (30 m x 0.25 mm i.d. x 0.10 µm, Phenomenex, CA, U.S.A.) was used as stationary phase and Helium (purity 99.99999%, Air Liquide, Germany) as mobile phase for the chromatographic separation. The temperature of the oven was heated from 35 °C to 320 °C with a rate of 10 °C min⁻¹ and hold for 15 min. 1 µL of samples was injected in the splitless mode. Mass spectra was acquired in full scan mode for m/z 60-900 with a resolution of 140,000 at m/z 200 and a scan rate of 1.5 Hz. The sheath gas was set to 8 arbitrary unit (a.u.).

6.3.5. Direct injection APPI FT MS Analysis

The samples analyzed by GC-APPI-FT MS were diluted in toluene (99.8%, Acros Organics, Germany) to a final concentration of 250 ppm, which were directly injected into a research type FT Orbitrap MS (Thermo Fisher Scientific, Bremen, Germany) with a flow rate of 20 µL min⁻¹. Samples were ionized using the same Krypton VUV lamp mentioned above. The vaporizer temperature, sheath, auxiliary and sweep gases were set to 350 °C, 20, 5 and 2 arb, correspondingly. Spectral stitching^{21, 31, 32} with mass windows of 30 Da and 5 Da overlap was used to record mass spectra from 125 to 1200 Da with a resolution of 480,000 at m/z 400.

6.3.6. Data Analysis

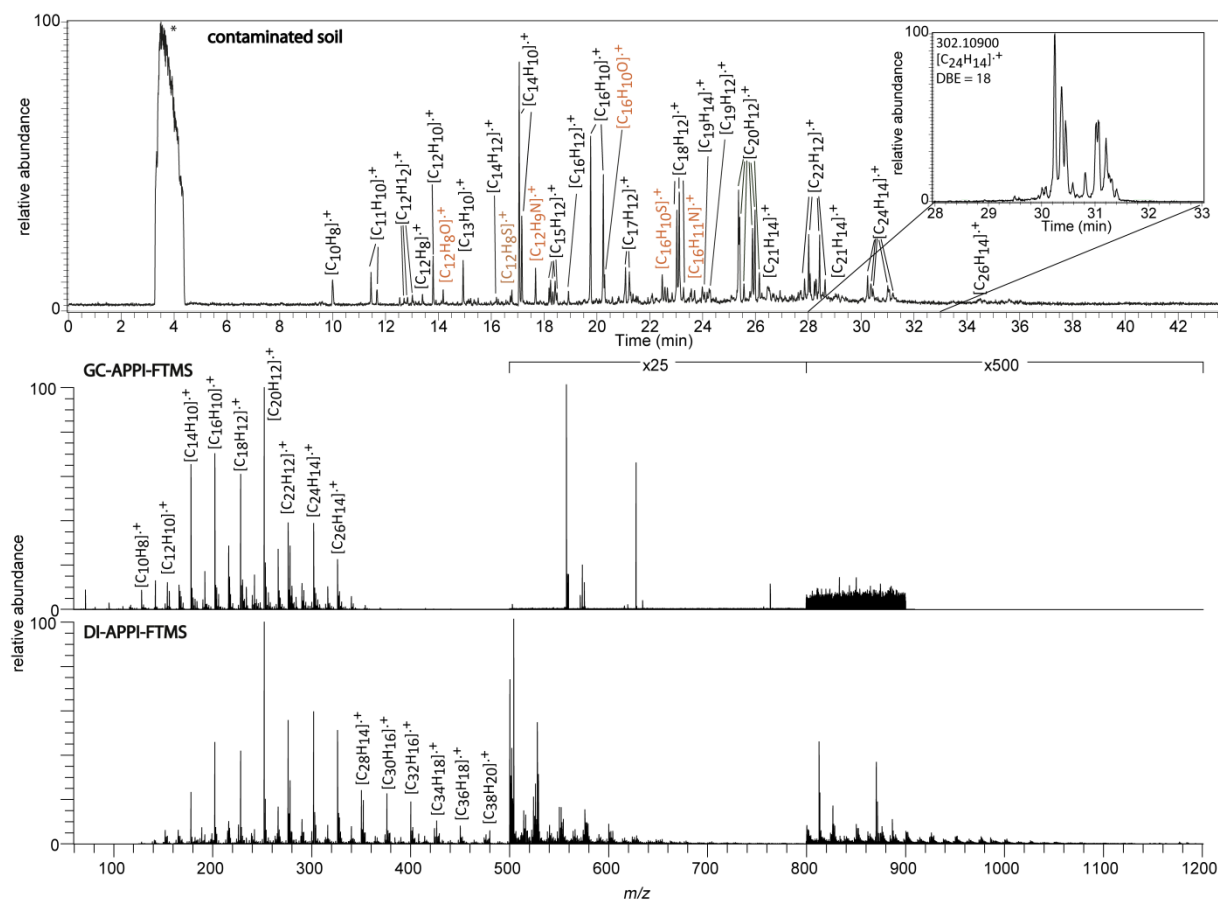
The data were recorded by Xcalibur 2.2 (Thermo Fisher Scientific, Bremen, Germany) and further processed using Composer v1.5.0 (Sierra Analytics, Modesto, CA, U.S.A) with the following chemical constraints: $0 < C < 200$, $0 < H < 1000$, $0 < N < 3$, $0 < S < 4$, $0 < O < 4$, $0 < \text{double bond equivalent (DBE)} < 100$, maximum mass error < 1 ppm.

6.4. Results and Discussion

6.4.1. Characterization of contaminated soil

The analysis of 16 EPA PAHs for assessing environmental quality has been applied for more than 40 years.³³ However, we know that neither the soil nor the contamination source is a simple system. The compositions of soils can vary from location to location drastically. The contamination source can contain besides these 16 PAHs, other higher molecular weight PAHs, PAHs containing different lengths of side chains as well as heteroatom containing PAHs.¹³⁻¹⁹ Owing to the continuing development of analytical techniques, especially the application of ultrahigh resolution FT MS²⁰ and its coupling to chromatographic separations,³⁴ it is possible to have more detailed view of contaminated soil samples, which helps to appraise the effect of remediation.^{29, 30, 35}

Figure 6-1 (top row) shows the total ion chromatogram for the contaminated soil, measured by GC-APPI-FTMS. Unlike the standard GC-FID analysis, which is the most universal but an unspecific method,³⁶ or GC-EI-MS analysis, which suffers from detecting the precursor ions



and can create incorrect assignments, when complex samples such as coal tar or crude oil are analyzed,³⁷ APPI is a soft ionization method, which produces molecular ions and protonated molecules. Using APPI in combination with ultrahigh resolution MS, polycyclic aromatic hydrocarbons with or without heteroatoms can be ionized efficiently and detected unambiguously.³⁸ In the contaminated soil radical cations of pure and alkylated PAHs dominated in the total ion chromatogram. Further adding to complexity, radical cations of heteroatom containing PAXHs, for example $[\text{C}_{12}\text{H}_9\text{N}]^+$, $[\text{C}_{16}\text{H}_{11}\text{N}]^+$, $[\text{C}_{12}\text{H}_8\text{S}]^+$, $[\text{C}_{16}\text{H}_{10}\text{S}]^+$, $[\text{C}_{12}\text{H}_8\text{O}]^+$, $[\text{C}_{16}\text{H}_{10}\text{O}]^+$, which are highlighted in orange in the total ion chromatogram, suggest the present of compounds containing pyrrole, thiophene or furan in the contaminated soil. In the end the chromatographic separation sophisticates the situation by providing isomeric information. As one example shown is the ion chromatogram for m/z 302.10900. At the retention time between 28 and 33 min, there were at least 12 partially separated peaks, which could all be assigned as $[\text{C}_{24}\text{H}_{14}]^+$ with a DBE of 18.

In the middle row of Figure 6-1 the recombined mass spectrum for the contaminated soil extract is shown, which was a result of averaging all mass spectra from the whole retention time after the solvent peak. The first overview shows a mass range of m/z 100-400 and a center at around m/z 250 for the contaminated soil, which mainly consists of pure PAHs. Here, radical PAHs predominate the spectrum.

When analyzing the natural soil²²⁻²⁵ or the contaminated soil,²⁶⁻²⁹ direct injection (DI) FTMS have been proved to be a versatile tool. Same as by the GC-MS measurements, here APPI was used as the ionization method. Additionally, the spectral stitching method provided more sensitive analysis for all possible compositions in the contaminated soil.³²

As can be seen in the bottom row of Figure 6-1, signal with highest intensity was around m/z 250, which is comparable to the results obtained from the GC-MS measurements. Here, signals appeared throughout the whole mass range (m/z 150-1200) for the contaminated soil extract.

To deal with very large data sets gained from ultrahigh resolution mass spectrometric analysis of complex mixtures, the accurately assigned signals are categorized according to their chemical formulas and summarized into the class distribution (Figure 6-2). Here, pure hydrocarbons including PAHs are grouped into the HC class, whilst compositions containing one or more heteroatoms, such as oxygen, nitrogen or sulfur, are sorted into the corresponding heteroatom classes. For example, azaarenes containing one nitrogen atom in the molecule,

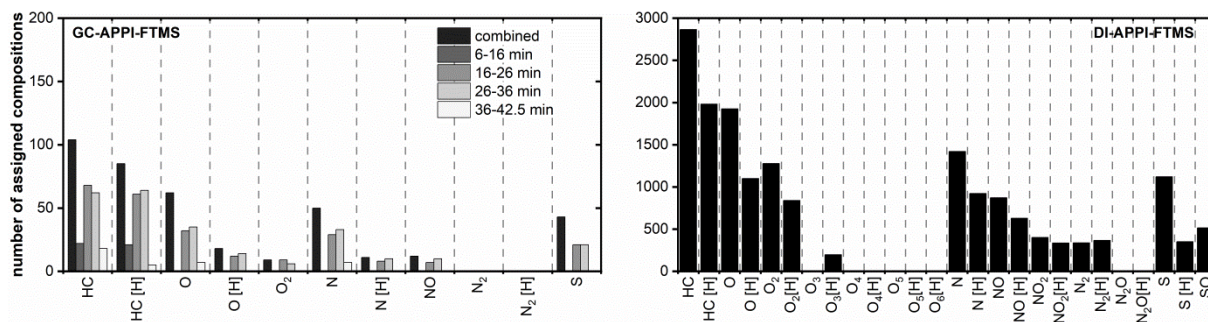


Figure 6-2. Class distributions for the contaminated soil extract, analyzed by GC- and DI-APPI-FT MS, respectively.

either pyrrolic or pyridinic structured, belong to the N_1 class. In addition to this, by using APPI, PAHs can be ionized as radicals and/or protonated molecules, which makes the data evaluation more complicated.³⁹ However, this can offer valuable structural information about one compound of interest. For instance, the pyrrolic PANHs (indole, carbazole, etc.) are preferentially ionized as radicals, though pyridinic PANHs (quinolone, acridine, etc.) as protonated molecules.^{40, 41}

In the left column of Figure 6-1 shown are the class distributions of assigned compositions from the whole retention time and different time intervals for the contaminated soil extract. During the GC-APPI-MS measurements, mass spectra were recorded at a frequency of 1.5 Hz. These will generate enormous amount of data. In order to reduce the data analysis time, time intervals of 10 min or shorter were taken. For the recombined mass spectrum from the contaminated soil extract, radical HC class delivered the highest number of assignments, followed by HC[H], O, N and S classes. The fact, that higher number of assignments was found for the radical N class compared to the N[H] class, implies that PANHs in the contaminated soil contained predominantly five-membered pyrrolic structures

In the right column of Figure 6-2 a total number of 11886 assigned compositions were found for the contaminated soil extract, which is about 37 times higher than the number of compositions detected by GC-MS (322). This is due to the fact, that during the measurement a more sensitive method in selected ion monitoring mode for each mass segment (30 Da) was applied.³² Apart from this, higher molecular weight PA(X)Hs and higher oxygenated class compounds can be more easily detected by direct injection MS than GC-MS.

A more detailed view of radical HC class compounds measured by GC- and DI-APPI-FTMS is shown in Figure 6-3. This is visualized by sorting all pure hydrocarbons according to their double bond equivalent (DBE) value and number of C-atoms per molecule. As the name already implies, DBE gives the information about the number of double bonds for a given

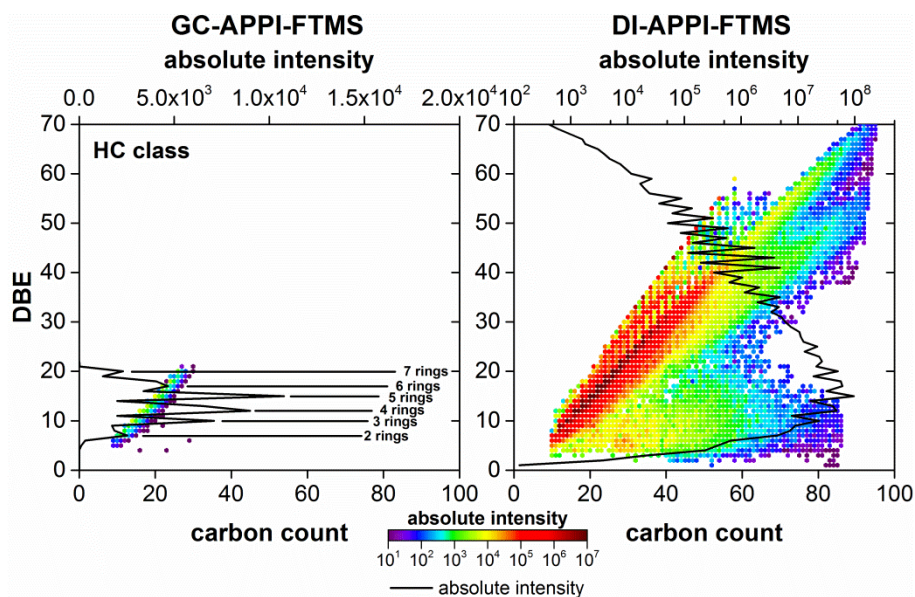


Figure 6-3. DBE vs. carbon count/absolute intensity plots for the radical HC class compositions in the contaminated soil extract, analyzed by GC- and DI-APPI-FTMS, respectively.

molecular formula. Additionally, the sum of monoisotopic abundance for hydrocarbons within a given DBE was linked with line.

In the GC-APPI-FTMS measurement (Figure 6-3, left column), pure hydrocarbons with DBE up to 21 and carbon counts up to 30 were detected. Hydrocarbons with higher intensity are mainly placed at the planar limit, which is defined as lines connecting the maximum DBE value at a given carbon count.⁴² These compounds correspond to non-alkylated PAHs. Hydrocarbons containing the same core aromatic structure but increasing length of side chains will have the same DBE value but increased number of carbon counts. In the contaminated soil extract alkylated PAHs with side chain length up to 7 were detected, and the intensity of them decreases gradually when the length of side chain increases. The highest absolute intensity for a given DBE appears at DBE of 15, which corresponds to benzo[*a*]pyrene and its isomers as well as alkylated derivatives with 5 aromatic benzene rings. Other peak values at DBE of 7, 10, 12, 17/18 and 20 represents structures containing 2 to 7 aromatic benzene rings, respectively.

In the DI-APPI-FTMS measurement (Figure 6-3, right column), a broader distribution of hydrocarbons was detected for the contaminated soil. Here, a total number of 2867 elemental compositions with DBE ranging from 2 to 70 were assigned to the radical HC class. Similar to results obtained from GC-APPI-FTMS measurement, compounds with highest absolute intensity represent non-alkylated PAHs containing up to 24 aromatic rings. Detailed structural discussion about these compounds is published elsewhere.

6.4.2. Pyrolysis of contaminated soil

For the purpose of selecting the desired temperature for the pyrolysis experiment, we first performed the thermogravimetric analysis for the pre-separated contaminated soil and the black solid aggregates. Figure 6-4 presents the weight loss and the weight loss rate for the samples during thermogravimetric analysis. For the contaminated soil a constant decrease of the soil weight was observed. A higher weight loss rate at below 100 °C indicated the release of water in the form of moisture. Another higher weight loss rate for the contaminated soil was observed at above 650 °C. This is resulted through release of CO₂ from carbonate containing minerals, such as magnesite or calcite.^{8,43}

Since the weight of contaminants, in terms of solvent extractable organics, compared to the total soil weight is very low (around 1%, see Figure 6-5). It is difficult to determine the efficient pyrolysis temperature for the contaminants. Therefore, the black solid aggregates, which were characterized to have high amount of solvent extractable organics, was subjected to thermogravimetric analysis.

Over 50% weight loss was gained, when the sample was heated up to 750 °C. The resulting residue cannot be dissolved in common organic solvents, such as toluene, dichloromethane or methanol, which leads to the assumption, that coke was formed during the process. For both samples a comparable weight loss rate at temperature below 100 °C and above 600 °C were observed, which indicates the release of water and CO₂ from minerals. However, an incredible high weight loss rate up to 3% min⁻¹ was detected between 200 °C and 600 °C for the black solid aggregates. This gives the range, where the transfer and decomposition of contaminants occur.

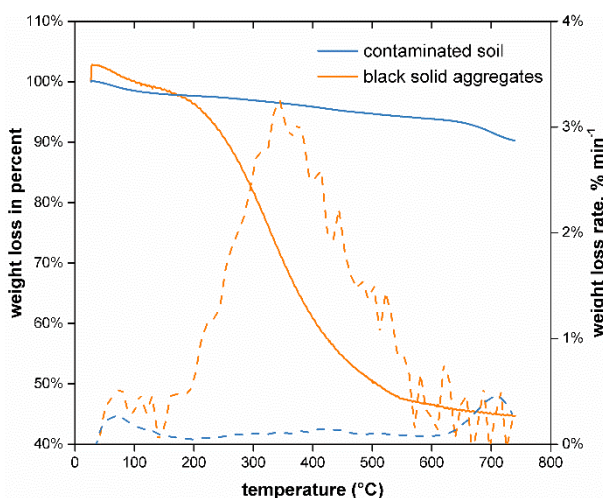


Figure 6-4. Thermogravimetric analysis of the contaminated soil (blue) and the black solid aggregates found in the soil (orange), weight loss in solid and weight loss rate in dashed lines.

In order to examine the pyrolysis efficiency, temperatures of 300 °C and 450 °C were selected, which represent a temperature lower or higher than the temperature for the maximum weight loss rate. Additionally, pyrolysis at 300 °C under vacuum was performed. Results can offer valuable information about the impact of the atmospheric condition on the remediation efficiency.

Pyrolysis belongs to thermal remediation techniques. Unlike other techniques, such as incineration, which are operated under an accelerated temperature and therefore have a higher energy demand, pyrolysis is aimed to lower the cost and remain the soil fertility.^{9, 44}

As results shown in Figure 6-5 are the amounts of solvent extractable organics (SEO) in the soil residue after pyrolysis compared to the amount in the contaminated soil before the treatment, as well as the yields of corresponding heavy and light volatile oil fractions. Here, the amount of SEO was used for the evaluation of the pyrolysis efficiency rather than the concentration of 16 EPA PAHs. It is a sum parameter similar but not only restricted to the total petroleum hydrocarbons, which is used together with the concentration of 16 EPA PAHs for monitoring soil quality and assessing remediation efficiency.⁸⁻¹¹ We want to move from a targeted to a non-targeted approach, and the amount of SEO represents a better view into the reality of what is present as contaminants in the soil.

A dramatic reduction of SEO from around 11,000 mg kg⁻¹ to 860 mg kg⁻¹ was the result of pyrolysis at 450 °C. Furthermore, around 1,000 mg kg⁻¹ heavy and light oil fractions were produced during the pyrolysis. About four times higher was the amount of SEO (32,600 mg kg⁻¹) after pyrolysis at 300 °C under Argon atmosphere, and accordingly, yields

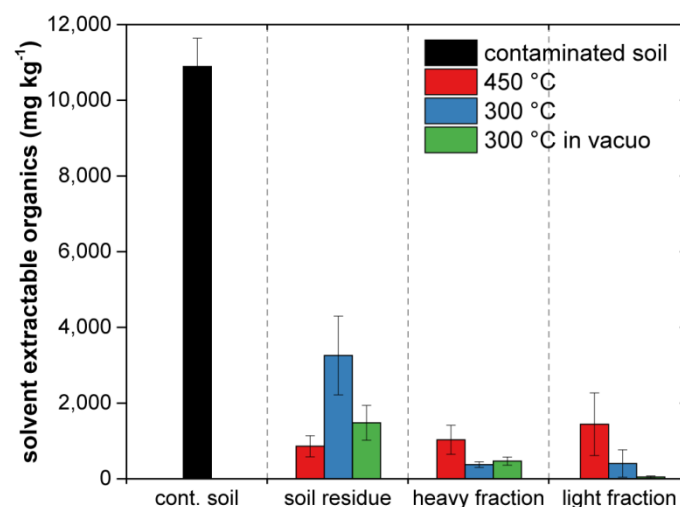


Figure 6-5. The amount of solvent extractable organics in the contaminated soil and soil residues after pyrolysis at 450 °C, 300 °C under Argon and 300 °C in vacuo, as well as the corresponding heavy and light oil fractions.

of heavy and light volatile fractions were only one third of the yields by pyrolysis at 450 °C. However, when changing from Argon atmosphere to vacuum condition, the amount of SEO was reduced to 1480 mg kg⁻¹. Results reveal that under same atmospheric condition, higher temperature can result in higher remediation efficiency. Nevertheless, it is feasible to lower the temperature but gaining the comparable result as at higher temperature by using vacuum. An early study from Roy et al. has shown that a reduction of total organic matter, which is equal to SEO in our content, from over 10,000 mg kg⁻¹ to around or even below 100 mg kg⁻¹ could be achieved by pyrolysis at a temperature between 450 and 550 °C under vacuum.⁴⁵ In order to better understand the pyrolysis process and compare results from different conditions, more advanced non-targeted analytical techniques are required.

For this purpose the soil residue extracts after pyrolysis at different conditions were analyzed using GC- and DI-APPI-FTMS, which were compared to the results gained for the contaminated soil extract. Figure 6-6 summarized both population and intensity based class

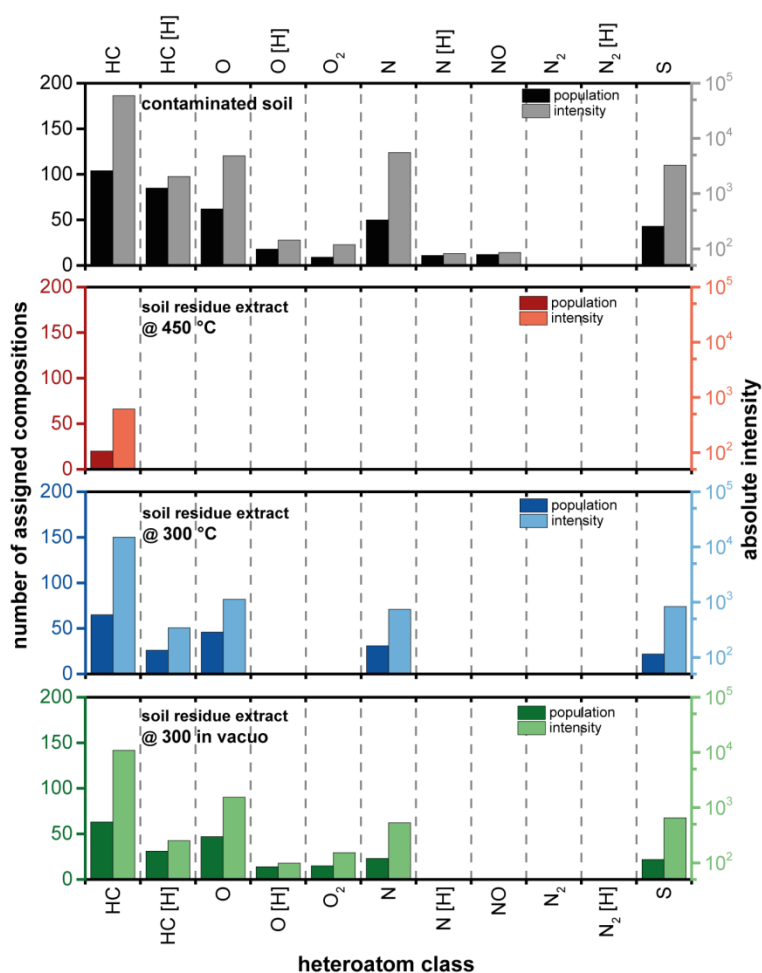


Figure 6-6. Population (darker color) and intensity (lighter color) based class distributions for the contaminated soil extract and soil residue extracts after pyrolysis at 450 °C, 300 °C as well as 300 °C in vacuo (from top to bottom), analyzed by GC-APPI-FTMS.

distributions for the contaminated soil extract and soil residue extracts from different pyrolysis conditions. It is clear to see, that in comparison to the contaminated soil extract there is a strong decrease in number of assigned compositions and absolute intensity for the soil residue extract after pyrolysis at 450 °C.

While for the GC-APPI-FTMS measurement, the number of assignments for the HC class is reduced significantly, for the DI-APPI-FTMS measurement, around 80% of the assigned HC compositions in the contaminated soil can still be detected (see Figure A6-1). Results indicate that the concentration of volatile compounds in the contaminated soil is decreased by pyrolysis, so that they are below the detection limit of GC-FTMS analysis, however detectable by the more sensitive DI-FTMS using spectral stitching method.³² Moreover, results point out that high molecular weight and more polar PAXHs, which have difficulty to be detected by GC-MS, are still present in the contaminated soil treated by pyrolysis.

A less pronounced reduction in both population and intensity can be observed for compositions in the soil residue extracts after pyrolysis at 300 °C and 300 °C in vacuo (Figure 6-6). Still, about half of the PAH, PANH as well as PASH were removed and the intensity was decreased to one tenth of the original value. The effect of applying vacuum during the pyrolysis can be better seen in Figure A6-1. The soil residue extract after pyrolysis at 300 °C showed similar distributions compared to the contaminated soil extract. Only radical S and SO class compounds exhibit a significant removal. In contrast to this, when vacuum was applied during the treatment, a reduction in number of assigned compositions can also be observed for HC, HC[H] and O, N, NO classes. Results demonstrate clearly that at a same pyrolysis temperature, better removal of contaminants from the soil can be achieved when vacuum is applied.

A closer look into the radical HC class compositions found in soil residue extracts after pyrolysis under different conditions is shown in Figure 6-7. The intensity of individual points in the plot was compared to the intensity obtained for the contaminated soil extract.

In the GC-APPI-MS measurement, the intensities of only 18 HC class compositions found in the soil residue extract after pyrolysis at 450 °C (instead of 104 in the contaminated soil extract) were reduced to around 1% (Figure 6-7, left column). Most of the alkylated PAHs with side chains are removed totally, remaining the parent PAHs and PAHs with up to one side chain. In the soil residue extracts after pyrolysis at 300 under argon atmosphere or vacuum alkylated PAHs with 3-4 side chains can still be detected, but a remarkable reduce for

PAHs can be seen. In comparison to the Argon condition, under vacuum condition the removal of PAHs with 2 to 6 rings was promoted. Similar results were obtained for the N class compositions in the contaminated soil (Figure A6-2, left column). After pyrolysis at 450 °C, PANHs were not detectable in the soil residue extract. In the extracts at 300 °C PANHs were reduced to containing 1 to 2 side chains.

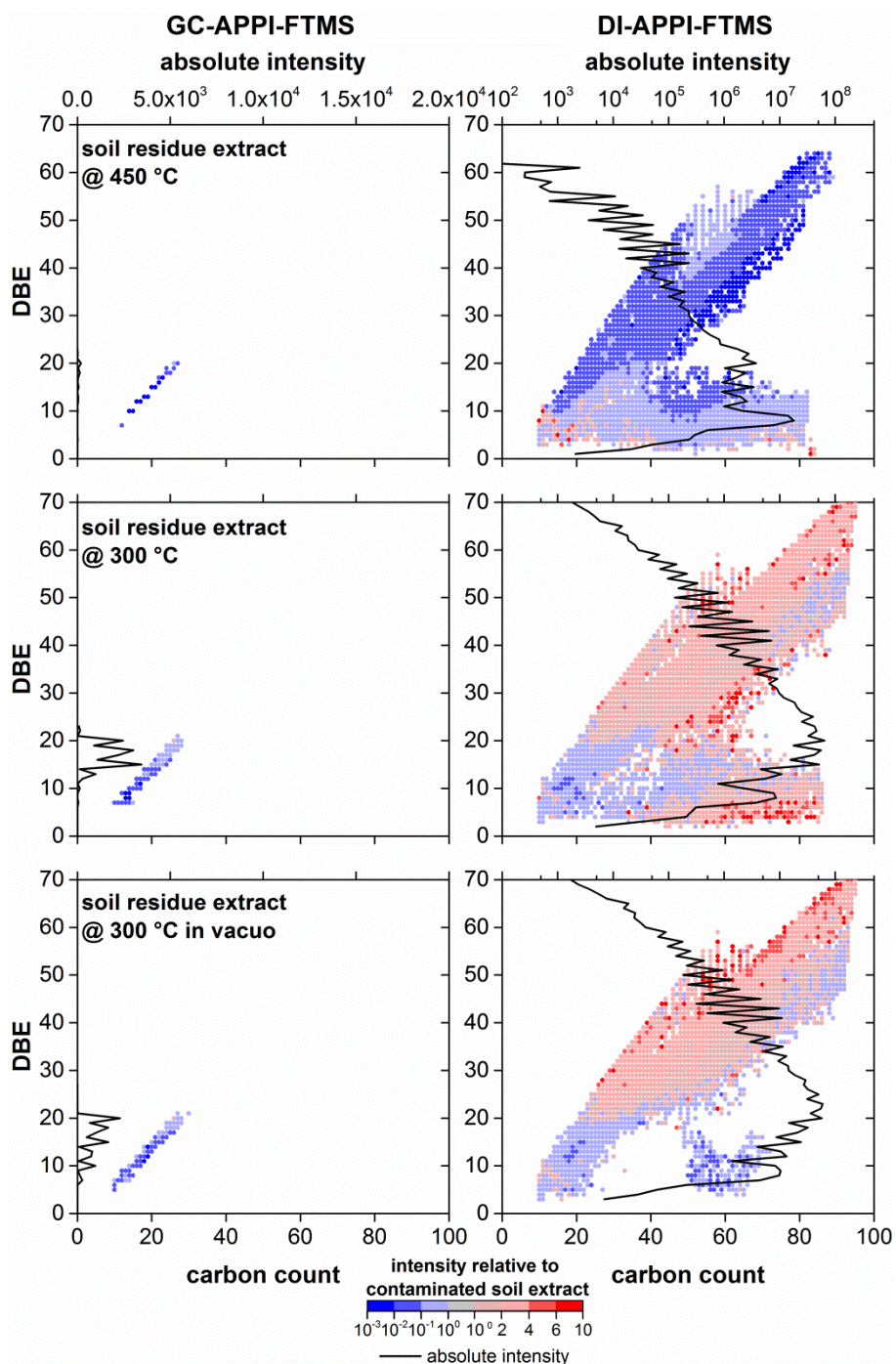


Figure 6-7. DBE vs. carbon count/absolute intensity plots for the radical HC class compositions in the soil residue extracts after pyrolysis at 450 °C, 300 °C as well as 300 °C in vacuo (from top to bottom), compared to the contaminated soil extract and analyzed by GC- and DI-APPI-FTMS.

In the DI-APPI-MS measurement, high molecular weight PAHs with DBE up to 65 and carbon count up to 90 are still detectable for the soil residue extract after pyrolysis at 450 °C (Figure 6-7, right column). However, the intensity of compositions with DBE over 9 has been reduced to less than 10% of the intensity in the contaminated soil extract. Differences between soil residue extracts from pyrolysis at 450 °C and 300 °C under argon atmosphere implied, that at lower temperature, hydrocarbons with DBE higher than 20 and alkylated hydrocarbons with extreme long side chains (carbon count exceeding 50) cannot be removed sufficiently. The application of vacuum improved the removal of long-chain hydrocarbons with DBE lower than 20. For PANHs in the contaminated soil, an overall reduction to 1% of the original intensity was resulted by the pyrolysis at 450 °C (Figure A6-2, right column). In the soils pyrolyzed at lower temperature, the intensity of PANHs with DBE below 20 (which corresponds to 7 rings) was decreased, while PANHs with higher DBE values was accumulated in the soil residue.

Results from both analytical methods show that at higher pyrolysis temperature, almost all PAXHs can be removed from the soil. At lower temperature, especially when vacuum was applied during the pyrolysis, PAXHs with DBE lower than 20 can be removed sufficiently. Since the DBE value of 17 for Benzo[*g,h,i*]perylene and Indeno[*1,2,3-cd*]pyrene is lower than 20, which is the highest value among the 16 EPA PAHs, it is feasible to run the pyrolysis under vacuum condition to cut down the energy consumption and reduce the damage for the soil at the same time.

6.4.3. Characterization of pyrolyzed oil

It is intensively investigated, using lignocellulosic biomass^{46, 47} or plastics⁴⁸ to produce pyrolysis oil as alternative to fossil fuels. However, little is known about the oil produced, when a contaminated soil is used as feedstock.

Figure 6-8 summarized the GC-APPI-FTMS measurement of the light and heavy oil fractions collected after the pyrolysis at 450 °C. Not only pure hydrocarbons, but also heteroatom containing contaminants are transferred into the oil fractions. When comparison has made between the four time intervals for the contaminated soil extract, the middle two time intervals (16-26 and 26-36 min) have the highest number of assignments (Figure 6-2, left column). This trend can also be observed for the oil fractions (Figure 6-8). In comparison to the contaminated soil extract, both two oil fractions showed an increase in number of assignments for the time interval between 16-26 min. This is obvious for the HC and HC[H]

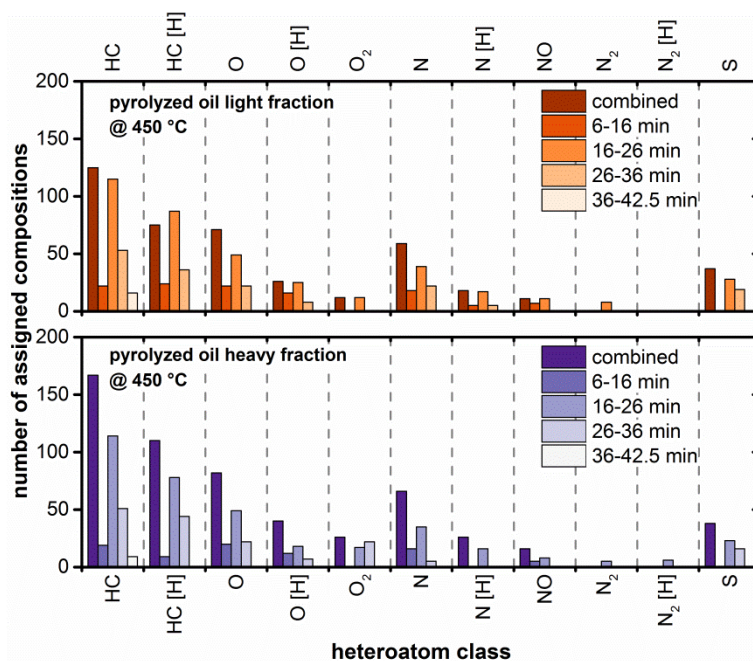


Figure 6-8. Population based class distributions for the light and heavy oil fraction after pyrolysis at 450 °C, analyzed by GC-APPI-FTMS.

classes, which demonstrates the formation of new low molecular weight hydrocarbons through pyrolysis.

Additionally, the results of DI-APPI-FTMS measurement for the oil fractions are shown in Figure A6-3. Here pure hydrocarbons followed by oxygen and nitrogen containing contaminants count as classes with highest absolute intensity. Compared with the contaminated soil extract and the corresponding soil residue extract (Figure A6-1), fewer hydrocarbons can be found in the oil fractions. Results show a clear mass transfer of volatile, low molecular weight contaminants from the soil into the light and heavy oil fractions during the pyrolysis, while high molecular weight contaminants either were decomposed.

A detailed view into the HC class compositions in the light and heavy oil fractions is shown in Figure 6-9. The results from GC-APPI-FTMS measurements showed, that the parent PAHs in oil fractions have a comparable intensity as in the contaminated soil extract. However, the intensity of alkylated or less aromatized PAHs in these two samples were higher than in the contaminated soil. Additionally, new compositions with low DBE were formed, which is shown in Figure A6-4.

In the DI-APPI-FTMS measurements (Figure 6-9, right column), hydrocarbons with DBE up to 50 can be transferred into the light and heavy oil fractions. Compared to the contaminated soil extract, these two fractions have an increased intensity for hydrocarbons with DBE

around 10 and carbon count between 10 and 40, which correspond to hydrocarbons containing 3 rings in the structure.

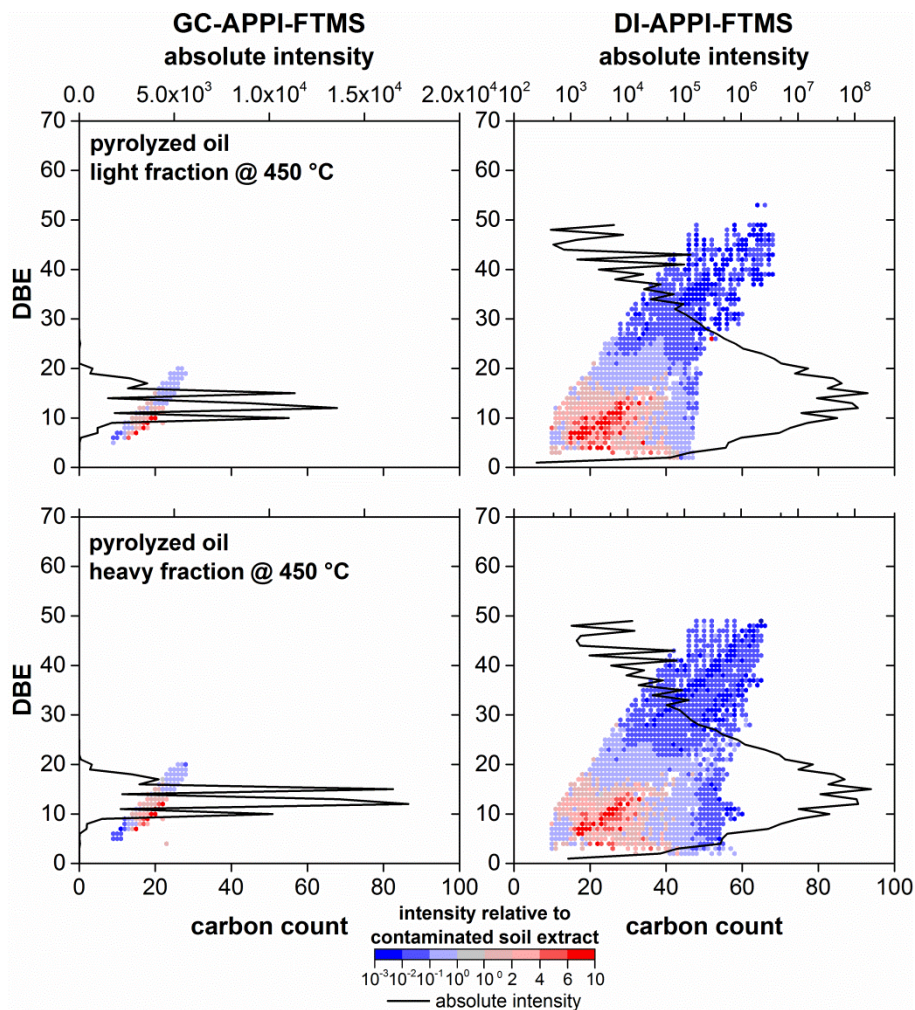


Figure 6-9. DBE vs. carbon count/absolute intensity plots for the radical HC class compositions in the light (upper row) and heavy (lower row) oil fractions after pyrolysis at 450 °C, compared to the contaminated soil extract and analyzed by GC- and DI-APPI-FTMS.

6.5. Conclusion

This work highlights the application of non-targeted analytical methods using both GC-APPI-FT MS and DI APPI FT MS for the analysis of a highly PAH contaminated soil before and after pyrolysis. By applying these techniques a detailed analysis of the pyrolyzed contaminated soil under different conditions is achieved on a molecular level. High molecular weight PAHs, PAHs with side chains and heteroatom containing PAXHs are considered at the same time. Results offer valuable information for assessing the pyrolytic remediation efficiency and demonstrate the possibility to use contaminated soil as feedstock and generate valuable fuels out of waste.

6.6. References

1. Manzetti, S., Polycyclic Aromatic Hydrocarbons in the Environment: Environmental Fate and Transformation. *Polycycl. Aromat. Comp.* **2013**, *33*, (4), 311-330.
2. Kanaly, R. A.; Harayama, S., Biodegradation of high-molecular-weight polycyclic aromatic hydrocarbons by bacteria. *J. Bacteriol.* **2000**, *182*, (8), 2059-2067.
3. Morillo, E.; Romero, A. S.; Maqueda, C.; Madrid, L.; Ajmone-Marsan, F.; Grcman, H.; Davidson, C. M.; Hursthouse, A. S.; Villaverde, J., Soil pollution by PAHs in urban soils: a comparison of three European cities. *J. Environ. Monitor.* **2007**, *9*, (9), 1001-1008.
4. Wilcke, W., Global patterns of polycyclic aromatic hydrocarbons (PAHs) in soil. *Geoderma* **2007**, *141*, (3), 157-166.
5. Gong, Z.; Wang, X.; Tu, Y.; Wu, J.; Sun, Y.; Li, P., Polycyclic aromatic hydrocarbon removal from contaminated soils using fatty acid methyl esters. *Chemosphere* **2010**, *79*, (2), 138-143.
6. Trelu, C.; Miltner, A.; Gallo, R.; Huguenot, D.; van Hullebusch, E. D.; Esposito, G.; Oturan, M. A.; Kästner, M., Characteristics of PAH tar oil contaminated soils—Black particles, resins and implications for treatment strategies. *J. Harzard. Mater.* **2017**, *327*, 206-215.
7. Khodadoust, A. P.; Bagchi, R.; Suidan, M. T.; Brenner, R. C.; Sellers, N. G., Removal of PAHs from highly contaminated soils found at prior manufactured gas operations. *J. Harzard. Mater.* **2000**, *80*, (1), 159-174.
8. Vidonish, J. E.; Alvarez, P. J. J.; Zygourakis, K., Pyrolytic Remediation of Oil-Contaminated Soils: Reaction Mechanisms, Soil Changes, and Implications for Treated Soil Fertility. *Ind. Eng. Chem. Res.* **2018**, *57*, (10), 3489-3500.
9. Vidonish, J. E.; Zygourakis, K.; Masiello, C. A.; Gao, X.; Mathieu, J.; Alvarez, P. J. J., Pyrolytic Treatment and Fertility Enhancement of Soils Contaminated with Heavy Hydrocarbons. *Environ. Sci. Technol.* **2016**, *50*, (5), 2498-2506.
10. Li, D.-C.; Xu, W.-F.; Mu, Y.; Yu, H.-Q.; Jiang, H.; Crittenden, J. C., Remediation of Petroleum-Contaminated Soil and Simultaneous Recovery of Oil by Fast Pyrolysis. *Environ. Sci. Technol.* **2018**, *52*, (9), 5330-5338.
11. Song, W.; Vidonish, J. E.; Kamath, R.; Yu, P.; Chu, C.; Moorthy, B.; Gao, B.; Zygourakis, K.; Alvarez, P. J. J., Pilot-Scale Pyrolytic Remediation of Crude-Oil-Contaminated Soil in a Continuously-Fed Reactor: Treatment Intensity Trade-Offs. *Environ. Sci. Technol.* **2019**, *53*, (4), 2045-2053.
12. Stout, S. A.; Emsbo-Mattingly, S. D.; Douglas, G. S.; Uhler, A. D.; McCarthy, K. J., Beyond 16 Priority Pollutant PAHs: A Review of PACs used in Environmental Forensic Chemistry. *Polycycl. Aromat. Comp.* **2015**, *35*, (2-4), 285-315.
13. Bandowe, B. A. M.; Lueso, M. G.; Wilcke, W., Oxygenated polycyclic aromatic hydrocarbons and azaarenes in urban soils: A comparison of a tropical city (Bangkok) with two temperate cities (Bratislava and Gothenburg). *Chemosphere* **2014**, *107*, 407-414.
14. Lundstedt, S.; Bandowe, B. A. M.; Wilcke, W.; Boll, E.; Christensen, J. H.; Vila, J.; Grifoll, M.; Faure, P.; Biache, C.; Lorgeoux, C.; Larsson, M.; Frech Irgum, K.; Ivarsson, P.; Ricci, M., First intercomparison study on the analysis of oxygenated polycyclic aromatic hydrocarbons (oxy-PAHs) and nitrogen heterocyclic polycyclic aromatic compounds (N-PACs) in contaminated soil. *TrAC-Trend. Anal. Chem.* **2014**, *57*, 83-92.
15. Wilcke, W.; Bandowe, B. A. M.; Lueso, M. G.; Ruppenthal, M.; del Valle, H.; Oelmann, Y., Polycyclic aromatic hydrocarbons (PAHs) and their polar derivatives (oxygenated PAHs, azaarenes) in soils along a climosequence in Argentina. *Sci. Total Environ.* **2014**, *473*, 317-325.

16. Chibwe, L.; Davie-Martin, C. L.; Aitken, M. D.; Hoh, E.; Massey Simonich, S. L., Identification of polar transformation products and high molecular weight polycyclic aromatic hydrocarbons (PAHs) in contaminated soil following bioremediation. *Sci. Total Environ.* **2017**, *599*, 1099-1107.
17. Richter-Brockmann, S.; Achten, C., Analysis and toxicity of 59 PAH in petrogenic and pyrogenic environmental samples including dibenzopyrenes, 7H-benzo[c]fluorene, 5-methylchrysene and 1-methylpyrene. *Chemosphere* **2018**, *200*, 495-503.
18. Manzano, C. A.; Marvin, C.; Muir, D.; Harner, T.; Martin, J.; Zhang, Y., Heterocyclic Aromatics in Petroleum Coke, Snow, Lake Sediments, and Air Samples from the Athabasca Oil Sands Region. *Environ. Sci. Technol.* **2017**, *51*, (10), 5445-5453.
19. Tian, Z.; Vila, J.; Wang, H.; Bodnar, W.; Aitken, M. D., Diversity and Abundance of High-Molecular-Weight Azaarenes in PAH-Contaminated Environmental Samples. *Environ. Sci. Technol.* **2017**, *51*, (24), 14047-14054.
20. Panda, S. K.; Andersson, J. T.; Schrader, W., Characterization of Supercomplex Crude Oil Mixtures: What Is Really in There? *Angew. Chem. Int. Edit* **2009**, *48*, (10), 1788-1791.
21. Vetere, A.; Schrader, W., Mass Spectrometric Coverage of Complex Mixtures: Exploring the Carbon Space of Crude Oil. *ChemistrySelect* **2017**, *2*, (3), 849-853.
22. Guigue, J.; Harir, M.; Mathieu, O.; Lucio, M.; Ranjard, L.; Lévêque, J.; Schmitt-Kopplin, P., Ultrahigh-resolution FT-ICR mass spectrometry for molecular characterisation of pressurised hot water-extractable organic matter in soils. *Biogeochemistry* **2016**, *128*, (3), 307-326.
23. Ohno, T.; Sleighter, R. L.; Hatcher, P. G., Comparative study of organic matter chemical characterization using negative and positive mode electrospray ionization ultrahigh-resolution mass spectrometry. *Anal. Bioanal. Chem.* **2016**, *408*, (10), 2497-2504.
24. Fleury, G.; Del Nero, M.; Barillon, R., Effect of mineral surface properties (alumina, kaolinite) on the sorptive fractionation mechanisms of soil fulvic acids: Molecular-scale ESI-MS studies. *Geochim. Cosmochim. Ac.* **2017**, *196*, 1-17.
25. Tfaily, M. M.; Chu, R. K.; Toyoda, J.; Tolic, N.; Robinson, E. W.; Pasa-Tolic, L.; Hess, N. J., Sequential extraction protocol for organic matter from soils and sediments using high resolution mass spectrometry. *Anal. Chim. Acta* **2017**, *972*, 54-61.
26. Lu, M.; Zhang, Z.; Qiao, W.; Guan, Y.; Xiao, M.; Peng, C., Removal of residual contaminants in petroleum-contaminated soil by Fenton-like oxidation. *J. Hazard. Mater.* **2010**, *179*, (1-3), 604-611.
27. Lu, M.; Zhang, Z.; Qiao, W.; Wei, X.; Guan, Y.; Ma, Q.; Guan, Y., Remediation of petroleum-contaminated soil after composting by sequential treatment with Fenton-like oxidation and biodegradation. *Bioresour. Technol.* **2010**, *101*, (7), 2106-2113.
28. Wang, J.; Zhang, X.; Li, G., Detailed characterization of polar compounds of residual oil in contaminated soil revealed by Fourier transform ion cyclotron resonance mass spectrometry. *Chemosphere* **2011**, *85*, (4), 609-615.
29. Noah, M.; Poetz, S.; Vieth-Hillebrand, A.; Wilkes, H., Detection of Residual Oil-Sand-Derived Organic Material in Developing Soils of Reclamation Sites by Ultra-High-Resolution Mass Spectrometry. *Environ. Sci. Technol.* **2015**, *49*, (11), 6466-6473.
30. Thomas, M. J.; Collinge, E.; Witt, M.; Palacio Lozano, D. C.; Vane, C. H.; Moss-Hayes, V.; Barrow, M. P., Petroleomic depth profiling of Staten Island salt marsh soil: 2 ω detection FTICR MS offers a new solution for the analysis of environmental contaminants. *Sci. Total Environ.* **2019**, *662*, 852-862.
31. Southam, A. D.; Payne, T. G.; Cooper, H. J.; Arvanitis, T. N.; Viant, M. R., Dynamic range and mass accuracy of wide-scan direct infusion nanoelectrospray Fourier

- transform ion cyclotron resonance mass spectrometry-based metabolomics increased by the spectral stitching method. *Anal. Chem.* **2007**, *79*, (12), 4595-4602.
32. Gaspar, A.; Schrader, W., Expanding the data depth for the analysis of complex crude oil samples by Fourier transform ion cyclotron resonance mass spectrometry using the spectral stitching method. *Rapid Commun. Mass Spectrom.* **2012**, *26*, (9), 1047-1052.
 33. Andersson, J. T.; Achten, C., Time to Say Goodbye to the 16 EPA PAHs? Toward an Up-to-Date Use of PACs for Environmental Purposes. *Polycycl. Aromat. Comp.* **2015**, *35*, (2-4), 330-354.
 34. Kondyli, A.; Schrader, W., High-resolution GC/MS studies of a light crude oil fraction. *J. Mass Spectrom.* **2019**, *54*, (1), 47-54.
 35. Barrow, M. P.; Peru, K. M.; Headley, J. V., An Added Dimension: GC Atmospheric Pressure Chemical Ionization FTICR MS and the Athabasca Oil Sands. *Anal. Chem.* **2014**, *86*, (16), 8281-8288.
 36. Li, D.-X.; Gan, L.; Bronja, A.; Schmitz, O. J., Gas chromatography coupled to atmospheric pressure ionization mass spectrometry (GC-API-MS): Review. *Anal. Chim. Acta* **2015**, *891*, 43-61.
 37. Zeigler, C. D.; Robbat, A., Comprehensive Profiling of Coal Tar and Crude Oil to Obtain Mass Spectra and Retention Indices for Alkylated PAH Shows Why Current Methods Err. *Environ. Sci. Technol.* **2012**, *46*, (7), 3935-3942.
 38. Vetere, A.; Schrader, W., 1- and 2-Photon Ionization for Online FAIMS-FTMS Coupling Allows New Insights into the Constitution of Crude Oils. *Anal. Chem.* **2015**, *87*, (17), 8874-8879.
 39. Gaspar, A.; Zellermann, E.; Lababidi, S.; Reece, J.; Schrader, W., Impact of Different Ionization Methods on the Molecular Assignments of Asphaltenes by FT-ICR Mass Spectrometry. *Anal. Chem.* **2012**, *84*, (12), 5257-5267.
 40. Purcell, J.; Rodgers, R.; Hendrickson, C.; Marshall, A., Speciation of nitrogen containing aromatics by atmospheric pressure photoionization or electrospray ionization fourier transform ion cyclotron resonance mass spectrometry. *J Am Soc Mass Spectrom* **2007**, *18*, (7), 1265-1273.
 41. Griffiths, M. T.; Da Campo, R.; O'Connor, P. B.; Barrow, M. P., Throwing light on petroleum: Simulated exposure of crude oil to sunlight and characterization using atmospheric pressure photoionization Fourier transform ion cyclotron resonance mass spectrometry. *Anal. Chem.* **2013**, *86*, (1), 527-534.
 42. Cho, Y.; Kim, Y. H.; Kim, S., Planar Limit-Assisted Structural Interpretation of Saturates/Aromatics/Resins/Asphaltenes Fractionated Crude Oil Compounds Observed by Fourier Transform Ion Cyclotron Resonance Mass Spectrometry. *Anal. Chem.* **2011**, *83*, (15), 6068-6073.
 43. Patterson, J. H.; Hurst, H. J.; Levy, J. H., Relevance of carbonate minerals in the processing of Australian Tertiary oil shales. *Fuel* **1991**, *70*, (11), 1252-1259.
 44. Kuppusamy, S.; Thavamani, P.; Venkateswarlu, K.; Lee, Y. B.; Naidu, R.; Megharaj, M., Remediation approaches for polycyclic aromatic hydrocarbons (PAHs) contaminated soils: Technological constraints, emerging trends and future directions. *Chemosphere* **2017**, *168*, 944-968.
 45. Roy, C.; de Caumia, B.; Blanchette, D.; Pakdel, H.; Couture, G.; Schwerdtfeger, A. E., Vacuum pyrolysis process for remediation of hydrocarbon - contaminated soils. *Remediation* **1994**, *5*, (1), 111-130.
 46. Mohan, D.; Pittman, C. U.; Steele, P. H., Pyrolysis of Wood/Biomass for Bio-oil: A Critical Review. *Energy Fuel* **2006**, *20*, (3), 848-889.
 47. Dhyani, V.; Bhaskar, T., A comprehensive review on the pyrolysis of lignocellulosic biomass. *Renew. Energ.* **2018**, *129*, 695-716.

48. Al-Salem, S. M.; Antelava, A.; Constantinou, A.; Manos, G.; Dutta, A., A review on thermal and catalytic pyrolysis of plastic solid waste (PSW). *J. Environ. Manage.* **2017**, *197*, 177-198.

Appendix for Chapter 6

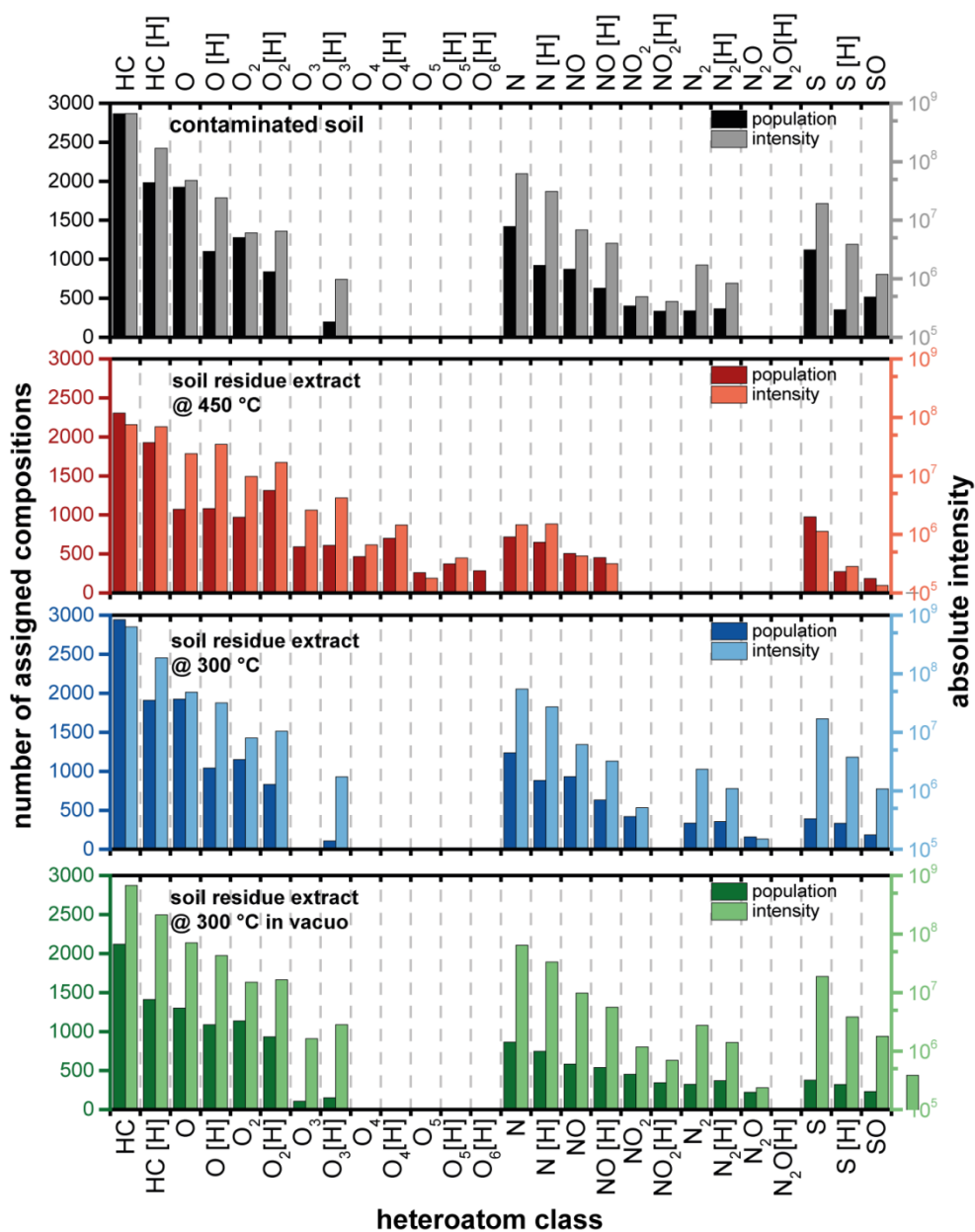


Figure A6-1. Population (darker color) and intensity (lighter color) based class distributions for the contaminated soil extract and soil residue extracts after pyrolysis at 450 °C, 300 °C as well as 300 °C in vacuo (from top to bottom), analyzed by DI-APPI-FTMS.

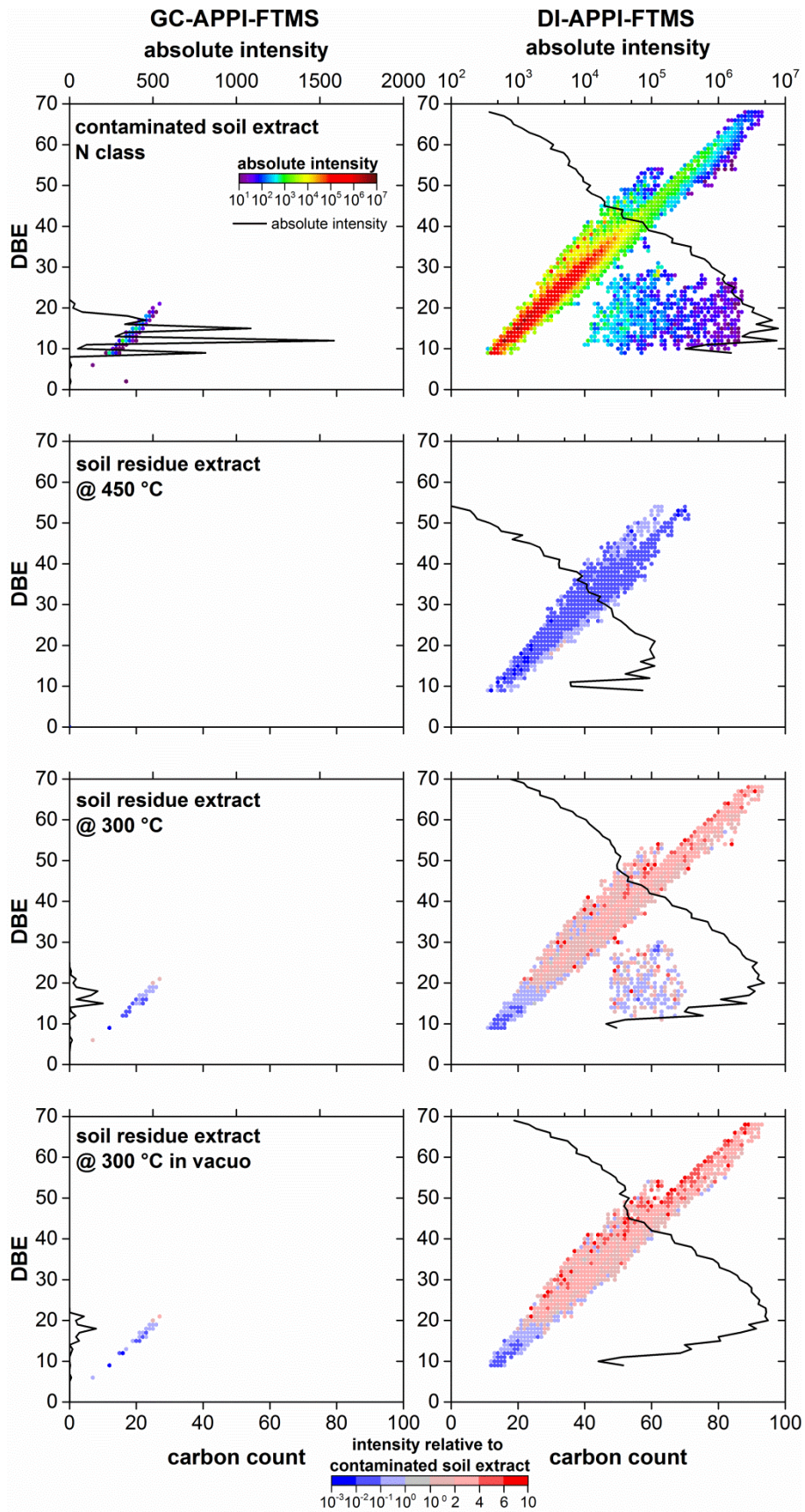


Figure A6-2. DBE vs. carbon count/absolute intensity plots for the radical N class compositions in the contaminated soil extract, compared to the composition in soil residue extracts after pyrolysis at 450 °C, 300 °C as well as 300 °C in vacuo (from top to bottom), analyzed by GC- and DI-APPI-FTMS.

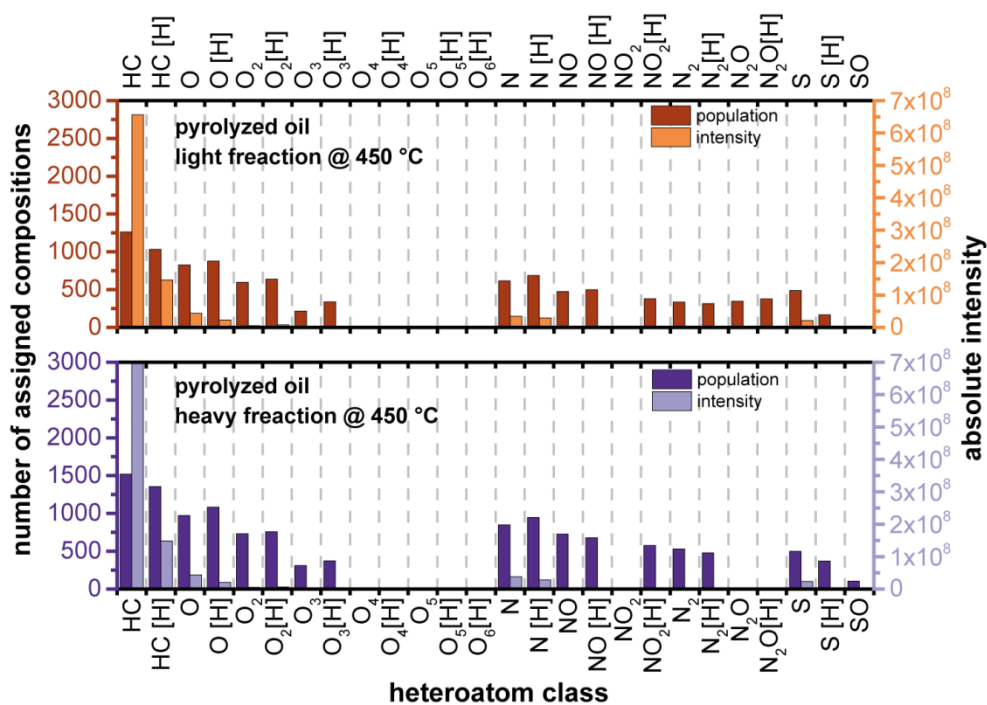


Figure A6-3. Population (darker color) and intensity (lighter color) based class distributions for the light and heavy oil fractions after pyrolysis at 450 °C, analyzed by DI-APPI-FTMS.

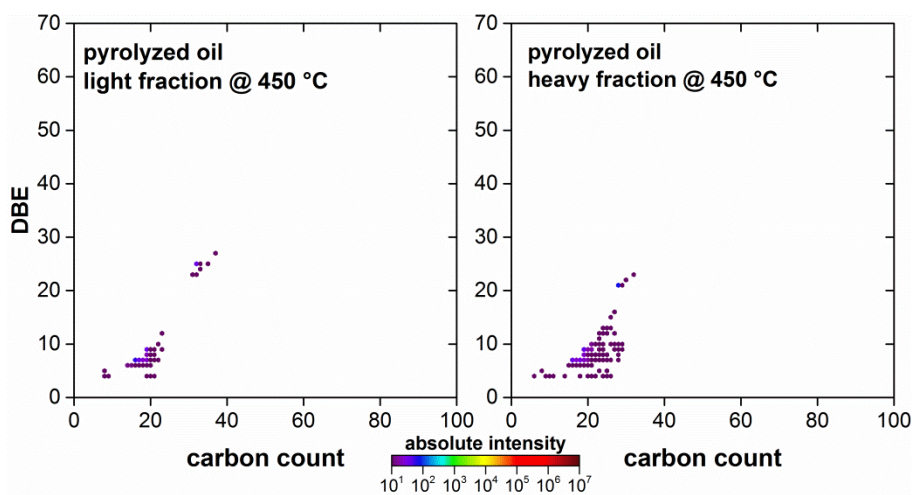


Figure A6-4. DBE vs. carbon count plots for newly formed radical HC class compositions in the light and heavy oil fractions after pyrolysis at 450 °C, analyzed by GC -APPI-FTMS.

Chapter 7. Conclusion

Polycyclic aromatic hydrocarbons (PAH) are ubiquitous in the environment. Over the last 40 years the standard method for measuring the concentration of PAH in the environment was to quantify the amount of 16 selected PAH, which were categorized as priority pollutants by the U.S. Environmental Protection Agency (EPA). Even only for these 16 PAH an elevated concentration exceeding $1,000 \text{ mg kg}^{-1}$ can be found in contaminated soils from industrial sites, such as manufactured gas plants and coking as well as petrochemical plants. Also the assessment of remediation techniques for the contaminated soil is based on the measurement of the concentration of the 16 EPA PAH in the soil after treatment.

It was not until recently, that studies with a higher priority focus on other high molecular weight (alkylated) PAH as well as polycyclic aromatic heterocycles (PAXH (X = N, S, O)), which can occur in the contaminated soil, were initiated. In order to gain a more comprehensive view for the contamination source and achieve a better assessment for remediation techniques, a non-targeted analysis for the ultra-complex environmental samples, such as contaminated soils, must be performed. This requires the state-of-the-art analytical instrumentation, such as Fourier transform mass spectrometry (FTMS) with various atmospheric pressure ionization (API) methods.

Environmental analysis starts with the sample preparation, which is the most crucial step, especially for the complex soil samples. Yet, almost all of the extraction methods applied for the PAH analysis in the contaminated soil have been optimized only for the 16 EPA PAH. In this work, the standard extraction methods for the 16 PAH analysis, which include Soxhlet extraction using different solvents and supercritical fluid extraction (SFE) using CO_2 , were extended to a broader range of analytes from a model sample containing crude oil as contaminant spiked in pure sand. Results from the non-targeted analysis by FTMS with various API methods reveal, that SFE using CO_2 as one of the modern extraction method could only extract compounds with lower double bond equivalent (DBE) values. In comparison to this, the conventional Soxhlet extraction offered quite good recovery for petroleum hydrocarbons. Among other solvents tested, dichloromethane (DCM) provided the best result.

Subsequently, this best extraction method from the investigation was applied for a real soil sample heavily contaminated with PAH. High amount of solvent extractable organics (SEO) was determined in the contaminated soil ($64,500 \pm 9,500 \text{ mg kg}^{-1}$). The extract was characterized using positive/negative mode electrospray ionization (ESI)-, atmospheric

pressure chemical ionization (APCI) and atmospheric photoionization (APPI)-FTMS in a non-targeted approach. In comparison to extracts from a potting soil and spiked sand with crude oil the contaminated soil exhibited a unique distribution of contaminants. They were located on or close to a line with a slope of 0.75 in the DBE vs. carbon count plot, which indicates the presence of condensed aromatic structures. PAH with DBE up to 70 were detected. Besides, pyridine- and pyrrole-based PANH were also detected in the contaminated soil, which can be distinguished by positive and negative ESI. Results also show that the length of side-chains from alkylated PA(X)H in the contaminated soil was relative short in comparison to petroleum hydrocarbons. According to the above described observations we concluded that the contaminants in the soil had a pyrogenic origin. In the end, results present the suitability of using FTMS for the non-targeted characterization of complex environmental samples.

The characterized contaminated soil was then treated using different remediation methods. Also here, emphasis has been placed on the assessment of remediation efficiency by means of a non-targeted analysis.

First of all, the contaminated soil was physically separated in an aqueous solution containing 39% (*w/w*) calcium chloride via stirring, aeration or ultrasonication. Around 80% of SEO were removed from the soil, which were mostly associated in black solid aggregates (BSA) from the light fraction. A detailed analysis of these BSA show that around 67% of the assigned elemental compositions from HC and O_x classes and over 40% of N and NO_x class compounds comprise condensed aromatic structures. This pre-separation step for especially highly PAH contaminated soils significantly reduces the amount of chemical or biological material for the remediation, and therefore lowers the costs.

In the next step the pre-separated contaminated soil was further subjected to another physical remediation technique, namely solvent extraction, using used cooking oil methyl ester (UCOME). Additional three fourth of the contaminants were removed from the soil. A detailed analysis of the extract was performed using gas chromatography (GC)-APPI-FTMS and direct injection (DI)-APPI-FTMS. Results showed that a wide range of PA(X)H with DBE up to 70 and carbon count up to 80 were extracted. For the pure PAH with increasing length of side chains, the extraction efficiency first increased and then decreased. Overall, the maximum removal rate for PA(X)H was determined at DBE between 10 and 30 and carbon count between 10 and 60.

At the same time the pre-separated contaminated soil was also subjected to thermal remediation by dint of pyrolysis. Different temperature and operation pressure were investigated. The amount of SEO was further reduced to below 1000 mg kg^{-1} at a pyrolysis temperature of $450 \text{ }^\circ\text{C}$. A comparable result was produced by applying vacuum in the system and lowering the temperature to $300 \text{ }^\circ\text{C}$, which emphasizes the roll of operating pressure during pyrolysis. The resulting pyrolytic treated contaminated soils were analyzed using both GC- and DI-APPI-FTMS. Results show that PAH with low molecular weight ($10 < \text{carbon count} < 40$) and low DBE values (around 15) were generated and transferred into the volatile fractions. A significant removal of PA(X)H with DBE up to 70 was achieved.

All results lead to a better understanding and characterization of unknowns in complex environmental samples, such as contaminated soils, as well as a detailed assessment of remediation techniques

Chapter 8. Appendix

8.1. List of abbreviations

°C	degree Celsius
AceHex	acetone: <i>n</i> -hexane
AI	aromaticity index
APCI	atmospheric pressure chemical ionization
APLI	atmospheric pressure laser ionization
APPI	atmospheric pressure photoionization
ASE	accelerated-solvent extraction
BSA	black solid aggregates
CA	California
CARS	condensed aromatic ring structures
Da	Dalton
DAD	diode array detector
DBE	double bond equivalent
DCM	dichloromethane
DI	direct injection
DNA	deoxyribonucleic acid
DOM	dissolved organic matter
EDX	energy dispersive X-ray
EI	electron ionization
ESI	electrospray ionization
eV	electronvolt
FAME	fatty acid methyl ester
FID	flame ionization detector
FLD	fluorescence detector
FT	Fourier transform
g	gram

GC	gas chromatography
GC x GC	two-dimensional gas chromatography
H	hour
HC	hydrocarbon
HPLC	high performance liquid chromatography
ICR	ion cyclotron resonance
ISO	International Organization for standardization
Kg	kilogram
LRMS	low resolution mass spectrometry
LTQ	linear ion trap
m/z	mass-to-charge ratio
MAE	microwave-assisted extraction
MeOH	methanol
Mg	milligram
Min	minute
mL	milliliter
Mm	millimeter
MS	mass spectrometry
NOM	natural organic matter
PAH	polycyclic aromatic hydrocarbons
PAXH	polycyclic aromatic heterocycles
Ppb	parts per billion
Q	quadrupole
QqQ	triple quadrupole
SEO	solvent extractable organics
SFE	supercritical fluid extraction
SOM	soil organic matter
T	Tesla

TEM	transmission electron microscopy
TIC	total ion chromatogram
TOF	time of flight
Tol	toluene
TPH	total petroleum hydrocarbons
U.S. EPA	United States Environmental Protection Agency
UCOME	used cooking oil methyl ester
UV	ultraviolet
VUV	vacuum ultraviolet
w/w	weight/weight
μA	microampere
μg	microgram
μL	microliter
ρ	density

8.2. List of schemes

Scheme 1-1. Gas phase reactions leading to the formation of radical cations and protonated molecules of the analyte (M) by positive mode APCI.	13
Scheme 1-2. Gas phase reactions leading to the formation of radical anions and even-electron ions of analyte (M) by negative mode APCI.....	14
Scheme 1-3. Gas phase reactions leading to the formation of radical cations and protonated molecules of the analyte (M) through positive mode normal APPI and dopant-assisted APPI (S: solvent, D: dopant).	14

8.3. List of figures

Figure 1-1. Examples of polycyclic aromatic compounds.....	1
Figure 1-2. Occurrence and transfer of PAH in the environment.....	2
Figure 1-3. Masses, double bond equivalents (DBEs) and chemical structures for 16 EPA PAH. ①: Naphthalene, ②: Acenaphthene, ③: Acenaphthene, ④: Fluorene, ⑤: Anthracene, ⑥: Phenanthrene, ⑦: Pyrene, ⑧: Fluoanthene, ⑨: Benzo[<i>a</i>]anthracene, ⑩: Chrysene, ⑪: Benzo[<i>a</i>]pyrene, ⑫: Benzo[<i>b</i>]fluoranthene, ⑬: Benzo[<i>k</i>]fluoranthene, ⑭: Dibenzo[<i>a,h</i>]anthracene, ⑮: Benzo[<i>ghi</i>]perylene, ⑯: Indeno[<i>1,2,3-cd</i>]pyrene.....	4
Figure 1-4. Extraction methods for PAH in contaminated sediments or soils. MAE: microwave-assisted extraction; ASE: accelerated-solvent extraction; SFE: supercritical fluid extraction. Methods in blue have been investigated in this work.....	6
Figure 1-5. Analytical methods for the targeted and non-targeted analysis of PA(X)H in contaminated soils. Green: separation techniques; orange: detection methods.....	8
Figure 1-6. Different remediation techniques for PAXH contaminated soils. Methods in blue are investigated in this work.....	9
Figure 1-7. Schematic view of Thermo Fisher Scientific Orbitrap Elite, adapted from Scigelova and Makarov. ¹²⁰	15
Figure 1-8. Original and high-field Orbitrap mass analyzers, adapted from Makarov et al. ¹²¹⁻¹²³	16
Figure 1-9. Resolving power dependency on m/z for the high-field Orbitrap mass analyzer with enhanced FT (solid lines), compared to the 7 T FT ICR MS in magnitude mode (dashed lines), adapted from Vetere and Schrader. ⁹⁵	17
Figure 1-10. broadband (top) vs. spectral stitching (narrowband, bottom) measurement.	18
Figure 2-1. Recovery of heavy crude oil in the spiked sand using Soxhlet extraction (in green) with toluene (Tol), dichloromethane (DCM), acetone: <i>n</i> -hexane (1:1, $v:v$) (AceHex), methanol (MeOH) and supercritical CO ₂ extraction (extract in blue, residue in brown). 33	
Figure 2-2. Recombined (left column) and zoomed in mass spectra at m/z 400 (right column) for the original crude oil sample, analyzed by FT Orbitrap MS using positive mode ESI (red), negative mode ESI (blue), positive mode APCI (green) and APPI (orange), respectively.....	34
Figure 2-3. Zoomed in mass spectra at m/z 400 for the original crude oil (black), Soxhlet extract using dichloromethane (green), SFE extract (blue) and SFE residue (brown) using positive mode APPI FT Orbitrap MS. Some signals are highlighted with calculated	

- elemental compositions and double bond equivalent (DBE) values, separated with a comma..... 35
- Figure 2-4. Intensity based class distributions for the Soxhlet extracted sample using dichloromethane, analyzed by positive/negative mode ESI, positive mode APCI/APPI (top to bottom) FT Orbitrap MS with protonated/deprotonated molecules in red, radical cations in blue and molecules with sodium adduct in green. 36
- Figure 2-5. Intensity (top) and population (bottom) based class distributions for the original crude oil, spiked sand Soxhlet extracted using Tol, DCM, AceHex or MeOH and its SFE extract (SFE E) and residue (SFE R), analyzed by positive mode APPI FT Orbitrap MS. Protonated molecules and radical cations are denoted in red and blue, respectively. 38
- Figure 2-6. Intensity (top) and population (bottom) based class distributions for the original crude oil, spiked sand Soxhlet extracted using Tol, DCM, AceHex or MeOH and its SFE extract (SFE E) and residue (SFE R), analyzed by positive mode APCI FT Orbitrap MS. 39
- Figure 2-7. Intensity (top) and population (bottom) based class distributions for the original crude oil, spiked sand Soxhlet extracted using Tol, DCM, AceHex or MeOH and its SFE extract (SFE E) and residue (SFE R), analyzed by positive (left) and negative (right) mode-ESI FT Orbitrap MS. Protonated molecules and radical cations are denoted in red and blue, respectively. 40
- Figure 2-8. Intensity based DBE vs. class distributions for the original crude oil, Soxhlet extract using DCM, SFE extract and residue (from top to bottom) using positive mode APPI FT Orbitrap MS (radical cations: M, protonated molecules: M[H])..... 41
- Figure 2-9. DBE vs. carbon count/intensity (Kendrick) plots for the radical HC (left column), [N+H]⁺ (middle column) and [N-H]⁻ (right column) classes in the original crude oil, Soxhlet extract using DCM, SFE extract and residue (from top to bottom) using positive mode APPI or positive/negative mode ESI FT Orbitrap MS. Upper abscissa for the absolute intensity in a given DBE and lower abscissa for the number of carbon atoms in a assigned composition..... 43
- Figure A2-1. Schematic representation of the SFE system. 1. CO₂ supply 2. Valve 3. Compressor 4: temperature controlled capillary 5. Pressure gauge 6. Heated Oven 7. Stainless steel column for the sample 8. Cool trap with toluene 9. Gas meter..... 49
- Figure A2-2. Recombined (left) and zoomed in mass spectra at 400 m/z (right) for the spiked sand sample Soxhlet extracted using dichloromethane, analyzed by FT Orbitrap MS

- using positive mode ESI (red), negative mode ESI (blue), positive mode APCI (green) and APPI (orange), respectively. 51
- Figure A2-3. Recombined (left) and zoomed in mass spectra at 400 m/z (right) for SFE extract of spiked sand, analyzed by FT Orbitrap MS using positive mode ESI (red), negative mode ESI (blue), positive mode APCI (green) and APPI (orange), respectively. 51
- Figure A2-4. Recombined (left) and zoomed in mass spectra at 400 m/z (right) for SFE residue of spiked sand, analyzed by FT Orbitrap MS using positive mode ESI (red), negative mode ESI (blue), positive mode APCI (green) and APPI (orange), respectively. 52
- Figure A2-5. Intensity based DBE vs. class distributions for the original crude oil, Soxhlet extract using DCM, SFE extract and residue (from top to bottom) using positive mode-APCI FT Orbitrap MS (radical cations: M, protonated molecules: M[H]). 52
- Figure A2-6. Intensity based DBE vs. class distributions for the original crude oil, Soxhlet extract using DCM, SFE extract and residue (from top to bottom) using positive mode-ESI FT Orbitrap MS (radical cations: M, protonated molecules: M[H], molecules with sodium adduct M[Na]). 53
- Figure A2-7. Intensity based DBE vs. class distributions for the original crude oil, Soxhlet extract using DCM, SFE extract and residue (from top to bottom) using negative mode-ESI FT Orbitrap MS (deprotonated molecules: M[H]). 54
- Figure A2-8. DBE vs. carbon number/intensity plots for the radical S (left column) and N (right column) class in the original crude oil, Soxhlet extract using DCM, SFE extract and residue (from top to bottom) using positive mode-APPI FT Orbitrap MS. 55
- Figure 3-1. The amount of solvent extractable organics in spiked sand, contaminated soil (CS), spiked contaminated soil, potting soil (PS) and spiked potting soil (from left to right) after Soxhlet extraction, spiked samples (with 50 g kg⁻¹ heavy crude oil per solid matrix) are denoted with oblique lines in the column (n = 3). 61
- Figure 3-2. Recombined positive mode (left column), zoomed-in section at m/z 400 (middle column) and negative (right column) mode mass spectra for the contaminated soil extract using ESI (green), APCI (red) and APPI (blue) FT Orbitrap MS. The magnification factor of the m/z signals is indicated above each mass spectrum. 62
- Figure 3-3. Venn diagrams for numbers of assigned compositions obtained from the extract of original contaminated soil using multiple ionization methods in positive (left) and negative (right) mode. 63

Figure 3-4. Population (top) and intensity (bottom) based class distributions for the original contaminated soil, analyzed by positive and negative mode ESI (green), APCI (red) and APPI (blue) FT Orbitrap MS, only classes with relative abundance higher than 1% are shown.	64
Figure 3-5. Kendrick plots for protonated/deprotonated N class after positive (top) and negative (bottom) mode multiple ionization methods.	66
Figure 3-6. Population based DBE vs. class distribution for the original contaminated soil extract. Only classes with relative abundance higher than 1% are shown.	67
Figure 3-7. Kendrick plot for HC class from the original contaminated soil extract, analyzed using positive mode APPI FTMS.	68
Figure 3-8. Kendrick plot for the slope calculation (A) with the corresponding proposed possible structures (B).	69
Figure A3-1. Venn diagrams for numbers of assigned compositions obtained using positive (left) and negative mode multiple ionization methods in the spiked sand.	79
Figure A3-2. Venn diagrams for numbers of assigned compositions obtained using positive (left) and negative mode multiple ionization methods in the potting soil.	79
Figure A3-3. Population (top) and intensity (bottom) based class distributions for the contaminated soil, analysed by positive and negative mode ESI (green), APCI (red) and APPI (blue) FT Orbitrap MS.	80
Figure A3-4. Population based DBE vs. class distribution for selected classes from contaminated soil (left), spiked sand (middle) and potting soil.	80
Figure A3-5. Kendrick plots for HC class from contaminated soil (left), spiked sand (middle) and potting soil.	81
Figure 4-1. Physical separation of contaminated soil in calcium chloride solution using stirring, aeration or ultrasonication.	86
Figure 4-2. Mass and SEO distributions and weight proportion of SEO to the contaminated soil and its fractions after physical separation through stirring, aeration or ultrasonication in 39% CaCl ₂ solution ($\rho = 1.40 \text{ g cm}^{-3}$). *: Soxhlet extracted using pure water. **: Black solid aggregates manually separated from the contaminated soil sample.	87
Figure 4-3. The separated heavy (a) and light (d) fractions from the original soil with their TEM images (b and e) and corresponding EDX results (c and f).	89
Figure 4-4. Recombined mass spectra for the Soxhlet extract from BSA, analyzed by FT Orbitrap MS using positive mode APPI (top), ESI (middle) and negative mode ESI (bottom).	90

- Figure 4-5. Class distributions for the heavy fraction after stirring, original soil, light fraction after stirring and BSA (from dark to light red) as well as the water extract (selected classes only) denoted as orig. soil*, analyzed using positive mode APPI FT Orbitrap MS. 92
- Figure 4-6. Kendrick plots for radical hydrocarbon (left column) and protonated nitrogen (right column) classes from the heavy fraction after stirring, original soil, light fraction after stirring, BSA and original soil after Soxhlet extraction with water (from top to bottom), analyzed using positive mode APPI and ESI Orbitrap MS. 93
- Figure 4-7. Van Krevelen plots for Soxhlet extract from BSA (top), the unique compositions from the heavy fraction after stirring (middle), and the original soil Soxhlet extracted using water (bottom, denoted as orig. soil*), compared with BSA, analyzed by both positive mode APPI (HC) and negative mode ESI (O_x) FT Orbitrap MS. Compositions below the gray or black line have a aromaticity index (AI) higher than 0.5 or 0.67, respectively. 95
- Figure A4-1. Recombined positive mode APPI mass spectra for original soil (top), its heavy (middle) and light (bottom) fractions after stirring..... 100
- Figure A4-2. Recombined mass spectra for the original soil Soxhlet extracted using water, analyzed by FT Orbitrap MS using positive mode APPI (top), ESI (middle) and negative mode ESI (bottom). 100
- Figure A4-3. Class distributions for the heavy fraction after aeration, original soil, light fraction after aeration and the black solid aggregate (from dark to light red) as well as the water extract (selected classes only) denoted as orig. soil*, analyzed using positive mode APPI FT Orbitrap MS..... 101
- Figure A4-4. Class distributions for the heavy fraction after ultrasonication, original soil, light fraction after ultrasonication and the black solid aggregate (from dark to light red) as well as the water extract (selected classes only) denoted as orig. soil*, analyzed using positive mode APPI FT Orbitrap MS..... 101
- Figure A4-5. Class distributions for the heavy fraction after stirring, original soil, light fraction after stirring and the black solid aggregate (from dark to light blue) as well as the water extract (selected classes only) denoted as orig. soil*, analyzed using positive mode ESI FT Orbitrap MS. 102
- Figure A4-6. Class distributions for the heavy fraction after aeration, original soil, light fraction after aeration and the black solid aggregate (from dark to light red) as well as the

water extract (selected classes only) denoted as orig. soil*, analyzed using positive mode ESI FT Orbitrap MS.	102
Figure A4-7. Class distributions for the heavy fraction after ultrasonication, original soil, light fraction after ultrasonication and the black solid aggregate (from dark to light red) as well as the water extract (selected classes only) denoted as orig. soil*, analyzed using positive mode ESI FT Orbitrap MS.	103
Figure A4-8. Class distributions for the heavy fraction after stirring, original soil, light fraction after stirring and the black solid aggregate (from dark to light red) as well as the water extract (selected classes only) denoted as orig. soil*, analyzed using negative mode ESI FT Orbitrap MS.	103
Figure A4-9. Class distributions for the heavy fraction after aeration, original soil, light fraction after aeration and the black solid aggregate (from dark to light red) as well as the water extract (selected classes only) denoted as orig. soil*, analyzed using negative mode ESI FT Orbitrap MS.	104
Figure A4-10. Class distributions for the heavy fraction after ultrasonication, original soil, light fraction after ultrasonication and the black solid aggregate (from dark to light red) as well as the water extract (selected classes only) denoted as orig. soil*, analyzed using negative mode ESI FT Orbitrap MS.	104
Figure A4-11. Kendrick plots for radical hydrocarbon (left column) and protonated nitrogen (right column) classes from the heavy and light fractions after aeration and ultrasonication (from top to bottom), analyzed using positive mode APP and ESI Orbitrap MS.	105
Figure A4-12. Van Krevelen plots for the black solid aggregate (top), the unique compositions from the heavy fraction after stirring (middle), and the original soil Soxhlet extracted using water (bottom, denoted as orig. soil*), compared with the black solid aggregate, analyzed by negative mode ESI FT Orbitrap MS. Compositions below the gray or black line have a AI higher than 0.5 or 0.67, respectively.	106
Figure 5-1. Efficiency of solvent extraction using UCOME for highly PAH contaminated soil. UCOME was removed from the contaminated soil through filtration and subsequent supercritical CO ₂ extraction.	111
Figure 5-2. Total ion chromatogram for UCOME, contaminated soil and soil residue extracts, analyzed by GC-APPI-FT MS. *: solvent peak.	112
Figure 5-3. Recombined mass spectra (left column) and corresponding class distributions (right column) for UCOME (black), contaminated soil extract (red), soil residue extract	

- (green), oil extract (blue) and SFE extract (purple) and, analyzed by GC-APPI-FT MS. 113
- Figure 5-4. Recombined mass spectra (left column) and corresponding class distributions (right column) for UCOME (black), contaminated soil extract (red), soil residue extract (green), oil extract (blue), and SFE extract (purple), analyzed by DI APPI FT MS. 115
- Figure 5-5. Population (top) and intensity (bottom) based DBE distribution for the contaminated soil (red) and soil residue extract (green), analyzed by GC APPI FT MS (left) or DI APPI FT MS (right), respectively. 116
- Figure 5-6. DBE vs. carbon count plots for HC (top), N (middle) and S (bottom) classes from the contaminated soil extract as well as soil residue extract compared to the contaminated soil extract, analyzed by GC- and DI-APPI-FTMS,..... 117
- Figure 6-1. Total ion chromatogram (top) and the recombined mass spectra (middle and bottom) for the contaminated soil extract, analyzed by GC-APPI-FTMS or DI-APPI-FTMS. *: solvent peak..... 127
- Figure 6-2. Class distributions for the contaminated soil extract, analyzed by GC- and DI-APPI-FT MS, respectively..... 129
- Figure 6-3. DBE vs. carbon count/absolute intensity plots for the radical HC class compositions in the contaminated soil extract, analyzed by GC- and DI-APPI-FTMS, respectively..... 130
- Figure 6-4. Thermogravimetric analysis of the contaminated soil (blue) and the black solid aggregates found in the soil (orange), weight loss in solid and weight loss rate in dashed lines..... 131
- Figure 6-5. The amount of solvent extractable organics in the contaminated soil and soil residues after pyrolysis at 450 °C, 300 °C under Argon and 300 °C in vacuo, as well as the corresponding heavy and light oil fractions..... 132
- Figure 6-6. Population (darker color) and intensity (lighter color) based class distributions for the contaminated soil extract and soil residue extracts after pyrolysis at 450 °C, 300 °C as well as 300 °C in vacuo (from top to bottom), analyzed by GC-APPI-FTMS..... 133
- Figure 6-7. DBE vs. carbon count/absolute intensity plots for the radical HC class compositions in the soil residue extracts after pyrolysis at 450 °C, 300 °C as well as 300 °C in vacuo (from top to bottom), compared to the contaminated soil extract and analyzed by GC- and DI-APPI-FTMS. 135
- Figure 6-8. Population based class distributions for the light and heavy oil fraction after pyrolysis at 450 °C, analyzed by GC-APPI-FTMS..... 137

- Figure 6-9. DBE vs. carbon count/absolute intensity plots for the radical HC class compositions in the light (upper row) and heavy (lower row) oil fractions after pyrolysis at 450 °C, compared to the contaminated soil extract and analyzed by GC- and DI-APPI-FTMS..... 138
- Figure A6-1. Population (darker color) and intensity (lighter color) based class distributions for the contaminated soil extract and soil residue extracts after pyrolysis at 450 °C, 300 °C as well as 300 °C in vacuo (from top to bottom), analyzed by DI-APPI-FTMS. 143
- Figure A6-2. DBE vs. carbon count/absolute intensity plots for the radical N class compositions in the contaminated soil extract, compared to the composition in soil residue extracts after pyrolysis at 450 °C, 300 °C as well as 300 °C in vacuo (from top to bottom), analyzed by GC- and DI-APPI-FTMS..... 144
- Figure A6-3. Population (darker color) and intensity (lighter color) based class distributions for the light and heavy oil fractions after pyrolysis at 450 °C, analyzed by DI-APPI-FTMS..... 145
- Figure A6-4. DBE vs. carbon count plots for newly formed radical HC class compositions in the light and heavy oil fractions after pyrolysis at 450 °C, analyzed by GC -APPI-FTMS. 145

8.4. List of tables

Table 2-1. Calculated mean values of m/z , DBE, number of carbon atoms and X/C for the samples, analyzed using APPI(+) FT Orbitrap MS.	42
Table A2-1. The experimental m/z , calculated ion formula, double bond equivalent (DBE) and mass error for identified major ions at m/z 400 with absolute intensity higher than 500 found in the original crude oil, measured by APPI(+)-FT Orbitrap mass spectrometry.	50
Table 3-1. Mean values of m/z , DBE, number of carbon atoms per molecule and X/C for the original contaminated soil extract, analyzed using different API-FT Orbitrap MS. Values were calculated using all assigned elemental compositions with on weighting of their absolute intensity.	63
Table 4-1. The number of HC and O_x class compositions detected in total, $AI > 0.5$ or > 0.67 (proportion to total number in parenthesis) for different samples.	95
Table A3-1. Suggested molecular structures of 10 most abundant signals for the original contaminated soil extract, analyzed by positive mode ESI FT Orbitrap MS.	75
Table A3-2. Suggested molecular structures of 10 most abundant signals for the original contaminated soil extract, analyzed by positive mode APCI FT Orbitrap MS.	75
Table A3-3. Suggested molecular structures of 10 most abundant signals for the original contaminated soil extract, analyzed by positive mode APPI FT Orbitrap MS.	75
Table A3-4. Suggested molecular structures of 10 most abundant signals for the original contaminated soil extract, analyzed by negative mode ESI FT Orbitrap MS.	76
Table A3-5. Suggested molecular structures of 10 most abundant signals for the original contaminated soil extract, analyzed by negative mode APCI FT Orbitrap MS.	76
Table A3-6. Suggested molecular structures of 10 most abundant signals for the original contaminated soil extract, analyzed by negative mode APPI FT Orbitrap MS.	76
Table A3-7. Properties of 16 EPA PAHs.	77
Table A3-8. Calculated mean values of m/z , DBE, number of carbon atoms and X/C for the spiked sand sample, analysed using different API-FT Orbitrap MS.	78
Table A3-9. Calculated mean values of m/z , DBE, number of carbon atoms and X/C for the potting soil, analysed using different API-FT Orbitrap MS.	78
Table A4-1. The number of NO_x class compositions detected in total, $AI > 0.5$ or > 0.67 (proportion to total number in bracket) for different samples.	106

8.5. List of publications

8.5.1. Publications in peer-reviewed Journals

1. Luo, R.; Schrader, W., Development of a Non-Targeted Method to Study Petroleum Polyaromatic Hydrocarbons in Soil by Ultrahigh Resolution Mass Spectrometry Using Multiple Ionization Methods. *Polycycl. Aromat. Comp.* **2020**, 1-16.
2. Luo, R.; Schrader, W., Getting a Better Overview of a Highly PAH Contaminated Soil: a Non-Targeted Approach Assessing the Real Environmental Risk (submitted to *Environmental Science & Technology*).
3. Luo, R.; Schrader, W., Physical Separation of Highly PAXH Contaminated Soil as Well as Analysis of Its Fractions and Corresponding Water Phase Using Fourier Transform Mass Spectrometry (will be submitted to *Environment International*).
4. Luo, R.; Schrader, W., Investigation of Solvent Extraction for Highly PAH Contaminated Soil Using Used Cooking Oil Methyl Ester, (will be submitted to *International Journal of Environmental Research and Public Health*).
5. Luo, R.; Schrader, W., Pyrolytic Remediation of Highly PAH Contaminated Soil, Analyzed Using Ultrahigh Resolution Atmospheric Pressure Photon Ionization (APPI) Fourier Transform Mass Spectrometry and Gas Chromatography-APPI-Mass Spectrometry, (will be submitted to *Environmental Pollution*).

8.5.2. Poster and oral presentations

R. Luo, W. Schrader, Characterization of black solid aggregates in highly PAH contaminated soil as main contamination source, analyzed by FT MS, 52nd German mass spectrometry society annual meeting, 10. – 13. March **2019**, Rostock, Germany (poster presentation)

R. Luo, W. Schrader, Method development for Non-targeted analysis of PAXHs in soil using ultrahigh resolution Fourier transform Orbitrap mass spectrometry, Umwelt 2018, 9 – 12 September **2018**, Münster, Germany (poster presentation)

R. Luo, W. Schrader, Non-targeted characterization of PAXHs contaminated soil using API FT Orbitrap MS, European mass spectrometry conference, 11 – 15 March **2018**, Saarbrücken, Germany (oral presentation)

R. Luo, W. Schrader, FT Orbitrap mass spectrometric analysis of hydrocarbon contaminated soil using Soxhlet and supercritical fluid extraction, FTMS Interest Group Meeting, 21 – 22 September **2017**, Kaiserslautern, Germany (poster presentation)

R. Luo, W. Schrader, Supercritical fluid extraction as a soil remediation method for removal of crude oil related contaminations, analyzed by FT Orbitrap MS, 50th German mass spectrometry society annual meeting, 5 – 8 March **2017**, Kiel, Germany (poster presentation)

R. Luo, W. Schrader, High-field FT Orbitrap mass spectrometric investigation on photooxidation processes of crude oil, 64th ASMS conference on mass spectrometry and allied topics, 5 – 9 June **2016**, San Antonio, Texas, USA (poster presentation)

R. Luo, W. Schrader, Investigation on the photooxidative degradation of crude oil by FT Orbitrap MS, 49th German mass spectrometry society annual meeting, 28 February – 02 March **2016**, Hamburg, Germany (oral presentation)

8.6. Curriculum Vitae

The CV has been removed from the online version because of data privacy.

8.7. Erklärung

Hiermit versichere ich, dass ich die vorliegende Arbeit mit dem Titel

„Development of analytical and remediation methods for highly polycyclic aromatic hydrocarbon contaminated soils“

selbst verfasst und keine außer den angegebenen Hilfsmitteln und Quellen benutzt habe, und dass die Arbeit in dieser oder ähnlicher Form noch bei keiner anderen Universität eingereicht wurde.

Essen, im Juli 2020

UNTERSCHRIFT

8.8. Acknowledgment

I would like to thank my “Shifu”, Wolfgang. He introduced me into the world of FTMS. In his lab, I got the possibility to get in touch with all kinds of mass spectrometers, from the oldest Finnigan MAT 95 double-focusing instrument to the heaviest 7 T FT ICR mass spectrometer. The topic he offered me makes it possible for me to continue the research in the field of environmental analysis. I remember he said something like this: everybody makes mistakes, but don't make the same mistake twice.” I want to thank the trust, freedom and also challenges as well as comments he gave me, which strongly increased my practical experience for instruments and trained my own scientific thinking. I am glad to be one of his students.

My thanks also go to my second supervisor, also my second “Shifu”, Torsten. I enjoyed the lectures he has given during my bachelor and master studies, which built up my solid fundamental knowledge for the environmental analysis including sample preparation and with emphasis on water analysis. His strict working attitude, scientific way of thinking and dedication to environmental chemistry as well as analysis have inspired me a lot. Although now I am not working in the field of environmental analysis, I hope that at least he has enjoyed a little bit reading my thesis and of course I am waiting for critical questions.

The corporation partner Mr. Klaus Moraw owns my sincere thanks. Thank you very much for your support and discussion during the study.

During my PhD in the work group, I met other colleagues from all over the world. They are: Xuxiao Wang, Lilla Guricza, Alessandro Vetere, Almalesh Roy, Jandyson Santos, Aikaterini Kondyli, Zahra Farmani, Ilker Satilmis, Yun Xu, Oleksandra Kuzmich, Haifa Shamseldin, David Hamacher, Robert Kalnins, Jens Dreschmann, Martin Ohrt and Andrei Jarashneli. Besides the scientific exchange between us, there were also cultural exchanges. I would call this as an extra bonus for my PhD. I still remember the face of other colleagues, once they tasted the moon cakes I bought for them.

I would like to thank other technicians in the MS department, here especially Danial Margold and Dirk Kampen, who shared me with their valuable practical knowledge about GC-MS. In Addition, I want to thank Jürgen Lutz from the glass blowing workshop, Niklas Fuhrmann and Lars Winkel from the technical laboratories, Ralf Thomas, Knut Gräfenstein, Dirk Ullner and Wolfgang Kersten from the precision mechanics department for their technical supports.

My sincerely thanks go to my parents. Thank you for your trust, patience, and love. Without your continuous support it wouldn't be possible to finish my thesis. My special thanks go to my girlfriend Dong and now my wife. I was lucky to meet you and thank you for putting faith in me and accompanying me during the hardest time of my PhD.

All in all, like the title of one German song says "Alles hat ein Ende nur die Wurst hat zwei", there is going to be an end for my PhD, however I really enjoyed the process. It is my great pleasure to meet you all and **THANK YOU VERY MUCH!!!**